

Sixth Case Study: Reference Data and Codes

NWMO-TR-2016-10

December 2016

M. Gobien, F. Garisto, E. Kremer, C. Medri

Nuclear Waste Management Organization

nwmo

NUCLEAR WASTE
MANAGEMENT
ORGANIZATION

SOCIÉTÉ DE GESTION
DES DÉCHETS
NUCLÉAIRES



Nuclear Waste Management Organization

22 St. Clair Avenue East, 6th Floor

Toronto, Ontario

M4T 2S3

Canada

Tel: 416-934-9814

Web: www.nwmo.ca

Sixth Case Study Reference Data and Codes

NWMO-TR-2016-10

December 2016

M. Gobien, F. Garisto, E. Kremer, and C. Medri
Nuclear Waste Management Organization

Document History

Title:	Sixth Case Study: Reference Data and Codes		
Report Number:	NWMO-TR-2016-10		
Revision:	R000	Date:	December 2016
Nuclear Waste Management Organization			
Authored by:	M. Gobien, F. Garisto, E. Kremer, and C. Medri		
Verified by:	F. Garisto and R. Guo		
Reviewed by:	N. Hunt		
Approved by:	P. Gierszewski		

ABSTRACT

Title: Sixth Case Study: Reference Data and Codes
Report No.: NWMO-TR-2016-10
Author(s): M. Gobien, F. Garisto, E. Kremer and C. Medri
Company: Nuclear Waste Management Organization
Date: December 2016

Abstract

The Sixth Case Study is an illustrative postclosure safety assessment of a conceptual repository for used nuclear fuel located at 500 m depth at a hypothetical site on the Canadian Shield.

The conceptual design differs from the previous case studies in that it considers horizontal in room placement of smaller (48 bundle) used fuel containers. The reference used fuel container design has also been updated: it retains the outer copper for corrosion protection and inner steel vessel for structural support; however, the copper is now electroplated or cold-sprayed directly onto the outer steel vessel, rather than being a separate shell. This copper coating is much thinner than the copper shell.

The hypothetical site where the repository is excavated is the same as in the Fourth Case Study (NWMO 2012a); however, a different realization of the fracture system is used. In this study, the exact repository location has shifted approximately 3500m to the north west, the room spacing has decreased from 40 m to 20 m and the repository remains at 500 m Below Ground Surface (mBGS).

The main safety assessment codes used in the Sixth Case Study are:

- FRAC3DVS-OPG – for 3D groundwater flow and radionuclide transport;
- RSM – a simple screening model used to identify the key radionuclides;
- SYVAC3-CC4 – the primary safety assessment system model (container, repository, geosphere, biosphere);
- HIM – for calculating dose consequences for the inadvertent human intrusion scenario.

These codes and their datasets are maintained under a software quality assurance system at NWMO. The codes are described briefly in this report.

The reference datasets are based on a combination of the site conceptual model information and the repository design description, with most of the general material properties and other input parameters adopted from previous work. Updated data were used when available from more recent studies. This report provides a summary of all the data selected, and indicates the references where more details about the derivation of the data may be found.

TABLE OF CONTENTS

	<u>Page</u>
ABSTRACT	iii
1. INTRODUCTION	1
1.1 BACKGROUND.....	1
1.2 REPORT OUTLINE	1
2. OVERVIEW	3
2.1 REPOSITORY CONCEPT	3
2.2 CONCEPTUAL MODELS	3
2.3 DATA.....	6
2.3.1 Data Sources	6
2.3.2 Parameter Variability.....	7
3. COMPUTER MODELS	8
3.1 MODELS, DATA AND TOOLS.....	8
3.1.1 Reference Models.....	8
3.1.2 Reference Data.....	10
3.1.3 Software Tools.....	10
3.2 COMPUTER MODEL DESCRIPTIONS	11
3.2.1 SYVAC3-CC4	11
3.2.2 FRAC3DVS-OPG.....	11
3.2.3 RSM.....	11
3.2.4 HIM.....	12
3.2.5 Specialized Supporting Codes	12
3.3 SOFTWARE QUALITY ASSURANCE	16
4. USED FUEL DATA.....	19
4.1 USED FUEL WASTEFORM	19
4.2 USED FUEL COMPOSITION	20
4.3 NUCLIDE AND ELEMENT INVENTORIES OF UO₂ FUEL AND ZIRCALOY	22
4.4 CONTAMINATION ON EXTERNAL BUNDLE SURFACES	30
4.5 INSTANT RELEASE	31
4.5.1 UO ₂ Instant Release	31
4.5.2 Zircaloy Instant Release.....	40
4.6 CONGRUENT RELEASE	41
4.6.1 UO ₂ Fuel Dissolution.....	41
4.6.2 Zircaloy Corrosion.....	44
5. CONTAINER	45
5.1 CONTAINER DIMENSIONS	45
5.2 DEFECTIVE CONTAINER.....	46
5.3 FREE WATER DIFFUSION COEFFICIENT.....	47
5.4 WATER COMPOSITION	49
5.5 SOLUBILITY LIMITS.....	50
6. REPOSITORY DATA	53

6.1	PHYSICAL LAYOUT	53
6.2	BUFFER	62
6.3	BACKFILL	63
6.4	CONCRETE	64
6.5	ASPHALT	64
6.6	DIFFUSION COEFFICIENTS	64
6.6.1	Buffer	64
6.6.2	Backfill	65
6.6.3	Concrete	66
6.6.4	Asphalt.....	66
6.7	SORPTION COEFFICIENTS AND CAPACITY FACTORS	66
6.7.1	Buffer	66
6.7.2	Backfill	67
6.7.3	Concrete	67
6.7.4	Asphalt.....	67
6.8	EFFECT OF INCREASED TEMPERATURE	70
6.8.1	Physical Properties	70
6.8.2	Hydraulic Conductivity	70
6.8.3	Diffusion Coefficients	70
6.8.4	Sorption Coefficients.....	70
7.	GEOSPHERE DATA	71
7.1	GENERAL SITE DESCRIPTION	71
7.2	PHYSICAL AND CHEMICAL CHARACTERISTICS OF THE GEOSPHERE	72
7.3	GEOSPHERE TRANSPORT PARAMETERS	76
7.3.1	Effective Diffusivity	76
7.3.2	Dispersion Length	77
7.4	EXCAVATION DAMAGE ZONE TRANSPORT PARAMETERS	78
7.4.1	Excavation Damage Zone Thickness.....	78
7.4.2	Excavation Damage Zone Permeability	79
7.4.3	Excavation Damage Zone Dispersion Length	79
7.4.4	Excavation Damage Zone Porosity	80
7.4.5	EDZ Tortuosity	81
7.5	GEOSPHERE SORPTION PARAMETERS	82
7.6	WELL LOCATION AND DEPTH	85
7.7	OTHER GEOSPHERE PARAMETERS	87
7.8	GEOSPHERE NODE DATA	87
8.	BIOSPHERE DATA	88
8.1	SITE AND SURFACE WATER	88
8.2	DISCHARGE ZONES	88
8.2.1	River Watershed Areas	90
8.2.2	Surface Discharge Area	92
8.3	CLIMATE AND ATMOSPHERE	94
8.4	SOILS AND SEDIMENT	96
8.4.1	Soil Physical Characteristics	96
8.4.2	Plant/Soil Concentration Ratio	98
8.4.3	Soil Distribution Coefficient (K_d)	99
8.4.4	River Sedimentation Rate	101
8.5	FARMING YIELDS	103

9.	DOSE PATHWAYS DATA	104
9.1	HUMAN LIFESTYLE CHARACTERISTICS.....	104
9.2	HUMAN PHYSICAL CHARACTERISTICS.....	109
9.3	AIR CONCENTRATION PARAMETERS.....	109
9.4	MISCELLANEOUS PHYSICAL PARAMETERS	112
9.5	ANIMAL CHARACTERISTICS	113
9.6	DOSE COEFFICIENTS.....	115
9.6.1	Adult Ingestion Dose Coefficients	116
9.6.2	Adult Inhalation Dose Coefficients	116
9.6.3	Adult Ground Exposure and Air Immersion Dose Coefficients.....	116
9.6.4	Adult Water Immersion Dose Coefficients.....	117
9.6.5	Adult Building Exposure Dose Coefficients	117
9.7	No-Effect Concentrations for Non-Human Biota	120
9.8	Chemical Hazard.....	120
10.	SUMMARY	120
11.	REFERENCES	121
APPENDIX A: USED FUEL INVENTORY UNCERTAINTY		133
A.1	INTRODUCTION	133
A.2	VALIDATION OF ORIGEN-S FOR CANDU REACTORS AND ORIGEN-S UNCERTAINTIES.....	133
A.3	INVENTORY UNCERTAINTY DUE TO AVERAGE AGE OF FUEL IN CONTAINERS	140
A.4	INVENTORY UNCERTAINTY DUE TO VARIATION IN AVERAGE BURNUP AND POWER RATING OF FUEL IN EACH CONTAINER	140
A.5	SUMMARY OF INVENTORY UNCERTAINTIES	141
APPENDIX B: USED FUEL DISSOLUTION MODEL		144
APPENDIX C: SYVAC3-CC4 GEOSPHERE MODEL DATA.....		156

LIST OF TABLES

	<u>Page</u>
Table 2.1: Parameter Probability Density Function Types and Attributes	7
Table 3.1: Description of Software Tools.....	11
Table 3.2: SYVAC3-CC4, Version SCC4.09.2.....	13
Table 3.3: FRAC3DVS-OPG, Version 1.3	14
Table 3.4: RSM, Version 1.1	15
Table 3.5: HIM, Version 2.1.....	16
Table 4.1: Used Fuel Parameters.....	20
Table 4.2: Potentially Significant Radionuclides Included in the Assessment	21
Table 4.3: Potentially Hazardous Elements Included in the Assessment.....	22
Table 4.4: Discharge Burnup Percentiles on a Per Station Basis	23
Table 4.5: Inventories of Potentially Hazardous Radionuclides in UO ₂ Fuel	27
Table 4.6: Inventories of Potentially Hazardous Radionuclides of Interest in Zircaloy for 30 Years Decay Time	28
Table 4.7: Inventories of Potentially Hazardous Elements for 30 Year Decay Time	29
Table 4.8: Inventories of Potentially Hazardous Elements in Zircaloy for 30 Year Decay Time ..	29
Table 4.9: Instant Release Fractions for CANDU Fuel	32
Table 4.10: Rationale for Selection of Instant Release Fractions for Elements without Measured Data	38
Table 4.11: Instant Release Fractions for Zircaloy Cladding.....	41
Table 4.12: Radiation Doses at Fuel Surface (220 MWh/kgU)#	43
Table 4.13: Radiation Doses at Fuel Surface (280 MWh/kgU)#	43
Table 4.14: Used Fuel Dissolution Rate Parameters (see Appendix B).....	44
Table 5.1: Container internal parameters	45
Table 5.2: Defective Container Scenario Parameters.....	47
Table 5.3: Free Water Diffusivity	48
Table 5.4: Contact Water Composition.....	49
Table 5.5: Element Solubilities ¹	52
Table 6.1: Placement Room Parameters.....	57
Table 6.2: Central Access Tunnels, Panel Access Tunnels, Perimeter Tunnels, and Shafts	60
Table 6.3: Proposed Sealing System for Shafts	61
Table 6.4: Properties of as Placed Materials in the Repository.....	61
Table 6.5: Properties of Highly Compacted Bentonite in the Buffer Box and Spacer Blocks at Saturation.....	62
Table 6.6: Properties of Gapfill at Saturation	62
Table 6.7: Homogenized Bentonite Properties at Saturation	62
Table 6.8: Properties of Dense Backfill at saturation	63
Table 6.9: Properties of Light Backfill at saturation.....	63
Table 6.10: Properties of 70% bentonite / 30% sand at saturation	63
Table 6.11: Properties of Concrete at Saturation.....	64
Table 6.12: Properties of Asphalt at Saturation	64
Table 6.13: Buffer Effective Diffusion Coefficients at 25°C	65
Table 6.14: Backfill Effective Diffusion Coefficients at 25°C	66
Table 6.15: Sorption Coefficients in the Bentonite, Backfill and Concrete.....	68
Table 6.16: Capacity Factors for the Bentonite, Backfill and Concrete	69
Table 7.1: Physical Parameters of the Host Rock	73
Table 7.2: Geochemistry Parameters.....	76
Table 7.3: Effective Diffusivities in Geosphere Zones [m ² /a].....	77

Table 7.4: Excavation Damage Zone Properties	81
Table 7.5: Transverse, Radial, and Axial Excavation Damage Zone Properties	82
Table 7.6: Values of $[\rho_s(1-\epsilon_{\text{expt}})/\epsilon_{\text{expt}}]$ for Several Geological Materials	83
Table 7.7: Geosphere K_d Values for Fractures and Crushed Rock ¹	84
Table 7.8: Well Model Geosphere Parameters	86
Table 7.9: Other Geosphere Properties	87
Table 8.1: Surface water properties	91
Table 8.2: Discharge zone areas	94
Table 8.3: Climate and Atmosphere Parameters	95
Table 8.4: Soil properties	97
Table 8.5: Plant/soil concentration ratios ¹	99
Table 8.6: Soil K_d Values ¹ [L/kg]	100
Table 8.7: River Sedimentation Rates	102
Table 8.8: Farming yield data	103
Table 9.1: Human Lifestyle Characteristics for Farm Household	105
Table 9.2: Irrigation Rate Parameters	107
Table 9.3: Timing Parameters	108
Table 9.4: Human Physical Characteristics	109
Table 9.5: Volatilization Parameters	111
Table 9.6: Physical Parameters	112
Table 9.7: Food Energy and Water Content	112
Table 9.8: Nutrient Content of Foods ¹	113
Table 9.9: Domestic Animal Data ¹	113
Table 9.10: Animal Ingestion Transfer Coefficients ¹	114
Table 9.11: Animal Inhalation Transfer Coefficients ¹	115
Table 9.12: Adult Human Dose Coefficients ¹	118
Table 9.13: Parameters for Human Specific Activity Models	119
Table A.1: Measured and Calculated Atom Ratios for NDP Fuel Study	134
Table A.2: Measured and Calculated Atom Ratios for Bruce Fuel Study	135
Table A.3: Measured and Calculated Inventories for Pickering-A Fuel Study	136
Table A.4: Measured and Calculated Inventories for NEA ATM-104 Study	138
Table B.1: Alpha, Beta and Gamma Dose Rates (Gy/a) for 220 MWh/kgU and 280 MWh/kgU Burnups	147
Table C.1: SYVAC3-CC4 Simple Geosphere Network - Node Data	161
Table C.2: SYVAC3-CC4 Simple Geosphere Network - Segment Properties	162
Table C.3: SYVAC3-CC4 Simple Geosphere Network - Slope Values	163
Table C.4: SYVAC3-CC4 Simple Geosphere Network - Input Data File	164
Table C.5: SYVAC3-CC4 Full Geosphere Network – Node Data	172
Table C.6: SYVAC3-CC4 Full Geosphere Network – Segment Properties	177
Table C.7: SYVAC3-CC4 Full Geosphere Network – Slope Values	183
Table C.8: SYVAC3-CC4 Full Geosphere Network – Input Data File	188

LIST OF FIGURES

	<u>Page</u>
Figure 1.1: Illustration of the Multi-Barrier Deep Geological Repository Concept Considered in the Sixth Case Study.....	2
Figure 2.1: Base Case – General Conceptual Model Describing Releases from Defective Containers.....	5
Figure 2.2: Inadvertent Human Intrusion – General Conceptual Model	6
Figure 3.1: Illustration of Relationship between the Computer Models Used in the Sixth Case Study and Supporting Data	9
Figure 3.2: Software Change Control Process Followed for the NWMO Postclosure Safety Assessment Software and Data	18
Figure 4.1: Distribution of Burnups and Cumulative Distribution for all Fuel Bundles.....	24
Figure 4.2: Radioactivity of Used Fuel (220 MWh/kgU burnup) as a Function of Time after Discharge from the Reactor.....	30
Figure 4.3: Distribution of Maximum Linear Power Ratings and Cumulative Distribution for all Commercial Fuel Bundles (discharged up to 2012)	33
Figure 4.4: Fission Gas (gap) Release as a Function of Peak Linear Power Rating for CANDU Fuels with Burnups Less than 400 MWh/kgU	35
Figure 4.5: Total Instant Release Fractions (gap + grain boundary inventories) for Iodine and Cesium.....	35
Figure 4.6: Cl-36 Releases from CANDU Fuel	36
Figure 5.1: Container Design Showing Copper Coating, Inner Steel Vessel, and Fuel Assemblies inside support tubes.	46
Figure 6.1: Plan View of Underground Repository.....	55
Figure 6.2: Placement Room Longitudinal Section.....	56
Figure 6.3: Placement Room Geometry	56
Figure 6.4: Longitudinal View of the Placement Room Seal	58
Figure 6.5: Underground Repository Tunnel Sections	59
Figure 7.1: Hypothetical Subregional area	71
Figure 7.2: Fracture Network in 2D local	72
Figure 7.3: Conductivity versus Depth Profiles of the Rock Mass and Fractures	74
Figure 8.1: Repository Site and Surface Area	89
Figure 8.2: Surface Discharge Zones.....	89
Figure 8.3: Catchment Areas	91
Figure 8.4: Discharge Areas for Concentration Thresholds of 1 Bq/m ³ , 0.1 Bq/m ³ and 10 Bq/m ³	93
Figure A.1: Comparison of Calculated and Experimental Inventories for Actinide (left) and Fission Product (right) Using ENDF/B-V and ENDF/B-VII Libraries	139
Figure B.1: Corrosion Rates Measured as a Function of Specific Alpha Activity.....	148
Figure B.2: UO ₂ (fuel) Corrosion Rates (calculated at 100°C) Plotted Logarithmically as a Function of the Gamma or Beta Radiation Dose Rate	150
Figure B.3: UO ₂ Corrosion Rates from Various Literature Sources	152
Figure B.4: Radiation Dose Rate in Water at the Fuel Surface (220 MWh/kgU burnup)	153
Figure B.5: Calculated Total Fuel Dissolution Rate	153
Figure C.1: SYVAC3-CC4 Simple Model: Transport Network Connectivity	158
Figure C.2: SYVAC3-CC4 Full Model: Transport Network Connectivity – Part I	159
Figure C.3: SYVAC3-CC4 Full Model: Transport Network Connectivity – Part II	160

1. INTRODUCTION

1.1 BACKGROUND

The Sixth Case Study is a postclosure safety assessment of a deep geological repository in crystalline rock in the Canadian Shield as shown in Figure 1.1 (NWMO 2017). The main objective of the Sixth Case Study is to assess key aspects of the postclosure safety of a deep geological repository based on a more recent Canadian design concept. The key differences between the Sixth and previously completed Fourth Case Study (NWMO 2012a) is the use of a smaller container holding 48 fuel bundles (rather than the much larger container holding 360 fuel bundles) and the repository design changes made to accommodate the smaller container. The present report documents the data and computer codes used for this study. This information should be considered within the following context.

- The Study focusses on key scenarios, including the expected or Normal Evolution scenario and a variety of Disruptive Event Scenarios, but is not a complete postclosure safety assessment.
- The Study is based on a specific conceptual repository design.
- The site is hypothetical. It is assumed that a sufficient volume of competent rock is available for the repository. The depth of 500 m was assumed for this illustrative assessment, and would be optimized for a real site. There is no site-specific data and, hence, no Geosynthesis, i.e., a geoscientific explanation of the overall understanding of site characteristics and evolution (past and future) as they relate to demonstrating long-term repository performance and safety.

1.2 REPORT OUTLINE

This report describes the main computer codes and data used in the postclosure safety assessment calculations for the Sixth Case Study. It is organized as follows:

- **Section 2** provides an overview of the repository design, models and general data selection principles;
- **Section 3** summarizes the computer codes used and their main features, and the software quality assurance approach;
- **Section 4** provides the used fuel wastefrom data;
- **Section 5** provides the container data;
- **Section 6** provides the placement room and repository data;
- **Section 7** provides the geosphere data;
- **Section 8** provides the local surface biosphere data; and
- **Section 9** provides the biosphere data, specifically the data used for calculating dose rates to a critical human group assumed to be living at the site in the future.

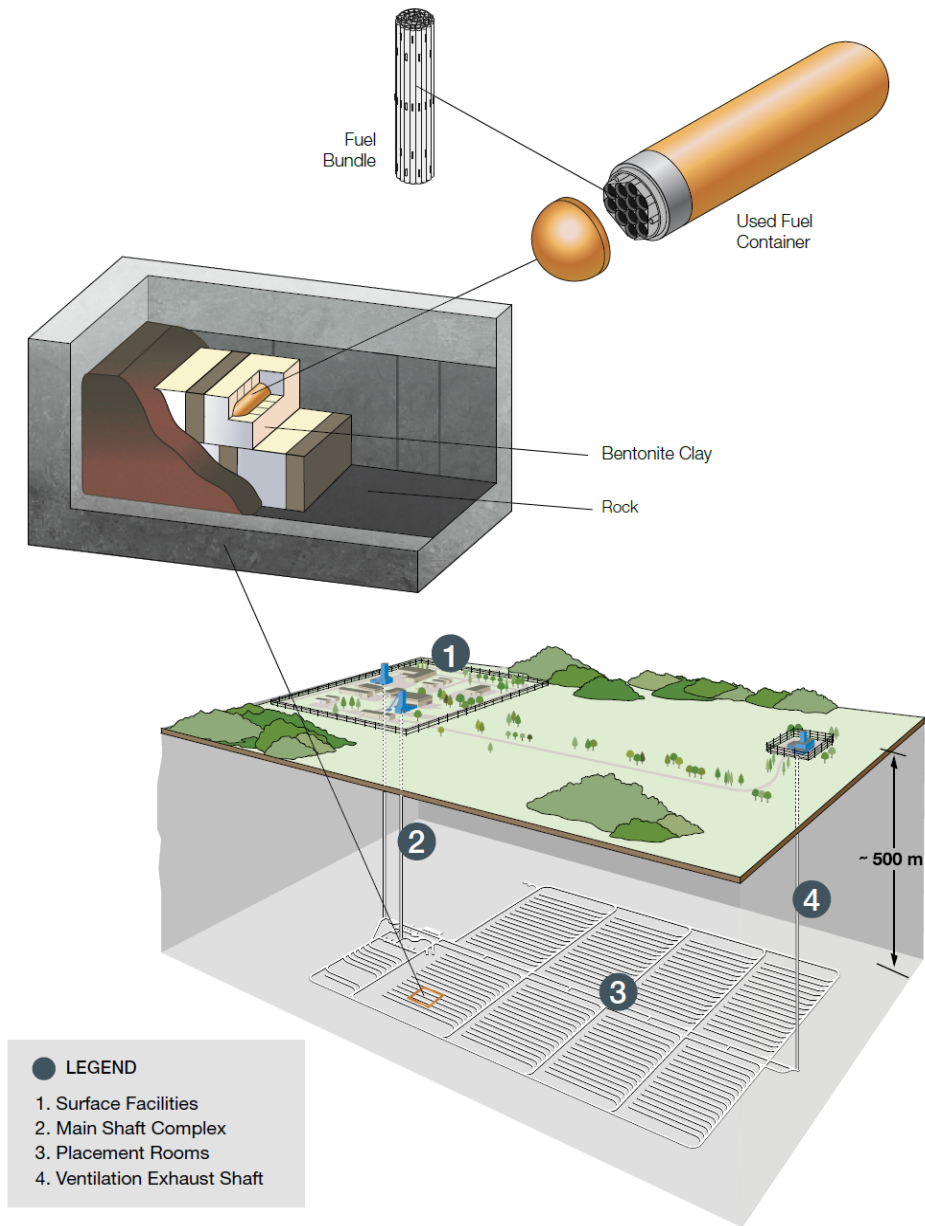


Figure 1.1: Illustration of the Multi-Barrier Deep Geological Repository Concept Considered in the Sixth Case Study

2. OVERVIEW

2.1 REPOSITORY CONCEPT

The main features of the conceptual repository are as follows (see also Figure 1.1):

- The repository is located at a depth of 500 m below the surface in granitic rock on the Canadian Shield.
- The repository is located in a region in which there are no known mineral deposits or other economically exploitable geological resources.
- The repository is constructed by the room-and-pillar method, with the repository excavated at a single level.
- The repository contains approximately 4.6 million bundles of used CANDU fuel.
- At the time of placement, the used-fuel bundles have been discharged from the reactor for a minimum of 30 years.
- Prior to placement, used-fuel bundles are sealed inside durable copper and steel containers.
- The used fuel containers are placed horizontally in an in-room configuration.
- The outer surface temperature of the container after placement is constrained (by design) to a maximum value of 100°C.
- Each container is surrounded by a 100% bentonite clay buffer material.
- As placement proceeds, the open space in each room is filled with compacted bentonite, and the filled rooms are closed off by composite seals made of clay-based and cement-based materials.
- At the end of a postclosure monitoring period, all tunnels, shafts, and exploration boreholes in the vicinity of the repository are sealed using backfill and a combination of clay-based and cement-based materials.

2.2 CONCEPTUAL MODELS

Five scenarios are considered in the Sixth Case Study:

1. The **Normal Evolution Scenario** is based on a reasonable extrapolation of present day site features and receptor lifestyles. It includes the expected evolution of the site and expected degradation of the disposal system. It illustrates the anticipated effects of the repository on people and on the environment.

The Normal Evolution Scenario is described in terms of a “Reference Case” and a series of associated sensitivity studies. The Reference Case represents the situation in which all repository components meet their design specification and function as anticipated. As such, the used fuel containers remain intact essentially indefinitely and no contaminant releases occur in the one million year time period of interest to the safety assessment.

The associated sensitivity studies illustrate repository performance for a range of reasonably foreseeable deviations from key Reference Case assumptions. These deviations arise as a result of components unknowingly placed in the repository that either (a) do not meet their design specification or (b) do not fully function as anticipated.

The most important sensitivity case is the **Base Case**. The “Base Case” sensitivity study assumes a small number of containers are fabricated with defects in their copper coating, and that a smaller number of these off-specification containers escape detection by the quality assurance program and are unknowingly placed in the repository.

2. An **Inadvertent Human Intrusion Scenario**, in which the engineered and natural repository barriers are bypassed by a borehole that is inadvertently drilled through a container, bringing used fuel material directly to the surface.
3. An **All Containers Fail Scenario**, in which all containers are assumed to fail at 60,000 years, the time of the first major ice-sheet advance over the repository site in the glacial cycle defined by NWMO (2017, Section 2).

A sensitivity case where all the containers are assumed to fail at 10,000 years is also assessed.

4. A **Repository Seals Failure Scenario**, in which there is rapid and extensive degradation of (1) the shaft seals and /or (2) the seals around the fracture passing through the repository footprint.

The conceptual models for analysing the Normal Evolution and Inadvertent Human Intrusion scenarios are described in more detail in NWMO (2017). However, in order to provide an outline of the code features and data required to support these analyses, a general conceptual model for these scenarios is provided in Figure 2.1 and Figure 2.2.

The conceptual models for the other three scenarios are identical to that for the Normal Evolution scenario since differences between the scenarios can be represented by modifying parameter values.

For quantitative analysis, these conceptual models are implemented as computer models or "codes". The main codes used are listed below, and described in Section 3:

Normal Evolution Scenario

- FRAC3DVS-OPG v1.3.0- Groundwater flow and transport in the repository and geosphere
- RSM v1.1 – Radionuclide screening model
- SYVAC3-CC4 Version SCC409.2 – Integrated system model

Inadvertent Human Intrusion Scenario

- HIMv2.1 – Inadvertent Human intrusion model

All Containers Fail Scenario

- FRAC3DVS-OPG v1.3.0- Groundwater flow and transport in the repository and geosphere
- SYVAC3-CC4 Version SCC409.2 – Integrated system model

Repository Seals Failure Scenario

- FRAC3DVS-OPG v1.3.0 - Groundwater flow and transport in the repository and geosphere

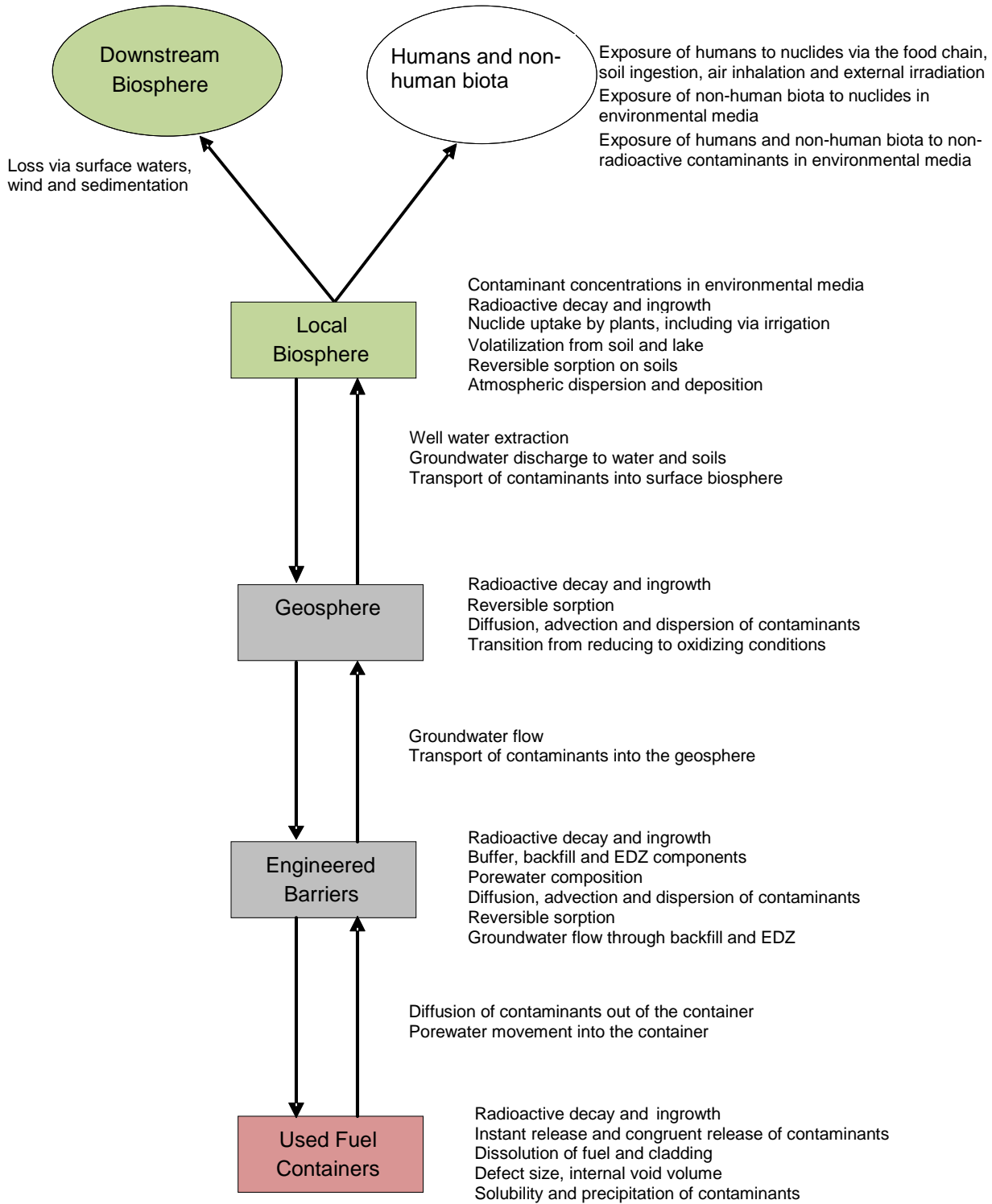


Figure 2.1: Base Case – General Conceptual Model Describing Releases from Defective Containers

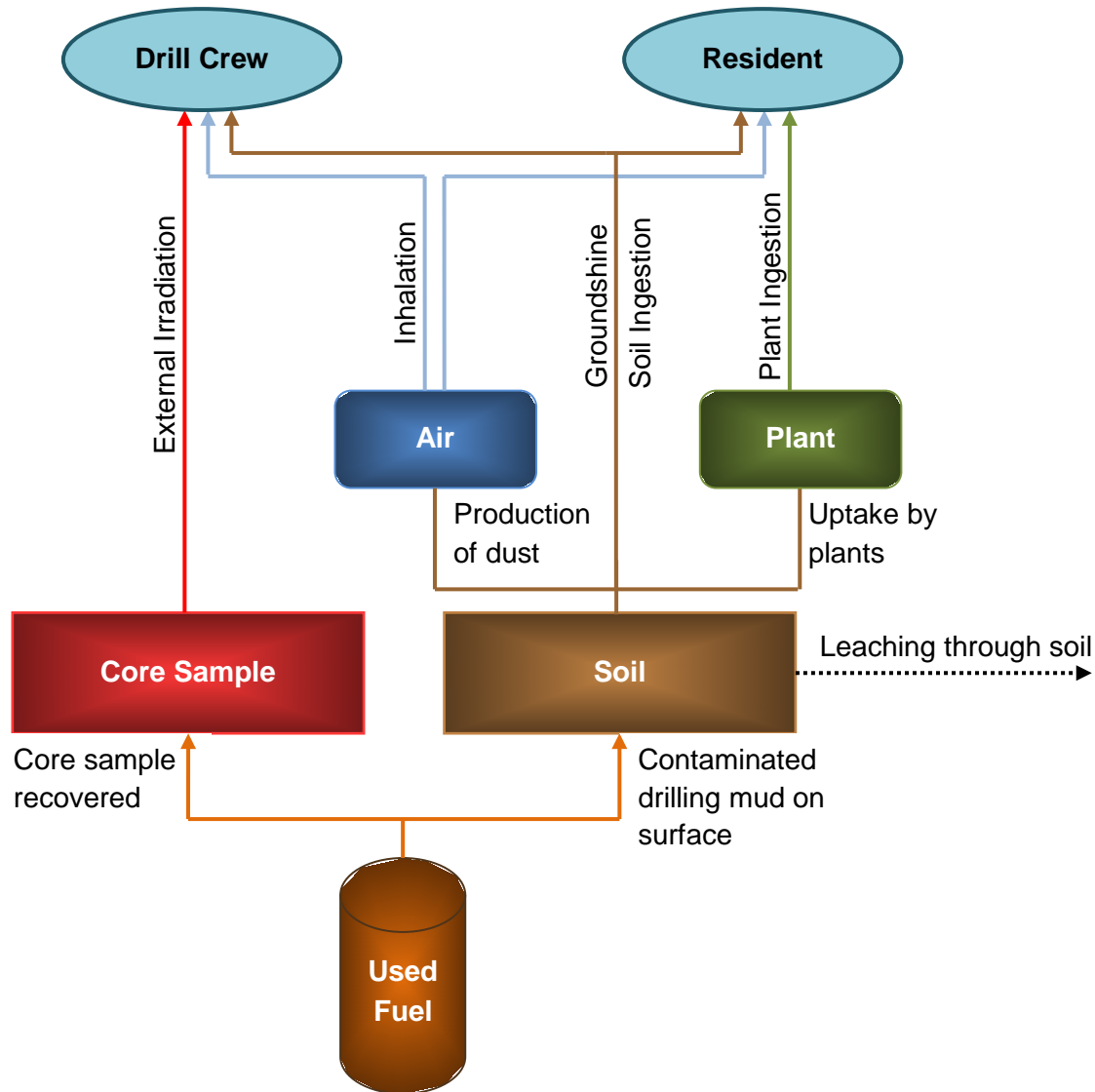


Figure 2.2: Inadvertent Human Intrusion – General Conceptual Model

2.3 DATA

2.3.1 Data Sources

For analyses of the Normal Evolution scenario, the starting point for the data used in the Sixth Case Study was that used in the Fourth Case Study (NWMO 2012a). The data needed for the Sixth Case Study were compared with those used in the Fourth Case Study (Garisto et al. 2012), and many of the latter values were judged to be reasonable and kept without change. Several parameters were revised, however, for the specific Sixth Case Study repository and geosphere setting (e.g., parameters describing the repository design).

Most parameter values used in the Sixth Case Study are defined in Sections 4 to 9 of this report. This includes all design, inventory, material, geosphere, biosphere, and dose conversion

data. Exposure-specific parameters for the Inadvertent Human Intrusion scenario are described in Medri (2015a).

2.3.2 Parameter Variability

For some model input parameters, there is a clearly appropriate value. However, for many parameters, a range of values may be possible because of natural variability or measurement uncertainties or uncertainties arising from the modelling basis. An example of natural variability is human diet - the amount that people eat is naturally variable from person to person, and from time to time. An example of model-based uncertainty is the sorption K_d parameter, since this is an effective parameter that represents the net effect of possibly several processes that may be occurring at the microscopic scale.

The format of the input data described here allows the specification of data using probability density functions to indicate both the likely values as well as their range. In particular, Table 2.1 lists the probability density function types supported within the Sixth Case Study data. Correlations between two parameters are supported if the two correlated parameters are described by either a normal distribution or a lognormal distribution. Presently, the SYVAC3-based computer models (RSM and CC4) can use this information directly; however other models (such as FRAC3DVS-OPG) must be supplied with specific input values.

Generally, even though a parameter may be described by a range, it is not so clear how to characterize that range in a probability density function. Mishra (2002) discusses general factors that can be considered in selecting a probability density function type, including the following suggestions in the absence of a mechanistic basis for selection:

- Uniform (log-uniform) - low state of knowledge (e.g., bounds only),
- Triangular (log-triangular) - low state of knowledge (e.g., bounds and best estimate),
- Normal - additive processes, and
- Lognormal - multiplicative processes.

Table 2.1: Parameter Probability Density Function Types and Attributes

Distribution Type	Attributes
Constant	Value
Uniform	Lower bound, upper bound
Loguniform	Lower bound, upper bound
Piecewise uniform	Lower and upper bound, probability for each piece
Triangular	Lower bound, peak value, upper bound
Normal	Mean, standard deviation, optional lower and upper bounds
Lognormal	Geometric mean, geometric standard deviation, optional lower and upper bounds

3. COMPUTER MODELS

The Sixth Case Study uses computer models (or "codes") to numerically represent the conceptual models considered. In this section, the computer models used are briefly described, as well as the general software quality assurance system supporting these codes.

3.1 MODELS, DATA AND TOOLS

3.1.1 Reference Models

There are two categories of computer models - detailed (or "process") models and integrated system models. In general, the detailed models address specific topics, usually with the inclusion of mechanistic effects or with greater resolution in space or time. These detailed models either provide supporting data or validation tests, or else identify the important parameters and processes for use in the integrated system models. The latter system models incorporate the most important features, events and processes describing the behaviour of the repository, from waste form to dose consequences.

Figure 3.1 identifies the codes used in the Sixth Case Study assessment, and their interrelationship. Initially, information from used fuel characteristics, engineering design, and site characterization are used in conjunction with specialized codes to develop a site-specific system description. For example, the initial inventory is determined using ORIGEN-S, while the site characterization information is collected into a detailed groundwater flow model under FRAC3DVS-OPG.

The results from the RSM model are used to screen the initial inventories of radionuclides in the fuel in order to identify a short list of most concern. Detailed transport calculations for scenarios involving groundwater transport of contaminants are then undertaken with the FRAC3DVS-OPG transport model and the SYVAC3-CC4 system model. FRAC3DVS-OPG calculates advective-dispersive transport through the repository and geosphere using a detailed 3-D model, and interfaces with SYVAC3-CC4 for source terms and biosphere consequence calculations. SYVAC3-CC4 contains a set of submodels that represent the whole repository, including the repository (used fuel, defective containers, etc.), the geosphere (advective and diffusive transport, well, etc.) and the biosphere (food chain model, surface waters, etc.). The FRAC3DVS-OPG and SYVAC3-CC4 models are complementary since they use very different numerical approaches and have different strengths.

The Inadvertent Human Intrusion scenario is separately analyzed using the Human Intrusion Model (Medri 2015a), which is built on the AMBER software platform (Quintessa 2016). AMBER is a graphical-user interface based software tool that allows users to build dynamic compartment models to represent, for example, the migration and fate of radioactive and non-radioactive contaminants in environmental systems.

In addition, the assessment is supported by detailed models, notably PHREEQC for solubilities.

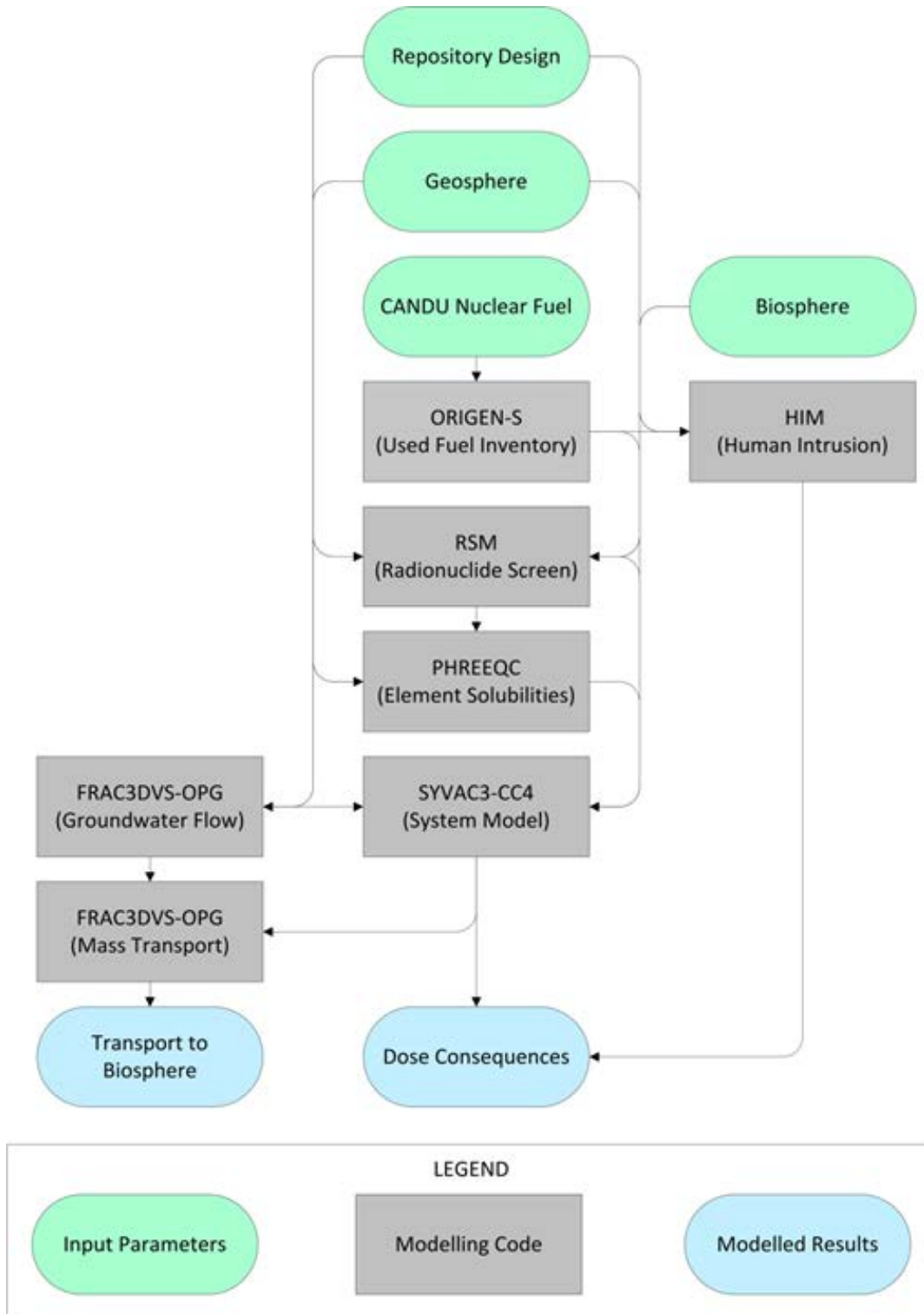


Figure 3.1: Illustration of Relationship between the Computer Models Used in the Sixth Case Study and Supporting Data

3.1.2 Reference Data

The main system model – SYVAC3-CC4 – has reference datasets associated with it. These are also maintained under a software configuration management system. Specific reference datasets are prepared as required; for example, for major safety assessments or major database updates. These reference datasets and their documentation are maintained under control of the NWMO.

All data are stored as text files, one for each parameter, in a XML format that is readable by the input file generation software. The data file format allows the description and storage of parameters as probability density functions and stores other information such as: parameter definition, data contributor, date data were entered, distribution bounds, any correlation, justification and references for the data, and information on when the data were checked and who checked it. This latter information is important for quality assurance.

The reference datasets are placed in controlled access directories. For example, the SYVAC3-CC4 dataset used in Sixth Case Study Base Case is “SCC4.09.2 XML Dataset (Base Case)”. The main purpose of this report is to describe the source of data in this SYVAC3-CC4 dataset.

The RSM dataset used in the Sixth Case Study is “6CS RSM Dataset”. The RSM dataset is described by Gobien and Garisto (2012). It contains data on many more radionuclides and chemical elements than does the SYVAC3-CC4 dataset.

Only part of the repository, geosphere and biosphere data required by the FRAC3DVS-OPG model are described in detail in this report. For example, the hydraulic conductivities of the buffer material and geosphere are described, but the detailed data describing the fracture locations and the surface topography are not provided here. These are however available in electronic format in the NWMO archives.

Finally, the data used by the Inadvertent Human Intrusion model HIMv2.1 is embedded directly within the AMBER code describing the model. These data are provided in Medri (2015a).

3.1.3 Software Tools

The safety assessment codes and system models are supported by software tools as listed in Table 3.1. They support the codes in various capacities such as post-processing the raw output, pre-processing input data, and improving software quality.

Continuing effort on improving coding, data and documentation of the safety assessment models has led to the development of several software quality assurance support tools. The coding tools, for example, ensure consistency between source code and coding standards, automate certain coding tasks, provide checking that units are balanced in coded equations, and help with the code documentation.

Table 3.1: Description of Software Tools

Output Analysis	
SyView, Version 1.3	A post-processor for SYVAC3-based codes, based on the mView graphical framework Geofirma Engineering Ltd.'s pre- and post-processor for FRAC3DVS-OPG
mView, Version 4.10	
Prepare Reference Datasets and Input Files for SYVAC3-based Codes	
SINGEN, Version 3.2	An application for generating input files for SYVAC3-based codes
Software Quality Assurance	
UNITCK, Version 9	Checks that units balance in Fortran source code

3.2 COMPUTER MODEL DESCRIPTIONS

The main documentation associated with each computer model is a theory manual, user manual and testing reports. Documentation for the individual codes is specified in Table 3.2 through Table 3.5.

3.2.1 SYVAC3-CC4

The system code for the Sixth Case Study is referred to as SYVAC3-CC4, Version SCC409.2 (NWMO 2012b, Table 3.2). It is a system model for assessment of groundwater transport of contaminants from the repository to the biosphere, as in the Normal Evolution scenario. It was designed for the postclosure safety assessment of a deep geological repository for used CANDU fuel placed in durable containers. It calculates the rate of contaminant releases from used fuel in contact with water, their transport out of defective containers, through the engineered barriers and host rock, and into the biosphere. Dose consequences are calculated for a critical group – a farming household, living in the vicinity of the repository and exposed to contaminants released from the repository.

3.2.2 FRAC3DVS-OPG

The reference groundwater flow and transport code used in the Sixth Case Study is FRAC3DVS-OPG, a 3-D finite-element/finite-difference code (Therrien et al. 2010, Table 3.3). FRAC3DVS-OPG is a version of a commercially available code. FRAC3DVS-OPG supports both equivalent-porous-medium and dual-porosity representations of the geologic media. The FRAC3DVS-OPG groundwater flow results are used to derive the parameters for the CC4 geosphere groundwater transport model (GEONET). Furthermore, the results of the FRAC3DVS-OPG radionuclide transport calculations can be compared to the corresponding CC4 calculations, allowing verification of the CC4 geosphere transport model.

3.2.3 RSM

One of the simpler models used in the Sixth Case Study analysis is called the Radionuclide Screening Model (Goodwin et al. 2001, Table 3.4) It models groundwater transport of radionuclides via a simple contaminant transport pathway from the defective containers to humans via a well. By conservative choice of input parameters, it can be used to screen radionuclides so as to objectively identify which are potentially important and should be included in more detailed models.

3.2.4 HIM

The Inadvertent Human Intrusion Model for the Sixth Case Study (HIMv2.1) assesses an inadvertent human intrusion scenario (Medri 2015a, Table 3.5). The model considers an exposure scenario where a nuclear waste container is unknowingly intersected by a drilled borehole, and used fuel is brought directly to surface, bypassing all the repository barriers. The dose consequences are estimated for the drill crew and a resident of a home built on the contaminated area.

3.2.5 Specialized Supporting Codes

Various specialized codes are used to address specific topics or processes.

ORIGEN-S is a CANDU-industry standard code that was used to calculate the radionuclide inventories in the used fuel and Zircaloy cladding at time of placement, based on a defined reactor exposure scenario (Tait et al. 2000, Tait and Hanna 2001). The ORIGEN-S code is not part of the Sixth Case Study safety assessment codes, but the results from ORIGEN-S were used to derive a reference used fuel inventory, as described in Section 4.

PHREEQC is a widely used computer code that performs aqueous geochemical calculations (Parkhurst and Appelo 1999). The program is based on equilibrium chemistry (i.e., chemical thermodynamics) of aqueous solutions interacting with minerals, gases, solid solutions and sorption surfaces. PHREEQC was used to calculate the solubilities of various elements within the defective containers (Duro et al. 2010).

Table 3.2: SYVAC3-CC4, Version SCC4.09.2

Parameter	Comments
Components:	
SYVAC3	Executive module, Version SV3.12.1
CC4	System model, Version CC4.09.1
ML3	SYVAC3 math library, Version ML3.03
SLATEC	SLATEC Common Mathematical Library, Version 4.1
Main	<i>SYVAC3-CC4 Theory Manual (NWMO 2012b)</i>
Documents	<i>SYVAC3-CC4 User Manual (Kitson et al. 2012)</i> <i>SYVAC3-CC4 Verification and Validation Summary (Garisto and Gobien 2013)</i>
Main Features	<ul style="list-style-type: none"> - Linear decay chains - Radionuclide release by instant release and by congruent dissolution - UO₂ dissolution rate calculated using radiation dose-rate based model - Precipitation in container when user-supplied solubility limits exceeded - Durable container, but some fail due to small defects - Cylindrical buffer and backfill layer that surrounds the container and inhibits groundwater flow and radionuclide transport - Multiple sector repository connected to the geosphere at sector-specific nodes chosen considering the local groundwater flow - Geosphere network of 1D transport segments that connect the repository to various surface discharge locations, including a well - Transport considers diffusion, advection / dispersion and sorption - Biosphere model that calculates field soil concentrations, well water concentrations, and uses a surface water body as a final collection point - Dose impacts to a self-sufficient human household that uses water body or well water, locally grown crops and food animals, local building materials and heating fuel - Flow-based models in repository and geosphere, concentration-based models in biosphere - Generally time-independent material properties and characteristics for the biosphere and geosphere model. Transitions from one geosphere (or biosphere) state to another at specific times can be accommodated - Ability to represent all input parameters with a probability density function and to run Monte-Carlo type simulations

Table 3.3: FRAC3DVS-OPG, Version 1.3

Parameter	Comments
Components:	
FRAC3DVS-OPG	Main code, Version 1.3
Main Documents	<p><i>A Three-dimensional Numerical Model Describing Subsurface Flow and Solute Transport</i> (Therrien et al. 2010)</p> <p><i>Verification and validation described in Therrien et al. (2010)</i></p>
Main Features	<ul style="list-style-type: none"> - Linear decay chains - 3 D groundwater flow and solute transport in saturated and unsaturated media - Variable density (salinity) fluid - 1D hydromechanical coupling - Equivalent porous medium or dual-continuum model; fractures may be represented as discrete 2D elements - Finite-element and finite-difference numerical solutions - Mixed element types suitable for simulating flow and transport in fractures (2D rectangular or triangular elements) and pumping / injection wells, streams or tile drains (1D line elements) - External flow boundary conditions can include specified rainfall, hydraulic head and flux, infiltration and evapotranspiration, drains, wells, streams and seepage faces - External transport boundary conditions can include specified concentration and mass flux and the dissolution of immiscible substances - Options for adaptive time-stepping and sub-gridding

Table 3.4: RSM, Version 1.1

Parameter	Comments
Components:	
SYVAC3	Executive module, Version SV3.10.1
RSM	System model, Version RSM 1.1
Main	<i>RSM Version 1.1 - Theory</i> (Goodwin et al. 2001)
Documents	<i>RSM Version 1.1 Verification and Validation</i> (Garisto 2001)
Main Features	<ul style="list-style-type: none"> - Linear decay chains - Radionuclide release by instant release and by congruent dissolution - UO₂ dissolution calculated from user-supplied time-dependent data - Precipitation in container when user-supplied solubility limits exceeded - Durable containers, some fail with small defects - 1D buffer and backfill layer that surrounds the container and inhibits groundwater flow and radionuclide transport - Repository model based on one room containing failed container(s) - Linear sequence of 1D transport segments that connect the repository to a well. Transport segments are user-supplied; transport is solved considering diffusion, advection/dispersion and sorption - Dose impacts to a self-sufficient human household that uses well water, based on conservative model for drinking, immersion, inhalation and ground exposure. Effect of other ingestion pathways is included through a user-input multiplier - Ability to represent all input parameters with a probability density function and to run Monte-Carlo type simulations - Time-independent material properties and biosphere characteristics - Database of all radionuclides with half-lives longer than 0.1 years as well as radionuclides with half-lives longer than one day if they have a parent with a half-life longer than 0.1 years

Table 3.5: HIM, Version 2.1

Parameter	Comments
Components:	
AMBER	Executive Code, Version 5.5
HIMv2.1	Main Model Version
Main Documents	<i>Human Intrusion Model for the Mark II Container in Crystalline and Sedimentary Rock Environments: HIMv2.1 (Medri 2015a)</i> <i>Verification and validation of HIMv2.1 are described in Medri (2015a)</i>
Main Features	- Linear decay chains - Dose consequences by external, inhalation and ingestion pathways to drill crew and site resident - Surface contamination decreases with time due to radioactive decay and soil leaching - Time-independent material properties and biosphere characteristics - Includes data for potentially relevant radionuclides

3.3 SOFTWARE QUALITY ASSURANCE

The Nuclear Waste Management Organization (NWMO) supports the management principles of CSA N286.7, and has defined a managed system that meets this commitment through a hierarchy of governing documents and procedures. These procedures include quality assurance requirements.

Software for use in postclosure safety assessments of a deep geological repository is being developed and maintained by the NWMO consistent with these governing documents and procedures, notably NWMO-PROC-EN-0002. For the main system codes and reference datasets used for the Sixth Case Study (SYVAC3-CC4, RSM, HIM, FRAC3DVS-OPG), this procedure identifies CSA N286.7-16 (CSA 2016) as the relevant software standard.

The CSA N286.7-16 software standard identifies requirements for:

- configuration management and change control;
- documentation; and
- verification.

The configuration management approach selected for the NWMO postclosure safety assessment software is based on controlled access, defined releases, and a formal change request system. Figure 3.2 summarizes the procedure followed for making changes to code and data for all codes and datasets developed by the NWMO.

The CSA N286.7-16 standard distinguishes between verification and validation testing. Verification is the process of ensuring that each phase of the software development is consistent with the previous phase. For example, it ensures that the source code is consistent with the code design, or that the installed version on a new system is consistent with the

archived version. Validation is the process of demonstrating that a model adequately represents the physical system that it is meant to describe. A model is validated when it provides a sufficiently good representation of the actual processes occurring in a real system, consistent with the intended use of the model.

The types of approaches and tests include:

- comparison with field or experimental data (e.g., short term or accelerated experiments or experiments involving specific processes);
- comparison with natural analogs;
- comparison with independently developed codes and models;
- peer review and acceptance; and
- use of conservative models and parameters.

Validation is best achieved by comparing model predictions with field or experimental observations. However, full validation of models for long-term assessment of nuclear fuel disposal is not possible for several reasons, notably the long time periods involved. Also, there is no firm criterion for determining what constitutes an acceptable level of validation or confidence in the results (CNSC 2006). Consequently, validation is approached through a range of tests that collectively provide confidence in the model results, and through an ongoing testing effort to continuously improve confidence in the long-term models.

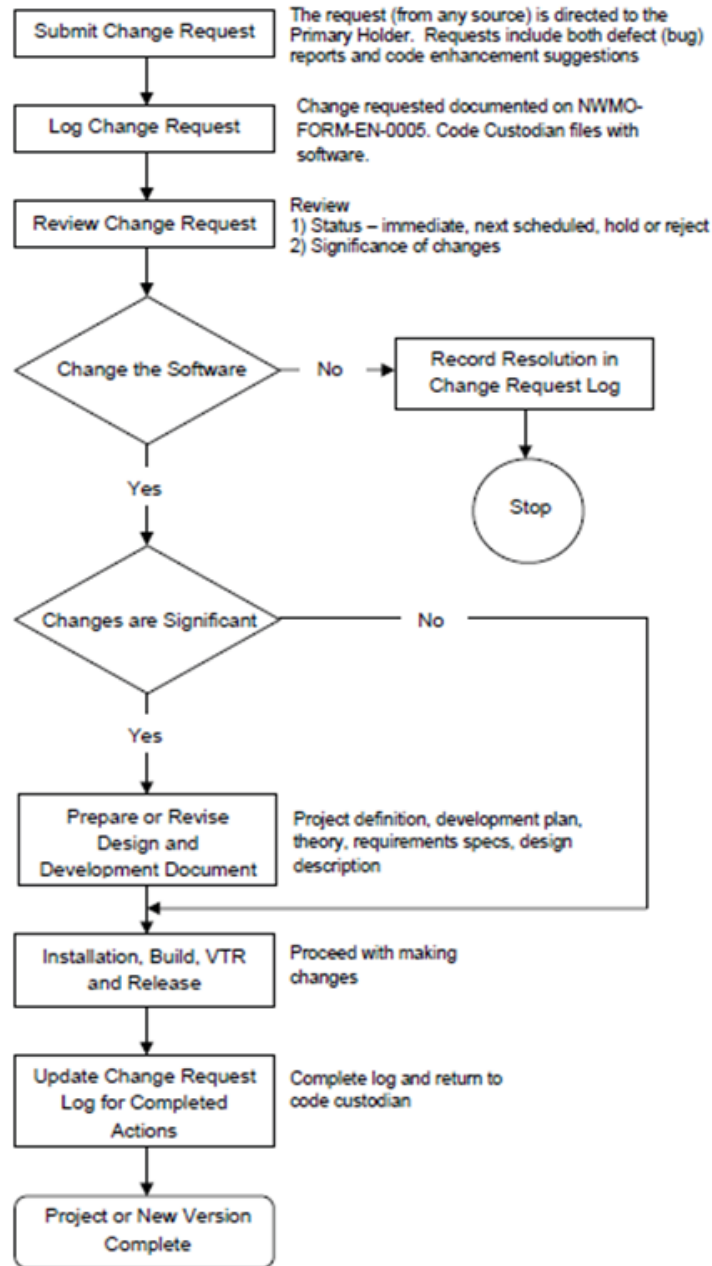


Figure 3.2: Software Change Control Process Followed for the NWMO Postclosure Safety Assessment Software and Data

4. USED FUEL DATA

This section describes the used fuel data for the Sixth Case Study. It provides a reference to the source(s) of the data, and a brief justification.

4.1 USED FUEL WASTEFORM

The inventory of used fuel in interim storage consists primarily of 28-element and 37-element natural uranium CANDU fuel bundles and their variants. Variants include the 37-element long length bundle and the 37m bundle¹, while additionally there are some older bundles that do not have the CANLUB coating (i.e., a thin graphite layer between the fuel pellet and the fuel sheath). Other fuel bundles in storage include small quantities of 18-element bundles², 19-element bundles³, and 43-element CANFLEX LVRF bundles⁴.

The storage inventory also includes very small quantities of more experimental fuel types (including some enriched in U-235) developed by AECL in prior decades. This fuel is currently the subject of ongoing characterization studies.

Given the overwhelming predominance of CANDU fuel in interim storage, the used fuel waste form adopted for this assessment is a post-discharge natural uranium UO₂ CANDU fuel bundle. The experimental fuel types mentioned above are not included due to the lack of data describing the fuel characteristics. This will be addressed in the future as the characterization studies come to fruition. Reprocessed wastes and other high-level waste forms are not considered.

The conceptual repository is assumed to contain 4.6×10^6 used bundles. This quantity is slightly greater (5 percent more) than the total used fuel inventory projected over the expected lifetime of the current fleet of Canadian CANDU power reactors (Garamszeghy 2015)⁵. Because the inventory projections indicate there will be 3.6×10^6 37-element bundles and only 8.1×10^5 28-element bundles, the standard 37-element (Bruce) fuel bundle is selected as the reference fuel bundle for this assessment. Sensitivity studies in Tait et al. (2000) show the differences in radionuclide inventories in the 28-element and 37-element designs are small enough (per kgU) to be ignored.

¹ A modified 37-element bundle (37m) will be entering service in some stations; however, the changes are minor and do not significantly affect inventory.

² A small quantity of 18-element fuel is currently in dry storage after use in the Gentilly 1 CANDU-BLW boiling water reactor prototype.

³ A small quantity of the 19-element fuel is currently in dry storage after use in the Douglas Point CANDU PHWR reactor prototype.

⁴ A 43-element bundle with a central element composed of Dysprosium was used in a limited fashion in Bruce B reactors and is an option for use in Enhanced CANDU 6 reactors.

⁵ The 4.6×10^6 value assumes refurbishment of Bruce A, Darlington, Point Lepreau and Gentilly-2, no further refurbishment of Pickering or Bruce B, and no new build. Because Gentilly-2 has decided to not proceed with refurbishment, the current projected used fuel inventory is slightly reduced about 4.4×10^6 bundles.

Specifically:

- For most fission products, inventories for the 37-element bundles are greater than those for the 28-element bundles.
- For most actinides, inventories for the 37-element bundles are generally less than those for the 28-element bundles.

Note that the age of the fuel when placed in the repository will vary. Because the earliest bundles date back to 1970 and because the repository is unlikely to open before 2035, some fuel will be over 60 years old at the time of placement. For this assessment, all fuel bundles are assumed to have an out-of-reactor decay time of 30 years.

The used fuel irradiation history can be characterized by its power rating and burnup. These are discussed in more detail in Sections 4.2 and 4.3.

The characteristics of the reference used fuel are summarized in Table 4.1.

Table 4.1: Used Fuel Parameters

Parameter	Value	Comment
Waste Form	37-element UO ₂ fuel bundle	Standard fuel bundle from Bruce and Darlington stations
Mass U/bundle	19.25 kg	Initial mass (before irradiation); 37r bundle
Mass Zircaloy/ bundle	2.2 kg	Includes cladding, spacers, end plates
Initial U-235	0.72 wt%	Natural uranium is used in all CANDU fuel, except a small number of research or test bundles
Burnup	220 MWh/kgU	For events affecting a large number of containers (such as the All Containers Fail Disruptive Event Scenario)
	280 MWh/kgU	For events affecting a small number of containers (such as the Normal Evolution Scenario)
Power Rating	455 kW/bundle	Nominal mid-range value
Fuel Age (when placed in repository)	30 years	e.g., 10 years in pools, 20 years in dry storage
Fuel Pellet Geometric Surface Area	8.47 cm ²	Surface area of undamaged pellet (37 element design)

4.2 USED FUEL COMPOSITION

Freshly discharged used fuel could contain a few hundred different radionuclides, as well as over 80 stable elements. However, most of these will be present in negligible amounts or will rapidly decay, so they are not a concern for postclosure safety assessment.

The reference dataset used for the Sixth Case Study contains inventory, half-lives, dose coefficients and related data for over 300 radionuclides. All radionuclides with half-lives greater

than 0.1 years are included in the dataset. A radionuclide with a half-life longer than 1 day is also included in the dataset, if any parent has a half-life longer than 0.1 years. The dose impacts of radionuclides with half-lives shorter than 1 day are incorporated through the dose coefficients of the parents (Gobien and Garisto 2012).

The analyses for the scenarios discussed in Section 2 start with this full list of radionuclides and chemical elements. However, screening studies are used to reduce the number of nuclides and chemical elements examined in more detail.

For clarity, data are not listed in this report for all the nuclides and chemical elements in the full dataset. Instead, data are presented for only the radionuclides and chemical elements that have been identified as of potential interest for the Normal Evolution Scenario (and its variants) and the All Containers Fail Scenario, based on the screening results for the Sixth Case Study (NWMO 2017).

The screening analysis identified 26 radionuclides from the UO₂ fuel and 2 radionuclides from the Zircaloy sheath as potentially important. Eleven additional radionuclides are included to ensure ingrowth is properly accounted for so that a total of 39 radionuclides are represented in the detailed assessment.

Table 4.2 shows the included radionuclides and their associated decay chains.

Table 4.2: Potentially Significant Radionuclides Included in the Assessment

Radionuclides	
Fuel	
Single Nuclides	Cl-36, I-129, C-14, Cs-135, Ca-41, Se-79, Sr-90
Chain Nuclides	Pu-239 → U-235 = Th-231 → Pa-231 = Ac-227 = Th-227 = Ra-223
	Pu-240 → U-236 → Th-232 = Ra-228
	Pu-242 → U-238 = Th-234 → U-234 → Th-230 → Ra-226 = Rn-222 = Pb-210 = Bi-210 = Po-210
	Am-241 → Np-237 = Pa-233 → U-233 → Th-229 = Ra-225 = Ac-225
	Sn-126 → Sb-126
Zircaloy	
Single Nuclides	C-14, Cl-36

Note: Red shows the screened-in radionuclides. The → indicates decay is modelled while the = indicates the species will be modelled in secular equilibrium with the parent. Radionuclides in black are added to account for ingrowth.

At the time of discharge the used fuel also contains essentially the entire periodic table of elements ranging from hydrogen to californium; however, only a small fraction of these could potentially pose a non-radiological hazard to humans or to the environment. As is the case for radionuclides, the subset of chemical elements of potential concern is identified via a screening analysis.

This screening analysis identified 21 elements of potential concern arising from the fuel and Zircaloy, where multiple isotopes of an element (i.e., U, Pb, and Ba) are considered as one element. To ensure that ingrowth is properly accounted for (leading to formation of these

elements), 30 radionuclides are also included in the chemical hazard analysis. Table 4.3 shows the included chemical elements and their associated decay chains.

Table 4.3: Potentially Hazardous Elements Included in the Assessment

Chemically Hazardous Elements	
Fuel	
Elements	Cd, Hg, I, Mo, Sb, Se, Tc, W
Chains	Pu-239 → U-235
	Pu-240 → U-236
	Pu-242 → U-238 = Th-234 → U-234 → Th-230 → Ra-226 = Rn-222 = Pb-210 = Bi-210
	Am-241 → Np-237 = Pa-233 → U-233 → Th-229 = Ra-225 = Ac-225 → Bi
Misc	Pd-107 → Ag
	Se-79 → Br
	Sn-126 → Sb-126 → Te
Zircaloy	
Elements	Te

Note: Red shows the screened-in isotopes. The → indicates decay is modelled while the = indicates the species is modelled in secular equilibrium with the parent. Radionuclides in black are added to account for ingrowth.

The data used in the postclosure safety assessment for the radionuclides and chemical elements in Table 4.2 and Table 4.3 are presented in this report.

4.3 NUCLIDE AND ELEMENT INVENTORIES OF UO₂ FUEL AND ZIRCALOY

The radionuclide and chemical element inventories in the fuel, at time of placement, will depend on how long it has been since the fuel was discharged from the reactor. In particular, there is significant decay of short-lived radionuclides during this initial period after discharge. Based on system schedule considerations (notably the projected start-up of the repository) as well as engineering design considerations (older fuel produces less thermal power), a minimum fuel age of 30 years has been selected as a design basis. Since the fuel age distribution is unknown at present, for safety assessment purposes it is conservatively assumed that all fuel is 30-years old at the time of placement.

The used fuel radionuclide and chemical element inventories for CANDU fuel of various burnups were calculated by Tait et al. (2000, 2001) using ORIGEN-S. The data of Tait et al. are used to calculate the average radionuclide and chemical element inventories in a container with 48 fuel bundles.

The uncertainties in these inventories are discussed below. It should be noted that what is important is the uncertainties in the average inventories in a container. These uncertainties are much smaller than the uncertainties in the inventories of a single fuel bundle, based on the central limit theorem and the number of fuel bundles in a container.

The total uncertainty in the average inventories in a container is the sum of

- 1) σ_{OR} , the uncertainties/errors in the inventories calculated by ORIGEN-S for a fuel bundle with a specified burnup and power history, which arise due ORIGEN-S model and input data uncertainties, and
- 2) σ_{PR} , the uncertainties in the inventories arising from the uncertainty in average fuel burnup and fuel power rating of the bundles in container (see below).

The validation of the ORIGEN-S code for predicting radionuclide inventories in CANDU fuel is discussed in Appendix A. Generally, the ORIGEN-S calculated inventories agree well with the measured values, with differences generally well within the measurement uncertainties. Consequently, the uncertainties/errors in the inventories calculated by ORIGEN-S, σ_{OR} , for a fuel bundle with a specified burnup and power history, are set equal to the measurement uncertainties, as discussed in Appendix A.

Nuclide inventories generally increase with fuel burnup (Tait et al. 2000). The distribution of fuel burnups for existing fuel bundles (up to 2012) from all Canadian CANDU reactors is shown in Figure 4.1. This distribution was obtained using data from Wilk (2013). Table 4.4 shows the corresponding discharge burnup percentiles on a per station basis for burnup values of 220 MWh/kgU and 280 MWh/kgU, where detailed radionuclide inventories are available (Tait et al. 2000).

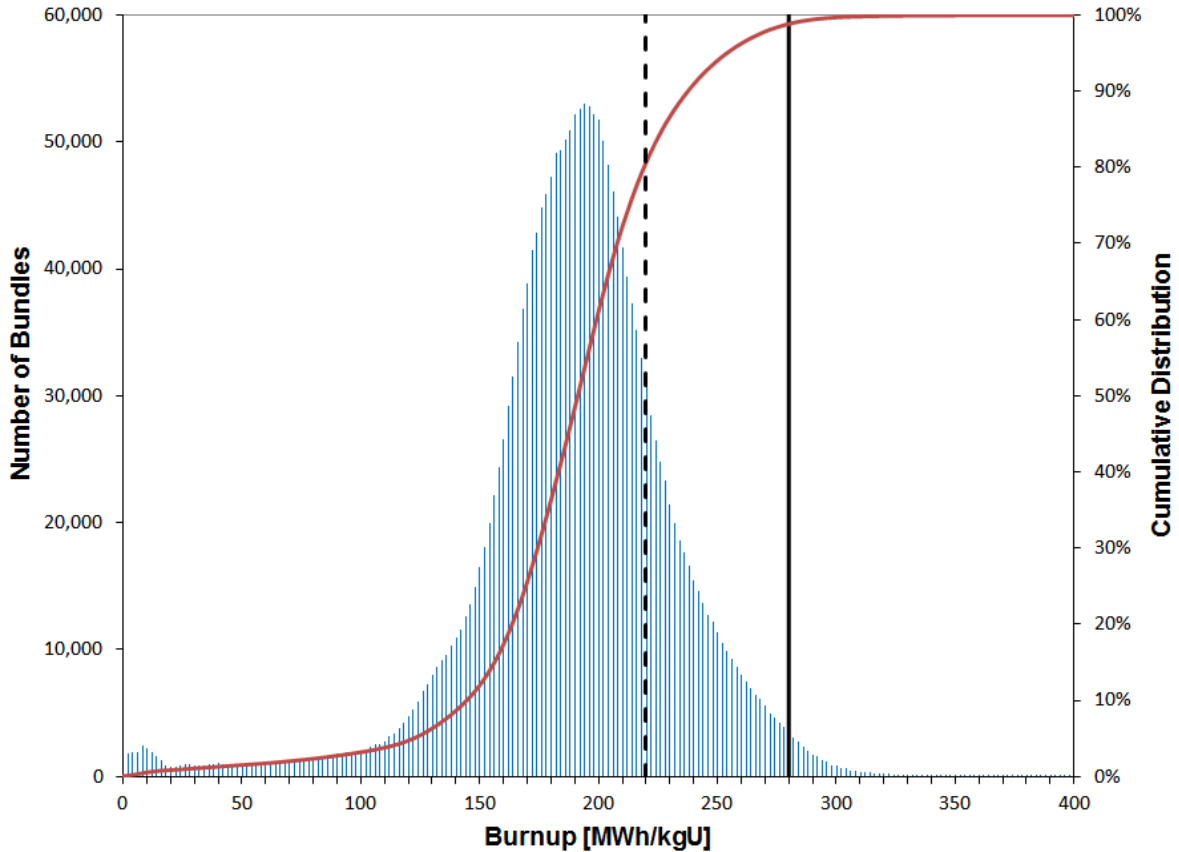
Table 4.4: Discharge Burnup Percentiles on a Per Station Basis

Reactor	Median Burnup [MWh/kgU]	Burnup Percentile for 220 MWh/kgU	Burnup Percentile for 280 MWh/kgU
Bruce A	195	62.9	96.7
Bruce B	188	92.3	99.7
Darlington A	201	75.3	99.7
Gentilly-2	174	93.3	99.9
Point Lepreau	170	93.0	99.9
Pickering A	202	71.5	95.0
Pickering B	191	87.3	99.8
Aggregate	192	80.7	98.8

Note: Based on Data from Wilk (2013)

The used fuel disposal container in the Sixth Case Study holds 48 fuel bundles. Each bundle inventory depends on its burnup. The total nuclide inventory in a container can be calculated from the average burnup of the bundles inside it. On average, across the entire repository, the average "container burnup" is the same as the average fuel bundle burnup, or 190 MWh/kgU, and the standard deviation in the average container burnup is about $42/(48)^{1/2}$ or 6.1 MWh/kgU, where 42 MWh/kgU is the standard deviation of the burnup distribution in Figure 4.1. The aggregate 95th percentile value is 254 MWh/kgU, with some exceptional fuel elements experiencing burnups as high as 706 MWh/kgU. On a per station per decade basis, the 95th percentile values vary between 224 MWh/kgU and 286 MWh/kgU. At these burnups, about 2% of the initial uranium is converted into other elements.

For the Sixth Case Study, the reference container inventories are conservatively calculated for a fuel burnup of 220 MWh/kgU and 280 MWh/kgU (Tait et al. 2000). When only a few containers fail in a scenario the fuel inventories are calculated assuming a burnup of 280 MWh/kgU; whereas when most containers in the repository fail the fuel inventories are calculated assuming a burnup of 220 MWh/kgU. Because these burnups are significantly larger than the median burnup (see Figure 4.1), there is no need to account for the uncertainty in the total inventories in a container due to the small uncertainty in the average container burnup.



Note: The vertical dashed and solid black lines correspond to burnups of 220 MWh/kgU and 280 MWh/kgU, while the red line represents the cumulative distribution. The figure is based on data in Wilk (2013) and includes data on bundles discharged up to 2012.

Figure 4.1: Distribution of Burnups and Cumulative Distribution for all Fuel Bundles

Although the calculated inventories are for a fuel power rating of 455 kW/bundle, Tait et al. (2000) show that the inventories of important radionuclides (i.e., the most significant contributors to radiological dose, decay heat or gamma radiation) are not sensitive to this value. In general, the differences in the concentrations of the important radionuclides at the minimum (200 kW/bundle), average (455 kW/bundle) and maximum (900 kW/bundle) powers were less than $\approx 2\%$. Thus, based on the central limit theorem, the uncertainty in the total inventory in a container due to the uncertainty in the average fuel power rating (of all bundles in a container), σ_{PR} , would be much smaller.

The radionuclide Cs-135, however, exhibited a substantial inverse dependence on concentration with power. The concentration of Cs-135 at the average power is about 2-fold lower than at the minimum power and about 1.8 times greater than at the maximum power. Since the distribution of bundle power ratings has a standard deviation of approximately 140 kW/bundle (see Figure 4.3), the uncertainty (σ_{PR} in %) in the total inventory of Cs-135 in a container due to the uncertainty in the average power rating of the fuel bundles in the container is conservatively estimated to be $140/(48)^{1/2} 100\%/(455-200) = 7.9\%$ (see Appendix A). This uncertainty is included in the calculation of the total uncertainty in the Cs-135 inventory in a container, as indicated in Table 4.5.

Finally, Tait et al. (2000) calculated inventories using an average bundle burnup calculation. However, elements in each ring of the fuel bundle will see a different neutron flux due to shielding of the surrounding elements, the burnup for each ring will be different. Hence, Tait et al. (2000) examined the differences between the fuel inventories calculated assuming an average fuel bundle burnup and those calculated by summing inventories produced in the individual rings of the fuel bundle. The latter are referred to as the “ring sum” inventories. The analysis indicated that most actinide inventories were under-predicted by the bundle average calculation (Tait et al. 2000, Appendix A). For the actinide radionuclides of most interest (i.e., the most significant contributors to radiological dose, decay heat or gamma radiation), the differences were: Cm-244 ($\approx 10\%$), Am-243 ($\approx 5\%$), Np-239 ($\approx 5\%$), Pu-242 ($\approx 2\%$) and less than 1% higher for the remaining actinides of interest.

The analysis also indicated that for the majority of fission products there was no consistent trend to either under- or over-prediction, and absolute differences between the bundle average and the “ring sum” inventories were $< 1\%$.

For the Sixth Case Study, corrections to the inventories calculated by Tait et al. (2000) were made to account for the difference in the bundle average and “ring sum” inventories only if differences exceeded $+1\%$. That is, corrections were not made if the bundle average calculation over-predicted the inventory. Corrections were required for the radionuclides Ac-227 (1%), Pa-231 (1.2%), Pu-242 (1.9%) and U-235 (1.7%). A correction was also required for the element Cd (1%).

Table 4.5 and Table 4.6 list the radionuclides of interest, their half-lives and their inventories in the fuel and Zircaloy respectively. Table 4.7 and Table 4.8 list the chemical elements of interest and their inventories in the fuel and Zircaloy respectively.

Table 4.5 through Table 4.8 also show the estimated uncertainties in the average inventories in a container arising from the potential differences between ORIGEN-S and measured concentrations, σ_{OR} , which are dominated by the measurement uncertainty, as well as uncertainties arising from the assumptions made by Tait et al. (2000), i.e., σ_{PR} . Thus, for most nuclides, the overall inventory is modelled as a normal probability density function with standard deviation σ_{Total} , and upper and lower bounds set to 5 standard deviations higher and lower than the mean (see Appendix A).

The concentrations of some radionuclides and chemical elements in fuel are affected by the decay of short-lived precursors with relatively large inventories (e.g., Pu-241 \rightarrow Am-241 and Pu-238 \rightarrow U-234). Since these precursors are not modelled directly in the simulations carried out for the Sixth Case Study, their influence is accounted for by adding the inventory of the precursor to that of the progeny. This affects the inventory of the radionuclides Am-241 and U-

234. Short-lived precursors such as Cm-245 and Am-243 with relatively small inventories are neglected in the simulations.

The inventories of C-14 and Cl-36 in Table 4.5 are not directly from Tait et al. (2000).

The inventory of the activation product C-14 in used fuel was calculated using an N impurity level of 15 $\mu\text{g/g}$ (Tait et al. 2000). Based on data in Stroes-Gascoyne et al. (1994), the range of measured C-14 concentrations in seven fuels is about 0.43 to 1.21 times the ORIGEN-S predicted values, with most values less than 55% of the ORIGEN-S values. Therefore, the C-14 inventory in fuel is described using a uniform distribution with lower and upper bounds equal to 0.45 times and 1.25 times the predicted inventory, respectively. The median value is 0.85 times the ORIGEN-S value, or 5.21×10^{-6} mol/kgU for a fuel burnup of 220 MWh/kgU and 6.73×10^{-6} mol/kgU for a fuel burnup of 280 MWh/kgU.

The inventory of the activation product Cl-36 was calculated using a conservative Cl impurity level of 5 $\mu\text{g/g}$ in used fuel (Tait et al. 2000). This leads to an overestimate of the Cl-36 inventory in fuel given that measured Cl impurity levels in fuel range from 1.6 to 3.0 $\mu\text{g/g}$ (Tait et al. 1997). Thus, the Cl-36 inventory is described as a uniform distribution with an upper bound equal to the ORIGEN-S prediction and a lower bound 10 times smaller. The median value is 0.55 times the ORIGEN-S values, or 5.42×10^{-6} mol/kgU for a fuel burnup of 220 MWh/kgU and 6.89×10^{-6} mol/kgU for a fuel burnup of 280 MWh/kgU.

Two radionuclides from the Zircaloy cladding (C-14 and Cl-36) were identified as significant in the screening analysis. The inventory for these species (Table 4.6) are assumed to be constant and are based on conservatively high impurity levels from Tait et al. 2000.

Table 4.5: Inventories of Potentially Hazardous Radionuclides in UO₂ Fuel

Nuclide	Half-life* [a]	280 MWh/kgU Inventory [moles/kgU initial]	220 MWh/kgU Inventory [moles/kgU initial]	σ_{OR} [%]	σ_{PR} [%]	σ_{Total} [%]
Ac-225	2.7380E-02	1.856E-14	1.662E-14	-	-	NA1
Ac-227	2.1770E+01	1.872E-11 [#]	1.573E-11 [#]	3	-	3
Am-241	4.3260E+02	1.544E-03 ^{&}	1.155E-03 ^{&}	15	-	15
Bi-210	1.3720E-02	5.225E-18	5.296E-18	-	-	NA1
¹ C-14	5.7000E+03	6.725E-06	5.207E-06	-	-	NA2
Ca-41	1.0200E+05	3.041E-06	2.354E-06	7	-	7
¹ Cl-36	3.0100E+05	6.886E-06	5.422E-06	-	-	NA3
Cs-135	2.3000E+06	3.455E-04	2.675E-04	7	7.9	10.6
I-129	1.5700E+07	5.486E-04	4.228E-04	7	-	7
Np-237	2.1440E+06	2.218E-04	1.708E-04	20	-	20
Pa-231	3.2760E+04	4.527E-08 [#]	3.820E-08 [#]	3	-	3
Pa-233	7.3850E-02	7.662E-12	5.901E-12	-	-	NA1
Pb-210	2.2200E+01	8.488E-15	8.604E-15	55	-	55
Pd-107	6.5000E+06	9.866E-04	6.901E-04	7	-	7
Po-210	3.7890E-01	1.443E-16	1.463E-16	-	-	NA1
Pu-239	2.4110E+04	1.152E-02	1.123E-02	3	-	3
Pu-240	6.5610E+03	6.788E-03	5.339E-03	4	-	4
Pu-242	3.7350E+05	7.773E-04 [#]	4.257E-04 [#]	7	-	7
Ra-223	3.1290E-02	2.669E-14	2.243E-14	-	-	NA1
Ra-225	4.0790E-02	2.747E-14	2.460E-14	-	-	NA1
Ra-226	1.6000E+03	2.282E-12	2.354E-12	55	-	55
Ra-228	5.7500E+00	8.309E-13	8.370E-13	-	-	NA1
Rn-222	1.0470E-02	1.493E-17	1.541E-17	-	-	NA1
Sb-126	3.3810E-02	3.356E-12	2.462E-12	-	-	NA1
Se-79	2.9500E+05	2.216E-05	1.762E-05	7	-	7
Sn-126	2.3000E+05	7.063E-05	5.182E-05	7	-	7
Sr-90	2.8790E+01	8.966E-04	7.561E-04	4	-	4
Tc-99	2.1110E+05	3.021E-03	2.409E-03	10	-	10
Th-227	5.1140E-02	4.308E-14	3.620E-14	-	-	NA1
Th-229	7.3400E+03	5.341E-09	4.783E-09	20	-	20
Th-230	7.5380E+04	1.571E-08	1.636E-08	55	-	55
Th-231	2.9110E-03	1.932E-14	2.944E-14	-	-	NA1
Th-232	1.4050E+10	2.078E-03	2.095E-03	4	-	4
Th-234	6.5980E-02	6.074E-11	6.091E-11	-	-	NA1
U-233	1.5920E+05	4.004E-05	3.608E-05	20	-	20
U-234 ^{&}	2.4550E+05	2.166E-04 ^{&}	2.089E-04 ^{&}	50	-	50
U-235	7.0380E+08	4.748E-03 [#]	7.238E-03 [#]	3	-	3
U-236	2.3420E+07	3.845E-03	3.501E-03	4	-	4
U-238	4.4680E+09	4.114E+00	4.125E+00	0	-	0

Notes:

NA1 = Nuclide assigned a constant inventory because it has a short half-life.

NA2 = Nuclide inventory calculated by ORIGEN-S is based on a N impurity level of 15 µg/gU. Inventory is assigned a uniform distribution with maximum value 1.25x the ORIGEN-S predicted inventory and minimum value equal to 0.45x the ORIGEN-S predicted inventory. Limits are based on measured C-14 values from Stroes-Gascoyne et al. 1994.

NA3 = Nuclide inventory is assigned a uniform distribution with maximum value equal to ORIGEN-S predicted value based on the Cl impurity level of 5µg/gU from Tait et al. (2000). The minimum value is set equal to maximum/10. Table shows the median value.

*Half-life from ENDF/B VII.1 (Chadwick et al. 2011) and converted as required using 365.25 days = 1 year.

#Median value from Tait et al. (2000) increased to account for “ring sum” correction: Ac-227 (1%), Pa-231 (1.2%), Pu-242 (1.9%) and U-235 (1.7%) (Appendix A, Tait et al. 2000)

&Includes inventory of short-lived precursor: Am-241 (Pu-241, 2.737E-4 mol/kgU) and U-234 (Pu-238, 2.259E-5 mol/kgU).

Table 4.6: Inventories of Potentially Hazardous Radionuclides of Interest in Zircaloy for 30 Years Decay Time

Nuclide	Half-life* [a]	280 MWh/kgZr Inventory [moles/kgZr initial]	220 MWh/kgZr Inventory [moles/kgZr initial]	σ _{OR} [%]	σ _{PR} [%]	σ _{Total} [%]
C-14	5.7000E+03	2.457E-05	2.180E-06	-	-	NA1
Cl-36	3.0100E+05	1.489E-05	9.860E-06	-	-	NA1

Notes:

NA1 = Nuclide assigned a constant inventory because it is formed by activation of impurity in the fuel, and impurity levels were assigned high values in Tait et al. (2000).

*Half-life from ENDF/B VII.1 (Chadwick et al. 2011) and converted as required using 365.25 days = 1 year.

Table 4.7: Inventories of Potentially Hazardous Elements for 30 Year Decay Time

Nuclide	Main Source ¹	280 MWh/kgU Inventory* [moles/kgU initial]	220 MWh/kgU Inventory* [moles/kgU initial]	σ_{OR} [%]	σ_{PR} [%]	σ_{Total} [%]
Ag	FP	4.628E-04	3.348E-04	7	-	7
Bi	IMP	9.603E-05	9.595E-05	-	-	NA1
Br	FP	1.475E-04	1.309E-04	7	-	7
Cd	FP	2.869E-04	1.908E-04	7	-	7
Hg	IMP	7.105E-06	6.719E-06	-	-	NA1
I	FP	7.023E-04	5.372E-04	7	-	7
Mo	FP	1.194E-02	9.488E-03	7	-	7
Sb	FP	3.687E-05	2.977E-05	7	-	7
Se	IMP	4.794E-04	4.361E-04	-	-	NA1
Te	FP	1.351E-03	1.048E-03	7	-	7
W	IMP	6.093E-05	5.956E-05	-	-	NA1

Notes:

*The inventories shown here exclude the concentrations of all short-lived isotopes of the element.

¹ Source of chemical element in fuel is either fission product (FP) or impurity in fuel (IMP).

NA1 = Nuclide assigned a constant inventory because it is formed by activation of impurity in the fuel, and impurity levels were assigned high values in Tait et al. (2000).

Table 4.8: Inventories of Potentially Hazardous Elements in Zircaloy for 30 Year Decay Time

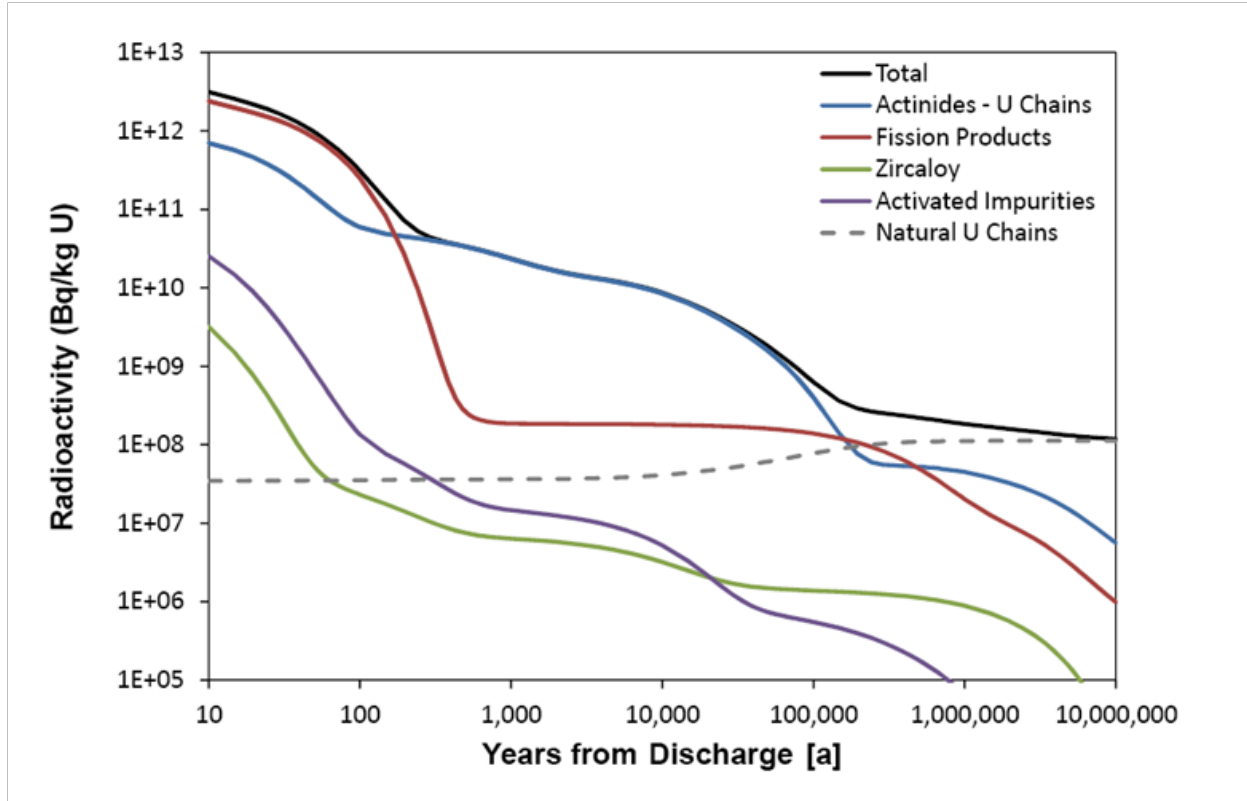
Nuclide	Main Source ¹	280 MWh/kgZr Inventory [moles/kgZr initial]	220 MWh/kgZr Inventory [moles/kgZr initial]	σ_{OR} [%]	σ_{PR} [%]	σ_{Total} [%]
Te	IMP	2.569E-05	2.157E-05	-	-	NA1

Notes:

¹ Source of chemical element in Zircaloy is an impurity in Zircaloy (IMP).

NA1 = Nuclide assigned a constant inventory because it is formed by activation of impurity in the fuel, and impurity levels were assigned high values in Tait et al. (2000).

Figure 4.2 shows the total radioactivity of the reference fuel and how it decreases with time. The radioactivity from light element activation and from the Zircaloy cladding is only a small contributor. After a few hundred years, the radioactivity is dominated by the actinides. The radioactivity levels out after about 1 million years. This residual activity is caused by the natural uranium chains remaining in the used fuel. Radioactivity of fuels with a burnup of 280 MWh/kgU are initially slightly higher but follows a similar trend overall.



Note: The blue line (Actinides – U Chains) shows the radioactivity of all actinides, except the U-238, U-235 and U-234 actinides and their progeny

Figure 4.2: Radioactivity of Used Fuel (220 MWh/kgU burnup) as a Function of Time after Discharge from the Reactor

4.4 CONTAMINATION ON EXTERNAL BUNDLE SURFACES

Corrosion products formed within the primary coolant circuit of a reactor can deposit on the surfaces of fuel bundles in the reactor core. Neutron activation of some of these corrosion products can generate radioactive isotopes. In addition, fission products and UO₂ fuel particulates released from defective fuel bundles can also deposit on the surfaces of fuel bundles. In the context of a geological repository for used fuel, these surface deposits provide a small additional source of radionuclides and potentially chemically toxic elements.

Fission product and uranium inventories in surface deposits are very low compared to the corresponding inventories within the fuel bundle itself (i.e., < 0.001%) (Chen et al. 1986) and, therefore, can be neglected in the Sixth Case Study postclosure safety assessment.

Data on metal (Fe, Ni, Cu, Cr and Co) concentrations in fuel surface deposits (Chen et al. 1986) indicate that, for these elements, the metal inventories in the surface deposit are a small fraction (up to 2.3%) of the corresponding metal inventory in the fuel. However, none of these 5 metals are included in the detailed safety assessment calculations carried out for the Sixth Case Study because they were screened out by the chemical hazard screening analyses. Hence, the inventories of these 5 metals on the external bundle surfaces are not included in the Sixth Case Study.

4.5 INSTANT RELEASE

4.5.1 UO₂ Instant Release

Radionuclides are released from used fuel by two processes - instant release and congruent dissolution release. Instant release is the rapid release of nuclides on contact of the used fuel with water. Congruent dissolution is the slower release of nuclides as the matrix material itself (either the UO₂ fuel or the Zircaloy cladding) dissolves.

The instant release process considers any radionuclide (or chemical element) inventory in the fuel-cladding gap or in the UO₂ fuel grain boundaries to be quickly exposed to water and to dissolve into the water. The degree of segregation of the various radionuclides (or chemical elements) is highly dependent on fuel operating parameters such as linear power rating and burnup, as well as on the properties of the radionuclides (or chemical elements).

The amount of a chemical element (or radionuclide) that is susceptible to instant release is defined as a fraction of the total inventory of that chemical element (or radionuclide) within the fuel. The instant release fraction data are given in Table 4.9. The range of values in the data allow for uncertainties. Radionuclides of the same element are all assumed to have the same instant release fraction. The sources of the instant release fraction data are described below.

The instant release fraction data for key elements such as I, Sr, and Cs, are based on the work of Stroes-Gascoyne (1996). The instant release fractions of these key elements were reviewed for the previous Case Study, including the possible implications of newer non-CANDU data (Johnson et al. 2004, 2005; SKB 2010). However, for CANDU fuel, Stroes-Gascoyne (1996) remains the best data source.

Stroes-Gascoyne (1996) found that the instant release fraction for Cs can be described using a normal distribution with mean 0.039 and standard deviation 0.019. The instant release fraction for I can be described using a normal distribution with mean 0.036 and standard deviation 0.024. This is higher than the instant release fraction used by SKB for light-water reactor fuel (SKB 2010).

The fuels used in the experiments of Stroes-Gascoyne (1996) had burnups and (peak) linear power ratings that were generally higher than those expected for typical CANDU fuel. For example, about 14% of CANDU fuel bundles have peak linear power ratings greater than 42 kW/m (see Figure 4.3, data from Wilk 2013), whereas in the work of Stroes-Gascoyne 57% of the fuels had peak linear power ratings greater than 42 kW/m. Thus, the measured instant release fractions from Stroes-Gascoyne should be conservative, based on the relationship between fission gas releases and linear power rating, as described below.

Generally fission (noble) gas releases from CANDU fuel bundles are low if the peak linear power rating of the fuel is less than about 42 kW/m, and increases with linear power rating for linear power rating values above 42 kW/m (Floyd et al. 1992), as illustrated in Figure 4.3. A threshold for fission gas release has also been found for BWR fuel (Kamimura 1992).

For light-water reactor fuel, fission gas releases are independent of fuel burnup for burnups less than about 1000 MWh/kgU and then increase with burnup (Johnson et al. 2004). Since CANDU burnups are much lower than 1000 MWh/kgU and there is no correlation between fuel burnup and linear power rating, fission gas releases from CANDU fuels are not correlated to fuel burnup.

Table 4.9: Instant Release Fractions for CANDU Fuel

Element	PDF Type	PDF Attributes*	Lower Limit	Upper Limit
Ac	constant	0	-	-
Ag	uniform	-	0	0.001
Am	constant	0	-	-
Bi	normal	(0.006, 0.0015)	0.0023	0.03
Br	normal	(0.06, 0.01)	0.01	0.2
C	normal	(0.027, 0.016)	0.0005	0.075
Ca	constant	0	-	-
Cd	normal	(0.006, 0.0015)	0.0023	0.03
Cl	normal	(0.06, 0.01)	0.01	0.2
Cs	normal	(0.04, 0.01)	0.015	0.20
Hg	normal	(0.04, 0.01)	0.015	0.20
I	normal	(0.04, 0.01)	0.015	0.20
Mo	lognormal	(0.01, 2)	0.0005	0.05
Np	constant	0	-	-
Pa	constant	0	-	-
Pb	normal	(0.006, 0.0015)	0.0023	0.03
Pd	lognormal	(0.01, 2)	0.0005	0.05
Po	normal	(0.04, 0.01)	0.015	0.20
Pu	constant	0	-	-
Ra	normal	(0.025, 0.008)	0.001	0.05
Rn	normal	(0.04, 0.01)	0.015	0.20
Sb	normal	(0.006, 0.0015)	0.0023	0.03
Se	normal	(0.006, 0.0015)	0.0023	0.03
Sn	uniform	-	0	0.001
Sr	normal	(0.025, 0.008)	0.001	0.05
Tc	lognormal	(0.01, 2)	0.0005	0.05
Te	normal	(0.006, 0.0015)	0.0023	0.03
Th	constant	0	-	-
U	constant	0	-	-
W	constant	0	-	-

*PDF attributes are (mean, standard deviation) for the normal PDF, and (geometric mean, geometric standard deviation) for the lognormal PDF.

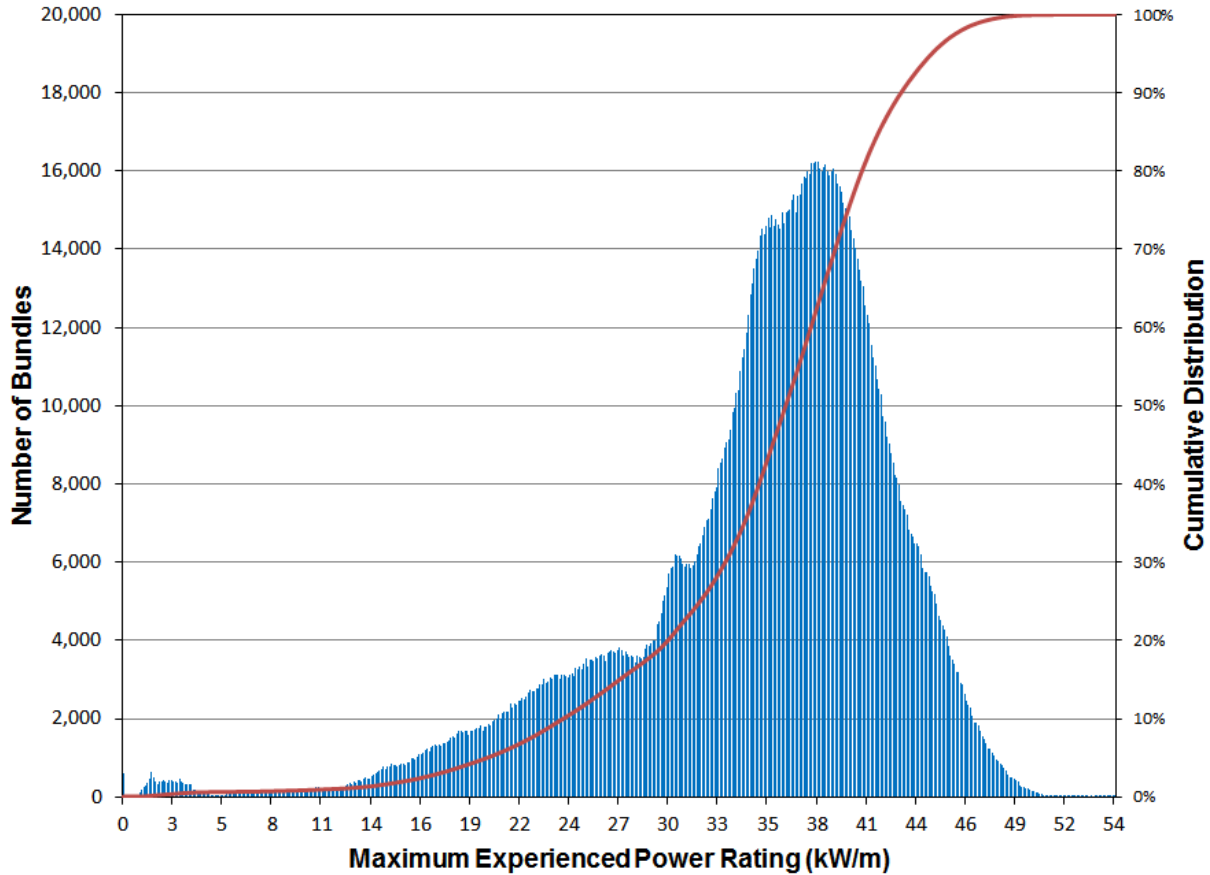


Figure 4.3: Distribution of Maximum Linear Power Ratings and Cumulative Distribution for all Commercial Fuel Bundles (discharged up to 2012)

Since iodine and cesium behave like noble gases (Iglesias et al. 2011), the I and Cs gap inventories should depend similarly on the fuel linear power rating. This is illustrated by plotting the instant release fractions for I and Cs (i.e., the sum of the gap and grain boundary inventories) versus the peak linear power rating, as shown in Figure 4.5. Because of the scarcity of data at low linear power ratings, no attempt was made to calculate an average Cs (or I) instant release fraction for the 48 fuel bundles in a fuel container from the distribution of bundle linear powers. Rather, the mean instant release fractions derived by Stroes-Gascoyne (1996), i.e., using unweighted averages, are used in the assessment. These are expected to be conservative given the relatively large number of high peak linear power rating fuels used by Stroes-Gascoyne (compare Figures 4.3 and 4.5).

The standard deviations in the instant release fractions found by Stroes-Gascoyne (1996) reflect mainly the differences between the 14 different fuels used in her experiments. For a larger quantity of fuel (i.e., the 48 fuel bundles in a used fuel container), the standard deviation for the average instant release fraction would be much smaller. For example, the standard deviation for the instant release fraction of I associated with having 48 bundles in a container, assuming that the measured variability is randomly distributed between fuel bundles, is $0.024/(48)^{1/2} = 0.0035$. However, the measured variability may include systematic biases and not just random measurement uncertainty; therefore, the standard deviation for the average instant release fraction for the fuel in a container has been set to a nominal value of 0.01.

In summary, for the Sixth Case Study, it is assumed that the instant release fraction for Cs and I are described by a normal distribution with mean 0.04 and standard deviation 0.01. The limits of the distribution are set at 0.015 to 0.20. The minimum value corresponds approximately to the smallest instant release fraction measured by Stroes-Gascoyne (1996) and the maximum value corresponds approximately to the calculated fission gas release from a high power rating/high burnup fuel (Iglesias et al. 2011).

The instant release fraction for Cl is derived from the Cl-36 release data of Tait et al. (1997), who suggest that most of the Cl-36 in the fuel originates from the fuel-cladding gap and that little is present in the grain boundaries. The instant release fraction for Cl increases with both the peak linear power rating and burnup of the fuel (see Figure 4.6). Thus, one could in theory use the relationship in Figure 4.6 along with the distribution of peak linear power ratings (Figure 4.3) to obtain the average expected Cl-36 instant release fraction from all fuel bundles. However, the data of Tait et al. (1997) are limited (i.e., most data are for low linear power rating, low burnups or for high linear power rating, high burnup fuels) and so the relationship shown in Figure 4.6 may not be generally applicable. Hence, a conservative estimate of the Cl-36 instant release fraction was made assuming, based on Tait et al. (1997), that fuels with low peak linear power rating (< 40 kW/m), low burnup (<190 MWh/kgU); intermediate linear power rating, intermediate burnup; and high linear power rating (> 43 kW/m) or high burnup (> 230 MWh/kgU) have Cl-36 instant release fractions of 0.7%, 4.5% and 15%, respectively. Using the distribution of fuel linear power rating and burnup data for the Pickering Nuclear Generating Station (for which linear power ratings and, hence, instant release fractions are the highest), the calculated Cl-36 instant release fraction is 0.06. Therefore, the instant release fraction for Cl-36 is described as a normal distribution with mean 0.06 and standard deviation of 0.01. This standard deviation accounts for the large quantity of fuel in a used fuel container, as discussed above for I and Cs. The limits of the distribution are set at 0.01 to 0.2, the approximate limits of the instant release fraction data measured by Tait et al. (1997).

Stroes-Gascoyne (1996) measured releases of Sr-90 from crushed CANDU fuel samples to derive the instant release fraction of Sr-90. The instant release fraction of Sr-90 was independent of the fuel power or burnup. Based on her data, the instant release fraction of Sr can be described by a normal distribution with a mean of 0.025, a standard deviation of 0.008, and a maximum instant release fraction of about 0.05.

Since Sr is mainly dissolved in the fuel matrix (Kleykamp 1985), segregation of Sr to the grain boundaries of the fuel is not expected. The measurements show otherwise. Segregation of the short-lived parents of Sr-90 has been proposed to explain why segregation of Sr-90 occurs in fuel (Stroes-Gascoyne 1996).

For CANDU fuel, Stroes-Gascoyne et al. (1994) measured C-14 releases from crushed fuel samples. No correlation of total C-14 release with fuel burnup or power rating was observed. The mean release from the fifteen fuel samples was 0.027, with a standard deviation of 0.016.

Technetium is not soluble in the UO₂ fuel and is present in used fuel in metallic form, typically in alloy inclusions (Kleykamp 1985). The results of leaching studies indicate that Tc gap and grain boundary releases are generally small, i.e., < 0.002 (Johnson and Tait 1997, Garisto and Gierszewski 2002). This may be due to the insolubility of the alloy inclusions in which Tc is found. The highest Tc releases, up to 5%, were observed in studies involving leaching of

CANDU fuel that was oxidized in air to U_3O_8 powder (Stroes-Gascoyne and Sellinger 1986). Although such conditions are not representative of fuel under repository conditions, they may provide a better estimate of the total grain boundary inventory of Tc.

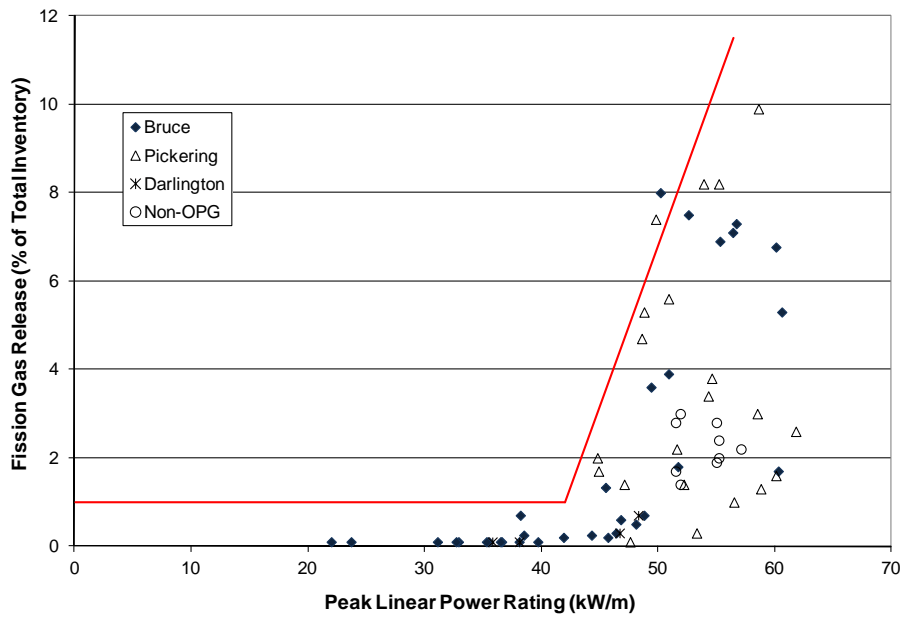


Figure 4.4: Fission Gas (gap) Release as a Function of Peak Linear Power Rating for CANDU Fuels with Burnups Less than 400 MWh/kgU

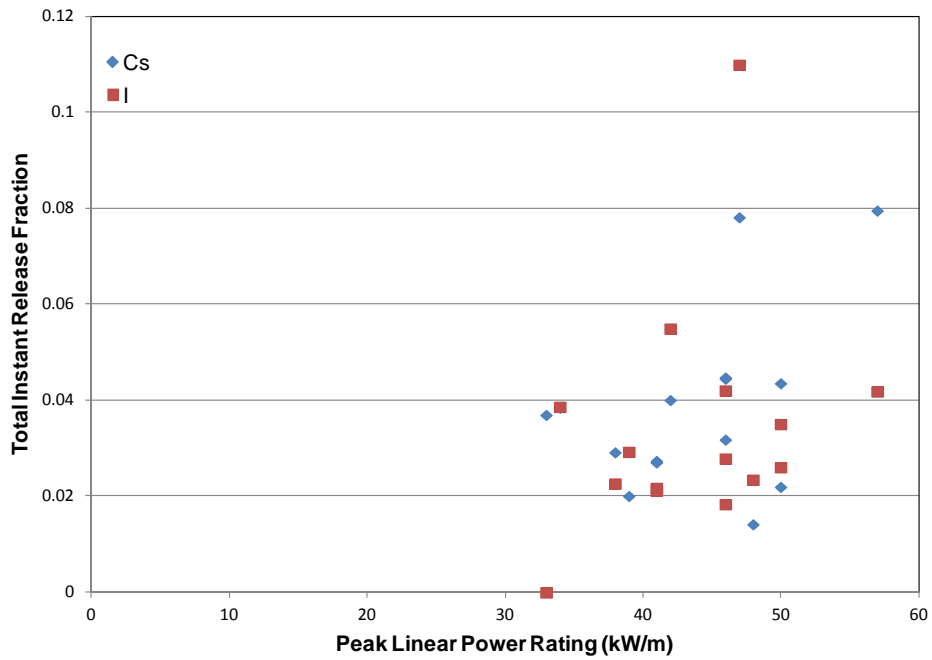


Figure 4.5: Total Instant Release Fractions (gap + grain boundary inventories) for Iodine and Cesium

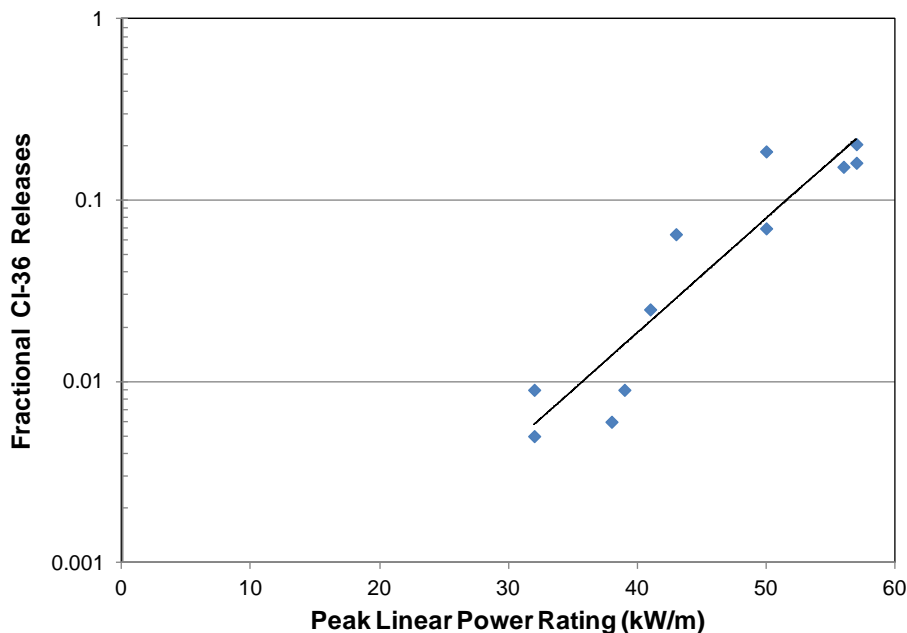


Figure 4.6: CI-36 Releases from CANDU Fuel

The Tc instant release fraction is taken from the review of Garisto and Gierszewski (2002). The Tc instant release fraction is lognormally distributed with a geometric mean of 0.01 and a geometric standard deviation of 2. This instant release fraction is larger than that used by SKB in their SR-Site safety assessment (SKB 2010) since it is based on results of leaching experiments with both slightly preoxidized (UO_{2+x} , $x < 0.25$) and non-oxidized CANDU fuels. This larger value was selected to account for the uncertainty in the amount of Tc that could be leached from the fuel grain boundaries over hundreds of years.

The instant release fractions of all actinides and lanthanides are taken to be zero, as in other studies (Johnson et al. 2004), since they form non-volatile oxides that are dissolved within the UO_2 fuel matrix.

The instant release fractions for the elements Sn and Se have not been measured for CANDU fuels. Wilson (1990a, 1990b) attempted to measure the instant release fractions of Se-79 and Sn-126 for light-water reactor fuels. However, the amount leached was less than the detection limit. From the “less than” data reported by Wilson, it is possible to infer maximum instant release fractions (Johnson et al. 2004, SKB 2010).

For Se, a semi-volatile element that is non-soluble in the UO_2 fuel, the maximum instant release fraction is less than 15% of the fission gas release. Such a low instant release fraction suggests that Se is not volatile in the fuel. Perhaps Se forms alloys in the fuel, e.g., BaSe, as suggested by Iglesias et al. (2011). For the Sixth Case Study, the instant release fraction of Se is set equal to 15% of the instant release fraction of I and Cs (following SKB 2010). Thus, the instant release fraction for Se is described by a normal distribution with mean 0.006 and standard deviation 0.0015. The limits of the distribution are set at 0.0023 to 0.03.

For Sn, a non-volatile element that is expected to be present as a metallic precipitate in used fuel (Kleykamp 1985), the maximum instant release fraction, based on the “less than” values from Wilson (1990a, 1990b) is low, i.e., less than 0.0001. Given the uncertainties in the experiments, the differences between CANDU and light-water reactor fuels and the fact that Sn is used as an analog for other elements (see below), it is conservatively assumed in the Sixth Case Study that the instant release fraction for Sn is described by a uniform distribution from 0.0 to 0.001, with a median value of 0.0005.

For the many chemical elements for which leaching measurements are not available, the only basis for estimating the instant release fractions are the diffusion coefficients of the elements in fuel and the chemistry of the elements in fuel. For example, an understanding of which elements form solid solutions with UO_2 and which elements form metallic or oxide precipitates in fuel would be important (Kleykamp 1985). This methodology is used to conservatively estimate the instant release fractions of elements for which measured data are not available.

Generally, fission products can be classified into 4 groups (Kleykamp 1985):

1. Gases and other volatiles:
Kr, Xe, Br, I
2. Fission products forming metallic precipitates:
Mo, Tc, Ru, Rh, Pd, Ag, Cd, In, Sn, Sb, Te
3. Fission products forming oxide precipitates (often referred to as the “grey phase”):
Rb, Cs, Ba, Zr, Nb, Mo, Te
4. Fission products dissolved in the fuel matrix:
Sr, Zr, Nb, Rare Earths, Y, La, Ce, Pr, Nd, Pm, Sm

Some elements fall into two categories. There is a continuous transition between categories 2 and 3 due to the similar oxygen potential of some fission product oxides and fuel, which changes composition during irradiation. Transitions can also occur between categories 3 and 4 due to the burnup dependent distribution of cations in both oxide phases. Furthermore, some fission products can react without participation of oxygen (e.g., Cs_2Te , CsI , etc.).

The key thermodynamic factor that influences the chemical state of the fission products in fuel is the oxygen potential, which in turn depends on the stoichiometry of the fuel, the temperature and burnup. The fuel is initially stoichiometric, i.e., the oxygen potential is very low (Lindemer and Besmann 1985), but burnup raises the ratio of oxygen to uranium because the O_2 released by fission of uranium cannot be completely bonded by the generated fission products (Cordfunke and Konings 1988). For near-stoichiometric fuels, the oxidation potential in the fuel may be buffered by the Mo/MoO_2 couple (Kleykamp 1985, Cubicciotti and Sanecki 1978), since this couple has an oxidation potential that is similar to that of slightly hyperstoichiometric fuel and the fission yield of Mo is relatively high.

The oxidation potential for formation of the oxide of each element, relative to the oxidation potential of the fuel, was used to assess the chemical state of the elements in fuel (Kleykamp 1985) and, thence, to estimate the instant release fractions of the elements for which no measured values are available. For an element for which measured instant release fractions are not available, the rationale for the selected instant release fraction is provided in Table 4.10.

Table 4.10: Rationale for Selection of Instant Release Fractions for Elements without Measured Data

Element	Chemical State of Element in Fuel	Element Boiling Point (K)	Rationale for Selected Instant Release Fraction
Ac, Am, Np, Pa, Pu, Th, U	Oxides dissolved in the fuel matrix	-----	Actinides are present in solid solution in the fuel matrix. Assume instant release fraction=0 for all actinides (Johnson and Tait 1997)
Ag	Metallic precipitate alloyed with other noble metals such as Cd and Sn (Kleykamp 1985).	2435	Boiling point of Ag is similar to that of Sn (2875 K). Since Ag is likely alloyed with Sn and other similar metals in fuel, assume instant release fraction for Ag is the same as that for Sn.
Bi	Metallic precipitate in fuel	1837	Boiling point of Bi is lower than that of Sn (2875 K) and higher than that of Se (958 K). For conservatism, assume instant release fraction is same as that of Se.
Br	Volatile, reactive gas	-----	Halogen like Cl and I. Assume instant release fraction of Br is equal to the instant release fraction of Cl.
C	Gaseous oxide (CO or CO ₂).	-----	Measured value (see text).
Ca	Oxide in fuel. CaO is soluble in fuel matrix	-----	CaO is likely present in solid solution in the UO ₂ fuel matrix, so the instant release fraction of Ca is set to zero.
Cd	Metallic precipitate in fuel, alloyed with, e.g., Ag, Sn and Pd.	1040	Boiling point of Cd is similar to that of Se (958 K), so assume instant release fraction of Cd is that same as that of Se.
Cl	Volatile, reactive gas	-----	Measured value (see text).
Cs	Found in various forms in fuel – dissolved in fuel, as Cs urinate, in grey phase and reacted with other fission products such as I and Te (Kleykamp 1985)	-----	Measure (see text)
Hg	Metallic precipitate in fuel, alloyed with other elements	630	The volatility of Hg is quite high at the temperature of fuel in the reactor; therefore, assume instant release fraction is similar to that of noble gases such as Rn.
I	Volatile, reactive gas	-----	Measured (see text)
Mo	Metallic precipitate alloyed with Tc, Ru, Rh and Pd, and dissolved in fuel matrix as oxide.	4912	Found in grain boundaries of fuel alloyed with Tc in epsilon particles. Assume instant release fraction of Mo is the same as for Tc.
Pb	Metallic precipitate in fuel	2022	Boiling point of Pb is lower than that of Sn (2875 K) and higher than that of Se (958 K). For conservatism, assume instant release fraction is same as that of Se.

Element	Chemical State of Element in Fuel	Element Boiling Point (K)	Rationale for Selected Instant Release Fraction
Pd	Metallic precipitate alloyed with a wide variety of metals in fuel, e.g., found in epsilon particles with Tc, Ru, Rh and Mo.	3236	Assume same instant release fraction of Pd is the same as for Tc, since found in grain boundaries of fuel alloyed with Tc in epsilon particles.
Po	Chemistry is similar to that of Bi and Te.	-----	Po has only short-lived isotopes, so for conservatism assume that instant release fraction of Po is the same as for noble gases such as Rn.
Ra	Oxide in fuel.	-----	Ra is likely dissolved in the fuel matrix. However, for conservatism, assume Ra behaves like Sr in fuel, since both are alkaline earth elements. Thus, assume instant release fraction of Ra is the same as that of Sr.
Rn	Non-reactive gas	-----	Rn is a noble gas. The instant release fractions of the Cs, I and the noble gases are similar. Therefore, instant release fraction for Rn is set equal to that of Cs or I.
Sb	Metallic precipitate alloyed with Pd, Sn and other metals	1860	Boiling point of Sb is lower than that of Sn (2875 K) and higher than that of Se (958 K). For conservatism, assume instant release fraction is same as that of Se.
Se	Likely in elemental form in fuel, alloyed with other fission products	958	Measured value (see text). Note that although boiling point of Se is relatively low, the measured values of the instant release fraction are not high. Perhaps alloys or compounds formed by Se are stable.
Sn	Metallic precipitate in fuel alloyed with other metals, e.g., Cd and Ag.	2875	Measured value (see text)
Sr	Oxide in fuel, dissolved in fuel matrix. Some evidence that it is also found in the grey oxide phase (Kleykamp 1985)	-----	Measured value. The instant release fraction of Sr-90 is non-zero even though SrO dissolves in the fuel matrix. This could be due to the volatile precursors of Sr-90 (Stroes-Gascoyne 1996).
Tc	Oxide in fuel	-----	Measured value (see text)
Te	Chemistry of Te is complex – it dissolves in UO ₂ , forms alloys with Pd and Sn, forms oxide precipitates (e.g., BaTeO ₃) and forms non-oxide compounds (e.g., Cs ₂ Te) (Kleykamp 1985).	1261	Assume Te behaves similarly to Se in the fuel. Therefore, the instant release fraction of Te is set equal to that of Se.

Element	Chemical State of Element in Fuel	Element Boiling Point (K)	Rationale for Selected Instant Release Fraction
W	Metallic precipitate in fuel	5828	Non-volatile, non-reactive metal. Since W concentration in fuel is so small, assume it can be accommodated in fuel matrix. Thus instant release fraction of W is equal to zero.

4.5.2 Zircaloy Instant Release

Because the impurities in the Zircaloy of the fuel bundles are likely uniformly distributed and the temperature of the cladding during reactor operation is relatively low, the activation products and impurities in the Zircaloy would be expected to be likewise uniformly distributed. Hence, for the Zircaloy wastefrom, the instant release fractions should be zero and contaminants are released congruently as the Zircaloy corrodes.

However, leaching experiments indicate that the C-14 within the oxide film on the Zircaloy is released relatively rapidly compared to the C-14 within the metal itself (Gras 2014, Yamaguichi et al. 1999, Smith and Baldwin 1993). The same leaching experiments suggest that the C-14 instant release fraction for the Zircaloy metal is zero. Consequently, the fraction of the C-14 within the oxide layer can be assumed to be instantly released after water breaches a used fuel container and contacts the fuel bundles and so the instant release fraction of C-14 from the Zircaloy wastefrom is non-zero.

In previous safety assessments, the instant release fraction for C-14 in the Zircaloy was based on pressurized water reactor data. This turns out to be very conservative since the oxide layer on the Zircaloy cladding of a CANDU fuel bundle is much thinner than for pressurized water reactor fuel and the thickness of the Zircaloy claddings is similar in the two fuel types. The derivation of the instant release fraction for C-14 for the Zircaloy wastefrom in a CANDU used fuel bundle is described below.

The concentration of C-14 in the Zircaloy oxide layer is higher than in the metal itself. Data from Tanabe et al. (2009) indicate that the concentration in the oxide layer is 1.5 to 1.7 times higher (on a weight basis) than in the metal. Thus, if Ω is the concentration of C-14 in the Zircaloy metal (in Bq/kg Zr) then the concentration of C-14 in the oxide layer is approximately 1.6Ω .

Based on information in the literature (Wasywich 1993, 1992), the thickness of the continuous oxide layer on the outer surface of the Zircaloy cladding of used CANDU fuel is less than $5 \mu\text{m}$. This oxide thickness is somewhat larger than the value determined using the correlation between the oxide thickness and the burnup of the fuel given in Gras (2014). For a burnup of 280 MWh/kgU (or 11.7 GWd/tU), this correlation gives an oxide thickness of $3.4 \mu\text{m}$.

The oxide layer on the inner surface of the Zircaloy cladding of CANDU fuel is generally patchy (Wasywich 1992) or non-existent. The patchy oxide layers were generally thicker in used fuel from early test reactors (e.g., Douglas Point) compared to used fuel from later power reactors (e.g. Pickering). The inner oxide layer was absent or patchy and thin ($< 2\mu\text{m}$) in fuels from and later power reactors was coated with CANLUB graphite. Thus, the amount of C-14 in the inner

oxide layer is small and is approximated by assuming that the inner oxide layer has a thickness of 1 μm .

If all the C-14 within the inner and outer oxide layers of the Zircaloy is released upon contact with water, the instant release fraction for C-14 in the Zircaloy wastefrom, $IRF_{C14,Zr}$, would be given by the following equation

$$IRF_{C14,Zr} = \frac{1.6\Omega\pi d\delta\rho_{ZrO_2}}{\Omega\pi d\omega\rho_{Zr}} \quad (4.1)$$

Where δ is the total thickness of the inner and outer oxide layers (6 μm), d is the outer diameter of the cladding, w is the thickness of the cladding (400 μm), ρ_{ZrO_2} is the density of zirconium dioxide (5680 kg/m^3) and ρ_{Zr} is the density of Zircaloy (6550 kg/m^3). Substituting the values of the parameters in Equation 1, one finds that $IRF_{C14,Zr} = 0.021$.

This value of the instant release fraction for C-14 from the Zircaloy wastefrom is approximately 10-fold smaller than the previous value of 0.20 which was based on data for high burnup pressurized water reactor fuel. This large difference is understandable given that the thickness of the Zircaloy oxide layer on the cladding of the higher burnup pressurized water reactor fuel is approximately 10-fold larger than the corresponding value for CANDU used fuel.

A summary of Zircaloy instant release fractions used in the Sixth Case Study is shown in Table 4.11.

Table 4.11: Instant Release Fractions for Zircaloy Cladding

Element	Value
C	0.021
All other elements	0

4.6 CONGRUENT RELEASE

4.6.1 UO_2 Fuel Dissolution

The UO_2 ceramic fuel matrix is durable, and dissolves slowly in water. The most important factor in the rate of dissolution of UO_2 in water is the redox conditions in the surrounding groundwater. Reducing conditions are expected to prevail in and around the container under the influence of the reducing groundwater, and consumption of any residual oxygen by reaction with the copper and steel container materials or with ferrous and organic material in the sealing materials. Under these reducing conditions, the UO_2 fuel would dissolve very slowly.

However, the conditions at the used fuel surface are likely to be oxidizing for a long time due to the production of oxidants in the water from radiolysis (Poinssot et al. 2005, Shoesmith 2007, He et al. 2012). Radiolysis of the groundwater would be caused by the α -, β -, and γ -radiations emitted by the used fuel, at rates that depend on the radiation type and that generally decrease with time as the radiation field strengths decrease (Garisto et al. 2009).

For the Sixth Case Study, an empirical model for radiolysis-driven dissolution is used. In this approach, the rates of dissolution of the used fuel matrix due to α -, β - and γ -radiolysis are assumed proportional to the corresponding dose rates, i.e.,

$$R_{\alpha} = A_{\text{cont}} G_{\alpha} f_{\alpha} [D_{\alpha}(t+t_C)]^{a\alpha} \quad (4.2)$$

$$R_{\beta} = A_{\text{cont}} G_{\beta} f_{\beta} [D_{\beta}(t+t_C)]^{a\beta} \quad (4.3)$$

$$R_{\gamma} = A_{\text{cont}} G_{\gamma} f_{\gamma} [D_{\gamma}(t+t_C)]^{a\gamma} \quad (4.4)$$

with the exponents $a\alpha = a\beta = a\gamma = 1$. The total matrix dissolution rate, R_{TOT} , is given by

$$R_{\text{TOT}} = R_{\alpha} + R_{\beta} + R_{\gamma} + R_{\text{ch}} * A_{\text{cont}} \quad (4.5)$$

where

R_{α} , R_{β} , and R_{γ} are the dissolution rates ($\text{mol}_U \cdot \text{a}^{-1}$) due to α -, β - and γ -radiation;

R_{ch} is the chemical fuel dissolution rate, i.e., the dissolution rate of the fuel in the absence of radiolysis ($\text{mol}_U \cdot \text{m}^{-2} \cdot \text{a}^{-1}$);

R_{TOT} is the total dissolution rate ($\text{mol}_U \cdot \text{a}^{-1}$);

$D_{\alpha}(t+t_C)$, $D_{\beta}(t+t_C)$ and $D_{\gamma}(t+t_C)$ are the time-dependent dose rates ($\text{Gy} \cdot \text{a}^{-1}$);

t is the time after placement of the fuel in the repository; t_C is the age of the fuel at the time of placement in the repository (i.e., the time between fuel removal from reactor and its placement in the repository) (years);

G_{α} , G_{β} and G_{γ} are empirical rate constants for fuel dissolution in the presence of alpha, beta and gamma radiation fields, respectively ($\text{mol}_U \cdot \text{m}^{-2} \cdot \text{Gy}^{-1}$);

f_{α} , f_{β} and f_{γ} are the alpha, beta and gamma dose variability factors; and

A_{cont} is the effective surface area of the dissolving fuel, per container (m^2).

The model and the derivation of the model parameter values are described in more detail in Appendix B. The parameter values recommended for the Sixth Case Study are summarized in Table 4.12 through Table 4.14.

Table 4.12: Radiation Doses at Fuel Surface (220 MWh/kgU)#

Time After Fuel Discharge (years)	Alpha Dose Rate (Gy/a)	Beta Dose Rate (Gy/a)	Gamma Dose Rate (Gy/a)
10	1.42E+06	3.77E+06	7.11E+05
20	1.72E+06	2.82E+06	5.30E+05*
30	1.89E+06	2.20E+06	3.95E+05*
40	1.99E+06	1.72E+06	2.95E+05*
50	2.03E+06	1.35E+06	2.20E+05
60	2.05E+06	1.06E+06	1.74E+05*
75	2.04E+06	7.38E+05	1.23E+05*
100	2.00E+06	4.04E+05	6.87E+04
150	1.88E+06	1.24E+05	2.16E+04*
200	1.77E+06	3.96E+04	6.80E+03
300	1.58E+06	6.66E+03	1.02E+03*
500	1.30E+06	2.69E+03	2.28E+01
1,000	9.03E+05	1.53E+03	1.55E+01
10,000	3.21E+05	3.78E+02	1.65 E+01
100,000	1.80E+04	1.68E+02	2.84 E+01
1,000,000	6.24E+03	1.49E+02	3.84 E+01
10,000,000	4.19E+03	1.15E+02	3.58 E+01

#Data from Garisto et al. (2009)

*Interpolated values assuming exponentially decaying function

Table 4.13: Radiation Doses at Fuel Surface (280 MWh/kgU)#

Time After Fuel Discharge (years)	Alpha Dose Rate (Gy/a)	Beta Dose Rate (Gy/a)	Gamma Dose Rate (Gy/a)
10	1.94E+06	4.56E+06	9.15E+05
20	2.31E+06	3.41E+06	6.82E+05*
30	2.52E+06	2.66E+06	5.08E+05*
40	2.63E+06	2.08E+06	3.80E+05*
50	2.68E+06	1.63E+06	2.79E+05
60	2.69E+06	1.28E+06	2.20E+05*
75	2.67E+06	8.92E+05	1.56E+05*
100	2.60E+06	4.90E+05	8.68E+04
150	2.43E+06	1.50E+05	2.73E+04*
200	2.28E+06	4.85E+04	8.60E+03
300	2.02E+06	8.48E+03	1.29E+03*
500	1.65E+06	3.56E+03	3.08E+01
1,000	1.11E+06	2.01E+03	2.15E+01
10,000	3.67E+05	4.66E+02	2.18E+01
100,000	1.93E+04	1.91E+02	3.20E+01
1,000,000	6.97E+03	1.59E+02	3.90E+01
10,000,000	4.22E+03	1.15E+02	3.57E+01

#Data from Garisto et al. (2009)

*Interpolated values assuming exponentially decaying function.

Table 4.14: Used Fuel Dissolution Rate Parameters (see Appendix B)

Parameter	Value	Probability Density Function
Fuel surface area per container	209.3 m ²	Lognormal PDF with GM=209.3 m ² , GSD = 3, bounds of 45.33 and 1048 m ²
Alpha, beta and gamma dose rates	Table 4.12 and Table 4.13	Variability included separately through the f _α , f _β and f _γ factors
Alpha dose rate variability factor, f _α	1.0	Triangular PDF with bounds of 0.80 and 1.20
Beta dose rate variability factor, f _β	1.0	Triangular PDF with bounds of 0.80 and 1.20
Gamma dose rate variability factor f _γ factor	1.0	Triangular PDF with bounds of 0.80 and 1.20
Age of fuel at time of placement, t _c	30 years	Design basis
G _α	1.4x10 ⁻¹⁰ mol·m ⁻² ·Gy ⁻¹	Lognormal PDF with GM= 1.4x10 ⁻¹⁰ mol·m ⁻² ·Gy ⁻¹ , GSD = 6.0, bounds of 3.5·10 ⁻¹² and 2.1·10 ⁻⁹ mol·m ⁻² ·Gy ⁻¹
G _β and G _γ	1.1x10 ⁻⁹ mol·m ⁻² ·Gy ⁻¹	Loguniform PDF with bounds of 3.7x10 ⁻¹¹ and 3.3x10 ⁻⁸ mol·m ⁻² ·Gy ⁻¹
Chemical dissolution rate	4.0x10 ⁻⁷ mol·m ⁻² ·a ⁻¹	Loguniform PDF with bounds of 4.0x10 ⁻⁸ and 4.0x10 ⁻⁶ mol·m ⁻² ·a ⁻¹

Notes: PDF = Probability Density Function, GM = Geometric mean, GSD = Geometric standard deviation

4.6.2 Zircaloy Corrosion

The Zircaloy sheath surrounding the fuel pellets in a CANDU fuel bundle naturally forms a thin layer of protective ZrO₂ on its surface when in contact with air or water. This oxide layer greatly inhibits the Zircaloy dissolution rate in the postclosure period in the event water gains access to the used fuel container (Shoosmith and Zagidulin 2010). Because the inventory of certain isotopes such as Cl-36 and C-14 within the fuel sheath can be significant relative to the amount present in the fuel (Gobien and Garisto 2012), dissolution of the Zircaloy is modelled in RSM and SYVAC3-CC4.

In the past the rate of dissolution of the zirconium oxide was calculated using a solubility-limited dissolution model. In this model, the concentration of zirconium in the failed container is set equal to the solubility limit of the zirconium oxide and the oxide dissolves at the rate required to maintain this zirconium concentration. In the Sixth Case Study, a kinetic dissolution model is used in which the zirconium dissolves at a rate proportional to the corrosion rate of Zircaloy in water and the surface area of the Zircaloy in contact with water. During corrosion, species trapped in the Zircaloy matrix are released. In the kinetic (corrosion) model, the dissolution rate, R_{cor}, of the Zircaloy is given by the following equation (4.6)

$$R_{cor} = k_{Zr} A_{Zr} \rho \tag{4.6}$$

where,

- k_{Zr} is the corrosion rate of ZrO_2 in water estimated to be approximately 5 nm/a (Shoesmith and Zagidulin 2010);
- A_{Zr} is the area of the Zircaloy exposed to water (0.75 m² per bundle or 36 m² for a 48 bundle container); and
- ρ is the density of the Zircaloy (6550 kg/m³)

Using the values specified above, R_{cor} is estimated to be 1.18×10^{-3} kg/a. Each container holds 105.6 kg of Zr (see Table 5.1) resulting in a complete dissolution of the Zircaloy in approximately 89,500 years.

5. CONTAINER

5.1 CONTAINER DIMENSIONS

The used fuel container design is illustrated in Figure 5.1. The main properties needed here are summarized in Table 5.1. The Sixth Case Study reference container design has changed to the copper coated MKII container which holds 48 bundles as opposed to the 360 bundle capacity IV-25 design used in the Fourth Case Studies.

The inner steel container provides structural support and is coated with copper for corrosion resistance. Inside this vessel are carbon steel baskets holding the used fuel bundles.

Table 5.1: Container Internal Parameters

Parameter	Value	Comments
Total number of fuel bundles in container	48	As per Chapter 4 of NWMO (2017)
Mass of uranium in container	924 kg	48 bundles x 19.25 kgU/bundle (pre-irradiation value) (Tait et al. 2000)
Mass of Zirconium in the container	105.6 kg	48 bundles x 2.2 kgZr/bundle (pre-irradiation value) (Tait et al. 2000)
Steel vessel outer diameter	556 mm	Nominal Dimension (NWMO 2017, Chapter 4)
Steel vessel thickness	Body 46.2 mm	Nominal Dimension (NWMO 2017, Chapter 4)
	Head 30 mm	Nominal Dimension (NWMO 2017, Chapter 4)
Inner vessel length	1950 mm	Length of cylindrical shell (NWMO 2017, Chapter 4)
	2506 mm	Overall length, apex head-to-head (NWMO 2017, Chapter 4)
Inner vessel internal volume	0.393 m ³	Calculated using CAD model
Internal void volume	0.266 m ³	Assumes basket (0.013 m ³ = calculated using CAD model) and 37 Standard Element Bruce Bundle (0.114 m ³ = 48 x 0.00238 m ³ from Tait et al. 2000)
Internal porosity fraction	0.677	(Internal void volume)/(Internal volume)
Copper cladding thickness	3 mm	Minimum Dimension (NWMO 2017, Chapter 4)

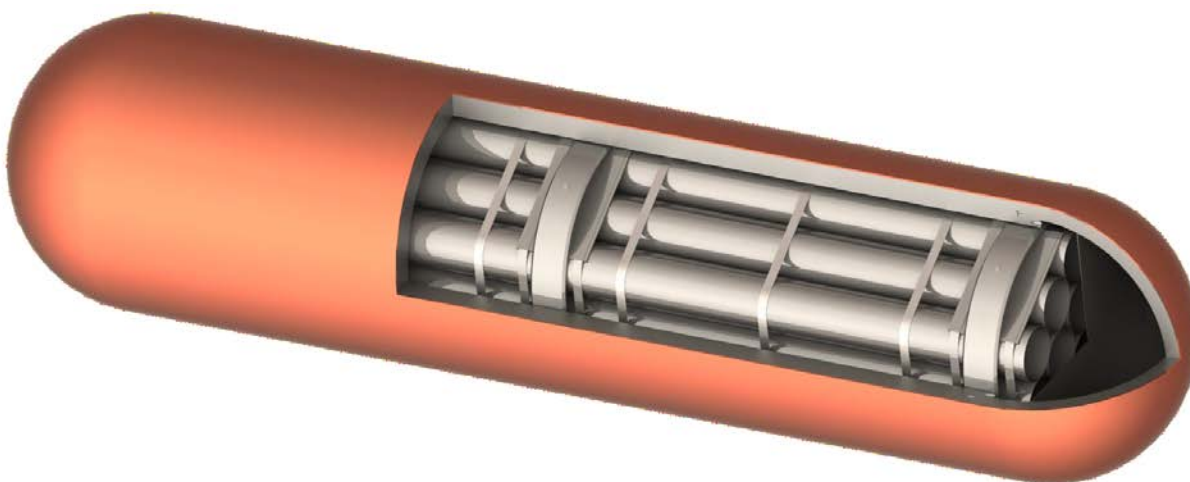


Figure 5.1: Container Design Showing Copper Coating, Inner Steel Vessel, and Inside Support Tubes

5.2 DEFECTIVE CONTAINER

The “Base Case” sensitivity study assumes a small number of containers are fabricated with defects in their copper coating, and that a smaller number of these off-specification containers escape detection by the quality assurance program and are unknowingly placed in the repository.

Studies are underway to determine the likelihood and number of off-specification containers that could potentially be present; however, the results of this work will not be available for quite some time. In the meantime, 10 containers with large undetected voids in the copper coating are assumed to be unknowingly placed in the repository. Postclosure safety studies with 10 defective containers are sufficient to illustrate repository performance and to provide a measure of the consequences that could be expected should such an event (or a similar one) actually occur.

The undetected voids in the copper coatings are assumed sufficiently large to cause each of the 10 containers to be breached within the first one million years. Because it is highly unlikely that all 10 containers would fail simultaneously, the failure times are assumed to be evenly spread over the one million year time period of interest, with the first failure occurring at 1000 years and subsequent failures occurring at a rate of one container every 100,000 years thereafter.

For the probabilistic case in which the number of defective containers is varied, the number of defective containers is described by a binomial distribution with the individual container failure probability selected such that 10 failed containers is the 95th percentile value.

The parameters used to describe this failure mode are listed in Table 5.2, and discussed further below.

Table 5.2: Defective Container Scenario Parameters

Parameter	Value	Comment
Probability of early failure	6.437x10 ⁻⁵ per container	Assumes a binomial distribution with the probability of failure set to a constant value and assumes 95,833 “trials” i.e number of containers (see Section 2.3.2 of NWMO 2012b). The probability of failure is set such that the probability of 10 containers failing is the 95 th percentile.
Container Failure Time, Deterministic Simulations	1000 a 100,000 a 200,000 a ... 900,000 a	For the Base Case the first failure occurs at 1000 years and subsequent failures occur at a rate of one container every 100,000 years thereafter
Container Failure Time, Probabilistic Simulations	1-1,000,000 a	Uniform distribution with a lower bound of 1 a and an upper bound of 1,000,000 a.
Defect Radius	5.623 m	Based on complete failure of container from Gobien and Garisto (2013). Although this is a non-physical defect radius, this value makes the calculated contaminant release rates agree with COMSOL model results.
Defect length	49.23 mm	Radial thickness of steel (46.23mm) and copper container (3mm).
Near field temperature	85°C	Normal probability density function with mean of 85°C, standard deviation of 10°C, and bounds of 30°C and 130°C (based on Guo 2016).

5.3 FREE WATER DIFFUSION COEFFICIENT

Contaminants will escape the breached container by diffusion. The free water diffusivity of various ions ranges from 0.025 to 0.067 m²/a at 25°C (Ohlsson and Neretnieks 1997) and are listed in Table 5.3. For Th, the free-water diffusivity in Ohlsson and Neretnieks seemed unusually low, and therefore its diffusivity was set equal to that for the other actinides such as U. Values for elements not listed in Ohlsson and Neretnieks were conservatively assumed to be the same as for cesium (0.067 m²/a).

Diffusivities would increase by a factor of about 3.2 at 85°C (assuming that the diffusivity can be scaled by the temperature/viscosity ratio, according to Rohsenow and Choi 1961, p.383). The free-water diffusivity therefore ranges from 0.08 m²/a to 0.21 m²/a, depending on the species and on the container temperature when the release occurs.

Table 5.3: Free Water Diffusivity

Element	Value (at 25°C) ^{1,2} [m ² /a]	Value (at 85°C) [m ² /a]
Ac	0.032	0.10
Ag	0.053	0.17
Am	0.032	0.10
Bi	0.067 [#]	0.21
³ Br	0.063	0.20
C	0.038	0.12
Ca	0.025 [*]	0.08
Cd	0.023	0.07
Cl	0.063	0.20
Cs	0.067	0.21
Hg	0.067 [#]	0.21
I	0.063	0.20
Mo	0.032	0.10
Np	0.032	0.10
Pa	0.032	0.10
Pb	0.067 [#]	0.21
Pd	0.032	0.10
Po	0.067 [#]	0.21
Pu	0.032	0.10
Ra	0.028	0.09
Rn	0.067 [#]	0.21
³ Sb	0.067 [#]	0.21
Se	0.032	0.10
³ Sn	0.032	0.10
³ Sr	0.025	0.08
Tc	0.032	0.10
Te	0.067 [#]	0.21
Th	0.032 [*]	0.10
U	0.032	0.10
W	0.032	0.10

¹Values are assumed to be normally distributed with a standard deviation of 0.01 and upper and lower bounds of 0.01 and 0.1 respectively

²Ohlsson and Neretnieks (1997), unless otherwise stated.

³Sixth Case Study analyses erroneously assumed free water diffusivities of 0.032 m²/a, 0.032 m²/a, 0.067 m²/a and 0.032 m²/a for Br, Sb, Sn, and Sr respectively.

[#]Value conservatively assumed to be the same as for Cs.

^{*}Values for Ca, Mo, W and Th set equal to Sr, Tc, Tc, and U values, respectively.

5.4 WATER COMPOSITION

The groundwater composition around the repository would need to be determined for any specific site. The range of measured groundwater compositions in Canadian Shield rock mass are described in McMurry (2004). A reference crystalline rock groundwater, CR-10, has been defined for the Sixth Case Study host rock based on the groundwaters found at a depth of around 500 m. Its composition is listed in Table 5.4 (Duro et al. 2010). It is a reducing Na-Ca-Cl groundwater, with total dissolved solids (TDS) of about 11.6 g/L.

Table 5.4: Contact Water Composition

Composition	CR-10 Equilibrated	CR-10 Bentonite-Iron Equilibration
pH	7.1	8.7
Environment	Reducing	Reducing
Eh (mV)	-194	-575
Element	Solutes (mg/L)	
Na	1,899	6,255
K	15	80
Ca	2,217	870
Mg	60	182
HCO ₃	50	4
SO ₄	1,243	4,314
Cl	6,099	6,059
Br	-	-
Sr	25	25
Li	-	-
F	2	2
I	-	-
B	-	-
Si	5	10
Fe	8	7
NO ₃	1	1
PO ₄	1	1
TDS	11,625	17,810

The composition of the water actually reaching the used fuel will be that of the surrounding host rock groundwater but conditioned by passage through the backfill, buffer and container. In particular, the concentrations of the species in the water reaching the used fuel will be affected by ion exchange with the bentonite buffer (e.g., calcium ions in the groundwater may be exchanged for sodium ions in the bentonite as the groundwater passes through the bentonite), the presence of the iron-canister, as well as the dissolution of the minor mineral components of the buffer, such as gypsum and calcite, which could lead to higher carbonate and sulphate concentrations in the contact water (Duro et al. 2010).

The composition of the contact water is also shown in Table 5.4. This was calculated by Duro et al. (2010) by equilibrating the selected CR-10 reference groundwater (see Table 5.4) with the bentonite buffer minerals and the steel canister. The assumed initial E_h of the groundwater is approximately -200mV but this is expected to decrease to approximately -560mV after equilibration of the groundwater with the carbon steel vessel.

5.5 SOLUBILITY LIMITS

After container failure, water can contact the fuel, and cause the release of contaminants. The rate at which contaminants are released from the fuel is determined by the used fuel dissolution model. In theory, the concentrations of a contaminant in the water in the container could reach the solubility limit for that element. Consequently, precipitation of contaminants could occur, especially within or near the container where concentrations are highest.

The element solubilities are listed in Table 5.5. These solubilities were calculated for 25°C and the reference water compositions in Table 5.4. Many solubility limits are temperature sensitive and the vault temperature is expected to be higher than 25°C (approximately 85°C) for thousands of years after repository closure. Despite this, solubility limits were calculated at 25°C since very little thermodynamic data exists for temperatures outside of 25°C. The solubility limits can also be quite sensitive to the groundwater composition which is also likely to vary somewhat throughout the repository due to non-homogeneities in mineral composition of the granitic rock and perhaps the buffer material. To account for uncertainties in the solubility due to the higher temperatures in the repository and the groundwater composition, the solubility values listed in Table 5.5 are increased by a factor of 10 from their original references for use in the safety assessment calculations.

For most elements, i.e., Am, Bi, C, Mo, Np, Pa, Pb, Pd, Pu, Ra, Se, Sn, Tc, Th, and U the solubilities were calculated by Duro et al. (2010) using PHREEQC and the ThermoChimie v7b database. ThermoChimie includes the thermodynamic data compiled by the NEA, when available, and uses the specific ion theory (SIT) activity corrections (Guillaumont et al. 2003). Due to uncertainty in the thermodynamic data as well as variability in the geochemical conditions at repository depth, the solubility limit is described using a lognormal distribution. For elements in which the thermodynamic data are well defined or the solubility limit is relatively insensitive to repository conditions, a lognormal distribution with a geometric standard deviation of 3.2 is assumed. This geometric standard deviation corresponds to the 95% confidence bounds being within a factor of 10 of the geometric mean. Conversely for Pa, for which the solubility is highly uncertain, a geometric standard deviation of 10 is used.

The elements Ag, Ba, Cd, and Sb are also expected to have limited solubilities on the basis of thermodynamic stabilities and observed behaviour in natural and experimental systems. The solubilities of these elements in the two groundwaters listed in Table 5.4 were calculated using

PHREEQC (version v2.18.5570) and the ThermoChimie database (v.7.d June 2011) that comes with PHREEQC. The higher of these two calculated solubility values is used in the assessment and is listed in Table 5.5.

The remaining elements (Ac, Ca, Cl, Cs, Hg, I, Po, Rn, Sr, Te, and W) are assigned a very high constant solubility (2 mol/kg) to ensure that precipitation does not occur. These elements are either expected to be highly soluble, or to have a low inventory in the fuel, or to exist only as short-lived radionuclides, or to be gaseous (i.e., they do not precipitate), or to have complex chemistries so that their solubility limit is highly uncertain.

Table 5.5: Element Solubilities¹

Element	Value ² (mol/kg)	GSD	Distribution Type	Comments
Ac	2.0	-	Constant	No solubility limit
Ag	1.1x10 ⁻⁴	3.2	Lognormal	Calculated, AgCl(s) controlling solid
Am	2.2x10 ⁻⁴	3.2	Lognormal	Duro et al. (2010)
Bi	1.2x10 ⁻⁴	3.2	Lognormal	Duro et al. (2010)
Br	2.0	-	Constant	No solubility limit
C	8.3x10 ⁻³	3.2	Lognormal	Duro et al. (2010)
Ca	2.0	-	Constant	No solubility limit
Cd	7.6x10 ⁻⁴	3.2	Lognormal	Calculated, CdCO ₃ controlling solid
Cl	2.0	-	Constant	No solubility limit
Cs	2.0	-	Constant	No solubility limit
Hg	2.0	-	Constant	No solubility limit
I	2.0	-	Constant	No solubility limit
³ Mo	8.7x10 ⁻⁸	-	Constant	Duro et al. (2010)
Np	1.1x10 ⁻⁸	3.2	Lognormal	Duro et al. (2010)
Pa	2.2x10 ⁻⁸	10	Lognormal	Duro et al. (2010)
Pb	8.0x10 ⁻⁵	3.2	Lognormal	Duro et al. (2010), Pb ₃ (CO ₃) ₂ controlling solid
Pd	4.1x10 ⁻⁵	3.2	Lognormal	Duro et al. (2010)
Po	2.0	-	Constant	No solubility limit
Pu	9.1x10 ⁻⁷	3.2	Lognormal	Duro et al. (2010)
Ra	1.6x10 ⁻⁶	3.2	Lognormal	Duro et al. (2010)
Rn	2.0	-	Constant	No solubility limit
Sb	5.7x10 ⁻⁴	3.2	Lognormal	Calculated, Sb ₂ O ₃ controlling solid
Se	1.3x10 ⁻⁷	3.2	Lognormal	Duro et al. (2010)
Sn	9.6x10 ⁻⁶	3.2	Lognormal	Duro et al. (2010)
Sr	2.0	-	Constant	No solubility limit
³ Tc	4.0x10 ⁻⁸	-	Constant	Duro et al. (2010)
Te	2.0	-	Constant	No solubility limit
Th	2.5x10 ⁻⁷	3.2	Lognormal	Duro et al. (2010)
U	3.5x10 ⁻⁸	3.2	Lognormal	Duro et al. (2010)
W	2.0	-	Constant	No solubility limit

¹The solubility values in this table are 10-fold larger than those listed in the original references to account for uncertainties, as discussed in the text.

²Constant value for the constant distribution function, and geometric mean for the lognormal distribution function.

³Sixth Case Study analyses erroneously assumed solubilities of 2.0 for Mo and Tc respectively.

6. REPOSITORY DATA

This section of the report describes the design of the deep geological repository, comprising the excavations for underground placement of the used fuel containers. Dimensions and parameters presented here are consistent with the current repository design (NWMO 2017, Chapter 4).

6.1 PHYSICAL LAYOUT

The deep geological repository consists of a system of access tunnels and placement rooms arranged in distinct panels. Figure 6.1 presents the design for the repository layout. The design consists of a total of 284 placement rooms, arranged in 8 panels. Placement rooms will be spaced a minimum of 20 m between centre-lines; the 20 m spacing is to prevent used fuel containers from reaching surface temperatures of over 100°C.

The repository is designed for a total capacity of 95,833 used fuel containers or 4,600,000 used fuel bundles. Assuming an ideal site, the minimum footprint of the underground repository would be approximately 1.7 km by 1.9 km (Figure 6.1). These dimensions do not account for any adaptations that may be required at an actual site to accommodate local conditions (e.g., specific rock structures, faults, or stress anomalies).

Each placement room will contain a maximum of 375 used fuel containers in buffer boxes. It is assumed that about 10% of the placement positions are unsuitable and that this space is filled with highly compacted bentonite blocks. This results in an average of 337.4 buffer boxes across the 284 placement rooms. Buffer boxes will be placed in the placement room in two levels and separated by blocks of highly compacted bentonite. The placement room is designed with a rectangular cross-section, as shown in Figure 6.2 and Figure 6.3 (NWMO 2017, Chapter 4). Placement room parameters are listed in Table 6.1.

The sealing materials used in placement rooms are:

- highly compacted bentonite blocks which surround the used fuel containers inside the buffer boxes;
- highly compacted bentonite blocks which act as 0.5-m-thick spacers between the buffer boxes; and
- gapfill which is placed on the floor before start of placement activities and in the nominal 100-mm-thick gap between the buffer boxes and spacer blocks and the rock wall and roof.

During the excavation process, drilled blast holes at the placement room perimeter are angled out by about 15 cm. This results in additional room volume which effectively increases the average placement room cross-sectional area by about 0.81 m². Although the angled “lookouts” are not explicitly modelled in the detailed FRAC3DVS-OPG models, the additional room volume is accounted for by using an average room width that incorporates the lookouts.

The excavation process will also create a ring of damaged rock surrounding all the placement rooms. This Excavation Damage Zone (EDZ) is more porous and has a higher hydraulic conductivity than the surrounding host rock. To minimize hydraulic flow between the placement rooms and access tunnels along the EDZ, bentonite clay will be keyed into the rock to interrupt

the EDZ transport path (see Figure 6.4). The excavation damaged zone is explicitly accounted for in the detailed FRAC3DVS-OPG models.

After closure of the repository, the access tunnels, perimeter tunnels, and panel access tunnels connecting the placement rooms would be backfilled with dense backfill blocks and light backfill, and tunnel bentonite seals with associated concrete bulkheads would be installed at strategic locations. Tunnel dimensions are shown in Figure 6.5 and tunnel parameters are listed in Table 6.2.

The repository design includes three shafts: main shaft, service shaft and ventilation shaft (see Figure 6.1). The excavated diameters of the main shaft, service shaft and ventilation shaft are 8 m, 7.5 m and 6.6 m, respectively. However, removal of the excavation damage zone, which will take place during decommissioning of the repository, will result in a nominal postclosure diameter of 9 m for the main shaft, 8.5 m for the service shaft and 7.6 m for the ventilation shaft. The proposed design for a shaft seal system is described in Table 6.3.

As-placed material properties of the engineered sealing materials used in the placement rooms, access tunnels, perimeter tunnels, panel access tunnels and shafts are listed in Table 6.4.

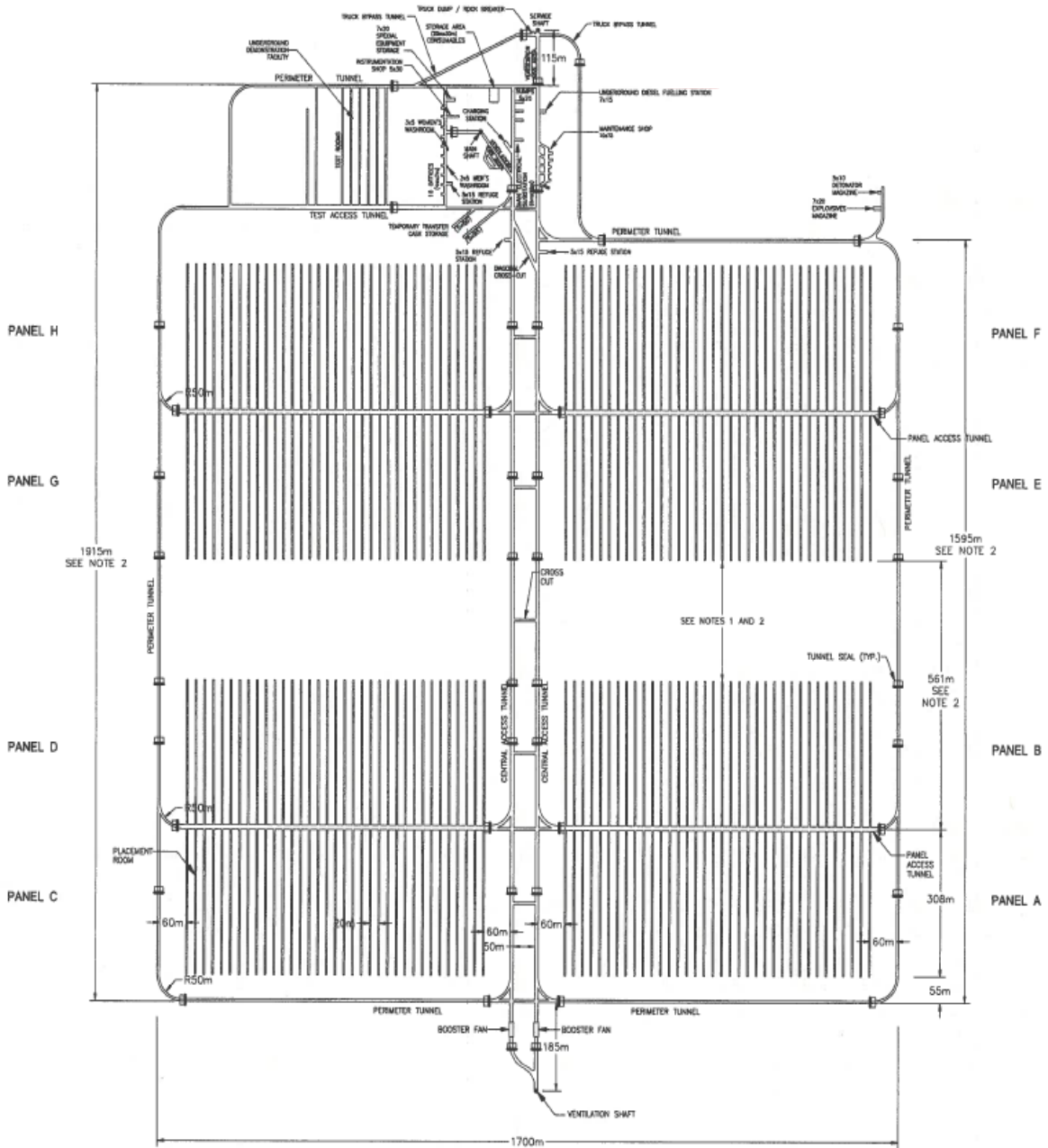


Figure 6.1: Plan View of Underground Repository

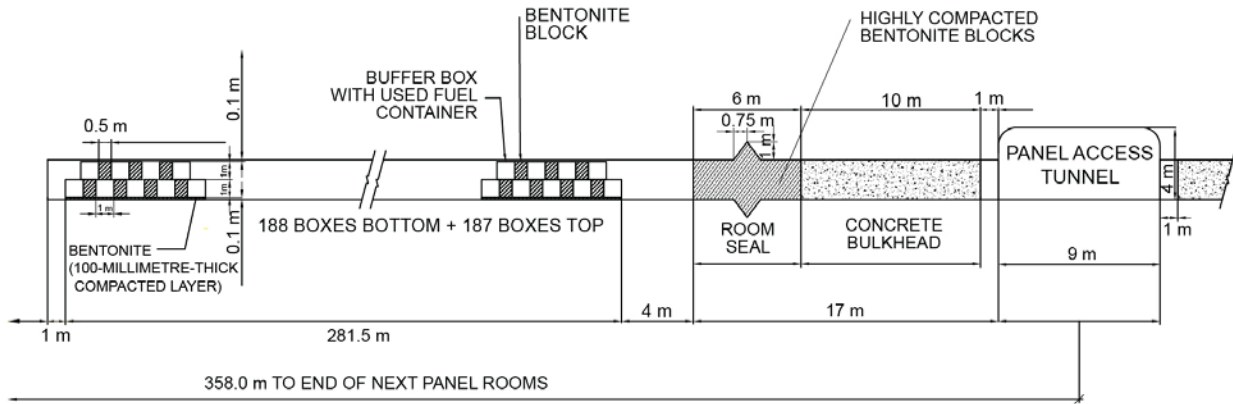


Figure 6.2: Placement Room Longitudinal Section

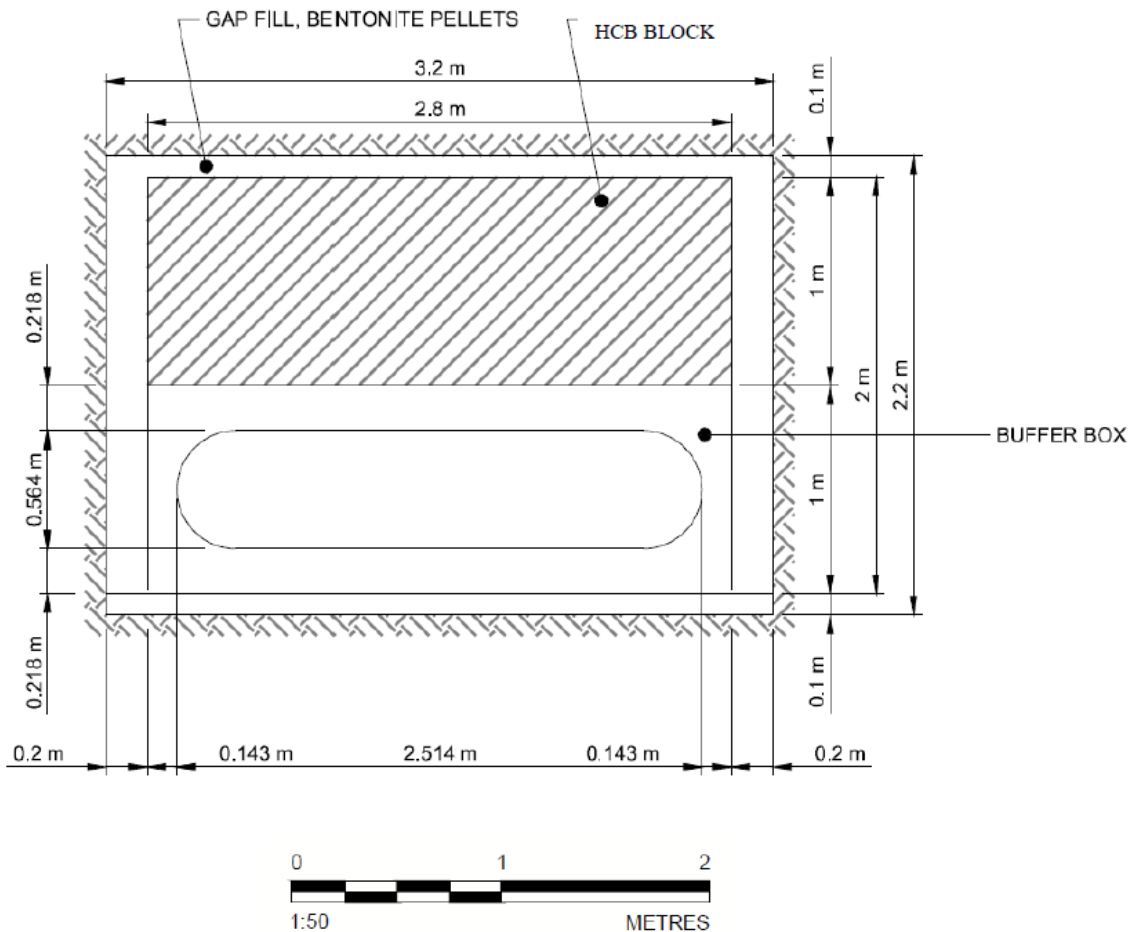


Figure 6.3: Placement Room Geometry

Table 6.1: Placement Room Parameters

Parameter	Value	Comment
Axial spacing between containers	1.5 m	NWMO (2017), Chapter 4
Placement room spacing	20 m	NWMO (2017), Chapter 4
Total number of containers	95,833	4.6x10 ⁶ fuel bundles, 48 bundles per container
Number of placement rooms	284	Arranged in eight panels as shown in Figure 6.1. Four panels with 35 placement rooms and four panels with 36 placement rooms.
Average number of Buffer Boxes (with containers) per placement room	337.4	95,833 Buffer Boxes (with containers) distributed across 284 placement rooms means an average of 337.4 Buffer Boxes per room. There are 375 Buffer Box positions per room available. It is assumed that 37.6 Buffer Box positions in each room (about 10% of the positions) are unsuitable and that this space is filled with 75.2 highly compacted bentonite blocks. The total volume occupied by 337.4 buffer boxes is 944.7 m ³ .
Placement room		
Width	3.20 m	Because the drilled blast holes at room perimeter are angled out by about 15 cm, there is additional room volume which effectively increases the average cross-section area by about 0.81 m ² .
Height	2.20 m	
Cross-sectional area	7.04 m ²	
Cross-sectional area with lookout	7.85 m ²	
Room Length	304 m	Distance from room end to room entrance
Useable Room Length	287 m	Distance from room end to inside surface of room seal
Volume of highly compacted bentonite per room with 338 Buffer Boxes in room	657 m ³	469.2 highly compacted bentonite blocks at 0.5m x 1.0m x 2.8m = 656.9 m ³ . There are 186 and 187 highly compacted bentonite blocks shown on top and bottom rows respectively and 17 dense backfill blocks between last row of Buffer Boxes and room seal. There is a nominal 1-m space at end of the room that would be filled by 6 highly compacted bentonite blocks. Last there are 75.2 highly compacted bentonite blocks filling unsuitable Buffer Box positions (see above). Total volume of room between end of room and the inside surface of room seal is 2253 m ³ (287m x 7.85m ²). Volume occupied by Buffer Boxes is 944.7 m ³ and by highly compacted bentonite blocks is 656.9 m ³ . Balance of space (651.4 m ³) is occupied by bentonite pellets.
Volume of 100% bentonite pellets per room with 338 Buffer Boxes in room	651 m ³	
Volume of highly compacted bentonite per room with 375 Buffer Boxes in room	552 m ³	394 highly compacted bentonite blocks at 0.5m x 1.0m x 2.8m = 551.6 m ³ . There are 186 and 187 highly compacted bentonite blocks shown on top and bottom rows respectively. There are 17 highly compacted bentonite blocks between last row of Buffer Boxes and room seal and there is a nominal 1-m space at end of the room that would be filled by 4 highly compacted bentonite blocks. Total volume of room between end of room and the inside surface of room seal is 2253 m ³ (287m x 7.85m ²). Volume occupied by Buffer Boxes is 1050 m ³ and by highly compacted bentonite blocks is 551.6 m ³ . Balance of space (651.4 m ³) is occupied by bentonite pellets.
Volume of 100% bentonite pellets per room with 375 Buffer Boxes in room	651 m ³	
Length of concrete bulkhead	10 m	
Volume of concrete	78.5 m ³	

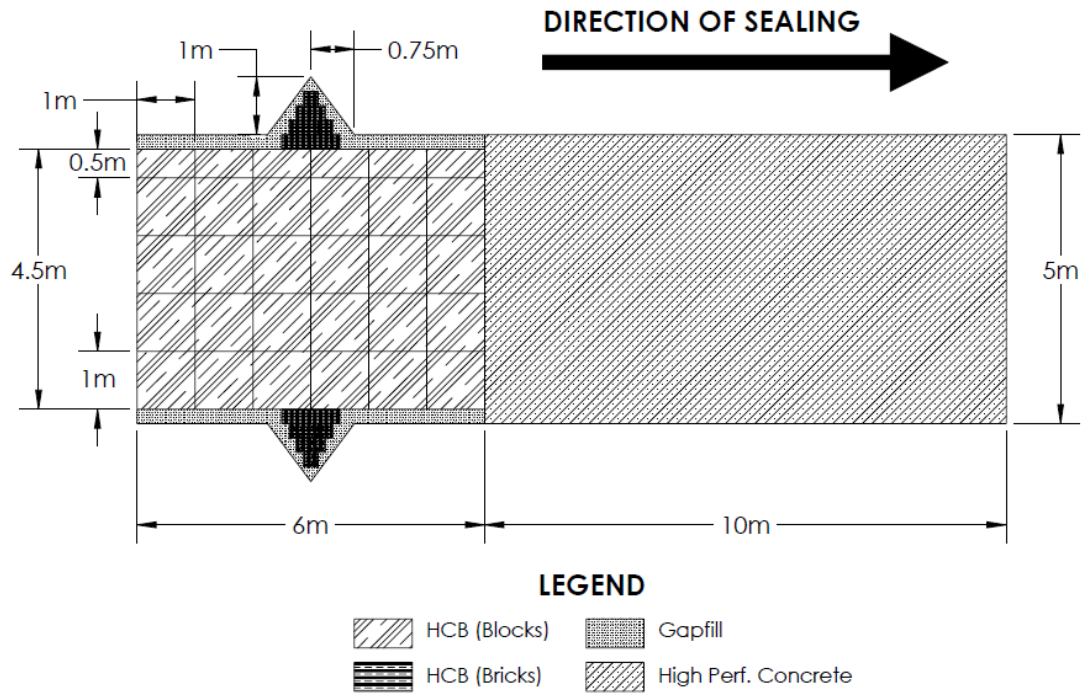
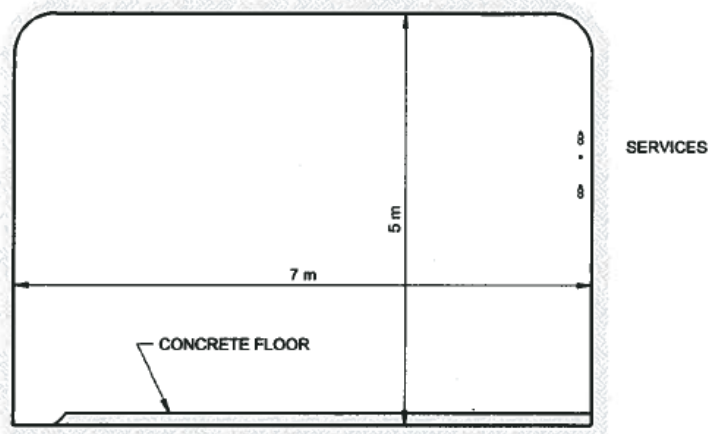
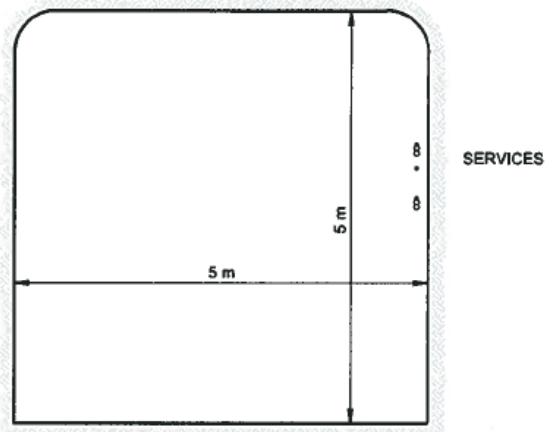


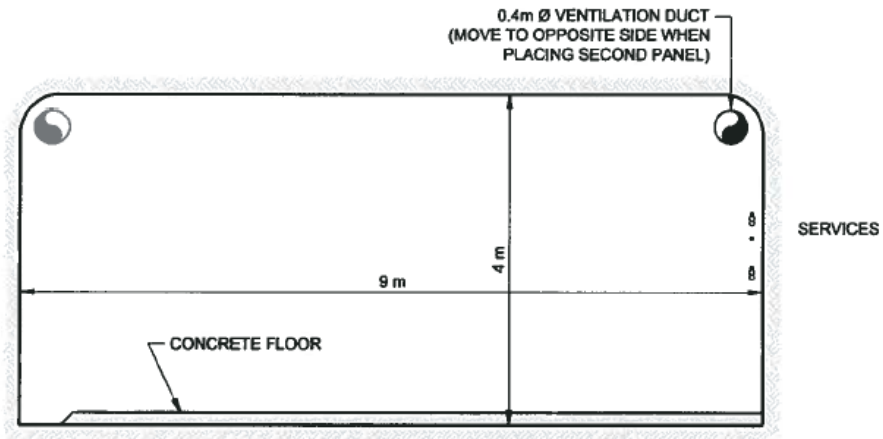
Figure 6.4: Longitudinal View of the Placement Room Seal



CENTRAL ACCESS TUNNEL



PERIMETER TUNNEL



PANEL ACCESS TUNNEL

5

Figure 6.5: Underground Repository Tunnel Sections

Table 6.2: Central Access Tunnels, Panel Access Tunnels, Perimeter Tunnels, and Shafts

Parameter	Value	Comment
Central Access Tunnels		
Width	7.0 m	See Figure 6.5
Height	5.0 m	
Area to be backfilled	35.0 m ²	An average of 264 mm-thick shell of light backfill pellets surrounding the dense backfill blocks including at the base of BDF blocks
Inner DGF blocks	28.9 m ²	
Outer light backfill pellets	6.1 m ²	
Panel Access Tunnels		
Width	9.0 m	See Figure 6.5
Height	4.0 m	
Area to be backfill	36.0 m ²	An average of 264 mm-thick shell of light backfill pellets surrounding the dense backfill blocks including at base of dense backfill blocks
Inner dense backfill blocks	29.4 m ²	
Outer bentonite pellets	6.6 m ²	
Perimeter Tunnels		
Width	5.0 m	See Figure 6.5
Height	5.0 m	
Area to be backfill	25.0 m ²	An average of 264 mm-thick shell of light backfill pellets surrounding the dense backfill blocks including at base of dense backfill blocks
Inner dense backfill blocks backfill	20.0 m ²	
Outer light backfill pellets	5.0 m ²	
Shafts		See NWMO 2017 (Chapter 4) for shaft design details.
Postclosure Main shaft Excavated diameter	9.0 m	The finished inside diameter of Main Shaft is 7.0 m. Assuming 500-mm-thick concrete liner, the excavated diameter will be 8000 mm. Assuming that a 500-mm-thick annulus of highly damaged rock is removed at time of shaft sealing, then the Postclosure nominal excavated shaft diameter will be 9.0 m.
Postclosure Service shaft Excavated diameter	8.5 m	
Postclosure Ventilation shaft excavated diameter	7.6 m	For the Service Shaft, the excavated diameter 7.5 m, and the Postclosure nominal shaft diameter will be 8.5 m
Backfill		For the ventilation Shaft, the excavated diameter 6.6 m, and the Postclosure nominal shaft diameter will be 7.6 m
		Shafts will be backfilled with sand, concrete, asphalt, and 70% bentonite/30% sand mixture (See Table 6.3)

Table 6.3: Proposed Sealing System for Shafts

Depth from Surface	Material
0 – 20 m	Low-heat high-performance concrete– concrete cap at surface
20 – 150 m	Shaft backfill - 70/30 bentonite/sand mixture compacted in-situ
150 – 170 m	Low-heat high-performance concrete for concrete bulkhead keyed into rock to a distance of 0.5 times the original radius of the shaft
170 – 330 m	Shaft backfill - 70/30 bentonite / sand mixture compacted in-situ
330 – 380 m	Asphalt or highly-compacted bentonite seal
380 – 480 m	Shaft backfill - 70/30 bentonite / sand mixture compacted in-situ
480 – 500 m	Concrete monolith – Low-heat high-performance concrete

Table 6.4: Properties of as Placed Materials in the Repository

Material ¹	Dry Density ^{2,3} [kg/m ³]	Saturation [%]	Porosity [%]	Bulk Density ⁴ [kg/m ³]	Thermal Conductivity ⁵ [W/m·K]	Heat Capacity ⁵ [J/kg·K]
Highly compacted bentonite (100% bentonite; MX-80 or equivalent)	1700	67	38.2	1955	1.0	1280
Dense backfill (5:25:70 bentonite:clay:aggregate)	2120	80	19.4	2276	2.0	1060
Gap fill (100% bentonite; MX-80 or equivalent)	1410	6	48.6	1439	0.4	870
Light backfill (50:50 bentonite:granitic sand)	1240	33	53.7	1418	0.7	1240
Shaft backfill (70:30 bentonite: granitic sand)	1600	80	41.1	1930	0.94	1360
Asphalt	N/A	N/A	2	1960	N/A	N/A
Concrete ⁶	N/A	50	5	2425	1.67	900

Notes:

1. Actual backfill compositions and their engineered physical properties will depend on the site-specific design requirements for a repository.
2. These data assume relative solid densities of 2.75, 2.67, 2.65, and 2.62 for MX-80 bentonite (80% montmorillonite), non-montmorillonite clay, silica sand, and granite (aggregate), respectively.
3. Dry densities represent a minimum requirement.
4. The density of water having 10 g/L salinity is 1005.8 kg/m³ at 20°C.
5. Material thermal conductivity and heat capacity are determined using calculations illustrated in Baumgartner (2006).
6. Concrete properties are from NWMO (2011) and Didry et al. (2000)

6.2 BUFFER

The containers are placed in buffer boxes comprised of highly compacted 100% bentonite. Upon placement, the buffer box surrounding the containers consists of a 1.0 m x 1.0 m x 2.8 m block of highly compacted bentonite, plus an additional 0.1 m of 100% bentonite pellets and gapfill between the buffer box and placement room walls (see Figure 6.3). Spaces between the buffer boxes are filled with highly compacted bentonite spacer blocks. The properties of the saturated buffer box and spacer block are listed in Table 6.5 and Table 6.6.

Table 6.5: Properties of Highly Compacted Bentonite in the Buffer Box and Spacer Blocks at Saturation

Property	Value	Comment
Dry density	1700 kg/m ³	
Porosity	38.2%	
Hydraulic conductivity	6x10 ⁻¹⁴ m/s	20°C value
Intrinsic permeability:	6x10 ⁻²¹ m ²	
Swelling pressure	11.5 MPa	

Note: Data listed are derived using calculations illustrated in Baumgartner (2006). It assumes that no volume change takes place for the material contained within the buffer box.

Table 6.6: Properties of Gapfill at Saturation

Property	Value	Comment
Dry density	1410 kg/m ³	
Porosity	48.6%	
Hydraulic conductivity	4x10 ⁻¹³ m/s	20°C value
Intrinsic permeability:	4x10 ⁻²⁰ m ²	
Swelling pressure	2.8 MPa	

Note: Data listed are derived using calculations illustrated in Baumgartner (2006).

With saturation, the highly compacted bentonite will swell and expand into the gapfill region, and the buffer layers will equilibrate to a uniform density. The properties of the homogenized bentonite at saturation are listed in Table 6.7.

Table 6.7: Homogenized Bentonite Properties at Saturation

Parameter	Value	Comment
Dry density	1600 kg/m ³	The highly compacted bentonite and bentonite Gap Fill pellets have equilibrated at saturation.
Porosity	41.6%	Averaged
Hydraulic conductivity	1x10 ⁻¹³ m/s	20°C value
Intrinsic permeability	1x10 ⁻²⁰ m ²	
Swelling pressure	7.1 MPa	Saturated

Note: Weighted average combined highly compacted bentonite and Gap Fill Material. Data listed are derived using calculations illustrated in Baumgartner (2006).

6.3 BACKFILL

Access and perimeter tunnels will be backfilled with dense backfill blocks during the closure of the repository. The dense backfill blocks are composed of 5 wt% bentonite, 25 wt% glacial clay, 70 wt% crushed granite aggregate (Dixon et al. 2001). To fill the gaps around the dense backfill blocks, light backfill pellets and gapfill are blown in; light backfill pellets are 50 wt% crushed granite and 50% bentonite (Dixon et al. 2001). The saturated properties of the backfilling materials are given in Table 6.8 and Table 6.9.

Table 6.8: Properties of Dense Backfill at saturation

Property	Value	Comment
Dry density	2120 kg/m ³	
Porosity	19.5%	
Hydraulic conductivity	9x10 ⁻¹¹ m/s	20°C
Intrinsic permeability:	9x10 ⁻¹⁸ m ²	
Swelling pressure	42 kPa	

Note: Data listed are derived using calculations illustrated in Baumgartner (2006).

Table 6.9: Properties of Light Backfill at saturation

Property	Value	Comment
Dry density	1240 kg/m ³	
Porosity	53.7%	
Hydraulic conductivity	1x10 ⁻¹¹ m/s	20°C
Intrinsic permeability:	1x10 ⁻¹⁸ m ²	
Swelling pressure	188 kPa	

Note: Data listed are derived using calculations illustrated in Baumgartner (2006).

The shaft seal design calls for a sealing backfill material comprised of 70% bentonite and 30% sand. Its properties at saturation are provided in Table 6.10.

Table 6.10: Properties of 70% bentonite / 30% sand at saturation

Property	Value	Comment
Dry density	1600 kg/m ³	Design provisions may be required to ensure that density does not fall below this absolute minimum value
Porosity	41.1%	
Hydraulic conductivity	5x10 ⁻¹³ m/s	20°C value
Intrinsic permeability:	5x10 ⁻²⁰ m ²	
Swelling pressure	2.30 MPa	

Note: Data listed are derived using calculations illustrated in Baumgartner (2006).

6.4 CONCRETE

The reference concrete is a Low-Heat High-Performance Concrete that is designed to minimize effects on the adjacent clay (Dixon et al. 2001). Transport modelling assumes degraded concrete properties from the time of closure, to account for degradation of concrete over tens of thousands of years (Quintessa and Geofirma 2011). The relevant properties of this concrete are summarized in Table 6.11.

Table 6.11: Properties of Concrete at Saturation

Property	Value	Comment
Dry density	2390 kg/m ³	
Porosity	10%	
Hydraulic conductivity	1x10 ⁻¹⁰ m/s	20°C value
Intrinsic permeability:	1x10 ⁻¹⁷ m ²	

Note: Data listed are provided in NWMO (2011).

6.5 ASPHALT

The shaft seal design concept includes a 50 m thick asphalt layer, as shown in Table 6.3. This provides a redundant low-permeable seal material. The reference asphalt mastic mix is the same as proposed for use in the Waste Isolation Pilot Plant (WIPP 2009). It contains 70% (by weight) silica sand, 20% asphalt and 10% hydrated lime. The high sand content provides a mechanical framework, the high asphalt content relative to conventional (road) asphalt provides this mixture with more plasticity, and the hydrated lime helps to stabilize the mixture and minimize microbial activity.

The relevant properties of the asphalt layer are provided in Table 6.12.

Table 6.12: Properties of Asphalt at Saturation

Property	Value	Comment
Bulk density	1960 kg/m ³	
Porosity	2%	
Hydraulic conductivity	1x10 ⁻¹² m/s	20°C value
Effective diffusivity	1x10 ⁻¹³ m ² /s	

Note: Data listed are provided in NWMO (2011).

6.6 DIFFUSION COEFFICIENTS

The diffusive transport of contaminants is described, in part, by their effective (or intrinsic) diffusivity in the medium (D_e).

6.6.1 Buffer

The measured effective diffusivity of contaminants in dense buffer materials under reducing conditions varies from about 10⁻¹² to 10⁻⁹ m²/s (Oscarson et al. 1995; Yu and Neretnieks 1997;

JNC 2000). Some nuclides are expected to be present in the buffer as anionic species, notably I and Cl (and possibly Se and Po as well, though not accounted for in this work). For these species, repulsion by the nominally negative surface charge on the clay particles results a lower effective porosity and, consequently, a lower effective diffusivity than for neutral or cationic species (Wersin and Schwyn 2004, Yu and Neretnieks 1997). The effective buffer porosity for anions is 0.165, based on the anion porosity (0.174) from SKB (2010) and the ratio of the porosities of the buffers in the SKB (0.44) and Sixth Case Study (0.416) repositories.

Effective diffusivities for the engineered clay-based sealing materials are listed in Table 6.13 and are described by a triangular probability density function. These values, which account for the possible effects of ion exclusion or surface diffusion on diffusive transport, are taken from SKB (2010), in which different elements are sorted into three categories: anionic elements, non-charged and hydrolyzable cationic elements, and cesium. The values listed for bentonite are sufficiently representative of all clay-based sealants in the repository design, except for dense backfill.

Table 6.13: Buffer Effective Diffusion Coefficients at 25°C

Element	Effective Diffusivity [m ² /a]		
	Peak Value	Lower Bound	Upper Bound
Anions (I, Cl, Br)	3.5x10 ⁻⁴	1.9x10 ⁻⁵	1.9x10 ⁻³
Neutral and hydrolysable cations (i.e., all other elements)	4.4x10 ⁻³	2.9x10 ⁻³	6.6x10 ⁻³
Cs	1.3x10 ⁻²	3.0x10 ⁻³	1.3x10 ⁻²

Note: Effective diffusivities are defined using triangular probability density functions. Data are based on SR-Site data report (SKB 2010); data are sufficiently representative of all clay-based sealants included in the vault design, except for dense backfill.

6.6.2 Backfill

For anionic species, repulsion by the nominally negative surface charge on the clay particles results in a lower effective porosity and, consequently, a lower effective diffusivity than for neutral or cationic species. The effective backfill porosity for anions is taken to be 0.077, based on the anion porosity (0.174) from SKB (2010) and the ratio of the porosities of the buffer in the SKB repository (0.44) and the backfill (0.195) in the Sixth Case Study repository.

Effective diffusivities for the backfill are listed in Table 6.14 and are described by a triangular probability density function. These values, which account for the possible effects of ion exclusion or surface diffusion on diffusive transport, are taken from the SKB (2006), in which elements are sorted into three categories: anionic elements, non-charged and hydrolysable cationic elements and cesium.

Table 6.14: Backfill Effective Diffusion Coefficients at 25°C

Element	Effective Diffusivity [m ² /a]		
	Peak Value	Lower Bound	Upper Bound
Anions (I, Cl, Br)	1.3x10 ⁻⁴	4.1x10 ⁻⁵	4.1x10 ⁻³
Neutral and hydrolysable cations (i.e., all other elements)	1.6x10 ⁻³	6.6x10 ⁻⁴	2.5x10 ⁻³
Cs	4.1x10 ⁻²	6.6x10 ⁻⁴	4.1x10 ⁻³

Note: Effective diffusivities are defined using triangular probability density functions. Values for the dense backfill are adopted from the SR-Can data report (SKB 2006).

6.6.3 Concrete

The effective diffusivity of all contaminants in concrete is taken to be 3.9x10⁻³ m²/a (Quintessa and Geofirma 2011).

6.6.4 Asphalt

The effective diffusivity of all contaminants in asphalt is 3.16x10⁻⁶ m²/a (Quintessa and Geofirma 2011).

6.7 SORPTION COEFFICIENTS AND CAPACITY FACTORS

Radionuclides can become attached to minerals found in the engineering sealing materials. This can be due to a number of physical or chemical processes. The net effect of these processes can be approximated through use of an adsorption coefficient. Adsorption coefficients are listed in Table 6.15 and are described by a triangular probability density function over the indicated range.

The sorption properties of the buffer can also be described by a capacity factor, $CF = \varepsilon + \rho \cdot K_d$, where ε is the porosity of the buffer or backfill, ρ is the dry bulk density, and K_d is the sorption coefficient. Capacity factors are listed in Table 6.16 and are described by a triangular probability density function over the indicated range.

6.7.1 Buffer

Where available, sorption coefficients are taken from Vilks (2011); otherwise, values for the highly-compacted bentonite buffer material are taken from SKB (2010). The SKB sorption coefficients are based on a comprehensive review of sorption data by Ochs and Talerico (2004). Both Vilks (2011) and SKB (2010) report the uncertainties and/or ranges in the sorption coefficient values.

Several sorption values are defined by use of chemical analogs: Ac by Am (trivalent actinides); Ca, Cd, and Sb by Sr (alkali earth metals or similar chemistry); Br by I (both halides); and Te by Se (chalcogens). Based on its likely speciation (as HCO₃⁻), the sorption coefficient of carbon

has been set to zero, i.e., carbon is not expected to sorb strongly onto any of the sealing materials. The sorption coefficients for Hg, Mo, and W are set to zero for conservatism.

Sorption coefficients are listed in Table 6.15 and capacity factors are listed in Table 6.16. The sorption coefficients are described by a triangular probability density function (with the lower and upper bounds equal to the pessimistic and optimistic values, respectively). The values listed for bentonite are sufficiently representative of all clay-based sealants in the repository design, except for dense backfill which is described in next section.

6.7.2 Backfill

Backfill sorption coefficients are listed in Table 6.15 and capacity factors are listed in Table 6.16. The sorption coefficients are described by a triangular probability density function (with the lower and upper bounds equal to the pessimistic and optimistic values, respectively).

Sorption coefficients are generally taken from SKB (2006), which are based on a comprehensive review of sorption data by Ochs and Talerico (2004). However, for conservatism, the sorption coefficients of C and Ra are set to zero.

Many sorption values are defined by use of chemical analogs: Ac by Am (trivalent actinides); Ca, Cd, and Sb by Sr (alkali earth metals or similar chemistry); Br by I (both halides); and Te by Se (chalcogens). Finally, for Ag, Hg, Mo, Po, and W, data are not available so the backfill sorption coefficient is conservatively set to zero.

6.7.3 Concrete

Sorption coefficients for concrete are from NAGRA (2004), where available, and are provided in Table 6.15 and capacity factors are listed in Table 6.16. Many sorption values are defined by use of chemical analogs: Ca, Cd, and Sb by Sr (alkali earth metals or similar chemistry); Br by I (halides); and Te by Se (chalcogens). For Ag, Bi, Hg, Mo, Pd, Rn, and W data are not available for concrete so the sorption coefficient is set to zero for conservatism.

6.7.4 Asphalt

Owing to a lack of sorption data, and due to the small porosity and small physical extent of this material, all sorption coefficients for the asphalt shaft seal are conservatively taken to be zero.

Table 6.15: Sorption Coefficients in the Bentonite, Backfill and Concrete

Element	Bentonite [m ³ /kg]			Backfill [m ³ /kg]			Concrete [m ³ /kg]		
	Median Value	Lower Bound	Upper Bound	Median Value	Lower Bound	Upper Bound	Median Value	Lower Bound	Upper Bound
Ac	61	10	380	19	3.2	110	80	20	300
Ag	0	0	15	3.5x10 ⁻³	7.0x10 ⁻⁴	4.5	0	0	0
Am	61	10	380	19	3.2	110	80	20	300
Bi	35	25	50	2.5	0.31	28	0	0	0
Br	0	0	0	0	0	0	0	0	0
C	0	0	0	0	0	0	0	0	0
Ca	4.5x10 ⁻³	7.5x10 ⁻⁴	0.027	1.5x10 ⁻³	2.8x10 ⁻⁴	9.7x10 ⁻³	1.0x10 ⁻³	7.0x10 ⁻⁴	1.0x10 ⁻³
Cd	4.5x10 ⁻³	7.5x10 ⁻⁴	0.027	1.5x10 ⁻³	2.8x10 ⁻⁴	9.7x10 ⁻³	1.0x10 ⁻³	7.0x10 ⁻⁴	1.0x10 ⁻³
Cl	0	0	0	0	0	0	5.0x10 ⁻³	3.0x10 ⁻³	7.0x10 ⁻³
Cs	0.093	0.015	0.56	0.036	6.1x10 ⁻³	0.19	5.0x10 ⁻⁴	3.0x10 ⁻⁴	7.0x10 ⁻⁴
Hg	0	0	0	0	0	0	0	0	0
I	0	0	0	0	0	0	0	0	0
Mo	0	0	0	0	0	0	0	0	0
Np	63	4	1100	19	1.2	330	80	20	300
Pa	3	0.2	45	0.97	0.095	14	0.1	0.07	0.1
Pb	74	12	460	22	3.6	140	0.5	0.3	0.7
Pd	5	0.3	75	1.5	0.09	23	0	0	0
Po	0.06	8.0x10 ⁻³	0.5	0	0	0	0	0	0
Pu	63	4	1100	19	1.3	330	80	20	300
Ra	4.5x10 ⁻³	7.5x10 ⁻⁴	0.027	0	0	0	0.05	0.03	0.07
Rn	0	0	0	0	0	0	0	0	0
Sb	4.5x10 ⁻³	7.5x10 ⁻⁴	0.027	1.5x10 ⁻³	2.8x10 ⁻⁴	9.7x10 ⁻³	1.0x10 ⁻³	7.0x10 ⁻⁴	1.0x10 ⁻³
Se	0	0	0	7.0x10 ⁻⁵	3.5x10 ⁻⁵	3.5x10 ⁻⁴	0.03	0.02	0.04
Sn	63	2.3	1800	19	0.69	530	10	2	30
Sr	4.5x10 ⁻³	7.5x10 ⁻⁴	0.027	1.5x10 ⁻³	2.8x10 ⁻⁴	9.7x10 ⁻³	1.0x10 ⁻³	7.0x10 ⁻⁴	1.0x10 ⁻³
Tc	63	2.3	1800	19	0.69	530	10	2	30
Te	0	0	0	7.0x10 ⁻⁵	3.5x10 ⁻⁵	3.5x10 ⁻⁴	0.03	0.02	0.04
Th	63	3.6	700	19	1.2	330	80	20	300
U	63	3.6	1100	19	1.2	330	2	1	2
W	0	0	0	0	0	0	0	0	0

Note: Adsorption coefficients are defined using triangular probability density functions, with the exception of a lognormal distribution for bismuth sorption on bentonite (geometric mean of 35, geometric standard deviation of 1.6, ranging from 25-50). The bentonite values are also used for light backfill and 70% bentonite.

Table 6.16: Capacity Factors for the Bentonite, Backfill and Concrete

Element	Bentonite [-]			Backfill [-]			Concrete [-]		
	Median Value	Lower Bound	Upper Bound	Median Value	Lower Bound	Upper Bound	Median Value	Lower Bound	Upper Bound
Ac	9.8x10 ⁴	1.6x10 ⁴	6.1x10 ⁵	4.0x10 ⁴	6.8x10 ³	2.3x10 ⁵	2.0x10 ⁵	5.0x10 ⁴	7.5x10 ⁵
Ag	0.416	0.416	24000	7.6	1.7	9.5x10 ³	0.1	0.1	0.1
Am	9.8x10 ⁴	1.6x10 ⁴	6.1x10 ⁵	4.0x10 ⁴	6.8x10 ³	2.3x10 ⁵	2.0x10 ⁵	5.0x10 ⁴	7.5x10 ⁵
Bi	5.6x10 ⁴	4.0x10 ⁴	8.0x10 ⁴	5.3x10 ³	660	5.9x10 ⁴	0.1	0.1	0.1
Br	0.165	0.165	0.165	0.077	0.077	0.077	0.1	0.1	0.1
C	0.416	0.416	0.416	0.195	0.195	0.195	0.1	0.1	0.1
Ca	7.6	1.6	44	3.4	0.79	21	2.6	1.8	2.6
Cd	7.6	1.6	44	3.4	0.79	21	2.6	1.8	2.6
Cl	0.165	0.165	0.165	0.077	0.077	0.077	12.6	7.6	17.5
Cs	149	24	900	76.5	13	400	1.35	0.85	1.8
Hg	0.416	0.416	0.416	0.195	0.195	0.195	0.1	0.1	0.1
I	0.165	0.165	0.165	0.077	0.077	0.077	0.1	0.1	0.1
Mo	0.416	0.416	0.416	0.195	0.195	0.195	0.1	0.1	0.1
Np	1.0x10 ⁵	6.4x10 ³	1.8x10 ⁶	4.0x10 ⁴	2.5x10 ³	7.0x10 ⁵	2.0x10 ⁵	5.0x10 ⁴	7.5x10 ⁵
Pa	4.8x10 ³	320	7.2x10 ⁴	2.1x10 ³	200	3.0x10 ⁴	250	175	250
Pb	1.2x10 ⁵	1.9x10 ⁴	7.4x10 ⁵	4.7x10 ⁴	7.6x10 ³	3.0x10 ⁵	1.2x10 ³	750	1.7x10 ³
Pd	8.0x10 ³	480	1.2x10 ⁵	3.2x10 ³	190	4.9x10 ⁴	0.1	0.1	0.1
Po	96	13	800	0.195	0.195	0.195	0.1	0.1	0.1
Pu	1.0x10 ⁵	6.4x10 ³	2.9x10 ⁶	4.0x10 ⁴	2.7x10 ³	7.0x10 ⁵	2.5x10 ⁴	5.0x10 ³	7.5x10 ⁴
Ra	7.6	1.6	44	0.195	0.195	0.195	124.65	74.83	174.47
Rn	0.416	0.416	0.416	0.195	0.195	0.195	0.1	0.1	0.1
Sb	7.6	1.6	44	3.4	0.79	21	2.6	1.8	2.6
Se	0.416	0.416	0.416	0.34	0.27	0.94	75	50	100
Sn	1.0x10 ⁵	3.7x10 ³	2.9x10 ⁶	4.0x10 ⁴	1.5x10 ³	1.1x10 ⁶	2.5x10 ⁴	5.0x10 ³	7.5x10 ⁴
Sr	7.6	1.6	44	3.4	0.79	21	2.6	1.8	2.6
Tc	1.0x10 ⁵	3.7x10 ³	2.9x10 ⁶	4.0x10 ⁴	1.5x10 ³	1.1x10 ⁶	2.5x10 ⁴	5.0x10 ³	7.5x10 ⁴
Te	0.416	0.416	0.416	0.34	0.27	0.94	75	50	100
Th	1.0x10 ⁵	9.6x10 ³	1.1x10 ⁶	4.0x10 ⁴	4.0x10 ³	4.5x10 ⁵	2.0x10 ⁵	5.0x10 ⁴	7.5x10 ⁵
U	1.0x10 ⁵	5.8x10 ³	1.8x10 ⁶	4.0x10 ⁴	2.5x10 ³	7.0x10 ⁵	5.0x10 ³	2.5x10 ³	5.0x10 ³
W	0.416	0.416	0.416	0.195	0.195	0.195	0.1	0.1	0.1

Note: Capacity factors are defined using triangular probability density functions, with the exception of a lognormal distribution for bismuth (geometric mean of 5.5x10⁴, geometric standard deviation of 1.6, ranging from 4.0x10⁴ to 8.0x10⁴). The bentonite values are also used for light backfill and 70% bentonite.

6.8 EFFECT OF INCREASED TEMPERATURE

As discussed in Section 5.2 and Guo (2016) it is anticipated that the sealing materials around the containers will experience an increase in temperature. The reference temperature in the highly compacted bentonite around the containers is assumed to be 85°C over the postclosure period. Backfilling materials used in the access tunnels and shafts as well as the host rock do not experience such a high increase, and temperatures are assumed to remain at ambient temperature at these locations.

6.8.1 Physical Properties

Density and porosity of the engineered sealing materials are not expected to be significantly affected by increased temperature. No correction is applied to these data.

6.8.2 Hydraulic Conductivity

Hydraulic conductivity (and correspondingly permeability) increases with increased temperature. Table 6.7 lists the homogenized buffer hydraulic conductivity as 1×10^{-13} m/s for 20°C. An increase in temperature to 85°C corresponds to a factor 3.1 times increase in the buffer hydraulic conductivity. Despite this increased hydraulic conductivity, groundwater velocities in the buffer are still expected to be extremely small and transport should remain diffusion dominant.

6.8.3 Diffusion Coefficients

Diffusivity increases with increased temperature. Assuming the diffusivity scales with temperature T and porewater viscosity $\mu(T)$ as described below (Rohsenow and Choi 1961, p.383) the resulting diffusivity is a factor 3.2 times higher at 85°C than at room temperature.

$$D_i = D_{i298k} \frac{T}{298K} \frac{\mu_{298K}}{\mu(T)}$$

Viscosity values are discussed in Table 7.9

6.8.4 Sorption Coefficients

Elemental sorption coefficients on buffer materials are not assumed to be significantly affected by increased temperature. No correction is applied to these data.

7. GEOSPHERE DATA

7.1 GENERAL SITE DESCRIPTION

The repository in the Sixth Case Study is located at a hypothetical but plausible Canadian Shield site. The surface topography of the ~200 km² subregional watershed area around the site is relatively flat, as illustrated in Figure 7.1. A major river passes through the watershed, which is bounded by topographic highs to the north and south. The reference repository location is north of the major river and enclosed by a smaller river system.

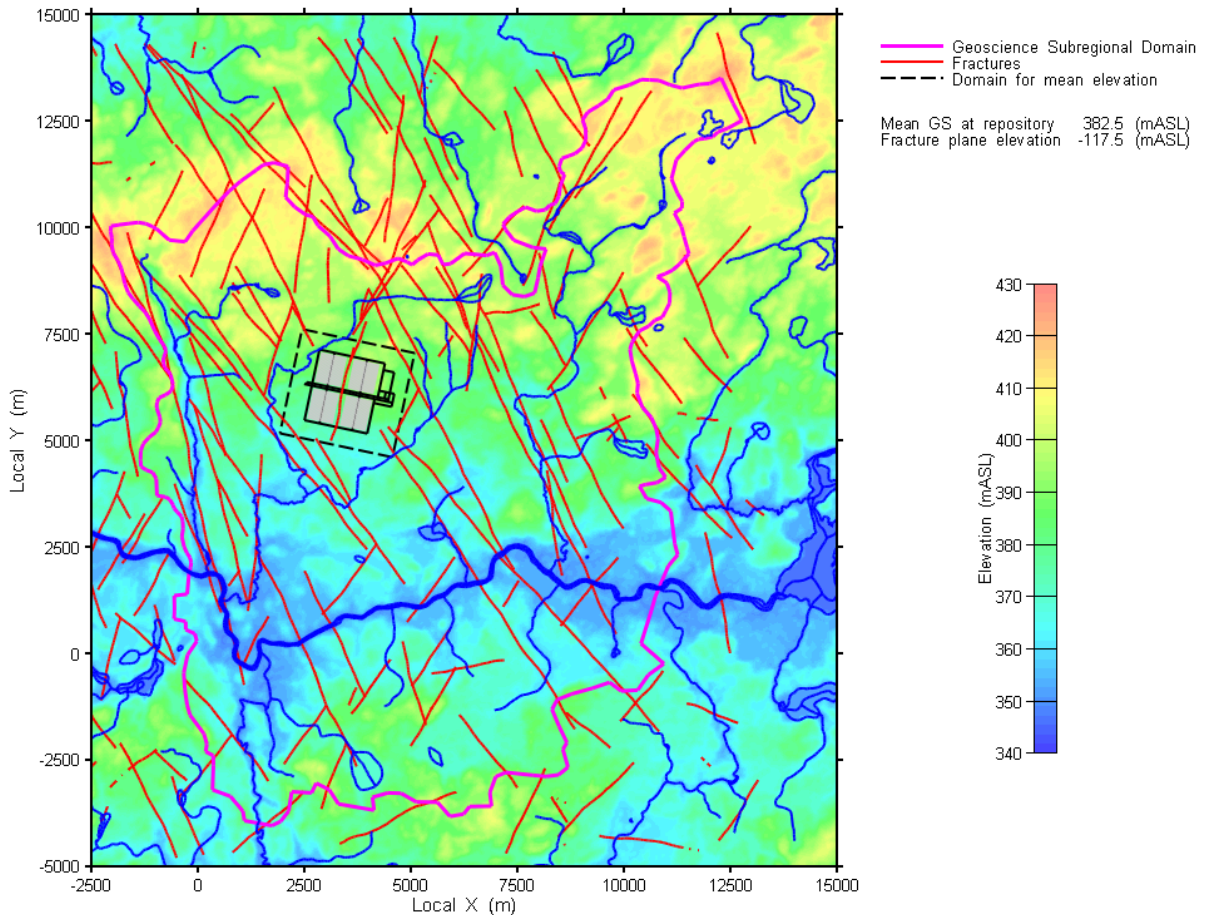


Figure 7.1: Hypothetical Subregional Area

Since the surface elevation varies, an absolute co-ordinate system has been defined relative to sea level. The ground surface above the repository is at approximately 382.5 m Above Sea Level (mASL) and the repository is located at -117.5 mASL.

For the hypothetical Sixth Case Study site, a set of major fractures (500 m or longer) was defined across the entire ~200 km² subregional area down to a depth of 1500 m (Srivastava 2002). The fracture network is illustrated in Figure 7.2. This figure illustrates the complexity of

the fracture network at the subregional level. Although not obvious from this figure, the network consists of a large number of intersecting features within the first few hundred meters depth, and much fewer larger and more vertical features extending to greater depths.

The bedrock around the site is Canadian Shield granite, extending up to close to the surface. The properties of this granite are largely based on the properties of granite at the Whiteshell (Manitoba) and Atikokan (Ontario) Research Areas (Stevenson et al. 1996, Ophori and Chan 1996).

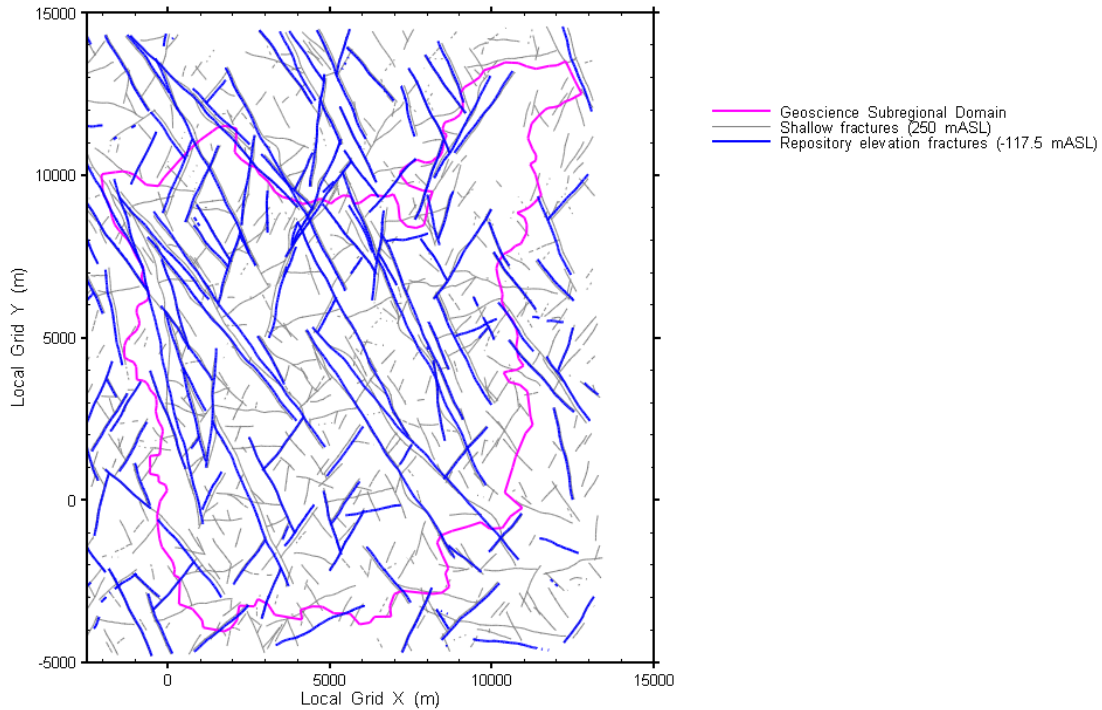


Figure 7.2: Fracture Network in 2D Local

7.2 PHYSICAL AND CHEMICAL CHARACTERISTICS OF THE GEOSPHERE

This section describes the physical and chemical properties of the host rock and fracture system.

Table 7.1 and Table 7.2 summarize the assumed physical and chemical characteristics of the geosphere zones at the Sixth Case Study site. The rock mass (hydraulic) conductivity is represented as a series of horizontally uniform layers with isotropic conductivity, and with conductivity decreasing with depth. The uncertainty in the conductivity is represented by considering a couple of cases of conductivity versus depth, as shown in Table 7.1 and Figure 7.3. Also shown in Figure 7.3, for comparison, are deep borehole data from two research locations on the Canadian Shield, Whiteshell and Atikokan.

Table 7.1: Physical Parameters of the Host Rock

Zone	Layer	Depth ¹ [mBGS]	Thick ness [m]	Conductivity [m/s]			Density ² [kg/m ³]	Porosity ³ [-]	Tortuosity [-]	Specific Storage [m ⁻¹]	Mineral Composition [%]
				Ref. Case	Sens. Case 1	Sens. Case 2					
Shallow Ground water Zone	Sediment	0 - 10	0 - 10	1x10 ⁻⁵	1x10 ⁻⁵	1x10 ⁻⁵	1537	0.5	0.75	1.0x10 ⁻⁷	70% clay 20% silt 10% sand
	Overburden	0 - 10	0 - 10	1x10 ⁻⁸	1x10 ⁻⁸	1x10 ⁻⁸	1250	0.42	1		100% organics
	Rock Mass Permeability Zone 1	10 - 150	140	2x10 ⁻⁹	2x10 ⁻⁸	2x10 ⁻¹⁰	2700	0.003	1		100% granite
	Shallow Fracture Zone	0 - 150	150	1x10 ⁻⁶			2400	0.1	1		100% granite
Inter- mediate Ground water Zone	Rock Mass Permeability Zone 2	150 - 700	550	4x10 ⁻¹¹	4x10 ⁻¹⁰	4x10 ⁻¹²	2700	0.003	0.06	1.0x10 ⁻⁷	100% granite
	Intermediate Fracture Zone	150 - 700	550	1x10 ⁻⁶			2400	0.1	1		100% granite
Deep Ground water Zone	Rock Mass Permeability Zone 3	700 - 1500	800	1x10 ⁻¹¹	1x10 ⁻¹⁰	1x10 ⁻¹²	2700	0.003	0.06	1.0x10 ⁻⁷	100% granite
	Deep Fracture Zone	700 - 1500	800	1x10 ⁻⁶			2400	0.1	1		100% granite

¹All values presented in metres Below Ground Surface (mBGS) are measured relative to the average metres Above Sea Level (mASL) for the topography contained within the footprint of the repository.

²Density Values taken from Davison et al. 1994, App. D

³Porosity values taken from Davison et al. 1994, App. D

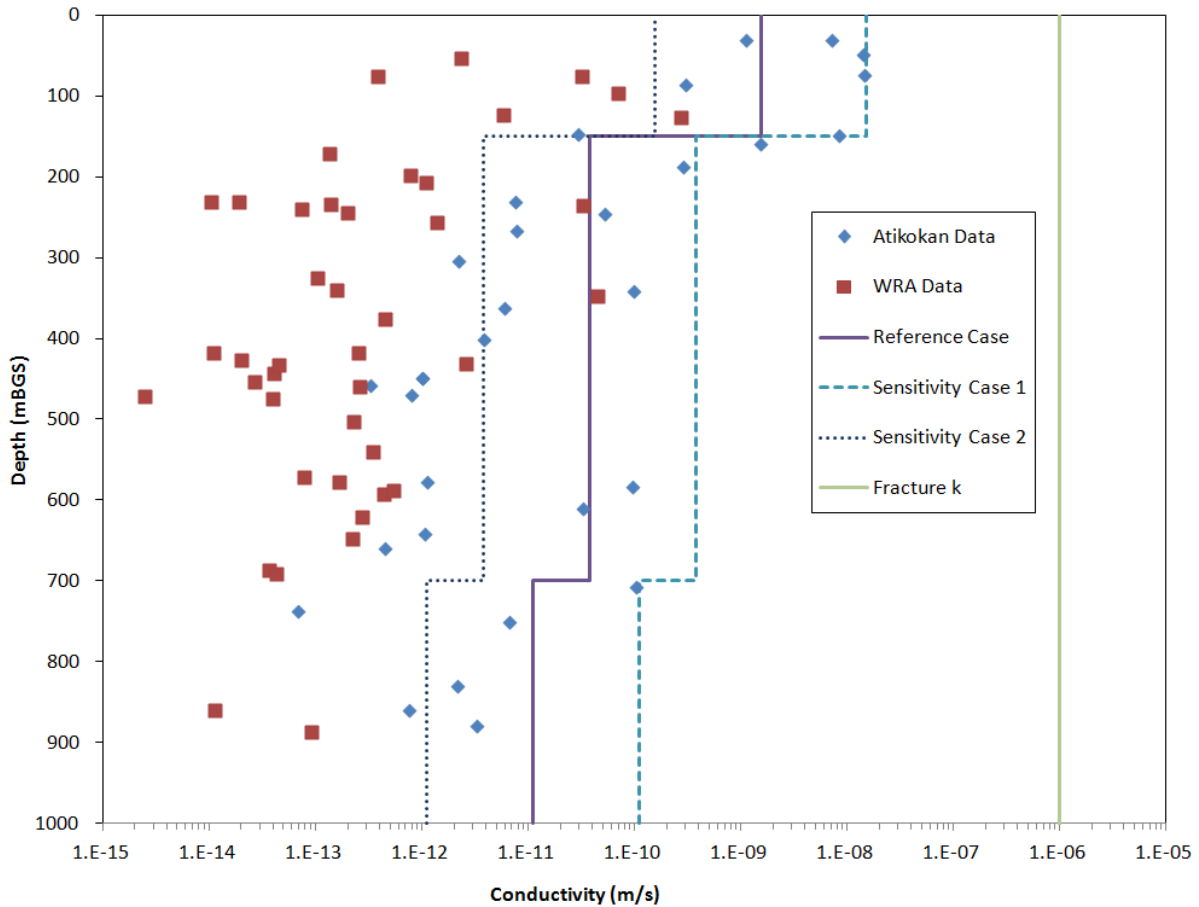


Figure 7.3: Conductivity versus Depth Profiles of the Rock Mass and Fractures

The Reference Case and Sensitivity Cases 1 and 2 conductivity profiles range between a sparsely fractured granitic rock and a more permeable rock. The conductivity profile for the Reference Case represents a medium permeability rock. Sensitivity Case 1 examines the influence of rock conductivity values 10-fold lower than those used in the Reference Case. The impact of higher conductivity values is examined in Sensitivity Case 2 in which the rock conductivity is 10-fold larger than in the Reference Case values for depths greater than 10 m.

The fractures identified in Table 7.1 are conservatively assumed to have a high conductivity of 1×10^{-6} m/s as indicated in Figure 7.3. The fractures are assumed to have an effective thickness of 1 m and a porosity of 0.1.

The rock temperature around the repository will vary with time as the heat load from the used fuel is dissipated into the rock. Preliminary analysis of the heat generated by the repository shows that the heat is largely contained within the repository itself and the heat does not extend any appreciable distance into the nearby rock (Guo 2016). It is assumed that the rock is at ambient temperature over time frames of interest for contaminant transport.

It is assumed that the bedrock is close to the surface. Specifically, the overburden thickness is characterized by a lognormal probability density function with a geometric mean of 4 m, a geometric standard deviation of 1.7 m, and range from 0 to 20 m, based on field experience with support from Singer and Cheng (2002). Davison et al. (1994, p.415) indicate that the sediment thickness under Canadian Shield lakes can be described as a lognormal probability density function with geometric mean of 3.7 m, geometric standard deviation of 2.2 m and bounds of 0.3 to 10 m. In the Sixth Case Study, the mean sediment thickness underneath the rivers near the repository was further reduced by a factor of 10 due to its higher flow rate. The overburden and sediment conductivities given in Table 7.1 are based on measurements at the Whiteshell site (Appendix D of Davison et al. 1994).

Colloids

Available evidence shows that the concentrations of natural colloids are low in the Canadian Shield (Davison et al. 1994, p.337), probably in the order of 0.04-4 mg/L. An additional potentially important source of colloids will be from the clay materials in the engineered barriers in the repository. However, while these concentrations could be on the order of 40 mg/L in low salinity water, the concentrations will be much lower for the expected salinities at the site (11.6 g/L, see Table 5.4), with values lower than 0.14 mg/L (Vilks and Miller 2006). In the Sixth Case Study, a total colloid concentration in the range 0.034 – 3.4 mg/L, from all sources, is assumed.

The nature of the colloids at the site is uncertain. For present purposes, it is assumed that the colloids are primarily montmorillonite as a basis for estimating their sorption characteristics, as indicated in Table 7.2. It is plausible that the colloids could be natural organics, which would imply that the colloid sorption properties would be similar to those for sediments. Furthermore, it is assumed that these same colloids continue to be dominant in the upper fracture and rock zones. As these zones are less saline, it is plausible that any bentonite colloids that reach the upper fracture zones will remain as colloidal particles rather than agglomerate. Although these colloids could be diluted by other natural colloids present in the upper zones, this possibility is neglected.

The colloid itself may move either with the groundwater or at a different rate characterized by the so-called colloid retardation factor. In the Reference Case of the Sixth Case Study, it is assumed that the colloids are not retarded and move with the groundwater, i.e., the colloid retardation factor = 1 (see Table 7.2).

Note that the ambient temperature at the repository horizon and redox divide are listed in Table 7.2. The redox divide determines the oxidation conditions of the rock zones. Rock zones above the redox divide are assumed to have oxidizing conditions and zones below the redox divide have reducing conditions.

Table 7.2: Geochemistry Parameters

Parameter	Value	Comment
Ambient temperature at repository horizon	11°C	Consistent with a 5°C average surface temperature and 0.012°C/m geothermal gradient.
Redox Divide	150 mASL	Normal PDF assumed with mean 150, a standard deviation of 75 m, and range from 50 to 300 m. Based on Whiteshell data (Gascoyne 2004). Note that surface elevation at repository location is approximately 382.5 mASL
Colloid Concentration	0.34 mg/L	Average colloid concentration in Whiteshell area is 0.34 mg/L (Davison et al. 1994, p.337). Range assumed 10-fold smaller to 10-fold higher, so colloid concentration described using loguniform PDF from 0.034–3.4 mg/L. Colloid grain density assumed to be 2700 kg/m ³ .
Colloid Transport Retardation Factor	1	Lognormal PDF with GM = 1.0, GSD = 5.0, bounds = 0.9 to 100.
Colloid Sorption Coefficient	See Table 6.15	Reference Case K _d value for element on bentonite used. All sampled values are directly correlated with bentonite sorption values.

7.3 GEOSPHERE TRANSPORT PARAMETERS

7.3.1 Effective Diffusivity

The effective or intrinsic diffusivity of contaminants in groundwater in saturated rock can be expressed in terms of the free-water diffusivity D_o , rock transport porosity ε , and tortuosity factor τ , where $D_e = \varepsilon \cdot \tau \cdot D_o$. Ohlsson and Neretnieks (1997) indicate that surface diffusion and anion exclusion are not important in granite under saline conditions (i.e., total dissolved solid concentrations over 10 g/L).

The selected free water diffusivities are from Ohlsson and Neretnieks (1997) and are the same as those in Table 5.3. Porosity and tortuosity values are listed in Table 7.1. These properties are defined at 25°C. This is higher than the host rock ambient temperature of about 11°C (Table 7.2). Since the rock is not expected to heat up significantly on timescales relevant to transport, no further temperature scaling is provided.

The calculated effective diffusivity values are shown in Table 7.3.

The tortuosity of the intact rock zones is described by a lognormal probability density function with a geometric mean 0.06, a geometric standard deviation of 1.7, a lower bound of 0.016 and an upper bound of 0.25. For the fracture and overburden zones, τ is constant and equal to one. For the sediment, τ is defined by a uniform probability density function with lower bound 0.5 and upper bound 1.

Table 7.3: Effective Diffusivities in Geosphere Zones [m²/a]

Element	Deep / Intermediate Rock	Shallow Rock	Fracture	Overburden	Sediment
Ac	5.8x10 ⁻⁶	9.6x10 ⁻⁵	3.2x10 ⁻³	1.3x10 ⁻²	1.2x10 ⁻²
Ag	9.5x10 ⁻⁶	1.6x10 ⁻⁴	5.3x10 ⁻³	2.2x10 ⁻²	2.0x10 ⁻²
Am	5.8x10 ⁻⁶	9.6x10 ⁻⁵	3.2x10 ⁻³	1.3x10 ⁻²	1.2x10 ⁻²
Bi	1.2x10 ⁻⁵	2.0x10 ⁻⁴	6.7x10 ⁻³	2.8x10 ⁻²	2.5x10 ⁻²
Br	1.1x10 ⁻⁵	1.9x10 ⁻⁴	6.3x10 ⁻³	2.6x10 ⁻²	2.4x10 ⁻²
C	6.8x10 ⁻⁶	1.1x10 ⁻⁴	3.8x10 ⁻³	1.6x10 ⁻²	1.4x10 ⁻²
Ca	4.5x10 ⁻⁶	7.5x10 ⁻⁵	2.5x10 ⁻³	1.1x10 ⁻²	9.4x10 ⁻³
Cd	4.1x10 ⁻⁶	6.9x10 ⁻⁵	2.3x10 ⁻³	9.7x10 ⁻³	8.6x10 ⁻³
Cl	1.1x10 ⁻⁵	1.9x10 ⁻⁴	6.3x10 ⁻³	2.6x10 ⁻²	2.4x10 ⁻²
Cs	1.2x10 ⁻⁵	2.0x10 ⁻⁴	6.7x10 ⁻³	2.8x10 ⁻²	2.5x10 ⁻²
Hg	1.2x10 ⁻⁵	2.0x10 ⁻⁴	6.7x10 ⁻³	2.8x10 ⁻²	2.5x10 ⁻²
I	1.1x10 ⁻⁵	1.9x10 ⁻⁴	6.3x10 ⁻³	2.6x10 ⁻²	2.4x10 ⁻²
Mo	5.8x10 ⁻⁶	9.6x10 ⁻⁵	3.2x10 ⁻³	1.3x10 ⁻²	1.2x10 ⁻²
Np	5.8x10 ⁻⁶	9.6x10 ⁻⁵	3.2x10 ⁻³	1.3x10 ⁻²	1.2x10 ⁻²
Pa	5.8x10 ⁻⁶	9.6x10 ⁻⁵	3.2x10 ⁻³	1.3x10 ⁻²	1.2x10 ⁻²
Pb	1.2x10 ⁻⁵	2.0x10 ⁻⁴	6.7x10 ⁻³	2.8x10 ⁻²	2.5x10 ⁻²
Pd	5.8x10 ⁻⁶	9.6x10 ⁻⁵	3.2x10 ⁻³	1.3x10 ⁻²	1.2x10 ⁻²
Po	1.2x10 ⁻⁵	2.0x10 ⁻⁴	6.7x10 ⁻³	2.8x10 ⁻²	2.5x10 ⁻²
Pu	5.8x10 ⁻⁶	9.6x10 ⁻⁵	3.2x10 ⁻³	1.3x10 ⁻²	1.2x10 ⁻²
Ra	5.0x10 ⁻⁶	8.4x10 ⁻⁵	2.8x10 ⁻³	1.2x10 ⁻²	1.1x10 ⁻²
Rn	1.2x10 ⁻⁵	2.0x10 ⁻⁴	6.7x10 ⁻³	2.8x10 ⁻²	2.5x10 ⁻²
Sb	1.2x10 ⁻⁵	2.0x10 ⁻⁴	6.7x10 ⁻³	2.8x10 ⁻²	2.5x10 ⁻²
Se	5.8x10 ⁻⁶	9.6x10 ⁻⁵	3.2x10 ⁻³	1.3x10 ⁻²	1.2x10 ⁻²
Sn	5.8x10 ⁻⁶	9.6x10 ⁻⁵	3.2x10 ⁻³	1.3x10 ⁻²	1.2x10 ⁻²
Sr	4.5x10 ⁻⁶	7.5x10 ⁻⁵	2.5x10 ⁻³	1.1x10 ⁻²	9.4x10 ⁻³
Tc	5.8x10 ⁻⁶	9.6x10 ⁻⁵	3.2x10 ⁻³	1.3x10 ⁻²	1.2x10 ⁻²
Te	1.2x10 ⁻⁵	2.0x10 ⁻⁴	6.7x10 ⁻³	2.8x10 ⁻²	2.5x10 ⁻²
Th	5.8x10 ⁻⁶	9.6x10 ⁻⁵	3.2x10 ⁻³	1.3x10 ⁻²	1.2x10 ⁻²
U	5.8x10 ⁻⁶	9.6x10 ⁻⁵	3.2x10 ⁻³	1.3x10 ⁻²	1.2x10 ⁻²
W	5.8x10 ⁻⁶	9.6x10 ⁻⁵	3.2x10 ⁻³	1.3x10 ⁻²	1.2x10 ⁻²

7.3.2 Dispersion Length

The dispersion length is a parameter that approximates the spreading of a contaminant plume due to inherent variability in the local rock or fracture permeability. As a general rule of thumb, a dispersion length is roughly 5-10% of the total path length. For the present repository, the path length of interest for the contaminant plume (i.e., when it reaches the surface) ranges from 400 m (the shortest direct distance from the repository to the bottom of the well) to 500 m (shortest direct distance from repository to the surface). Since a lower dispersion results in less spreading of the contaminant plume, the current study assumes a constant longitudinal dispersion length of 20 m or 5% of the 400 m total path length. The transverse dispersion length is assumed to be 10% of the longitudinal dispersion length or 2 m (uniform distribution with a lower bound of 1.6 m and an upper bound of 2.4 m).

7.4 EXCAVATION DAMAGE ZONE TRANSPORT PARAMETERS

In the Sixth Case Study, the excavation of the shafts, tunnels, placement rooms and boreholes will create zones of disturbed rock in which there is significantly increased porosity and flow permeability. These zones are referred to as excavation damage zones (EDZ). The extent and severity of the EDZ is dependent on the excavation method, size of the excavation, localized rock stress and residual heat generated by the fuel. Beyond the EDZ, the rock may be disturbed with respect to stress redistribution, but no significant change to the flow and transport properties of the rock is expected.

The selected EDZ parameters used in the Sixth Case Study are summarized in Table 7.4 and Table 7.5, and are described below.

7.4.1 Excavation Damage Zone Thickness

The shafts, placement rooms, and tunnels are assumed to be excavated by a controlled drill-and-blast technique resulting in an EDZ in the rock around the periphery of the shafts and tunnels. However, by considering the stress state in the host rock the extent of the EDZ can be minimized.

Martino (2000) and Chan et al. (1999) provide reviews of EDZ properties in Canadian Shield granite, including measurements made in the Mine-by Tunnel and Tunnel Sealing Experiments at the AECL Underground Research Laboratory. Bäckblom (2008) summarizes the results of several international experiments. These reviews focus on drill-and-blast excavated tunnels but include some limited discussion of tunnels excavated by a tunnel boring machine or mechanical excavation. The reports concluded that the severity of the EDZ significantly decreases the further away from tunnel surface. Based on these reviews, in the Sixth Case Study, the damaged zone around the placement rooms, access tunnels and shafts are divided into four regions, an inner damaged zone, an outer excavation damage zone, a seal inner excavation damage zone and a seal outer excavation damage zone.

The inner EDZ around the placement room is assumed to be relatively narrow, extending out 1 m from the floor, roof and walls of tunnels. The outer EDZ extends an additional 2 m from the inner EDZ placement room floor, roof, and walls. The outer EDZ has very similar properties to the host rock (Table 7.4).

At the end of each placement room, a bentonite seal will be keyed into the rock with the intent of restricting flow through the excavation damage zone (see Figure 6.4). The room seal will be carefully excavated to reduce the likelihood of an additional EDZ forming. However, it is possible additional layers of inner and outer EDZ could form around the seal. In the Sixth Case Study, the room seal inner and outer EDZ is included in the detailed modelling. It is assumed the inner EDZ is 1.1 m thick and the outer EDZ is assumed to extend out an additional 1.9 m. The room seal EDZ layers are assigned transport properties consistent with the inner EDZ defined above.

The central access tunnels, perimeter tunnel and panel access tunnels will also have regions of inner and outer EDZ similar to the placement room.

Shafts in the Sixth Case Study scenario are roughly circular and the local stress field around the shafts is expected to be high. The inner and outer EDZ layers of the shafts are defined in terms of the shaft radii. The main shaft, service shaft and ventilation shaft radii are 9.0 m, 8.5 m, and 7.6 m respectively. The inner and outer EDZ layers are $0.42 \times R$ and $0.64 \times R$, where R is the shaft radius, respectively. Similar to the placement rooms the shaft seals are also assumed to have an inner and outer EDZ layer. The seal inner EDZ and outer EDZ are assumed to be $0.54 \times R$ and $0.64 \times R$ respectively (see Table 7.4).

7.4.2 Excavation Damage Zone Permeability

EDZ measurements in Canadian Shield granite at the AECL Underground Research Laboratory indicated that the transmissivity of the inner EDZ was about two to three orders of magnitude higher than of the intact rock (Martino 2000). EDZ tests at other sites report a 1 to 10^5 times increase over the host rock permeability for the inner EDZ, and outer EDZ (Chan et al. 1999, Appendix A; Bäckblom 2008).

Seepage measurements along the floor of the AECL Mine-by Tunnel experiment gave permeability values of 10^{-13} m^2 occurring in a small 0.004 m^2 area, while similar tests in the Tunnel Sealing Experiment floor gave values of $2.5 \times 10^{-15} \text{ m}^2$, occurring over 0.2 m^2 (Martino 2000). This is consistent with other observations in tunnels in highly stressed rock where "notches" at the roof or floor have greater rock damage and corresponding increased permeability.

Some of these seepage measurements also explored the axial connectivity of the EDZ permeability. In the AECL Room 209 tests over a 6-m floor section, it was found that the EDZ did not form a continuous path beyond one blast round (about 3 m) (Martino 2000). However, in the Mine-by Tunnel, no drop in permeability was noted over 1 to 4 m (Martino 2000). For the Sixth Case Study, it is conservatively assumed that the EDZ permeability is axially connected along the placement rooms, tunnels and shafts.

For this study, the reference value for the axial inner EDZ permeability is selected to be 100 times the host rock permeability. Since values range from 10 to 1000 times the intact rock permeability, the EDZ permeability is defined by a lognormal probability density function with a geometric mean of 100 times the intact rock permeability and a geometric standard deviation of 3.2, so that 95% of the values of the distribution are within 10 to 1000 times the intact rock permeability. Bounds are set at 10 and 1000 times the intact rock permeability. The inner EDZ permeability is also assumed to be correlated to the porosity of the inner EDZ with a correlation coefficient of 0.8 (higher porosity implies higher permeability). The inner EDZ permeability in the radial direction is set to 0.1 times the axial value.

The outer EDZ permeability is lognormally distributed the a geometric mean of 10 times the host rock permeability, a geometric standard deviation of 3.2 and with lower and upper limits of 1 and 100 times the host rock permeability, respectively.

7.4.3 Excavation Damage Zone Dispersion Length

The axial-flow EDZ dispersion length is defined parallel (longitudinal) or transverse to the room axis direction. Although the room length is 304 m, it is expected that the contaminant path

length through the EDZ will normally be less than 100 m, considering that the failed container location can vary and that contaminants can also move radially.

Johnson et al. 1996 (p.181) uses a fit of dispersion data from a range of laboratory and field studies that gives a 14 m (best estimate) to 45 m (95% confidence bound) dispersion length for axial transport along a 100-m path (i.e., 14 to 45% of the path length). Flow measurements in the EDZ in the Mine-by Tunnel indicated a dispersion length of 0.60 m for a test region of 1.5 m, i.e., 40% of the scale length. Results from the TRUE tracer tests on a 3-m scale implied a 10% dispersion length (SKB 2001, p.99, p.161).

In the Sixth Case Study CC4 models, the longitudinal dispersion length for axial transport in the EDZ is described by a uniform probability density function from 10 to 40 m, corresponding to 10% to 40% of a 100-m path length. However, in the FRAC3DVS-OPG calculations, the longitudinal dispersion coefficient in the EDZ is selected to be 10 m based on Quintessa and Geofirma (2011) to avoid unrealistic transport results, i.e., large upstream dispersion. Upstream dispersion does not occur in the CC4 geosphere transport model (NWMO 2012b).

Johnson et al. 1996 (p.181) suggests that the transverse dispersion is about 1% of the longitudinal dispersion, whereas other “rules of thumb” suggest 10% (Chan et al. 1999). For the Sixth Case Study, these give a transverse dispersion length range of either 0.1 to 0.4 m, or 1 to 4m. Since the EDZ radial thickness is about 1.0 m, the transverse dispersion length is selected to be 1% of the longitudinal dispersion length. Thus, in the CC4 model calculations, the EDZ transverse dispersion length is described by a uniform probability density function from 0.1 to 0.4 m and in the FRAC3DVS-OPG calculations the EDZ transverse dispersion length is 0.1 m.

In the CC4 model, a radial flow component is separately modelled and assigned its own longitudinal and transverse dispersion lengths. These are set to 1% of the corresponding longitudinal and transverse dispersion lengths for axial flow.

7.4.4 Excavation Damage Zone Porosity

It is expected that the porosity of the EDZ is comparable to or larger than that of the host rock. Two measurements along the tunnel floor in the AECL Mine-by Tunnel experiment (Chan et al. 1999, Appendix A) indicated a transport porosity of around 3%, compared to the intact rock porosity of about 0.3%. However, these tests also indicated very high permeabilities, and so it is likely that the measured porosity represents the porosity of the bottom EDZ notch rather than the bulk EDZ porosity. In the AECL EDZ study (Chan et al. 1999), the porosity of the inner EDZ was modelled as 0.5%, and the center notches were treated as either 0.5% or 3%, compared with the rock porosity of 0.3%.

For the Sixth Case Study, the best-estimate porosity of the intact rock is 0.3%. The porosity is 0.6% for the tunnel inner EDZ, and 0.3% for the tunnel outer EDZ. However, in CC4, only the inner EDZ is modelled. To account for this, the EDZ porosity is described by a lognormal probability density function with a geometric mean of 0.6%, a geometric standard deviation of 3.2, and bounding values of 0.06% and 6%. Furthermore, the EDZ porosity is positively correlated with the EDZ permeability, so that the porosities are large when the permeability is large. Although there is no specific data, it is judged that this should be a fairly tight correlation - a correlation coefficient of 0.8 is used.

7.4.5 EDZ Tortuosity

As previously noted, the tortuosity, τ , used in the Sixth Case Study is defined so that the effective diffusivity is given by $D_e = \varepsilon \cdot \tau \cdot D_0$. The inner EDZ tortuosity is described by a lognormal probability density function with geometric mean = 0.1, geometric standard deviation = 1.7 and bounds from 0.06 to 0.44. For the more highly damaged shaft bulkhead EDZ, the tortuosity is set equal to the maximum tortuosity value used for the inner EDZ tortuosity, i.e., 0.44.

Table 7.4: Excavation Damage Zone Properties

EDZ ZONE	Description	Distance from Rock Face	Porosity [-]	Tortuosity [-]	Permeability (m ²)
Placement Rooms (3.2 m x 2.2 m)²					
Inner EDZ	Tunnel Top & Bottom	1 m	2xrock	0.1	100 x Rock
	Tunnel Sides	1 m			
Outer EDZ	Tunnel Top & Bottom	3 m	1xrock	0.1	10 x Rock
	Tunnel Sides	3 m			
Seal EDZ ¹	Tunnel Top & Bottom	Seal + 10% I.EDZ = Seal + 0.1 m	2xrock	0.1	100 x Rock
	Tunnel Sides	Seal + 10% I.EDZ = Seal + 0.1 m			
Seal Outer EDZ	Tunnel Top & Bottom	3	1xrock	0.1	10 x Rock
	Tunnel Sides	3			
Main, Service, and Vent Shafts (R = shaft radius in meters)³					
Inner EDZ	-	0.42 x R	2 x Rock	0.1	100 x Rock
Outer EDZ	-	0.64 x R	1 x Rock	0.1	10 x Rock
Seal Inner EDZ ¹	-	Seal + 10% I.EDZ = Seal + 0.042R	2 x Rock	0.44	100 x Rock
Seal Outer EDZ	-	0.64 x R	1 x Rock	0.1	10 x Rock

¹The extent of the seal EDZ is measured from the excavation surfaces of placement rooms and shafts, not from the keyed-in excavations of the seals. The EDZ at placement room and shaft seal locations is conservatively assumed to extend beyond the keyed-in depth of the seal (1m in the placement rooms and 0.5 x R in the shafts) by an additional depth of approximately 10% of the inner EDZ thickness. For the purpose of this study only, the permeability of seal inner EDZ is equal to that of inner EDZ (i.e., 100 x Rock).

²The EDZ characteristics of the placement rooms should be assumed for the central access, panel access and perimeter tunnels.

³The distance from the rock face for the shaft EDZ is specified as a function of the shaft radius.

Table 7.5: Transverse, Radial, and Axial Excavation Damage Zone Properties

Parameter	Value	Comment
Axial flow, axial dispersion length	25 m	Uniform probability density function from 10 m to 40 m. (In FRAC3DVS-OPG, the axial dispersion length is set at 10 m to avoid unrealistic transport, i.e., upstream dispersion.)
Axial flow, transverse dispersion length	0.25 m	Uniform probability density function from 0.1 to 0.4 m. (In FRAC3DVS-OPG, transverse dispersion length is set to 10% of longitudinal value or 1 m.)
Radial flow, ratio of radial to axial dispersion length	0.01	Assumed to be 1%
Radial flow, ratio of radial to axial transverse dispersion length	0.01	Assumed to be 1%
Ratio of radial EDZ permeability to axial EDZ permeability	0.1	Assumed to be 10%

7.5 GEOSPHERE SORPTION PARAMETERS

Chemical species will, to different degrees, interact with the mineral surfaces surrounding the pores in the rock. Sorption of a radionuclide in the geosphere may be modelled using a linear relation (justified by the expected low radionuclide concentrations) between the concentration of the sorbed species and the aqueous concentration. The proportionality constant is called the sorption coefficient K_d (m^3/kg)

Sorption properties of the rock depend on a number of factors, such as groundwater chemical composition, groundwater redox potential, rock type, degree of fracturing, etc. Many of the factors controlling radionuclide sorption onto the host rock are site-specific, and experimental data obtained for other conditions may not be applicable or may need to be adapted. At present, many of the site-specific conditions are unknown and, therefore, the sorption data used are partly generic.

Radionuclide sorption during transport through the geosphere is incorporated in SYVAC-CC4 using a retardation factor R given by

$$R = 1 + [\rho_s(1-\varepsilon)/\varepsilon] K_{d,in} \quad (7.1)$$

where ρ_s is the material grain density, ε is the porosity of the geological material and $K_{d,in}$ is the radionuclide sorption coefficient for intact rock. $K_{d,in}$ and R are element dependent.

To correct from experimentally measured sorption data on crushed rock samples to those for intact rock, a normalization factor is applied to the experimental sorption coefficient K_d (Vandergraaf 1997, Vandergraaf and Ticknor 1994) to account for the larger sorption area of the crushed rock, i.e.,

$$K_{d,in} = [(1-\varepsilon_{\text{expt}})/\varepsilon_{\text{expt}}] [(1-\varepsilon)/\varepsilon]^{-1} K_d \quad (7.2)$$

where ϵ_{expt} is the porosity of the unconsolidated material used in the experimental measurement of K_d . SKB also uses such a normalization factor (Crawford et al. 2006), but that used in Equation 7.2 (Vandergraaf and Ticknor 1994) is more conservative, i.e., generates smaller $K_{d,\text{in}}$ values. Substituting Equation (7.2) into Equation (7.1) leads to the following expression for the retardation factor

$$R = 1 + [\rho_s(1-\epsilon_{\text{expt}})/\epsilon_{\text{expt}}] K_d \quad (7.3)$$

Table 7.6 lists values of $[\rho_s(1-\epsilon_{\text{expt}})/\epsilon_{\text{expt}}]$ for various geological materials (Vandergraaf and Ticknor 1994).

In general, the geosphere includes an overburden on top of the bedrock, and the compacted (deep) sediment layer at the bottom of lakes. The normalization factors for the overburden materials were calculated with Equation 7.2 assuming a solid density of 2.65 kg/L and a porosity of 0.42 (Davison et al. 1994, p.366). For the compacted sediment, a density of 2.5 kg/L (Davis et al. 1993, p. 82) and a porosity of 0.5 (Davison et al. 1994, p. 366) were used. For granite, a density of 2.7 kg/L (Davison et al. 1994) and a porosity of 0.5 (Davison et al. 1994) were used.

Table 7.6: Values of $[\rho_s(1-\epsilon_{\text{expt}})/\epsilon_{\text{expt}}]$ for Several Geological Materials

Geological Material	$\rho_s(1-\epsilon_{\text{expt}})/\epsilon_{\text{expt}}$ [kg/m³]
granite	2700
sand	3660
silt	3660
clay	3660
sediment	2500

In the CC4 model, the experimental K_d values are input into the code and then the normalization factor is applied within the model. A complete list of K_d values are shown in Table 7.7. The K_d values are generally described using a lognormal probability density function. No distinction is made between sorption values for the bulk granite and for fracture materials, given the limited data available for fracture materials.

In general, the K_d values are taken from Crawford et al. (2006), when available. The geometric mean of the distribution is set equal to their recommended K_d value, and the geometric standard deviation was calculated assuming that the lower limit selected by SKB is 3 standard deviations from the geometric mean.

Table 7.7: Geosphere K_d Values for Fractures and Crushed Rock¹

Element	Distribution	Salinity ² / Oxidation ³	GM	GSD	Lower Limit	Upper Limit
			[m ³ /kg]	[-]	[m ³ /kg]	[m ³ /kg]
Ac	Lognormal	-	3	1.4	1	5
Ag	Lognormal	Non-Saline	0.5	1.7	0.1	1
		Saline	0.05	1.7	0.01	0.1
Am	Lognormal	-	13	3.9	0.22	190
Bi ⁴	Lognormal	-	0.001	2.2	0.0001	0.01
Br	Constant	-	0		-	
C	Lognormal	-	0.001	1.3	5.0x10 ⁻⁴	2.0x10 ⁻³
Ca ⁶	Lognormal	Non-Saline	1.3x10 ⁻²	2.4	1.0x10 ⁻³	6.1x10 ⁻¹
		Saline	9.8x10 ⁻⁵	1.9	1.4x10 ⁻⁵	5.0x10 ⁻⁴
Cd	Lognormal	Non-Saline	0.1	1.3	0.05	0.5
		Saline	0.02	1.3	0.01	0.1
Cl	Constant	-	0		-	
Cs	Lognormal	Non-Saline	0.18	4.7	1.7x10 ⁻³	9.6
		Saline	0.042	4.7	4.0x10 ⁻⁴	2.0
Hg ⁵	Constant	-	0		-	
I	Constant	-	0		-	
Mo ⁵	Constant	-	0		-	
Np	Lognormal	Oxidizing	0.018	2.1	2.0x10 ⁻³	2.2x10 ⁻¹
		Reducing	0.96	2.7	4.7x10 ⁻²	20
Pa	Lognormal	-	1	1.3	5.0x10 ⁻¹	5
Pb ⁸	Lognormal	-	1.26	4	0.02	80.6
Pd ⁸	Lognormal	-	2.75	5	0.022	344
Po ⁷	Lognormal	-	0.1	2.2	0.01	1
Pu	Lognormal	-	5	1.7	1	10
Ra ⁴	Lognormal	-	0.175	3.16	5.5x10 ⁻³	5.5
Rn ⁵	Constant	-	0		-	
Sb ⁵	Constant	-	0		-	
Se	Lognormal	-	0.001	1.3	5.0x10 ⁻⁴	5.0x10 ⁻³
Sn ⁴	Lognormal		0.71	6.3	2.8x10 ⁻³	177
Sr	Lognormal	Non-Saline	1.3x10 ⁻²	2.4	1.0x10 ⁻³	6.1x10 ⁻¹
		Saline	9.8x10 ⁻⁵	1.9	1.4x10 ⁻⁵	5.0x10 ⁻⁴
Tc	Constant	Oxidizing	0		-	
	Lognormal	Reducing	1	1.3	0.5	3
Te ⁵	Constant	-	0		-	
Th	Lognormal	-	1	1.3	5x10 ⁻¹	10
U	Lognormal	Oxidizing	0.0063	2.3	5.0x10 ⁻⁴	1.2x10 ⁻¹
		Reducing	6.3	5.1	4.8x10 ⁻²	280
W ⁵	Constant	-	0		-	

¹ K_d values for granite are from Crawford et al. (2006, Table 7.1-7.3), except as noted.

²Saline groundwater in Crawford et al (2006) is defined as [Cl⁻] > 500 mg/L, and non-saline otherwise. In the Sixth Case Study, the groundwater has a [Cl⁻] of 6000 mg/L (see Table 5.4). “-” indicates the groundwater salinity was not found to affect the K_d .

³Oxidizing values used in geosphere zones above redox divide, see Table 7.2. “-” indicates the element K_d is not sensitive to oxidation state of the groundwater.

⁴ K_d values are from Ticknor and Vandergraaf (1996).

⁵ K_d values are assumed to be zero.

⁶ K_d value is based on chemical analogue. Ca is assumed to have the same K_d as Sr from Crawford et al (2006).

⁷ K_d value is from Baston et al. (1999).

⁸ K_d value based on Crawford (2010).

7.6 WELL LOCATION AND DEPTH

An important pathway for human exposure to contaminants released from the repository is through a well, which can supply water for drinking, domestic use and irrigation. As a conservative assumption for safety assessment, the location and depth of the well are selected so as to maximize the possibility that the well water becomes contaminated. However, this must be tempered with the knowledge that some well locations would be unrealistic. For instance, the water could be unacceptably saline or the rock might not be sufficiently permeable to provide the amount of water required.

A survey of wells drilled around the Whiteshell Research Area was used to derive a statistical distribution of well depths. The results were described by a lognormal probability density function with geometric mean of 37 m, geometric standard deviation of 2.2 m, and a range from 0 to 200 m (Davison et al. 1994, p.386). The wells were judged to draw all or part of their water from weathered and fractured bedrock.

The FRAC3DVS-OPG groundwater flow modelling requires a specific well location and depth. For the Sixth Case Study, a reference well location and depth was defined. The location was selected to maximize uptake of contaminants from the repository. A reference (bottom) well depth of about 100 m was chosen as a plausible but conservative value for the following reasons:

- The well is located to maximize uptake of contaminants from the repository;
- The well intersected a fracture, ensuring good water supply;
- Salinity increases with depth, making the water from deeper wells less suitable for use; and
- This well depth is about 2.5 times as deep as typical Canadian Shield practice, according to data from Davison et al. 1994 (p. 386).

The well was analytically tested to be capable of supplying a range of well demands of interest. If the well is not capable of supplying all the water needed by the critical group, then it is assumed that the water demand that cannot be satisfied by the well is taken from the Lake. More information on the well location, and on the groundwater flow around the well, is provided in NWMO (2017).

Table 7.8 summarizes the reference well properties (well demand is discussed in Section 8).

Table 7.8: Well Model Geosphere Parameters

Parameter	Value	Comment
Well depth	100 m	Bottom of well, relative to ground surface.
Well casing radius	0.0508 m	75% of wells on Canadian Shield are 0.0508 m radius while 25% are 0.0762 m radius (4 or 6 inches diameter). (Davison et al. 1994, p.416).
Well bypass discharge minimum fraction	1.0	Minimum fraction for the reduction of the discharge area associated with the well bypass. Set to one representing no reduction of the discharge area due to well demand.
Well divergent break point A	911 m ³ /a	Break Points A, B, and C (BP _a , BP _b , and BP _c) are used for segments leading away from divergent nodes in the SYVAC3-CC4 geosphere model that exhibit changes in flow amounts due to different well demands. The break point values are used in combination with the change of the fractional flow per unit well demand for the three ranges (Appendix C).
Well divergent break point B	1500 m ³ /a	
Well divergent break point C	3500 m ³ /a	
Well demand maximum	3500 m ³ /a	If the water demand exceeds this value surface water will be used as a secondary water source.

7.7 OTHER GEOSPHERE PARAMETERS

Table 7.9 lists values of other miscellaneous parameters used by the CC4 geosphere model.

Table 7.9: Other Geosphere Properties

Parameter	Reference Value	Comment
Water density ρ_0 at 25°C for density equation	997.1 kg/m ³	Value used in calculation of density at other temperatures. (CRC 1993).
Compressibility of water β_{water} at 25°C for the density equation	4.57x10 ⁻¹⁰ Pa ⁻¹	CRC (1993) ¹
Coefficient a for density equation	-3.17x10 ⁻⁴ K ⁻¹	CRC (1993) ¹
Coefficient b for density equation	-2.56x10 ⁻⁶ K ⁻²	CRC (1993) ¹
Coefficient a for viscosity equation	2.38x10 ⁻⁶ kg/s/m	Based on Data from Kestin et al. (1978)
Coefficient b for viscosity equation	1.76x10 ³ K	Based on Data from Kestin et al. (1978)
Reference water density	1000 kg/m ³	Reference water density used for input hydraulic head data. Value corresponds to freshwater at atmospheric pressure and 6°C.
Reference water viscosity	1.472x10 ⁻³ kg/m/s	Reference water viscosity used for input hydraulic conductivity data. Value corresponds to freshwater at atmospheric pressure and 6°C.
0°C	273.15 K	Used in °C to K conversion

¹Density of water = $\rho_0 (1 + \beta_{\text{water}} \Delta p + \mathbf{a}(\Delta T) + \mathbf{b}(\Delta T)^2)$, where $\Delta T = T[^\circ\text{C}] - 25^\circ\text{C}$ and $\Delta p = \text{head difference from hydrostatic [Pa]}$. Calculated densities match values in CRC (1993) within 1% over the range 0-100°C.

²Viscosity of water = $\mathbf{a}e^{\mathbf{b}/\mathbf{T}[\text{K}]}$. Calculated viscosities match values in Kestin et al. (1978) within 3.8% over the range 20-85°C.

7.8 GEOSPHERE NODE DATA

The geosphere is represented by either 3D finite-element models in FRAC3DVS-OPG, or as a network of 1-D transport paths in SYVAC3-CC4.

The FRAC3DVS-OPG representations typically involve several million nodes, and are not included here. Further details about these detailed models are given in NWMO (2017). The SYVAC3-CC4 geosphere transport model uses a simplified representation of the FRAC3DVS-OPG groundwater flow field. The input parameters used in this latter model are described in Appendix C of this report.

8. BIOSPHERE DATA

The Sixth Case Study repository is located in the same area of the Canadian Shield as the repository in the Fourth Case Study (NWMO 2012a). Thus, many of the biosphere parameter values are unchanged from those used in the Fourth Case Study, although some values have been updated where more appropriate data were available.

The following sections summarize the biosphere parameter values used in the Sixth Case Study and provide links to the original sources of the data.

8.1 SITE AND SURFACE WATER

The Sixth Case Study is based on a hypothetical but plausible Canadian Shield site. The surface topography of this site is relatively flat. The sub-regional watershed containing the repository is bounded by topographic highs to the north and south; a major east-west river crosses through the sub-regional watershed area. The repository is approximately in the centre of this area.

The area around the repository is shown in Figure 8.1. The surface water features closest to the repository are two small rivers to the east and west of the repository that merge to the south of the repository. A wetland exists between the two river systems. All water drainage from the area local to the repository eventually reaches the river system around the repository.

The biosphere characteristics are typical of the Canadian Shield. A general description of the Canadian Shield biosphere is provided in Davis et al. (1993).

8.2 DISCHARGE ZONES

Contaminants released from the repository can eventually move through the geosphere and, if they do not decay first, reach the biosphere. In general, they will reach the biosphere at specific discharge zones that will depend upon details of the repository location, geosphere properties, and surface topography. Typically, these discharge zones are topographic low areas and often are associated with bodies of water.

Transport modelling results shown in Figure 8.2 indicate that the main discharge areas for contaminants released from the repository are the West River, the East River, the South River and the Central Wetland. Each discharge area has a terrestrial and an aquatic discharge associated with it.

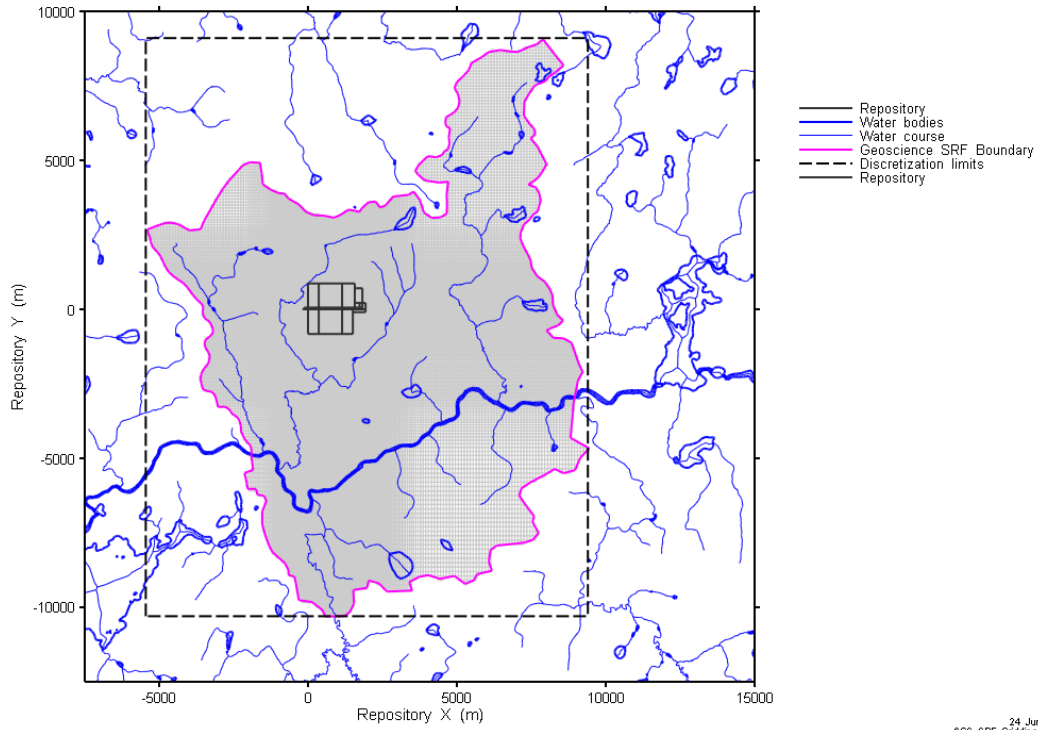


Figure 8.1: Repository Site and Surface Area

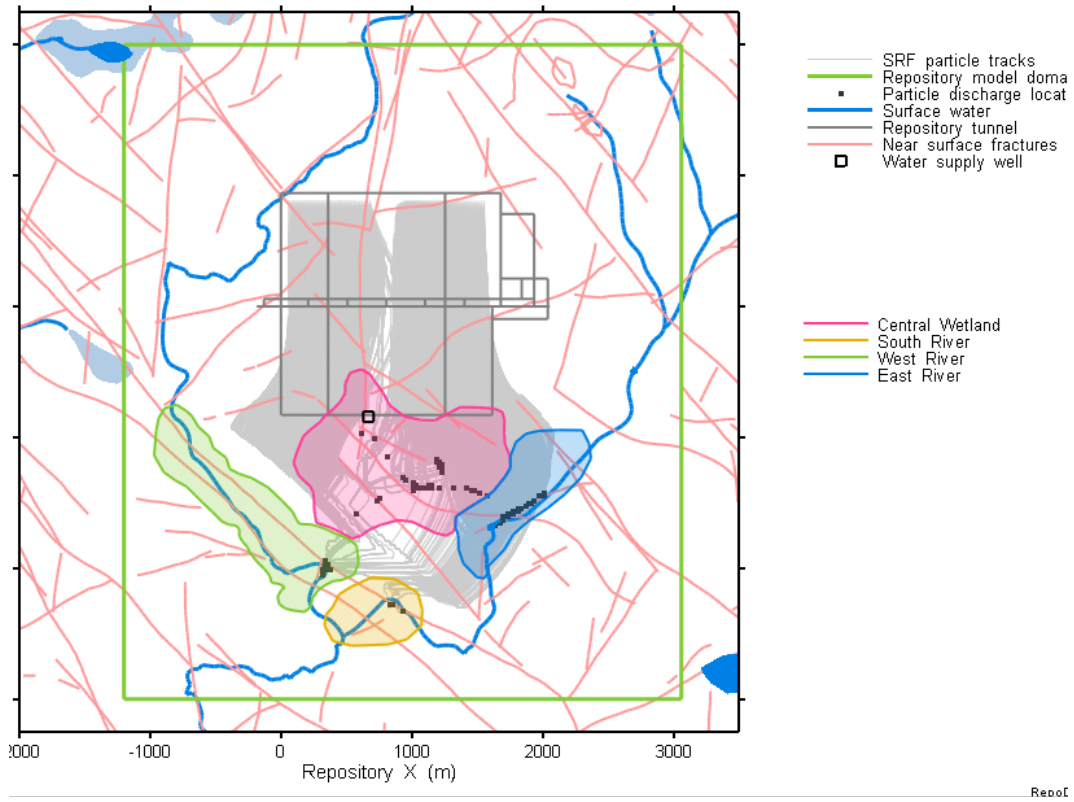


Figure 8.2: Surface Discharge Zones

The terrestrial portion of the discharge areas are used as various fields by the critical group. The fields are assigned to the terrestrial discharge areas in the following order: West River, Central Wetland, East River, and South River, based on the fraction of particle tracks arriving at these discharge locations when the well is operating.

The aquatic portion of the discharge areas are used as water sources by the critical group if the well is not operating or the well cannot supply a sufficient amount of water to support the critical group. Ultimately, contaminants released into the aquatic discharges are either trapped in deep sediments under these water bodies, or transported out of the local watershed. People living downstream from the repository, could be exposed to all the contaminants that reach the surface. However, there would be significant dilution because there is a large watershed area upstream of the repository.

8.2.1 River Watershed Areas

The total watershed area of the West, East and South Rivers was calculated to be 33.3 km² based on topographic information of the area. The West, East and South River watershed areas were estimated using FRAC3DVS and are approximately 13.4 km², 12.4 km², and 7.5 km², respectively (See Figure 8.3). These values, which are assumed to be constant in time, are used to calculate the water flow rate through the river system, based on the precipitation and runoff values defined in the next section.

In the Sixth Case Study safety assessment, doses are calculated to a human critical group living close to the well location, which is in the vicinity of the Central Wetland. It is also assumed that all discharged contaminants flow into the West River (even if they are captured by the well) in order to conservatively estimate contaminant concentrations in surface waters and to account for runoff of contaminated water (from, for example, farm fields irrigated with well water).

The characteristics of the river system are summarized in Table 8.1.

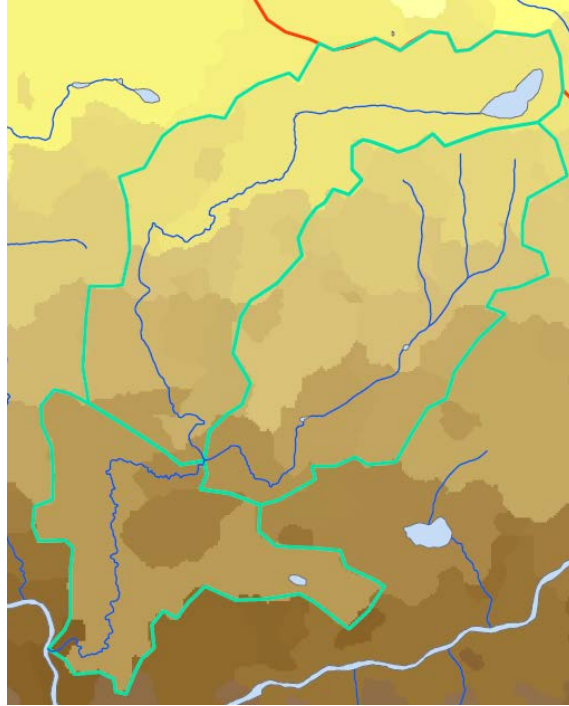


Figure 8.3: Catchment Areas

Table 8.1: Surface Water Properties

Parameter	Value	Comment
River watershed areas	1.34x10 ⁷ m ² 1.24x10 ⁷ m ² 7.50x10 ⁶ m ²	West River East River South River
West River surface area	5,000 m ²	Triangular distribution based on the west river aquatic area. Lower and upper bounds of 1,500 m ² and 30,000 m ² .
Mean West River depth	4.6 m	Value is geometric mean, geometric standard deviation is 2.0 with lower and upper bounds of 1 m and 10 m respectively.
Sedimentation rate	0.16 kg _{dry sed.} /m ² a	Lognormal PDF with GM=0.16 kg/(m ² .a), GSD=2.5, and bounds of 0.01 and 15 kg/(m ² .a) (Davis et al. 1993, p.99).
General sediment layer thickness	0.4 m	The thickness of river sediments is assumed to be lognormal PDF with GM=0.4 m, GSD=2.2 and bounds of 0.03 to 1.
Mixed sediment thickness	0.01-0.1 m	Uniform PDF over 0.01-0.1 m (Davis et al. 1993, p. 99).
Thickness of sediment removed for use in fields	0.3 m	Set to minimum value of 0.3 m allowed by CC4
Sediment dry bulk density	400 kg _{dw} /m ³	CSA (2008)

8.2.2 Surface Discharge Area

Discharge areas used in the Sixth Case Study were estimated as the area bounded by the 1 Bq/m³ concentration contour, as determined by the detailed FRAC3DVS modelling. Since exposure will likely occur at some time in the future, the future discharge areas are uncertain. Therefore, sensitivity cases in which the surface discharge area was bounded by concentration contours of 0.1 Bq/m³ and 10 Bq/m³ were also calculated. Figure 8.4 and Table 8.2 show the resulting discharge areas as well as the aquatic and terrestrial fractions of the discharge areas.

Discharge areas and terrestrial and aquatic discharge fractions are assumed to be triangularly distributed with lower, peak and upper bound values corresponding with concentration thresholds of 10 Bq/m³, 1 Bq/m³ and 0.1 Bq/m³ respectively.

Note that in the CC4 system model the East and South Rivers are amalgamated due to the negligible discharge to the South River. It should also be noted that despite the Central Discharge being classified as a wetland it will not be used as a potable water source.

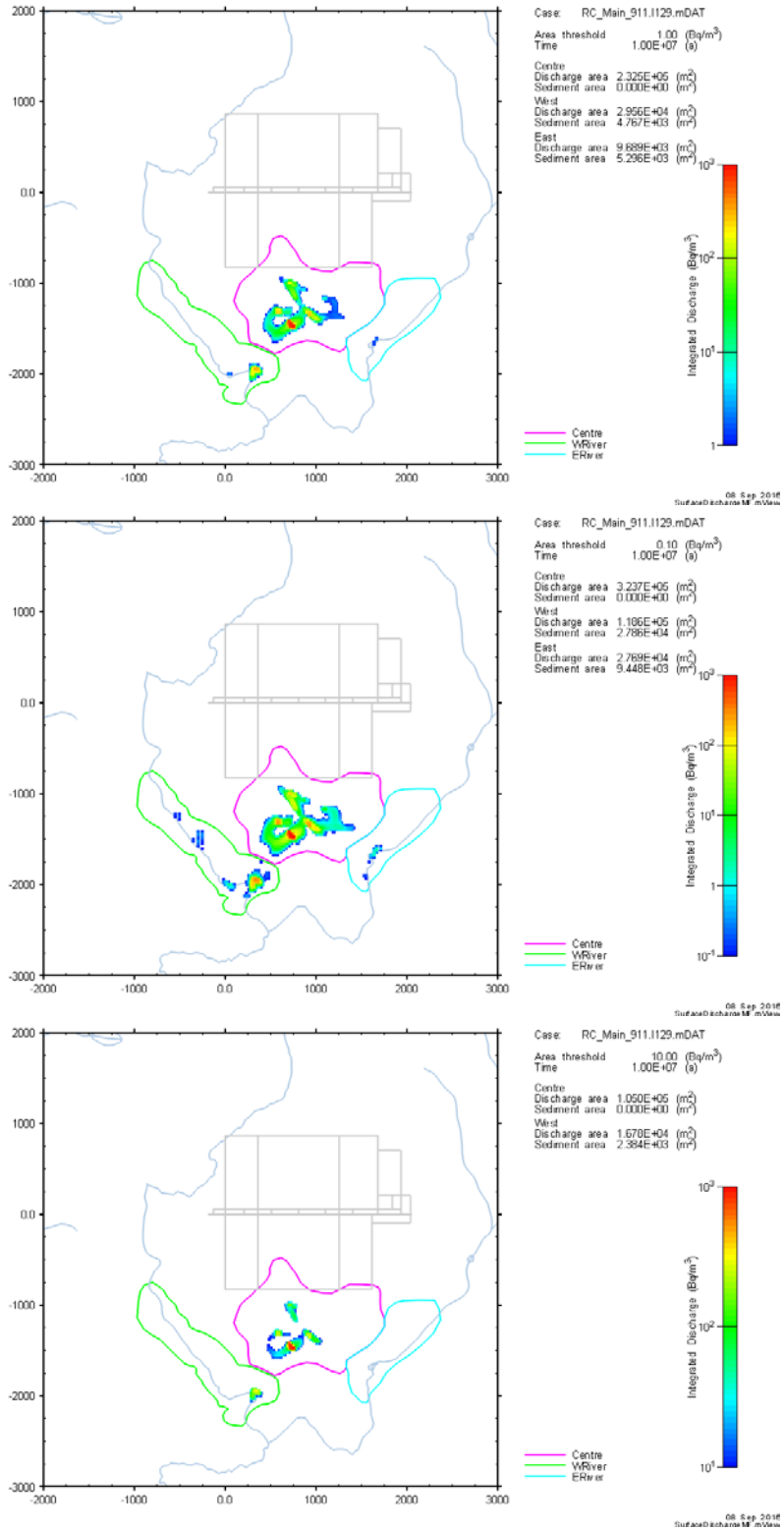


Figure 8.4: Discharge Areas for Concentration Thresholds of 1 Bq/m³, 0.1 Bq/m³ and 10 Bq/m³

Table 8.2: Discharge zone areas

Discharge zone	Area of discharge zone¹ [m²]	Lower Bound Area [m²]	Upper Bound Area [m²]	Aquatic discharge fraction² [%]	Terrestrial discharge fraction² [%]
West River	34,000	19,000	146,000	14 (12 - 19)	86 (81 - 88)
East/South River ³	15,000	6,000	37,000	35 (25 - 45)	65 (55 - 75)
Central Wetland	232,000	105,000	324,000	100	0

¹Discharge areas are assumed to be triangularly distributed

²Aquatic and terrestrial discharge fractions for the west, and east/south rivers are triangularly distributed and presented as follows peak(lower bound – upper bound). The aquatic and terrestrial discharge fractions for the central discharge is constant and assumed to be 100% terrestrial.

³The East and South River discharge areas have been amalgamated in the SYVAC3-CC3 model due to the negligible discharge to the South River.

8.3 CLIMATE AND ATMOSPHERE

The climate and atmospheric parameters are summarized in Table 8.3. These values reflect CSA (2008) values when available for a Canadian Shield site; otherwise the values are taken from Davis et al. (1993). The variation in these parameter values represents the natural variation across the Canadian Shield for present-day climate conditions.

Table 8.3: Climate and Atmosphere Parameters

Parameter	Value	Comment
Annual total precipitation	0.76 m/a	Geometric mean of annual averages from 1983 to 2006 in Geraldton (ON), which was identified as having a climate representative of the Canadian Shield. Normal PDF with a SD of 0.12 and bounds of 0.28 and 1.92 m/a (CDCD 2006). Lower and upper bounds represent half the minimum and double the maximum annual precipitation.
Annual average runoff	0.31 m/a	This is the balance between total precipitation and evapotranspiration, and includes surface runoff as well as infiltration into the water table. Normal PDF with mean of 0.31 m/a, standard deviation of 0.08 m/a, and bounds of 0.01 and 0.71 m/a. Correlated to total precipitation with a correlation coefficient of 0.80 (Davis et al. 1993, p.151, 279).
Average wind speed ¹	2.36 m/s	Normal PDF with mean of 2.36 m/s (8.5 km/h), standard deviation of 0.64 m/s, and bounds of 0.44 and 6 m/s. (Davis et al. 1993, p.196).
Average temperature	17°C July -15°C Jan.	Mean daily temperatures observed on Canadian Shield (Fisheries and Environmental Canada 1978).
Climate state	Temperate	Current climate.
Dry deposition velocity	0.006 m/s	Lognormal PDF with GM of 0.006 m/s and GSD of 2 (Amiro 1992).
Atmospheric dust load ²	$3.2 \times 10^{-8} \text{ kg}_{\text{drysoil}} / \text{m}^3_{\text{air}}$	Lognormal PDF with GM calculated from suspended particulate matter concentrations in ON, NB, QC and SK during years 1996 to 2002. GSD of 1.7 with bounds of 7.0×10^{-9} and $7.5 \times 10^{-8} \text{ kg}_{\text{drysoil}} / \text{m}^3_{\text{air}}$. (NAPS 1996 to 2002)
Atmospheric aerosol load ²	$2.9 \times 10^{-10} \text{ m}^3_{\text{water}} / \text{m}^3_{\text{air}}$	Lognormal PDF with geometric mean of $2.9 \times 10^{-10} \text{ m}^3_{\text{water}} / \text{m}^3_{\text{air}}$, and geometric standard deviation of 1.41. Based on estimate for sea salt aerosol over oceans (Davis et al. 1993, p.191).
Washout Ratio	630 000	CSA (2008) washout ratio for deposition to plants for all elements other than noble gases and iodine. This value is conservative for iodine. CSA (2008) recommends 200 000 for elemental iodine and 8400 for organic iodine.

¹Davis et al. (1993) values are judged more representative for a site on the Shield than the CSA (2008) values.

²Values for these parameters are not available in CSA (2008).

8.4 SOILS AND SEDIMENT

8.4.1 Soil Physical Characteristics

The physical characteristics of the soil at the hypothetical site are described in Table 8.4. These reflect mostly the values in CSA (2008), where available. Otherwise, the values from Garisto et al. 2012 are retained.

In SYVAC3-CC4, two soil models are considered: an upland soil and a shallow soil. For the upland soil, which is more typical, the water table is a reasonable distance below the ground surface. For the shallow soil, the water table extends into the surface soil on a regular and extended basis. The distinction between these two cases is important in determining how readily contaminated groundwater can reach the surface. In the upland soil case, it must be transported by processes such as capillary action. In the shallow soil case, the groundwater is directly discharged into the soil layer.

For the upland soil model, a simple approach is used to account for upward movement of contaminated groundwater into the surface soil. Specifically, the model requires information on the surface soil moisture content, and parameters describing the downward flow rate of surface water (precipitation and irrigation) and upward flow rate of groundwater. The water leaching fraction is the fraction of net precipitation or irrigation, after evapotranspiration, which penetrates deep into the soil rather than running off along the surface. On exposed bedrock, the fraction would be small. However, it is assumed that any farming would be on locations with suitable soil, and so a higher fraction would be expected. Since the specific value is uncertain, a large range from 0.1 to 1 is assumed.

Other soil model characteristics are also shown in Table 8.4.

Table 8.4: Soil Properties

Parameter	Value	Comment
Soil types	Sandy	On the Canadian Shield soil types are distributed as follows: 57% sand, 14% organic, 24% clay, and 5% loam (Davis et al. 1993, p.146).
Surface soil bulk density	1500 kg dry soil/m ³ soil (sandy soil)	The densities of the four soil types are as follows: 1500, 1300, 1400 and 400 kg dry soil/m ³ soil for sand, loam, clay and organic soils, respectively (CSA 2008).
Active surface soil depth	0.2 m	This is the active or root zone layer for which nuclide concentrations in the soil are determined (CSA 2008).
Soil Depth to water table	1.5 m	The depth of Canadian Shield soils vary considerably, from very shallow soils to 5 m or more. However, most soils cannot exert sufficient matric potential to pull groundwater up through the profile to the root zone if the water table lies more than 2.5 m below the surface. To ensure that the critical group and other biota are always exposed to groundwater contamination, a maximum soil depth of 2.5 m is adopted. This value as an upper truncation limit to a normal distribution with a mean of 1.5 m and an SD of 0.5 (Davis et al. 1993, p.148).
Minimum soil depth to water table for upland soil model	0.5 m	This is the minimum depth-to-water-table at which the upland soil model is used. For smaller depths, a shallow soil model is used that allows for flooding of the surface soil by contaminated groundwater. (Davis et al. 1993, p.137.)
Upland soil leach rate fraction	0.55	Fraction of net precipitation (precipitation + irrigation - evapotranspiration) that infiltrates into soil. Uniform PDF from 0.1 to 1.
Fraction of runoff entering the overburden	0.10	Uniform distribution with a lower bound of 0.03 and an upper bound of 0.17 (Singer and Cheng 2002).
Surface soil moisture content fraction	0.1 (0.05-0.13) sand 0.2 (0.15-0.27) loam 0.3 (0.25-0.42) clay 0.4 (0.3-0.56) organic	Triangular PDF assumed, with the bracketed numbers correspond to the upper and lower bounds. The lower bound is the average wilting point (Beals 1985) and the upper bound is the average field capacity (Beals 1985). The most probable values are from CSA (2008), except for organic soils for which the most probable value is set to the mid range between the wilting point and average field capacity.
Surface soil summer water deficit	0.20 m/a	Climate-based parameter. Value is based on water budget summaries (Coligado et al. 1968, 1969a-e) for various locations in the Ontario portion of the Canadian Shield. Value selected is the amount of water needed to eliminate the deficit yet not deplete the soil moisture. It is assumed to represent the maximum amount of water that would flow upward from a shallow water table.
Groundwater upflow exponent	3	Value is based on data for a fine sandy loam (Hillel 1980), and so likely overestimates upward flow for other soil types.
Bioturbation rate	0 /a	Not significant in Canadian Shield podzolic soils.

8.4.2 Plant/Soil Concentration Ratio

Table 8.5 lists the plant/soil concentration ratios for the different elements and the source of the data. The SYVAC3-CC4 biosphere model distinguishes between "garden" plants grown for human consumption, and "forage" plants which are used for animal consumption. Specifically, the model allows for different plant/soil concentration ratios for these different plants.

Plant/soil concentration ratios are inconsistently recorded on a dry or fresh weight basis. Conversion between the two is inaccurate unless the dry/fresh weight ratio is known. For consistency in the values reported here, a dry/fresh weight ratio of 0.53 and 0.35 are used for forage and garden crops, respectively. These values were calculated from the dry/fresh weight ratios given in CSA (2008). The dry/fresh weight ratio for forage crops is the average of the dry/fresh weight ratio of 0.19 for forage (e.g., fresh grass) and 0.86 for feed (e.g., grains), and assumes that animals eat 50% forage and 50% feed over the year. Similarly, the dry/fresh weight ratio for garden crops is calculated assuming that the critical group plant intake is 1/3 grain (dry/fresh weight ratio of 0.86) and 2/3 fruits and vegetables (dry/fresh weight ratio of 0.1).

The CSA (2008) plant/soil concentration ratios, which are expressed on a dry weight basis, were converted to a fresh weight basis using the dry/fresh weights shown above. The plant/soil concentration data in Davis et al. (1993) are expressed in a plant fresh weight basis, and were obtained from the original data using a plant dry/fresh weight ratio of 0.25. For consistency, the Davis et al. (1993) values were converted to a fresh weight basis using the dry/fresh weight ratios selected for this study.

The plant/soil concentration ratio is described using a lognormal probability density function with the geometric mean given in Table 8.5 and a geometric standard deviation of 5.7 for most elements (unless otherwise specified), as recommended by BEAK (2002).

Table 8.5: Plant/Soil Concentration Ratios¹

Element	Garden¹ (Bq/kg wet)/ (Bq/kg drysoil)	Forage¹ (Bq/kg wet)/ (Bq/kg dry soil)	Reference
Ac	0.0012	0.0019	Davis et al. (1993)
Am	0.00022	0.00034	CSA (2008)
Bi	0.0046 (2)	0.01 (2)	Sheppard et al. (2009)
C	7.7	11	CSA (2008)
Ca	0.022	0.025 (5.6)	Sheppard et al. (2010)
Cl	3.7	4.2	Sheppard et al. (2004a)
Cs	0.018	0.028	CSA(2008)
I	0.005 (10)	0.027 (10)	Sheppard et al. (2002)
Np	0.0006 (6.7)	0.0046 (10)	Sheppard et al. (2004b)
Pa	0.013	0.02	CSA(2008)
Pb	0.00084 (2.5)	0.0012 (2.5)	Sheppard et al. (2010)
Po	0.00088	0.0013	Davis et al. (1993)
Pu	0.000049	7.40E-05	CSA(2008)
Ra	0.0041 (7.5)	0.017 (11)	Sheppard et al. (2005a)
Rn	0	0	Davis et al. (1993)
Sb	0.00053	0.0008	CSA(2008)
Se	0.15	0.23	CSA(2008)
Sn	0.14	0.22	CSA(2008)
Sr	0.30	0.46	CSA (2008)
Th	0.0012	0.0018	CSA(2008)
U	0.00079 (6.3)	0.0027 (8.4)	Sheppard et al. (2005b)

¹Data for chemically hazardous elements (Ag, Br, Cd, Hg, Mo, Pd, Se, Tc, Te, and W), have been excluded from the dose model data.

²Values are lognormally distributed, with GM as listed and GSD = 5.7, with exceptions shown in brackets.

8.4.3 Soil Distribution Coefficient (K_d)

Table 8.6 provides the soil K_d values. The K_d values are taken from CSA 2008 when available. Note that CSA (2008) has adopted many soil K_d values of Thibault et al. (1990) and Davies et al. (1993). The geometric mean values for Cl, I, Np, Ra and U are from Sheppard et al. (2002, 2004a, 2004b, 2005a and 2005b, respectively). The soil K_d values for Rn and W are taken from Gobien and Garisto (2012).

Most soil K_d values are assumed to be lognormally distributed with a geometric standard deviation of 10 as per Davis et al (1993). Notable exceptions include I in organic soil for which the geometric standard deviation = 22 (Sheppard et al. 2002), Ra in all soils for which the geometric standard deviation = 4.9 (Sheppard et al. 2005a), and U in all soils for which the geometric standard deviation = 20 (Sheppard et al. 2005b). Rn is somewhat unique in that it's K_d value is conservatively assumed to be constant and zero for all soil types.

There is a strong inverse correlation between plant uptake of elements and the soil K_d values. Therefore, the K_d values are correlated to the plant/soil concentration ratio values (Table 8.6) with a correlation coefficient of -0.7 (Sheppard et al. 2010).

Table 8.6: Soil K_d Values¹ [L/kg]

Element	Sand	Loam	Clay	Organic	Reference
Ac	450	1500	2400	5400	Davis et al. (1993, p. 155)
Ag	90	120	180	15000	CSA (2008, Table G.2)
Am	2000	9600	8100	110 000	CSA (2008, Table G.2)
Bi	100	450	600	1500	Davis et al. (1993, p. 155)
Br	15	49	74	180	CSA (2008, Table G.2)
C	5	20	1	70	CSA (2008, Table G.2)
Ca	5	30	50	90	Davis et al. (1993, p. 155)
Cd	80	40	560	800	Davis et al. (1993, p. 155)
Cl	0.10	0.10	0.10	2200	Sheppard et al. (2002)
Cs	270	4400	1800	270	CSA (2008, Table G.2)
Hg	16	55	84	194	CSA (2008, Table G.2)
I	8.0	18	12	76	Sheppard et al. (2004a)
Mo	10	125	90	25	CSA (2008, Table G.2)
Np	2.5	13	21	530	Sheppard et al. (2004b)
Pa	540	1800	2700	6600	CSA (2008, Table G.2)
Pb	270	16 000	550	22 000	Davis et al. (1993, p. 155)
Pd	55	180	270	670	Davis et al. (1993, p. 155)
Po	150	400	3000	7300	Davis et al. (1993, p. 155)
Pu	540	1200	4900	1800	CSA (2008, Table G.2)
Ra	47	47	47	47	Sheppard et al. (2005a)
Rn ²	0.0	0.0	0.0	0.0	Gobien an Garisto (2012)
Sb	45	150	240	540	CSA (2008, Table G.2)
Se	150	490	740	1800	CSA (2008, Table G.2)
Sn	130	450	670	1600	CSA (2008, Table G.2)
Sr	13	20	110	150	CSA (2008, Table G.2)
Tc	0.14	0.1	1.2	1.5	CSA (2008, Table G.2)
Te	125	500	720	1900	CSA (2008, Table G.2)
Th	3000	3300	5400	89 000	CSA (2008, Table G.2)
U	42	220	180	2200	Sheppard et al. (2005b)
W	100	360	540	1250	Gobien an Garisto (2012)

¹Values are lognormally distributed with GM as stated and GSD=10, except for I in organic soil with GSD=22, Ra in all soils with GSD=4.9 and U in all soils with GSD=20.

²Rn soil K_d assumed to be constant and zero for all soil types.

8.4.4 River Sedimentation Rate

Table 8.6 provides data for the sedimentation rate of the different chemical elements in rivers. This parameter is defined as the fraction of the element in the water column that is lost to the sediments per unit time. It is the net rate of sedimentation, accounting for any resuspension of sediments back into the water column.

The river sedimentation rates were calculated from the equation (CSA 2008):

$$\lambda_{river} = \frac{DR \cdot \rho \cdot A \cdot K_d}{V}$$

where:

- λ_{river} is the river sedimentation rate (1/a);
- DR is the sediment accumulation rate, 1 mm/a (CSA 2008);
- ρ is the sediment density, 400 kg_{dw}/m³ (CSA 2008);
- A is the area of the river, m² (see Table 8.1)
- K_d is the solid-to-liquid partition coefficient, m³/kg_{dw}; and
- V is the West River volume (m³) (see Table 8.1)

CSA (2008) recommends setting the sediment solid-to-liquid partition coefficient to be 5 times the K_d of loam. Values of the lake sedimentation rate are lognormally distributed with geometric mean values shown in Table 8.7 and the geometric standard deviation equal to that for the loam K_d values. Namely, a geometric standard deviation of 10 is used except for I in organic soils (GSD=22), Ra in all soils (GSD=4.9), U in all soils (GSD=20) and Rn in all soils (constant parameter).

Table 8.7: River Sedimentation Rates

Element	Sediment¹ K_d [m³/kg]	Sedimentation Rate [1/a]
Ac	7500	815
Ag	600	65
Am	48,000	5200
Bi	2250	245
Br	245	27
C	100	11
Ca	150	16
Cd	200	22
Cl	0.5	0.1
Cs	22,000	2390
Hg	275	30
I	90	10
Mo	625	68
Np	65	7
Pa	9000	978
Pb	80,000	8700
Pd	900	98
Po	2000	217
Pu	6000	652
Ra	235	26
Rn ²	0	0.0
Sb	750	82
Se	2450	266
Sn	2250	245
Sr	100	11
Tc	0.5	0.1
Te	2500	272
Th	16,500	1800
U	1100	120
W	1800	196

¹Values are lognormally distributed with GM as stated and GSD=10, except for I in organic soil with GSD=22, Ra in all soils with GSD=4.9 and U in all soils with GSD=20.

²Rn sediment K_d assumed to be constant and zero.

8.5 FARMING YIELDS

Table 8.8 summarizes the properties relevant for determining the productivity of the area used for farming and building purposes. The data are from CSA (2008), if available; otherwise the data are from Davis et al. (1993).

Table 8.8: Farming Yield Data

Parameter	Value	Comment
Forest renewal time	50 a	This is the average time for a forest to regenerate, used in estimating woodlot size. Normal PDF with mean 50 a, standard deviation 10 a, and bounds of 25 and 100 a. Davis et al. (1993) used a fixed value of 50 a.
Forest yield in fire	2.2 kg/m ²	Lognormal PDF with geometric mean of 2.2 kg/m ² and geometric standard deviation of 1.6 (Davis et al. 1993, p.260). Note only small fraction of the forest mass is consumed in a fire.
Forest yield for wood	10.5 kg/m ²	Fixed value (Davis et al. 1993, p.260).
Soil contamination of plants	5x10 ⁻⁴ kg _{drysoil} /kg _{wetbio}	Fixed value (Davis et al. 1993, p.258).
Plant yield (plant)	0.8 kg _{fw} /m ²	The yield per harvest of plant used to feed people. Corresponds to a plant human diet of 2/3 fruits and vegetables and 1/3 grain as per CSA (2008, Table G.5). Normal PDF with bounds 0.1 to 8 and standard deviation of 1, calculated using grain (winter wheat, spring wheat, fall rye, buckwheat, oats, barley, mixed grain, canola and coloured beans) data from OMAFRA (2012) and fruits and vegetable data from OMAFRA (2011a, 2011b).
Plant yield (milk)	0.6 kg _{fw} /m ²	The yield per harvest of plants used to feed milk and meat producing animals, such as dairy cattle, beef cattle and chicken. Assume all animals eat generic feed crop (CSA 2008, Table G.5). Normal PDF with bounds of 0.1 to 4 and standard deviation of 1.3, where bounds and standard deviation were determined using the yield from 2001 to 2011 for grain corn, soybeans, dry white beans, fodder corn from OMAFRA (2012).
Plant yield (meat)	0.6 kg _{fw} /m ²	
Plant yield (bird)	0.6 kg _{fw} /m ²	

9. DOSE PATHWAYS DATA

9.1 HUMAN LIFESTYLE CHARACTERISTICS

For the present-day temperate climate, the reference human group or "critical group" for dose assessment purposes is defined as a self-sufficient farm household living near the repository. Davis et al. (1993, p.274) indicated that up to 50% of rural residents in Ontario used wells; therefore, lakes and wells were equally likely sources of water within the probabilistic safety analyses. In the Sixth Case Study, the critical group is conservatively assumed to use a well, since contaminant concentrations should be higher in well water than in surface waters due to lower dilution.

The number of people living in the reference household was modelled based on the 1987 Canadian census data, which considers households of up to 36 people, and the 1996 Canadian census data, which lumps households of 6 people and more into the same count. The data follows a lognormal distribution with upper and lower bounds of 1 to 12 people per household. This distribution was fitted by a piece-wise uniform distribution so that only an integer number of people per household would be considered. According to the 1996 Canadian census, the average Ontario farm had 3.2 people per farm (Statistics Canada 2002). Since the models are to be applied for long time frames, it is judged that this piece-wise distribution, with a best-estimate of 3 persons per household, and a large probability density function range, is a reasonable estimate for the critical group size.

Table 9.1 summarizes the lifestyle characteristics that describe the reference farm household.

As noted in Table 9.1, vegetable crops in general would be more likely to be irrigated than forage crops. Furthermore, they are also likely to receive a larger amount of water. The amount of irrigation water required also depends on the soil type - sandy soils in particular are distinctly different in terms of the amount of water they can store for crop use. The recommended irrigation amounts are listed in Table 9.2. These were largely based on 30-year irrigation data from northern Ontario as summarized in Sheppard (1985). The data are represented by a normal probability density function, where the standard deviation was calculated using the 95th percentile from Coligado (1968). The lower limit of 0.02 m/a is recommended based on the argument that, when irrigation is invoked, this represents the minimum amount of water that would be applied. The upper bound was set at approximately three standard deviations beyond the mean.

The amount of irrigation water will be strongly inversely correlated to the amount of precipitation. The preferred measure would be the effective precipitation, the amount that actually infiltrates the soil. However, total precipitation is the input parameter in SYVAC3-CC4. Therefore, the irrigation rate is correlated to total annual precipitation with a negative correlation coefficient of -0.9.

Table 9.1: Human Lifestyle Characteristics for Farm Household

Parameter	Value	Comment
People per household	3	Piece-wise uniform PDF from 1 to 12 people per household (Statistics Canada 1996; Davis et al. 1993, p.270)
Domestic water demand per person	110 m ³ /a	Lognormal PDF with geometric mean 110 m ³ /a, GSD of 2 and bounds of 40 and 240 m ³ /a. Calculated from data in Environment Canada (2007)
Man's air inhalation rate	8400 m ³ /a	95 th percentile from CSA (2008)
Man's water ingestion rate	840 L/a	90 th percentile from CSA (2008)
Man's total energy need	18744 kJ/d	90 th percentile from CSA (2008)
Man's meat ingestion rate	103 g/d	Median intakes for male adult (CSA 2008, Table G.9a). Defined as lognormal PDF with GM equal to median and GSD=1.65 (Zach and Sheppard 1992). For a total energy intake of 18744kJ/d, this intake is prorated to 249 g/d.
Man's milk ingestion rate	283 g/d	Median intakes for male adult (CSA 2008, Table G.9a). Defined as lognormal PDF with GM equal to median and GSD=1.35 (Zach and Sheppard 1992). For a total energy intake of 18744kJ/d, this intake is prorated to 685 g/d.
Man's plant ingestion rate	796 g/d	Median intakes for male adult (CSA 2008, Table G.9a). Defined as lognormal PDF with GM equal to median and GSD=1.65 (Zach and Sheppard 1992). For a total energy intake of 18744 kJ/d, this intake is prorated to 1928 g/d.
Man's poultry ingestion rate	53 g/d	Median intakes for male adult (CSA 2008, Table G.9a). Defined as lognormal PDF with GM equal to median and GSD=1.65 (Zach and Sheppard 1992). For a total energy intake of 18744 kJ/d, this intake is prorated to 128 g/d.
Man's fish ingestion rate	7.9 g/d	Median intakes for male adult (CSA 2008, Table G.9a). Defined as lognormal PDF with GM equal to median and GSD=4.48 (Zach and Sheppard 1992). For a total energy intake of 18744 kJ/d, this intake is prorated to 19 g/d.
Soil ingestion rate	0.12 kg/a	95 th percentile value from CSA (2008).
Probability of irrigation	0.9 garden 0.02 forage	Fixed value (Davis et al. 1993, p.157). Probability of irrigating woodlot and peat bog are set to zero.
Irrigation period	100 a	Lognormal PDF with GM = 100 a, GSD = 4, and bounds of 50 and 10000 a (Davis et al. 1993, p.158).
Probability of using fresh lake sediments on fields	0.01	Fixed value. This is uncommon in the Canadian Shield. Infilled lakes are not included in this category, but are considered normal organic-soil fields (Davis et al. 1993, p.158).
Dredged sediment thickness	0.2 m	Fixed value. Thickness of lake sediment used as surface soil for farming, same value as soil thickness.
Cropping frequency	1/a garden 1/a forage 1/50 a woodlot 0 peat bog	Fixed value (Davis et al. 1993, p.137)
Cropping period, non-irrigated fields	50 a	Fixed value (Davis et al. 1993, p. 137). Period over which non-irrigated fields are farmed.
Cropping soil contaminant loss fraction	0.05	Fixed value (Davis et al. 1993, p.157).

Parameter	Value	Comment
Annual energy consumption per household	1.2x10 ⁵ MJ/a	Normal PDF with GM of 1.2x10 ⁵ MJ/a, standard deviation of 8x10 ³ MJ/a and bounds of 10 ⁵ MJ/a and 1.3x10 ⁵ MJ/a (Natural Resources Canada 2011).
Probability of burning peat for energy	1%	Fixed value (Davis et al. 1993, p.196). Burning peat as a fuel is not common in Canada.
Household lifetime	50 a	Fixed value (Garisto et al. 2004). Average duration for household to farm a particular area. Only used to estimate peat fuel requirements.
Building width	9.7 m	Lognormal PDF with GM = 9.7 m, GSD = 1.2, bounds of 8.4 and 24 m (Davis et al. 1993, p.197).
Building height	2.4 m	Fixed value for single-story house (Davis et al. 1993, p.197).
Building volume	228 m ³	Lognormal PDF with GM = 228 m ² , GSD = 1.42, bounds of 168 and 1382 m ³ , based on Height * (Width) ² . Fully correlated with building width.
Building occupancy factor	0.8	Fixed value (CSA 2008).
Building air infiltration rate	0.35 /hr	Fixed value (CSA 1989), minimum recommendation for tightly-sealed house.
Building wake plume entrainment factor	2	Fixed value (Davis et al. 1993, p.198). Value is conservatively set to maximize entrainment.
Probability of being located downwind from energy fires	0.25	Fixed value (Davis et al. 1993). This factor represents how much exposure a person has to nuclides released from a chimney due to burning contaminated wood or peat fuel.
Outdoor or ground exposure factor	0.2	Fixed value (CSA 2008)
Water immersion occupancy factor	0.042	Fixed value (CSA 2008).
Frequency of agricultural fires	1/a	Fixed value (Davis et al. 1993, p.180).
Frequency of land-clearing fires	1/(50 a)	Fixed value (Davis et al. 1993, p. 183).

Table 9.2: Irrigation Rate Parameters

Soil Type	Mean Irrigation Rate ¹ [m/a]	Standard Deviation [m/a]	Lower Bound [m/a]	Upper Bound [m/a]
Garden				
Sandy soil	0.2	0.06	0.02	0.4
Other soils	0.1	0.05	0.02	0.25
Forage field				
Sandy soil	0.1	0.06	0.02	0.3
Other soils	0.06	0.09	0.02	0.3

¹ Normal Probability Density Function.

Table 9.3 summarizes various timing-related parameters.

For example, the fish holdup time is the time between catching a fish and consuming the fish. Davis et al. (1993) state that locally caught fish are generally consumed within one day, while commercially processed fish are stored for an average of 10 days. A self-sufficient farmer would furthermore store food for the winter, so one might further expect that some of the fish consumed would be 3 to 6 months old. A shorter time minimizes decay, while a longer time maximizes ingrowth. Thus, a holdup time of 0.5 d is recommended.

Similarly, the building holdup time allows for any decay of radionuclides from soil or tree equilibrium levels till occupancy of the building. The values used in Davis et al. (1993) for these holdups were set to 1 or 6 months for soil and wood, respectively. Since buildings would likely have lifetimes on the order of 100 years, during which the radionuclides would be decaying, the decay is minimized.

Whether decay or ingrowth is more important, and so whether a shorter or longer time is more conservative, depends on the nuclide. For the long-lived radionuclides that tend to dominate the postclosure safety assessments, for example, a holdup of even 100 years is not an important factor. On the other hand, many biosphere models do not take credit for these holdup delays at all (e.g., CSA 2008). Since these holdups are likely to be of low importance, the values are set to those recommended by Davis et al. (1993).

Table 9.3: Timing Parameters

Parameter	Value	Comment
Fish holdup time	0.5 d	Time between catching and eating fish (Davis et al. 1993, p.249). Conservatively assume that the critical group eats local fish which is eaten within a day of being caught.
Plant holdup time	1 d	Time between plant absorbing nuclides and being consumed by man (Davis et al. 1993, p.248). Conservatively assume that the critical group eats local produce which is consumed 1 day after harvesting.
Animal feed holdup time	1 d milk 1 d bird 5 d meat	Time between removal of feed or forage from a field and the consumption of animal food types by man. (Davis et al. 1993, p.249). Conservatively assume that, in addition to the plant hold-up time (1d), the critical group consumes fresh milk and birds (0 d) and that they age their meat slightly (4d).
Animal drinking water holdup time	0 milk 0 bird 4 d meat	Time between water being consumed by animal, and animal (or milk) being consumed by man (Davis et al. 1993, p.249). Because animals drink fresh water from the lake or well, there is no delay between consumption of water and slaughter/milking of animals. Conservatively assume that the critical group consumes fresh milk and birds (0 d) and that they age their meat slightly (4d).
Animal air holdup time	0 milk 0 bird 4 d meat	Time between air inhaled by animal and animal (or milk) being consumed by man (Zach et al. 1996, p.36). Because animals inhale fresh air, there is no delay between inhalation and slaughter/milking of animals. Conservatively assume that the critical group consumes fresh milk and birds (0 d) and that they age their meat slightly (4d).
Animal soil holdup time	0 milk 0 bird 4 d meat	Time between soil being consumed by animal and animal (or milk) being consumed by man (Davis et al. 1993, p.249). Because animals ingest soil while grazing, there is no delay between ingestion of soil and slaughter/milking of animals. Conservatively assume that the critical group consumes fresh milk and birds (0 d) and that they age their meat slightly (4d).
Food exposure time	100 d plant 50 d milk 100 d bird 50 d meat	Time that plants consumed by people or by domestic animals are exposed to possible contamination (Davis et al. 1993, p.250).
Man's water holdup time	0 d	Time between removing water from source and its consumption by man (Davis et al. 1993, p.250).
Inorganic building material holdup time	30 d	Time between inorganic materials (e.g., sand, clay, rock) being removed from the ground and placed into buildings occupied by man (Davis et al. 1993, p.250). Conservatively assume that these materials are handled relatively rapidly.
Wood building material holdup time	180 d	Time between wood being harvested from woodlot and placed into building occupied by man (Davis et al. 1993, p.250). Normal holdup time is approximate half a year (for harvesting, processing, transporting, storing and building).
Tree age when harvested for building material	60 a	Time from seedling to mature tree. Mean rotation ages for Canadian spruces and firs (typical trees for building materials) from Bowles and Prickett (2001).
Element removal rate from vegetation	12 d	Half-life for physical loss of an element from exposed plant material (leaves), other than radioactive decay. Lognormal PDF with GM=12 d and GSD=2 (Davis et al. 1993, p.251). Bounds of 0.01 and 400 d.

9.2 HUMAN PHYSICAL CHARACTERISTICS

Table 9.4 summarizes the physical characteristics of the reference (adult) human used for dose calculations.

Table 9.4: Human Physical Characteristics

Parameter	Value	Comment
Hydrogen concentration in tissue	105 g/kg	Hydrogen content of bulk soft tissue is 10.5% by mass (ICRP 2002, Table 13.2)
Carbon content of soft tissue	16.0 kg	Carbon content of bulk soft tissue is 25.6% by mass (ICRP 2002, Table 13.2)
Chlorine content of soft tissue	0.13 kg	Chlorine content of bulk soft tissue is 0.2% by mass (ICRP 2002, Table 13.2).
Mass of soft tissue	62.5 kg	Difference between mass of reference man and mass of skeletal system ICRP (2002)
Mass of thyroid	0.020 kg	Fixed value (ICRP 2002).
Stable iodine content of thyroid	1.2x10 ⁻⁵ kg	Fixed value (Sheppard et al. 2002).

9.3 AIR CONCENTRATION PARAMETERS

The dispersion of contaminants into the atmosphere is characterized by several parameters. For contaminants that become airborne as fine particulates, the air concentration due to suspension of particulates from water bodies (i.e., aerosols) is calculated from $C_{air}^w = A_{DL,w} \cdot C_w$, and the air concentration due to suspension of dust particulates from land is calculated from $C_{air}^t = A_{DL,t} \cdot C_s$, where $A_{DL,w}$ is the aerosol load (m³ water/m³ air), $A_{DL,t}$ is the atmospheric dust load (kg/m³), and C_w and C_s are the radionuclide concentrations in water (mol/m³) and surface soil (mol/kg) (see Table 8.3).

In addition, for potentially gaseous nuclides (e.g., Rn-222, I-129, and C-14), additional volatilization terms are considered from both terrestrial sources (soils) and surface waters. The contributions of these sources to the nuclide concentrations in air are calculated as the product of the flux of the radionuclide from the source (i.e., a soil layer or a water body) and an atmospheric dispersion factor. These atmospheric dispersion factors are dependent on the source type (i.e., soil or water).

Aquatic degassing for all nuclides is defined by the following equation:

$$C_{air,AG}^i = \frac{\lambda_{vol}^i}{3.15 \times 10^7 \text{ s/a}} C_L^i Z_L D_L \quad (8.1)$$

where

λ_{vol}^i is the water-to-air loss rate constant for nuclide i for surface water [a^{-1}],
 C_L^i is the concentration of the nuclide i in river water [$mol\ m^{-3}$],
 Z_L is the depth of the river [m] (see Table 8.1), and
 D_L is the semi-empirical dispersion parameter over water described by equation (8.4) [$m^2_{water}\ m^{-3}_{air}$]

No empirical data are available for values of λ_{vol}^i for Rn and I. Therefore, the following equations are used to determine values of λ_{vol}^i for I and Rn:

$$\lambda_{vol}^{Rn} = \frac{K_{water}^{Rn} 3.15 \times 10^7 s/a}{Z_L} \quad (8.2)$$

$$\lambda_{vol}^{I129} = \frac{I_{MLA} 3.15 \times 10^7 s/a}{Z_L D_L} \quad (8.3)$$

where

K_{water}^{Rn} is the radon transfer coefficient from fresh water to air, 6.7×10^{-6} (mol/m^2s)/(mol/m^3) (Sheppard et al. 2002),

I_{MLA} is the iodine aquatic mass-loading parameter described by equation (8.5) [$m^3_{water}\ m^{-3}_{air}$], and

D_L and I_{MLA} are calculated as follows:

$$D_L = \frac{u_s}{u_{ref}} e^{5 \ln(\ln A_L) - 9} \left[\frac{s}{m} \right] \quad (8.4)$$

$$I_{MLA} = \frac{F_i k_v \sqrt{A_L}}{u_s Z_a} \quad [-] \quad (8.5)$$

where

u_{ref} is the annual wind speed across the Canadian shield (m/s) (see Table 8.3),

u_s is the annual wind speed at the repository site, assumed to be the same as u_{ref} (m/s),

A_L is the area of the river (m^2) (see Table 8.1),

F_i is a correction factor (=0.80) to account for ice and lower temperatures in the winter months

k_v is the iodine volatilization constant = 8.8×10^{-3} m/a (Connan et al. 2008), and

Z_a is the height of the air compartment = 2 m.

The values for these and other dispersion parameters are listed in Table 9.5.

Table 9.5: Volatilization Parameters

Parameter	Value	Comment
Degassing rate from river water	0.92/a for C 1.34x10 ⁻² /a for I 45.9/a for Rn 0 for others	Value for C from Davis et al. (1993). Value for I is calculated from Equation 8.3 using parameter values described in the text. Value for Rn is calculated from Equation 8.2 using parameter values described in the text.
Gas evasion (degassing) rate from soil	13.6/a for C 9.47x10 ⁻⁴ /a for Cl 2.11x10 ⁻² /a for I 3.16x10 ⁻² /s for Se 0 for others	Only C, I, Cl and Se are considered volatile. Rn is treated separately. Lognormal PDF with GM as given on left and GSD of 3.3 for C (Zach et al. 1996) and GSD of 10 for Cl (Sheppard et al. 2004a), I (Sheppard et al. 2002) and Se (Davis et al. 1993).
Radon emission rate from soil	2.7x10 ⁻⁹ (mol/m ² .s)/(mol/kg)	Lognormal PDF with GM=2.7x10 ⁻⁹ (mol _{Rn222} /m ² .s) / (mol _{Ra226} /kg _{dry soil}), GSD = 2.16 (Sheppard et al. 2005b).
Radon indoor transfer coefficient	1.0x10 ⁻⁵ (mol/m ³)/(mol/kg)	Lognormal PDF with GM =1.0x10 ⁻⁵ (mol _{Rn222} /m ³ _{air}) / (mol _{Ra226} /kg _{dry soil}), GSD = 2.6 (Sheppard et al. 2005b).
Release fraction from indoor water use	Varies by element	Most elements are not volatile under domestic water conditions of E _n and pH. Values are as follows (Zach et al. 1996, p.14): Rn, Xe, Ar, Kr - Triangular PDF with most probable value of 0.52 and range from 0.3 to 0.9 C - uniform PDF from 0.25 to 1.0 All others - loguniform PDF from 0.00052 to 0.052
Release fraction from agricultural fires	Varies by element	Set to 0.2 for all elements, except for Ar, C, Cl, H, I, Kr, Rn, and Xe for which value is 1 (Davis et al. 1993, p.195).
Release fraction from energy fires	Varies by element	Set to 0.2 for all elements, except for Ar, C, Cl, H, I, Kr, Rn, and Xe for which value is 1 (Davis et al. 1993, p.195).
Release fraction from land clearing (or forest) fires	1	These fires can burn hotter than energy and agricultural fires (Davis et al. 1993, p.195).

9.4 MISCELLANEOUS PHYSICAL PARAMETERS

The miscellaneous physical parameters used in the biosphere model are listed in Table 9.6. The physical properties of the various human foods are given in Table 9.7 and Table 9.8.

Table 9.6: Physical Parameters

Parameter	Value	Comment
Hydrogen content of water	112,000 g/m ³	Mass H = 1.00794, mass O = 15.994, density of water at 16°C = 999 kg/m ³ .
Energy content of peat	5 MJ/kg	Fixed value. Based on average 10 MJ/kg for milled peat, used in wood stove with 50% efficiency (Davis et al. 1993, p.194).
Energy content of wood	5.5 MJ/kg	Fixed value. Based on average 11 MJ/kg for Canadian wood, used in wood stove with 50% efficiency (Davis et al. 1993, p.194).
Hydrogen content of wood	63 g/kg	Average for hardwoods and softwoods in Table 3 of Ragland and Aerts (1991)
Plant interception fractions for food	0.05 irrigation, 1.0 atmospheric	Fraction of the aerial nuclide deposition (wet or dry) that is retained on exposed plant parts and consumed by humans or animals (Davis et al. 1993, p.258)
Plant interception fractions for wood	1.0	This is the fraction of the aerial nuclide deposition that is retained on wood used for building material (Davis et al. 1993, p.259)
Soil to building density conversion factor	1	No change in density of inorganic materials between natural form and as used in building materials (Davis et al. 1993, p.264).
Dry/wet soil conversion factor	0.95	(Davis et al. 1993, p.263)
Wet/dry wood conversion factor	1.7	(Davis et al. 1993, p.264)

Table 9.7: Food Energy and Water Content

Parameter	Value	Comment
Carbohydrate fuel value	16.3 kJ/g	CSA (2008) Table G.8
Fat fuel value	37.7 kJ/g	CSA (2008) Table G.8
Protein fuel value	16.7 kJ/g	CSA (2008) Table G.8

Table 9.8: Nutrient Content of Foods¹

	Plant	Milk	Meat	Bird	Fish
Carbohydrate content [g/kg]	169	32.0	5.4	3.2	0.0
Fat content [g/kg]	25.6	191	203	43.9	62.6
Protein content [g/kg]	49.4	114	170	198	178

¹CSA (2008), Table G.8. Units are per kg of wet biomass for plant, meat, bird and fish, and per L for milk.

9.5 ANIMAL CHARACTERISTICS

The feeding rates of the various domestic animals are given in Table 9.9.

The animal feed ingestion rate corresponds to the allometric feed intake from Table G.6 of CSA (2008), converted to a wet weight basis using the dry/wet weight ratio of 0.53 for forage plants, described in Section 8.4. The animal water consumption rate corresponds to the allometric water intake from Table G.6 of CSA (2008). The inhalation rate corresponds to the allometric inhalation rate from CSA (2008). The soil ingestion rate is calculated from CSA (2008) values assuming that half the soil load is from grazed feed and the other half from harvest feed, in addition to soil from “other contaminated sources”, as reported in CSA (2008). The standard deviation and bounds are from Davis et al. (1993) and are prorated to match the mean derived from the CSA (2008) values. Human food yields are from Davis et al. (1993).

Table 9.9: Domestic Animal Data¹

Parameter	Bird	Dairy cow	Beef cow
Human food yield [Quantity/a/animal]	2.03 kg/a	4600 L/a	145 kg/a
Animal feed consumption rate [kg _{wet weight} /d]	Normal PDF M=0.2 SD=0.047 LB=0.047 UB=0.42	Normal PDF M=37 SD=9.3 LB=9.3 UB=84	Normal PDF M=25 SD=6.2 LB=6.2 UB=56
Animal water consumption rate [L/d], with 0.75 correlation with animal feed consumption	Normal PDF M=0.1 SD=0.03 LB=0.03 UB=0.18	Normal PDF M=75 SD=19 LB=19 UB=130	Normal PDF M=31 SD=8 LB=8 UB=54
Animal soil ingestion rate [kg/d], with 0.75 correlation with animal feed consumption	Normal PDF M=0.013 SD=0.003 LB=0.003 UB=0.029	Normal PDF M=1.6 SD=0.4 LB=0.4 UB=3.6	Normal PDF M=0.56 SD=0.14 LB=0.14 UB=1.3
Animal air inhalation rate [m ³ _{air} /d], with 0.75 correlation with animal feed consumption	Normal PDF M=1 SD=0.3 LB=0.3 UB=2.3	Normal PDF M=87 SD=22 LB=21 UB=198	Normal PDF M=87 SD=22 LB=22 UB=196

¹PDF = probability density function, M = mean, SD = standard deviation, LB = lower bound, UB = Upper bound.

Table 9.10 summarizes the mean values for the animal food ingestion transfer coefficients. These values describe the amount of a contaminant in the animal's daily food intake that appears in their produce as used for human food. For example, in the case of dairy cattle, it is the amount of contaminant (mol/kg) in the cow food intake (kg/d) that appears in the milk (mol/L) and has units of (mol/L)/(mol/kg * kg/d) = (d/L).

Table 9.10: Animal Ingestion Transfer Coefficients¹

Element	Milk [d/L]	Meat (beef) [d/kg _{wetbio}]	Bird (poultry) [d/kg _{wetbio}]	Freshwater fish [L/kg _{wetbio}]
Ac	2.0 x 10 ⁻⁵	2.5 x 10 ⁻⁵	2.5 x 10 ⁻³	2.5 x 10 ¹
Am	1.1 x 10 ⁻⁶	1.6 x 10 ⁻⁵	1.2 x 10 ⁻³	3.0 x 10 ¹
Bi	5.0 x 10 ⁻⁴	4.0 x 10 ⁻⁴	4.0 x 10 ⁻²	1.5 x 10 ¹
C	2.8 x 10 ⁻²	8.8 x 10 ⁻²	8.5 x 10 ⁰	5.7 x 10 ³
Ca	1.1 x 10 ⁻²	1.6 x 10 ⁻³	4.4 x 10 ⁻¹	4.0 x 10 ¹
Cl	1.5 x 10 ⁻²	2.0 x 10 ⁻²	2.0 x 10 ⁰	5.0 x 10 ¹
Cs	7.5 x 10 ⁻³	3.7 x 10 ⁻²	4.4 x 10 ⁰	3.5 x 10 ³
I	7.6 x 10 ⁻³	1.2 x 10 ⁻²	7.5 x 10 ⁰	6.0 x 10 ⁰
Np	5.0 x 10 ⁻⁶	2.0 x 10 ⁻⁴	2.0 x 10 ⁻²	1.5 x 10 ²
Pa	5.0 x 10 ⁻⁶	1.1 x 10 ⁻⁵	2.0 x 10 ⁻³	1.0 x 10 ¹
Pb	2.6 x 10 ⁻⁴	4.0 x 10 ⁻⁴	4.0 x 10 ⁻²	3.0 x 10 ²
Po	3.4 x 10 ⁻⁴	4.5 x 10 ⁻³	4.5 x 10 ⁻¹	5.0 x 10 ²
Pu	6.0 x 10 ⁻⁷	2.1 x 10 ⁻⁵	9.2 x 10 ⁻⁴	3.0 x 10 ¹
Ra	6.2 x 10 ⁻⁴	9.0 x 10 ⁻⁴	1.3 x 10 ⁻¹	5.0 x 10 ¹
Rn	0.0	0.0	0.0	0.0
Sb	7.0 x 10 ⁻⁵	4.4 x 10 ⁻⁴	1.0 x 10 ⁻¹	1.5x 10 ¹
Se	1.0 x 10 ⁻²	1.0 x 10 ⁻¹	9.0 x 10 ⁰	2.0 x 10 ²
Sn	1.1 x 10 ⁻³	1.1 x 10 ⁻²	1.2 x 10 ⁰	3.0 x 10 ³
Sr	2.0 x 10 ⁻³	2.1 x 10 ⁻³	7.6 x 10 ⁻²	2.0 x 10 ⁰
Th	2.4 x 10 ⁻⁵	1.2 x 10 ⁻⁴	1.0 x 10 ⁻²	1.0 x 10 ²
U	3.7 x 10 ⁻⁴	4.0 x 10 ⁻⁴	1.2 x 10 ⁰	5.0 x 10 ¹

¹Data for chemically hazardous elements (Ag, Br, Cd, Hg, Mo, Pd, Se, Tc, Te, and W), have been excluded from the dose model data.

The Cl, I, Np, Ra and U values are from Sheppard et al. (2002, 2004a, 2004b, 2005a and 2005b, respectively). The remaining values are preferentially taken from CSA (2008, Table G.3), and supplemented with values from Davis et al. (1993, p.233) for Ac, Bi, Ca, Pb and Po. The CSA values for milk were expressed in d/kg and these were converted to d/L using a milk density of 1.032 L/kg (Wong et al. 1999). For all elements, except those listed below, a lognormal distribution with a geometric standard deviation of 3.2 was recommended in Davis et al. (1993), reflecting the natural variability in both animals and their feed. For I in milk, a geometric standard deviation of 2.9 was recommended by Sheppard et al. (2002); for Cl in birds, milk and meat, a geometric standard deviation of 2.2 was recommended by Sheppard et al. (2004a); and for Ra in birds, a geometric standard deviation of 7 was recommended by Sheppard et al. (2005a).

Table 9.10 also lists the geometric mean values for the transfer coefficients for freshwater fish. This is the bioaccumulation factor, or the ratio between the nuclide concentrations in fish flesh (mol/kg_{wet biomass}) to that in water (mol/L). The geometric standard deviation is 12 for all

elements. The sources of these data are the same as discussed above for the animal food ingestion transfer coefficients, except that they are from Table A.25a in CSA (2008).

Table 9.11 provides the geometric mean values for terrestrial animal inhalation transfer coefficients - the amount of contaminant in the animal's daily intake by inhalation that appears in the animal produce used by humans for food. A geometric standard deviation of 5.2 is used for all elements (Zach et al. 1996). The data sources are the same as those for the ingestion transfer coefficients above, except that for the data from CSA (2008), the ingestion transfer coefficients from Table 9.10 were multiplied by the inhalation/ingestion ratios given in Table G.7 of CSA (2008).

Table 9.11: Animal Inhalation Transfer Coefficients¹

Element	Dairy cattle (milk) [d/L]	Beef cattle (meat) [d/kg _{wetbio}]	Bird (poultry or eggs) [d/kg _{wetbio}]
Ac	1.0 x 10 ⁻²	1.3 x 10 ⁻²	1.3 x 10 ⁰
Am	2.7 x 10 ⁻⁴	3.9 x 10 ⁻³	2.9 x 10 ⁻¹
Bi	5.5 x 10 ⁻³	4.4 x 10 ⁻³	4.4 x 10 ⁻¹
C	5.6 x 10 ⁻⁴	1.8 x 10 ⁻³	1.7 x 10 ⁻¹
Ca	1.3 x 10 ⁻²	1.9 x 10 ⁻³	5.3 x 10 ⁻¹
Cl	1.7 x 10 ⁻²	8.0 x 10 ⁻²	8.0 x 10 ⁰
Cs	4.7 x 10 ⁻³	2.3 x 10 ⁻²	2.8 x 10 ⁰
I	0.0	0.0	0.0
Np	7.5 x 10 ⁻⁵	8.3 x 10 ⁻⁴	8.3 x 10 ⁻²
Pa	1.2 x 10 ⁻³	2.7 x 10 ⁻³	4.8 x 10 ⁻¹
Pb	7.8 x 10 ⁻⁴	1.2 x 10 ⁻³	1.2 x 10 ⁻¹
Po	1.9 x 10 ⁻³	2.5 x 10 ⁻²	2.5 x 10 ⁰
Pu	1.4 x 10 ⁻⁴	5.1 x 10 ⁻³	2.2 x 10 ⁻¹
Ra	5.6 x 10 ⁻⁴	1.3 x 10 ⁻³	1.3 x 10 ⁻¹
Rn	0.0	0.0	0.0
Sb	1.2 x 10 ⁻⁴	7.5 x 10 ⁻⁴	1.7 x 10 ⁻¹
Se	7.5 x 10 ⁻³	7.5 x 10 ⁻²	6.8 x 10 ⁰
Sn	2.7 x 10 ⁻²	2.7 x 10 ⁻¹	2.9 x 10 ¹
Sr	1.8 x 10 ⁻³	1.9 x 10 ⁻³	6.9 x 10 ⁻²
Th	2.3 x 10 ⁻³	1.2 x 10 ⁻²	1.0 x 10 ⁰
U	4.1 x 10 ⁻³	2.2 x 10 ⁻³	1.3 x 10 ⁻¹

¹Data for chemically hazardous elements (Ag, Br, Cd, Hg, Mo, Pd, Se, Tc, Te, and W), have been excluded from the dose model data.

9.6 DOSE COEFFICIENTS

The International Commission on Radiological Protection (ICRP) 2007 recommendations are considered to be the best estimate of dose response for humans (ICRP 2007) and replace the 1990 recommendations (ICRP 1991). The new recommendations do not lead to changes in dose limits.

The recommendations are based on the Linear No-Threshold model, although account was taken of dose and dose-rate effects in their derivation.

In the Sixth Case Study, radiological exposures to humans are converted to dose rates using

dose coefficients based on the 1990 ICRP recommendations (ICRP 1991), since dose coefficients based on the 2007 recommendations are not yet available. However, dose coefficients are not expected to change substantially (Wrixon 2008).

9.6.1 Adult Ingestion Dose Coefficients

The adult human ingestion dose coefficients are presented in Table 9.12 and are taken from Gobien and Garisto (2012). They are based on ICRP 72 (ICRP 1996) which is consistent with ICRP 60 recommendations (ICRP 1991). Gobien and Garisto (2012) included in the dose coefficients of parent radionuclides the contributions from progeny with half-lives less than 1-day. That is, the dose coefficients assume that an amount of progeny in secular equilibrium with the parent is eaten (the ICRP values only account for ingrowth of progeny within the body). Since the present study does not explicitly model radionuclides with half-lives less than one day, this ensures that doses from these short-lived nuclides are fully included in any dose calculations involving their parent.

The biosphere model also includes a groundwater limit to the internal I-129, Cl-36 and C-14 human doses (NWMO 2012b, Section 5.6). The groundwater dose limit for I-129 is attained when the ratio of I-129 to total iodine in the thyroid is equal to that in groundwater (well water or water discharging into the lake). For Cl-36 (or C-14), the groundwater dose limits are attained when the ratio of Cl-36 to stable chlorine (or C-14 to stable carbon), in the soft tissue of man's body is equal to that in groundwater. These limits reflect that the human body does not distinguish between isotopes when incorporating these elements into its tissue, and in particular will not concentrate the radioisotopes.

The calculation of the groundwater internal dose limits requires data on the concentration of stable I, Cl and C in groundwater and on the human internal dose conversion factors for I-129, Cl-36 and C-14. The values for these parameters are listed in Table 9.13. For I-129, the internal dose conversion factor is based on the thyroid specific-activity model described above; for Cl-36 and C-14, the internal dose conversion factors are on a soft tissue specific activity model.

9.6.2 Adult Inhalation Dose Coefficients

The adult inhalation doses coefficients are presented in Table 9.12, and are from Gobien and Garisto (2012). These were based on the values in ICRP 72 recommendations (ICRP 1996). The dose coefficients of parent nuclides include contributions from daughters with half-lives less than 1-day, so that doses from these short-lived nuclides are included in any dose calculations involving their parent.

9.6.3 Adult Ground Exposure and Air Immersion Dose Coefficients

The adult ground exposure and air immersion dose coefficients are presented in Table 9.12, and are from Gobien and Garisto (2012). These were based on the values in Eckerman and Leggett (1996), which are consistent with ICRP 60 (ICRP 1991). Gobien and Garisto (2012) included in the dose coefficient of parent nuclides contributions from any progeny with half-lives less than 1 day.

9.6.4 Adult Water Immersion Dose Coefficients

Eckerman and Leggett (1996) calculate adult water immersion dose coefficients based on the recommendations in ICRP 60 (ICRP 1991). These data were selected for use in the Sixth Case Study unless otherwise stated. The values are presented in Table 9.12.

The dose coefficients in Eckerman and Leggett (1996) do not include any contributions from progeny. Although radionuclides with half-lives less than one day are not explicitly modelled in the Sixth Case Study, their contribution to the total water immersion dose is accounted for by adding their water immersion dose coefficient or a fraction thereof (depending on the decay scheme) to that of the parent radionuclide, to derive effective water immersion dose coefficients for the parent, as was done for other dose coefficients (Gobien and Garisto 2012).

9.6.5 Adult Building Exposure Dose Coefficients

Whole body building dose coefficients were derived from Holford (1989), who lists building dose coefficients, in units of (Sv/a)/(Bq/kg), for three building types: concrete, wood-log and wood-frame house.

The building dose coefficients in Holford (1989) are based on ICRP26/28 recommendations. However, MacDonald and Laverock (1996) compare air, water and soil external dose coefficients based on the ICRP26/28 and ICRP60 recommendations. Thus, the ICRP60 whole body building dose coefficients, for each building type, were estimated by dividing the ICRP26/28 dose coefficients from Holford (1989) for a nuclide by the smallest value of the ICRP26/28-to-ICRP60 dose coefficient ratio listed in MacDonald and Laverock (1996) for that particular nuclide.

Radionuclides with half-lives less than one day are not explicitly modelled in the Sixth Case Study assessment. Instead, their contribution to the total building exposure dose rate is accounted for by adding their building dose coefficient or a fraction thereof (depending on the decay scheme) to that of the parent radionuclide to derive an effective building dose coefficient for the parent.

The CC4 biosphere model does not simulate the ingrowth of radionuclides in building materials. This may be a non-conservative approximation if the building dose coefficient of the progeny is higher than that of the parent and ingrowth contributes significantly to the progeny concentration in building materials. Hence, radionuclides with half-lives less than 2 years are assumed to be in secular equilibrium with their parents in all building materials, and their contribution to the total building exposure dose rate is accounted for by adding their effective building dose coefficient to that of the parent radionuclide. In this case, the building dose coefficient of the short-lived progeny is set to zero (see Table 9.12).

For each nuclide, the largest of the building dose coefficients for the three building types was conservatively chosen for use in the Sixth Case Study. The effective building dose coefficients are presented in Table 9.12.

Table 9.12: Adult Human Dose Coefficients¹

Radio-nuclide	Air immersion (Sv/a)/ (Bq/m ³)	Ground exposure (Sv/a)/ (Bq/kg soil)	Building exposure (Sv/a)/ (Bq/kg dry material)	Water immersion (Sv/a)/ (Bq/m ³)	Ingestion (Sv/Bq)	Inhalation (Sv/Bq)
Ac-225*	3.26E-07	3.20E-07	0.00E+00 [#]	6.96E-10	2.43E-08	8.53E-06
Ac-227*	1.12E-09	7.97E-10	1.17E-06	2.39E-12	1.10E-06	5.50E-04
Am-241	2.13E-08	1.00E-08	4.70E-08	4.86E-11	2.00E-07	9.60E-05
Bi-210	8.14E-09	1.47E-09	0.00E+00 [#]	9.40E-12	1.30E-09	9.30E-08
C-14	8.20E-11	2.97E-12	0.00E+00	9.09E-14	5.80E-10	5.80E-09
Ca-41	0.00E+00	0.00E+00	0.00E+00	0.00E+00	1.90E-10	1.80E-10
Cl-36	5.24E-09	6.72E-10	5.70E-10	6.15E-12	9.30E-10	7.30E-09
Cs-135	3.00E-10	8.68E-12	0.00E+00	3.28E-13	2.00E-09	8.60E-09
I-129	8.87E-09	2.58E-09	2.00E-08	2.07E-11	1.10E-07	3.60E-08
Np-237	2.80E-08	1.88E-08	6.47E-07	6.28E-11	1.10E-07	5.00E-05
Pa-231	4.95E-08	4.77E-08	1.10E-07	1.08E-10	7.10E-07	1.40E-04
Pa-233	2.70E-07	2.54E-07	0.00E+00 [#]	5.90E-10	8.70E-10	3.90E-09
Pb-210	1.41E-09	5.35E-10	4.05E-09	3.28E-12	6.90E-07	5.60E-06
Po-210	1.23E-11	1.33E-11	0.00E+00 [#]	2.66E-14	1.20E-06	4.30E-06
Pu-239	1.10E-10	7.12E-11	2.40E-10	2.47E-13	2.50E-07	1.20E-04
Pu-240	1.08E-10	3.04E-11	2.60E-10	2.52E-13	2.50E-07	1.20E-04
Pu-242	9.15E-11	2.68E-11	2.20E-10	2.13E-13	2.40E-07	1.10E-04
Ra-223*	4.11E-07	3.76E-07	0.00E+00 [#]	8.76E-10	1.00E-07	8.71E-06
Ra-225	7.57E-09	2.33E-09	0.00E+00 [#]	1.66E-11	9.90E-08	7.70E-06
Ra-226	8.96E-09	7.88E-09	6.32E-06	1.97E-11	2.80E-07	9.50E-06
Ra-228	1.42E-06	1.53E-06	3.97E-06	3.06E-09	6.90E-07	1.60E-05
Rn-222*	2.63E-06	2.86E-06	0.00E+00 [#]	5.71E-09	2.50E-10	3.50E-09
Sb-126	4.04E-06	4.34E-06	0.00E+00 [#]	8.77E-09	2.40E-09	3.20E-09
Se-79	1.24E-10	4.14E-12	0.00E+00	1.37E-13	2.90E-09	6.80E-09
Sn-126	2.27E-06	2.39E-06	6.76E-06	4.93E-09	4.74E-09	2.80E-08
Sr-90	3.10E-09	1.75E-10	0.00E+00	3.44E-12	2.80E-08	1.60E-07
Th-227	1.40E-07	1.30E-07	0.00E+00 [#]	3.06E-10	8.80E-09	1.00E-05
Th-229	1.06E-07	7.83E-08	9.67E-07	2.36E-10	4.90E-07	2.40E-04
Th-230	4.67E-10	2.89E-10	1.00E-09	1.05E-12	2.10E-07	1.00E-04
Th-231	1.45E-08	8.68E-09	2.90E-08	3.19E-11	3.40E-10	3.30E-10
Th-232	2.28E-10	1.23E-10	5.20E-10	5.18E-13	2.30E-07	1.10E-04
Th-234*	5.65E-08	4.21E-08	9.50E-08	1.03E-10	3.40E-09	7.70E-09
U-233	4.48E-10	3.42E-10	8.90E-10	9.94E-13	5.10E-08	9.60E-06
U-234	1.93E-10	9.29E-11	4.60E-10	4.39E-13	4.90E-08	9.40E-06
U-235	2.04E-07	1.78E-07	4.40E-07	4.51E-10	4.70E-08	8.50E-06
U-236	1.22E-10	4.80E-11	3.00E-10	2.81E-13	4.70E-08	8.70E-06
U-238	7.89E-11	2.15E-11	1.90E-10	1.85E-13	4.50E-08	8.00E-06

*Identifies radionuclides whose dose coefficients include contributions from secular-equilibrium progeny with half-lives less than one day.

[#]The building dose coefficient is set to zero for short-lived nuclides for which the building dose coefficient is added to the building dose coefficient of a longer lived parent.

¹Data for chemically hazardous elements (Ag, Br, Cd, Hg, Mo, Pd, Se, Tc, Te, and W), have been excluded from the dose model data.

Table 9.13: Parameters for Human Specific Activity Models

Parameter	Units	Value	Comment
Stable iodine concentration in groundwater	kg/L	7.0×10^{-9}	GM of lognormal PDF with GSD of 8.0 and bounds of 1.0×10^{-10} to 4.0×10^{-7} (Sheppard and Gascoyne 1997).
Stable chlorine concentration in groundwater	kg/L	3.0×10^{-5}	GM of lognormal PDF with GSD of 6.0 and bounds of 8.0×10^{-7} to 1.0×10^{-3} (Sheppard and Gascoyne 1997).
Stable carbon concentration in groundwater	kg/L	4.0×10^{-5}	GM of lognormal PDF with GSD of 3.0 and bounds of 4.0×10^{-6} to 2.0×10^{-4} (Sheppard and Gascoyne 1997). Upper bound set to maximum observed concentration.
^{129}I internal dose conversion factor (based on thyroid specific activity model)	(Sv/a)/ (Bq/kg thyroid)	1.6×10^{-8}	Zach et al. (1996, p.32)
^{36}Cl internal dose conversion factor (based on specific activity model)	(Sv/a)/ (Bq/kg soft tissue)	1.38×10^{-6}	Zach et al. (1996, p.31)
^{14}C internal dose conversion factor (based on specific activity model)	(Sv/a)/ (Bq/kg soft tissue)	2.50×10^{-7}	Davis et al. (1993)
^3H internal dose conversion factor (based on specific activity model)	(Sv/a)/ (Bq/kg soft tissue)	2.9×10^{-8}	Davis et al. (1993)

9.7 No-Effect Concentrations for Non-Human Biota

Potential radiological impacts on non-human biota are assessed using the equations and data from Medri and Bird (2014) and are documented in NWMO (2017).

9.8 Chemical Hazard

The proposed values for protection of humans and non-human biota from potentially chemically hazardous elements are listed in Medri (2015b) and are based on Canadian guideline values for concentrations in environmental media relevant to human health and environmental protection, supplemented as needed.

10. SUMMARY

For the Sixth Case Study, several codes were used to support the safety assessment. The data and codes used for this project have been maintained under configuration management and have been documented according to the NWMO software procedure. This report briefly describes the codes and data. For further details, references to the original documentation are provided.

Most of the model parameters are the same as the Canadian dataset developed as part of the Fourth Case Study (NWMO 2012a). The notable model parameters changes are:

- new repository site location;
- new MKII container with a 48 bundle capacity;
- revised repository design to accommodate the new MKII container design, with in-room container placement and 20 m room spacing;
- revised geosphere transport network, based on the new site geosphere model;
- changes in groundwater discharge areas, resulting from new site geosphere model and new repository location;
- main groundwater discharge from repository is to a river rather than a lake;
- new Zr corrosion rate model and data; and
- additional data for bundles with 280 MWh/kgU burnup.

11. REFERENCES

- Amiro, B.D. 1992. The atmosphere submodel for the assessment of Canada's nuclear fuel waste management concept. Atomic Energy of Canada Limited Report, AECL-9889, COG-91-199. Pinawa, Canada.
- Bäckblom, G. 2008. Excavation damage and disturbance in crystalline rock – results from experiments and analyses. SKB Technical Report TR-08-08. Stockholm, Sweden.
- Baston, G.M.N., J.A. Berry, M. Brownsword, T.G. Heath, D.J. Ilett, R. McCrohon, C.J. Tweed and M. Yui. 1999. The sorption of polonium, actinium and protactinium onto geological materials. Mat. Res. Soc. Symp. Proc. 556, 1107-1114.
- Baumgartner, P. 2006. Generic thermal-mechanical-hydraulic (THM) data for sealing materials – Volume 1: Soil-water relationships. Ontario Power Generation Report 06819-REP-01300-10122-R00. Toronto, Canada.
- BEAK International. 2002. Guidance for calculation of Derived Release Limits for radionuclides in airborne and liquid effluents from Ontario Power Generation Nuclear Facilities - Appendices. Ontario Power Generation Report N-REP-03482-10000-R00. Toronto, Canada.
- Beals, D.I. 1985. Soil and climate parameters for post-closure biosphere assessment of nuclear fuel waste disposal. Atomic Energy of Canada Limited Technical Record, TR-285. Pinawa, Canada.
- Bowles, I.A. and G.T. Prickett. 2001. Footprints in the Jungle. Oxford University Press. NY, USA. p137
- CDCD (Canadian Daily Climate Data). 2006. National Climate Data and Information Archive. Retrieved online at: <ftp://arcdm20.tor.ec.gc.ca/pub/dist/CDCD/>
- Chadwick, M.B., M. Herman, P. Obložinský, M.E. Dunn, Y. Danon, A.C. Kahler, D.L. Smith, B. Pritychenko, G. Arbanas, R. Arcilla, R. Brewer, D.A. Brown, R. Capote, A.D. Carlson, Y.S. Cho, H. Derrien, K. Guber, G.M. Hale, S. Hoblit, S. Holloway, T.D. Johnson, T. Kawano, B.C. Kiedrowski, H. Kim, S. Kunieda, N.M. Larson, L. Leal, J.P. Lestone, R.C. Little, E.A. McCutchan, R.E. MacFarlane, M. MacInnes, C.M. Mattoon, R.D. McKnight, S.F. Mughabghab, G.P.A. Nobre, G. Palmiotti, A. Palumbo, M.T. Pigni, V.G. Pronyaev, R.O. Sayer, A.A. Sonzogni, N.C. Summers, P. Talou, I.J. Thompson, A. Trkov, R.L. Vogt, S.C. van der Marck, A. Wallner, M.C. White, D. Wiarda, P.G. Young. 2011. ENDF/B-VII.1 Nuclear data for science and technology: Cross section, covariances, fission product yields, and decay data. *Nuclear Data Sheets*: 112-12, 2887-2996 (2011).
- Chan, T., M. Kolar, P.A. O'Connor, N.W. Scheier and F.W. Stanchell. 1999. Finite-element sensitivity analysis of effects of an excavation damage zone on ¹²⁹I transport from a used CANDU fuel waste disposal repository. Ontario Hydro Report 06819-REP-01200-0022-R00. Toronto, Canada.
- Chen, J.D., P.A. Seeley, R. Taylor, D.C. Hartrick, N.L. Pshhyshlak, K.H. Wasywich, A. Rochon and K.I. Burns. 1986. Characterization of corrosion deposits and the assessment of fission products released from used CANDU fuel. Proceedings 2nd International

- Conference on Radioactive Waste Management. Winnipeg, Canada, 7-11 September 1986. Canadian Nuclear Society, Canada.
- CNSC (Canadian Nuclear Safety Commission). 2006. Assessing the Long Term Safety of Radioactive Waste Management. CNSC Regulatory Guide G-320. Ottawa, Canada.
- Coligado, M.C., W. Baier and W.K. Sly. 1968. Risk Analyses of Weekly Climatic Data for Agricultural and Irrigation Planning, Kapuskasing, Ontario, Technical Bulletin 31, Canada Land Inventory, Dept of Forestry and Rural Development, Agriculture Canada, p8.
- Coligado, M.C., W. Baier and W.K. Sly. 1969a. Risk Analyses of Weekly Climatic Data for Agricultural and Irrigation Planning, Armstrong, Ontario, Technical Bulletin 64, Canada Land Inventory, Dept of Forestry and Rural Development, Agriculture Canada. 8 pp.
- Coligado, M.C., W. Baier and W.K. Sly. 1969b. Risk Analyses of Weekly Climatic Data for Agricultural and Irrigation Planning, Fort Frances, Ontario, Technical Bulletin 65, Canada Land Inventory, Dept of Forestry and Rural Development, Agriculture Canada. 8 pp.
- Coligado, M.C., W. Baier and W.K. Sly. 1969c. Risk Analyses of Weekly Climatic Data for Agricultural and Irrigation Planning, Guelph, Ontario, Technical Bulletin 66, Canada Land Inventory, Dept of Forestry and Rural Development, Agriculture Canada. 8 pp.
- Coligado, M.C., W. Baier and W.K. Sly. 1969d. Risk Analyses of Weekly Climatic Data for Agricultural and Irrigation Planning, North Bay, Ontario, Technical Bulletin 67, Canada Land Inventory, Dept of Forestry and Rural Development, Agriculture Canada. 8 pp.
- Coligado, M.C., W. Baier and W.K. Sly. 1969e. Risk Analyses of Weekly Climatic Data for Agricultural and Irrigation Planning, White River, Ontario, Technical Bulletin 68, Canada Land Inventory, Dept of Forestry and Rural Development, Agriculture Canada. 8 pp.
- Connan, O., E. Tessier, D. Maro, D. Amouroux, D. Hebert, M. Rozet, C. Vaiseux and L. Solier. 2008. Water to atmosphere fluxes of ^{131}I in relation with alkyl-iodide compounds from the Sein Estuary (France). *J. Environ. Radioactivity* 99, 1102-1110.
- Cordfunke, E.H.P. and R.J.M. Konings. 1988. Chemical interactions in water-cooled nuclear fuel: A thermodynamic approach. *J. Nucl. Mat.* 152, 301-309.
- Crawford, J. 2010. Bedrock K_d data and uncertainty assessment for application in SR-Site geosphere transport calculations. SKB Research Report R-10-48. Stockholm, Sweden.
- Crawford, J., I. Neretnieks and M. Malmström. 2006. Data and uncertainty assessment for radionuclide K_d partitioning coefficients in granitic rock for use in SR-Can calculations. SKB Research Report R-06-75. Stockholm, Sweden.
- CRC. 1993. CRC Handbook of chemistry and physics, 73rd ed. CRC Press, Ann Arbor, USA.
- CSA (Canadian Standards Association). 2016. Quality assurance of analytical, scientific, and design computer programs. CSA Standard CSA N286.7-16. Toronto, Canada.

- CSA (Canadian Standards Association). 2008. Guidelines for calculating derived release limits for radioactive material in airborne and liquid effluents for normal operation of nuclear facilities. Canadian Standards Association Report CSA-N288.1-08. Toronto, Canada.
- CSA (Canadian Standards Association). 1989. Residential mechanical ventilation requirements. Canadian Standards Association Preliminary Standard F326.1-M1989. Toronto, Canada.
- Cubicciotti, D. And J.E. Sanecki. 1978. Characterization of deposits on inside surfaces of LWR cladding. J. Nucl. Mat. 78, 96-111.
- Davis, P.A., R. Zach, M.E. Stephens, B.D. Amiro, G.A. Bird, J.A.K. Reid, M.I. Sheppard and M. Stephenson. 1993. The disposal of Canada's nuclear fuel waste: The biosphere model, BIOTRAC, for postclosure assessment. Atomic Energy of Canada Limited Report AECL-10720. Pinawa, Canada.
- Davison, C.C., T. Chan, A. Brown, M. Gascoyne, D. Kamineni, G. Lodha, T. Melnyk, B.W. Nakka, P. O'Connor, D. Ophori, N. Scheier, N. Soonawala, F. Stanchell, D. Stevenson, G. Thorne, T. Vandergraaf, P. Vilks and S. Whitaker. 1994. The disposal of Canada's nuclear fuel waste: The geosphere model for postclosure assessment. Atomic Energy of Canada Limited Report AECL-10719, COG-93-9. Pinawa, Canada.
- Didry, O., M.N. Gray, A. Cournut and J. Graham. 2000. Modelling the early age behaviour of a low heat concrete bulkhead sealing an underground tunnel. Canadian Journal of Civil Engineering 27. 112-124.
- Dixon, D.A., N.A. Chandler and P.M. Thompson. 2001. The selection of sealing system components in AECL's 1994 Environmental Impact Statement. Ontario Power Generation Report 06819-REP-01200-10074-R00. Toronto, Canada.
- Duro, L., V. Montoya, E. Colàs and D. García. 2010. Groundwater equilibration and radionuclide solubility calculations. Nuclear Waste Management Organization Technical Report NWMO TR-2010-02. Toronto, Canada.
- Eckerman, K.F. and R.W. Leggett. 1996. DCFPAK: Dose Coefficients Data File Package for Sandia National Laboratory. Oak Ridge National Laboratory Report ORNL/TM-13347. Oak Ridge, US. (<http://homer.hsr.ornl.gov/vlab/VLcodeDF.html>)
- Environment Canada. 2007. Municipal Water Use 2004 Statistics. Ontario, Canada.
- Fisheries and Environment Canada. 1978. Hydrological atlas of Canada. Department of Fisheries and Environment Canada, Printing and Publishing Supply Services Canada. Ottawa, Canada.
- Floyd, M.R., J. Novak and P.T. Truant. 1992. Fission-gas release in fuel performing to extended burnups in Ontario Hydro Nuclear Generating Stations. Proceedings of a Technical Committee Meeting on Fission Gas Release and Fuel Rod Chemistry Related to Extended Burnup, Pembroke, Ontario, Canada, 28 April – 1 May 1991. IAEA-TECDOC-697, p. 53. Vienna, Austria.

- Garamszeghy, M. 2015. Nuclear Fuel Waste Projections in Canada - 2014 Update. Nuclear Waste Management Organization Report NWMO TR-2015-19. Toronto, Canada.
- Garisto, F. 2001. Radionuclide Screening Model (RSM) version 1.1 verification and validation. Ontario Power Generation Report 06819-REP-01300-10029-R00. Toronto, Canada.
- Garisto, F. and P. Gierszewski. 2002. Technetium-99: Review of properties relevant to a Canadian geologic repository. Ontario Power Generation Report 06819-REP-01200-10081-R00. Toronto, Canada.
- Garisto, F., A. D'Andrea, P. Gierszewski and T. Melnyk. 2004. Third Case Study - Reference Data and Codes. Ontario Power Generation Report 06819-REP-01200-10107-R00. Toronto, Canada.
- Garisto, F., D.H. Barber, E. Chen, A. Ingot and C.A. Morrison. 2009. Alpha, beta and gamma dose rates in water in contact with used CANDU fuel. Nuclear Waste Management Organization Technical Report NWMO TR-2009-27. Toronto, Canada.
- Garisto, F., M. Gobien, E. Kremer and C. Medri. 2012. Fourth Case Study: Reference Data and Codes. Nuclear Waste Management Organization Technical Report NWMO TR-2012-08. Toronto, Canada.
- Garisto, F. and M. Gobien. 2013. SYVAC3-CC4 Verification and Validation Summary. Nuclear Waste Management Organization Technical Report NWMO TR-2015-14. Toronto, Canada.
- Gascoyne, M. 2004. Hydrogeochemistry, groundwater ages and sources of salts in a granitic batholith on the Canadian Shield, southeastern Manitoba. *Appl. Geochem.* 19, 519-560.
- Gobien, M. and F. Garisto. 2012. Data for radionuclide and chemical element screening. Nuclear Waste Management Organization Technical Report NWMO TR-2012-11. Toronto, Canada.
- Gobien, M. and F. Garisto. 2013. Modelling Container Failure in a Deep Geologic Repository. In Proceedings of the 14th International High-Level Radioactive Waste Management Conference, Albuquerque, New Mexico, USA.
- Goodwin, B.W., P. Gierszewski and F. Garisto. 2001. Radionuclide Screening Model (RSM) Version 1.1 - Theory. Ontario Power Generation Report 06819-REP-01200-10045-R00. Toronto, Canada.
- Gras, J.-M. 1996. Corrosion Assessment of Metal Containers for the Geological Disposal of HLW. Part 1: Carbon Steels, Low Alloy Steels, Cast Iron. EDF Report No. HT/40/96/002/A, Electricité de France, Moret-sur-Loing, France
- Guillaumont, R., J. Fanghänel, V. Neck, J. Fuger, D.A. Palmer, I. Grenthe, and M.H. Ran. 2003. Chemical Thermodynamics 5. Update on the Chemical Thermodynamics of Uranium, Neptunium, Plutonium, Americium and Technetium. NEA OECD, Elsevier, Amsterdam.

- Guo, R. 2016. Thermal Response of a Mark II Conceptual Deep Geological Repository in Crystalline Rock. Nuclear Waste Management Organization Technical Report NWMO-TR-2016-03. Toronto, Canada.
- He, H., M. Broczkowski, K. O'Neil, D. Ofori, O. Semenikhin and D. Showsmith. 2012. Corrosion of nuclear fuel (UO₂) inside a failed nuclear waste container. Nuclear Waste Management Organization Technical Report NWMO TR-2012-09. Toronto, Canada.
- Hillel, D. 1980. Application of Soil Physics. Academic Press, Toronto, Canada.
- Holford, R.M. 1989. Supplement to dose conversion factors for air, water, soil and building materials. Atomic Energy of Canada Limited Report AECL-9825-1. Pinawa, Canada.
- ICRP (International Commission on Radiological Protection). 1991. 1990 recommendations of the International Commission on Radiological Protection. Annals of the ICRP 21 (1-3), ICRP Publication 60. Pergamon Press, Oxford, UK.
- ICRP (International Commission on Radiological Protection). 1996. Age-dependent doses to members of the public from intake of radionuclides: Part 5, Compilation of ingestion and inhalation dose coefficients. Annals of the ICRP 26 (1), ICRP Publication 72. Pergamon Press, Oxford, UK.
- ICRP (International Commission on Radiological Protection). 2002. Basic Anatomical and Physiological Data for Use in Radiological Protection Reference Values. Ann. ICRP 32 (3-4), 2002. Vienna, Austria.
- ICRP (International Commission on Radiological Protection). 2007. The 2007 recommendations of the International Commission on Radiological Protection. Annals of the ICRP 37(2-4), ICRP Publication 103. Pergamon Press, Oxford, UK.
- Iglesias, F., M. Kaye and B. Lewis. 2011. Estimate of instant release fractions using ORIGEN-S and FEMAXI. Nuclear Waste Management Organization Technical Report NWMO TR-2011-19. Toronto, Canada.
- JNC. 2000. H12: Project to establish the scientific and technical basis for HLW disposal in Japan; Supporting Report 3; Safety assessment of the geological disposal system. Japan Nuclear Cycle Development Institute Report JNC TN1410 2000-004. Tokai, Japan.
- Johnson, L., C. Ferry, C. Poinssot and P. Lovera. 2005. Spent fuel radionuclide source-term model for assessing spent fuel performance in geological disposal. Part I: Assessment of the instant release fraction. J. Nucl. Mat. 346, 56-65.
- Johnson, L., C. Poinssot, C. Ferry and P. Lovera. 2004. Estimates of the instant release fractions for UO₂ and MOX fuel at t=0. NAGRA Technical Report NTB 04-08. Wettingen, Switzerland.
- Johnson, L.H. and J.C. Tait. 1997. Release of segregated nuclides from spent fuel. SKB Technical Report SKB TR 97-18. Stockholm, Sweden.

- Johnson, L.H., D.M. LeNeveu, F. King, D.W. Shoesmith, M. Kolar, D.W. Oscarson, S. Sunder, C. Onofrei, and J.L. Crosthwaite. 1996. The disposal of Canada's nuclear fuel waste: A study of postclosure safety of in-room placement of used CANDU fuel in copper containers in permeable plutonic rock, Volume 2: Vault model. Atomic Energy of Canada Limited Report AECL-11494-2. Pinawa, Canada.
- Kamimura, K. 1992. FP gas release behaviour of high burn-up MOX fuels for thermal reactors. Proceedings of a Technical Committee Meeting on Fission Gas Release and Fuel Rod Chemistry Related to Extended Burnup, Pembroke, Ontario, Canada, 28 April – 1 May 1991. IAEA-TECDOC-697, p. 82. Vienna, Austria.
- Kestin, J., M. Sokolov, and W.A. Wakeham. 1978. Viscosity of Liquid Water in the Range -8°C to 150°C. J. Phys. Chem. Ref. Data, Vol. 7, No. 3, 1978.
- Kitson, C., T. Melnyk, P. Gierszewski and L. Wojciechowski. 2012. SYVAC3-CC4 User Manual. Nuclear Waste Management Organization Technical Report NWMO TR-2012-21. Toronto, Canada.
- Kleykamp, H. 1985, The chemical state of the fission products in oxide fuels. J. Nucl. Mat. 131, 221-246.
- Lindemer, T.B. and T.M. Besmann. 1985. Chemical thermodynamic representation of $\langle \text{UO}_{2+x} \rangle$. J. Nucl. Mat. 130, 473-488.
- Macdonald, C.R. and M. Laverock. 1996. External ICRP 60 dose conversion factors for air and water immersion, groundshine and soil. Atomic Energy of Canada Limited Report TR-739. Pinawa, Canada.
- Martino, J. 2000. A review of excavation damage studies at the Underground Research Laboratory and the results of the excavation damage zone study in the Tunnel Sealing Experiment. Ontario Power Generation Report 06819-REP-01200-10018-R00. Toronto, Canada.
- McMurry, J. 2004. Reference water compositions for a deep geologic repository in the Canadian Shield. Ontario Power Generation Report 06819-REP-01200-10135-R01. Toronto, Canada.
- Medri, C. and G. Bird. 2014. Non-human Biota Dose Assessment Equations and Data. Nuclear Waste Management Organization Technical Report NWMO TR-2014-02. Toronto, Canada.
- Medri, C. 2015a. Human Intrusion Model for the Mark II Container in Crystalline and Sedimentary Rock Environments: HIMv2.1. Nuclear Waste Management Organization Technical Report NWMO TR-2015-04. Toronto, Canada.
- Medri, C. 2015b. Non-Radiological Interim Acceptance Criteria for the Protection of Persons and the Environment. Nuclear Waste Management Organization Technical Report NWMO TR-2015-03. Toronto, Canada.
- Mishra, S. 2002. Assigning probability distributions to input parameters of performance assessment models. SKB Technical Report TR-02-11. Stockholm, Sweden.

- NAGRA. 2004. Project Opalinus Clay – Integrated approach for the development of geochemical databases used for safety assessment. NAGRA Technical Report 03-06. Wettingen, Switzerland.
- NAPS (National Air Pollution Surveillance). 1996-2002. NAPS network annual data summaries. Retrieved online at: http://www.etc-cte.ec.gc.ca/publications/naps/naps_lib_e.html
- Natural Resources Canada. 2011. Office of Energy Efficiency Comprehensive Energy Use Database Table. Retrieved online at: http://oee.nrcan.gc.ca/corporate/statistics/neud/dpa/tablestrends2/res_ca_2_e_3.cfm?attr=0
- NWMO (Nuclear Waste Management Organization). 2011. OPG's Deep Geologic Repository for Low and Intermediate Level Waste: Postclosure Safety Assessment Data. Nuclear Waste Management Organization Technical Report NWMO DGR-TR-2011-32.
- NWMO (Nuclear Waste Management Organization). 2012a. Used fuel repository conceptual design and postclosure safety assessment in crystalline rock. Nuclear Waste Management Organization Technical Report NWMO TR-2012-16. Toronto, Canada.
- NWMO (Nuclear Waste Management Organization). 2012b. SYVAC3-CC4 Theory Manual. Nuclear Waste Management Organization Technical Report NWMO TR-2012-22. Toronto, Canada.
- NWMO (Nuclear Waste Management Organization). 2017. Postclosure Safety Assessment of a Used Fuel Repository in Crystalline Rock. Nuclear Waste Management Organization Technical Report NWMO-TR-2017-02. Toronto, Canada.
- Ochs., M. and C. Talerico. 2004. SR-Can. Data and uncertainty assessment – Migration parameters for the bentonite buffer in the KBS-3 concept. SKB Technical Report TR-04-18. Stockholm, Sweden.
- Ohlsson, Y. and I. Neretnieks. 1997. Diffusion data in granite. Recommended values. SKB Technical Report TR 97-20. Stockholm, Sweden.
- OMAFRA (Ontario Ministry of Agriculture, Food and Rural Affairs). 2011a. Area, production and farm value of specified commercial fruit crops, Ontario, 2009 - 2010. Retrieved online at: http://www.omafra.gov.on.ca/english/stats/hort/fruit_all09-10.htm
- OMAFRA (Ontario Ministry of Agriculture, Food and Rural Affairs). 2011b. Area, production and farm value of specified commercial vegetable crops, Ontario, 2009 - 2010. Retrieved online at: http://www.omafra.gov.on.ca/english/stats/hort/veg_all09-10.htm
- OMAFRA (Ontario Ministry of Agriculture, Food and Rural Affairs). 2012. Estimated area, yield, production and farm value of specified field crops, Ontario, 2001-2011. (Metric Units). Retrieved online at: http://www.omafra.gov.on.ca/english/stats/crops/estimate_metric.htm.

- Ophori, D.U. and T. Chan. 1996. Regional groundwater flow in the Atikokan Research Area: Model development and calibration. Atomic Energy of Canada Limited Report AECL-11081. Pinawa, Canada.
- Oscarson, D.W., N.G. Sawatsky, W.-J. Cho and J.-W. Choi. 1995. Compacted clays as barriers to radionuclide transport. In 5th Inter. Conf. on Radioactive Waste Management and Environmental Remediation, Berlin Germany, p.751-754.
- Parkhurst, D.L. and C.A.J. Appelo. 1999. User's guide to PHREEQC (version 2). A computer program for speciation, batch reaction, one dimensional transport and inverse geochemical calculations. U. S. Department of the Interior. U. S. Geological Survey, Water Resources Investigations. Reston, Virginia, USA.
- Poinssot, C., C. Ferry, M. Kelm, B.Grambow, A. Martinez-Esparza, L. Johnson, Z.Andriambololona, J. Bruno, C. Cachoir, J-M. Cavendon, H. Christensen, C.Corbel, C. Jegou, K.Lemmens, A. Loida, P. Lovera, F. Miserque, J. de Pablo, A. Poulesquen, J. Quinones, V. Rondinella, K. Spahiu and D.Wegen. 2005. Final report of the European project spent fuel stability under repository conditions. European Commission Report CEA-R-6093. Brussels, Belgium.
- Quintessa. 2016. AMBER 6.1 User Guide. Henley-On-Thames, UK.
- Quintessa Ltd. and Geofirma Engineering Ltd. 2011. Postclosure safety assessment: Data. Nuclear Waste Management Organization Report NWMO DGR-TR-2011-32 R000. Toronto, Canada.
- Ragland, K.W. and D.J.Aerts. 1991. Properties of wood for combustion analysis. Bioresource Technology 37, 161-168.
- Rohsenow, W. and H. Choi. 1961. Heat, mass and momentum transfer. Prentice-Hall, Englewood Cliffs, USA.
- Sheppard, M.I., S.C. Sheppard and B. Sanipelli. 2002. Recommended biosphere model values for iodine. Ontario Power Generation Report 06819-REP-01200-10090. Toronto, Canada.
- Sheppard, M.I., S.C. Sheppard and B. Sanipelli. 2004a. Recommended biosphere model values for chlorine. Ontario Power Generation Report 06819-REP-01200-10119-R00. Toronto, Canada.
- Sheppard, M.I., S.C. Sheppard and B. Sanipelli. 2004b. Recommended biosphere model values for neptunium. Ontario Power Generation Report 06819-REP-01200-10120-R00. Toronto, Canada.
- Sheppard, M.I., S.C. Sheppard and B. Sanipelli. 2005a. Recommended biosphere model values for uranium. Ontario Power Generation Report 06819-REP-01200-10088-R00. Toronto, Canada.
- Sheppard, M.I., J.C. Tait, B.L. Sanipelli and S.C. Sheppard. 2005b. Recommended biosphere model values for radium and radon. Ontario Power Generation Report 06819-REP-01200-10144-R00. Toronto, Canada.

- Sheppard, S. 1985. Use of the food chain model FOOD III and the soil model SCEMR to assess irrigation as a biosphere pathway. Atomic Energy of Canada Limited Report AECL-8380. Pinawa, Canada.
- Sheppard, S.C. and M. Gascoyne. 1997. Supplement to the database of groundwater iodine, chlorine and carbon concentrations. Ontario Hydro Report 06819-REP-01200-0005. Toronto, Canada.
- Sheppard, S.C., J.Long and B. Sanipelli. 2009. Field Measurements of the transfer factors for iodine and other trace elements. Nuclear Waste Management Organization Technical Report NWMO TR-2009-35. Toronto, Canada.
- Sheppard, S.C., J.M.Long, B.Sanipelli. 2010. Plant/soil concentration ratios for paired field and garden crops, with emphasis on iodine and the role of soil adhesion. Journal of Environmental Radioactivity 101, 1032-1037.
- Shoesmith, D.W. 2007. Used fuel and uranium dioxide dissolution studies – A review. Nuclear Waste Management Organization Technical Report NWMO TR-2007-03. Toronto, Canada.
- Shoesmith. S. and D. Zagidulin. 2010. The corrosion of Zirconium Under Deep Geological Repository Conditions. Nuclear Waste Management Organization Technical Report NWMO TR-2010-09. Toronto, Canada.
- Singer, S.N. and C.K. Cheng. 2002. An assessment of the groundwater resources of Northern Ontario. Ontario Ministry of the Environment, Environmental Monitoring and Reporting Branch, Report: Hydrogeology of Ontario Series (Report 2). Toronto, Ontario.
- SKB (Svensk Kärnbränslehantering AB). 2001. First TRUE stage - Transport of solutes in an interpreted single fracture. Proc. 4th Inter. Seminar Aspö, September 2000. Swedish Nuclear and Waste Management Company Technical Report SKB TR-01-24. Stockholm, Sweden.
- SKB (Svensk Kärnbränslehantering AB). 2006. Data report for the safety assessment SR-Can. SKB Technical Report TR-06-25. Stockholm, Sweden.
- SKB (Svensk Kärnbränslehantering AB). 2010. Data report for the safety assessment SR-Site. SKB Technical Report SKB TR-10-52. Stockholm, Sweden.
- Smith, H.D. and D.L. Baldwin. 1993. An investigation of thermal release of carbon-14 from PWR Zircaloy spent fuel cladding. J. Nucl. Mat. 200, 128-137.
- Srivastava, R.M. 2002. The discrete fracture network model in the local scale flow system for the Third Case Study. Ontario Power Generation Technical Report 06819-REP-01300-10061-R00. Toronto, Canada.
- Statistics Canada. 2002. Web pages: Private household by size data tables (1996 census) in www.statcan.ca/english/census96/oct14/hou.htm; Ontario farm population data tables in www.statcan.ca/english/census96/apr26/ont3.htm. Statistics Canada. Ottawa, Canada.

- Statistics Canada. 1996. Private households by size, showing structural type of dwelling, for Canada, Provinces and Territories, 1996 Census – 20% Sample data. Retrieved online at: <http://www.statcan.gc.ca/c1996-r1996/oct14-14oct/household-menages-eng.pdf>
- Stevenson, D.R., E.T. Kozak, C.C. Davison, M. Gascoyne and R.A. Broadfoot. 1996. Hydrogeologic characteristics of domains of sparsely fractured rock in granitic Lac du Bonnet batholith, southeastern Manitoba, Canada. Atomic Energy of Canada Limited Report AECL-11558. Pinawa, Manitoba.
- Stroes-Gascoyne, S. 1996. Measurements of instant release source terms for Cs-137, Sr-90, I-129, Tc-99 and C-14 in used CANDU fuel. *J. Nucl. Mat.* 238, 264-277.
- Stroes-Gascoyne, S. and D.M. Sellinger. 1986. The effect of fuel power on the leaching of cesium and iodine from used CANDU fuel. *In* Proceedings of the International Conference on CANDU Fuel, Chalk River, Canada, p. 383.
- Stroes-Gascoyne, S., J.C. Tait, R.J. Porth, J.L. McConnell and W.J. Lincoln. 1994. Release of ^{14}C from the gap and grain-boundary regions of used CANDU fuels to aqueous solutions. *Waste Management* 15, 385-392.
- Tait, J.C. and S. Hanna. 2001. Characteristics and radionuclide inventories of used fuel from OPG Nuclear Generating Stations, Volume 3 - Radionuclide inventory data. Decay times 10 to 300 years. Ontario Power Generation Report 06819-REP-01200-10029-R00. Toronto, Canada.
- Tait, J.C., H. Roman and C.A. Morrison. 2000. Characteristics and radionuclide inventories of used fuel from OPG Nuclear Generating Stations. Volume 1 - Main report; and Volume 2 – Radionuclide inventory data. Ontario Power Generation Report 06819-REP-01200-10029-R00. Toronto, Canada.
- Tait, J.C., R.J.J. Cornett, L.A. Chant, J. Jirovec, J. McConnell and D.L. Wilkin. 1997. Determination of Cl impurities and ^{36}Cl instant release from used CANDU fuels. *Mat. Res. Soc. Symp. Proc.* 465, 503-510.
- Therrien, R., R. G. McLaren, E. A. Sudicky, S.M. Panday, and, V. Guvanasen. 2010. FRAC3DVS-OPG: A three-dimensional numerical model describing subsurface flow and solute transport. User's guide. Groundwater Simulations Group, University of Waterloo. Waterloo, Canada.
- Thibault, D.H., M.I. Sheppard and P.A. Smith. 1990. A critical compilation and review of default soil solid/liquid partition coefficients, K_d , for use in environmental assessments. Atomic Energy of Canada Limited Report AECL-10125. Pinawa, Canada.
- Ticknor, K.V. and T.T. Vandergraaf. 1996. A revised compilation of sorption coefficients for use in geosphere models in performance assessments of used fuel disposal in granitic environments. Atomic Energy of Canada Limited Report AECL-11343, COG-96-71 Pinawa, Canada.
- Vandergraaf, T.T. 1997. The sorptive capacity of sparsely and moderately fractured rock. Atomic Energy of Canada Limited Technical Record TR-752. Pinawa, Canada.

- Vandergraaf, T.T. and K.V. Ticknor. 1994. A compilation and evaluation of sorption coefficients used in the geosphere model of SYVAC for the 1990 assessment of the Whiteshell Research Area. Atomic Energy of Canada Limited Report AECL-10546, COG-92-59. Pinawa, Canada.
- Vilks. P. 2011. Sorption of selected radionuclides on sedimentary rocks in saline conditions – Literature review. Nuclear Waste Management Organization Technical Report NWMO TR-2011-12. Toronto, Canada.
- Vilks, P. and N.H. Miller. 2006. Laboratory bentonite colloid migration experiments to support the Aspo Colloid Project. Ontario Power Generation Report 06819-REP-01300-10123. Toronto, Canada.
- Wasywich, K.M. 1993. Characteristics of used CANDU fuel relevant to the Canadian Nuclear Fuel Waste Management Program. Atomic Energy of Canada Limited Report AECL-10463, COG-91-340. Pinawa, Canada.
- Wasywich, K.M. 1992. Examination of spent CANDU fuel following 27 years of pool storage. Electric Power Research Institute Report TR-100674. Palo Alto, USA.
- Wersin, P. and B. Schwyn. 2004. Project Opalinus Clay - Integrated approach for the development of geochemical databases used for safety assessment. NAGRA Technical Report 03-06. Wetingen, Switzerland.
- Wilk, L. 2013. CANDU Fuel Burnup and Power Rating 2012 Update. Nuclear Waste Management Organization Technical Report NWMO TR-2013-02. Toronto, Canada.
- Wilson, C.N. 1990a. Results from NNWSI series 2 bare fuel dissolution tests. Pacific Northwest Laboratory Report PNL-7169. Richland, USA.
- Wilson, C.N. 1990b. Results from NNWSI series 3 spent fuel dissolution tests. Pacific Northwest Laboratory Report PNL-7170. Richland, USA.
- WIPP. 2009. Waste isolation pilot plant hazardous waste facility permit renewal application September 2009: Appendix I2, Appendix A, Material specification shaft sealing system compliance submittal design report. Waste Isolation Pilot Plant, U.S. Department of Energy, Carlsbad, USA.
- Wong, N.P., R. Jenness, M. Keeney, and E.H. Marth. 1999. Fundamentals of Dairy Chemistry (3rd Edition). Springer-Verlag.
- Wrixon, A.D. 2008. New ICRP recommendations. J. Radiol. Prot. 28, 161-168.
- Yamaguchi, I., S. Tanuma, I. Yasutomi, T. Nakayama, H. Tanabe, K. Katsurai, W. Kawamura, K. Maeda, H. Katao, and M. Saigusa. 1999. A study on chemical forms and migration behaviour of radionuclides in hull wastes. In ICEM'99 Conference Proceedings, Nagoya, Japan, Sept. 26-30. American Society of Mechanical Engineers. New York, USA.
- Yu, J.-W. and I. Neretnieks. 1997. Diffusion and sorption properties of radionuclides in compacted bentonite. SKB Technical Report TR 97-12. Stockholm, Sweden.

- Zach, R. and S.C. Sheppard. 1992. The food-chain and dose submodel, CALDOS, for the assessment of Canada's nuclear fuel waste management concept. Atomic Energy of Canada Limited Report, AECL-10165, COG-91-195. Pinawa, Canada.
- Zach, R., B.D. Amiro, G.A. Bird, C.R. Macdonald, M.I. Sheppard, S.C. Sheppard and J.G. Szekely. 1996. The disposal of Canada's nuclear fuel waste: A study of postclosure safety of in-room placement of used CANDU fuel in copper containers in permeable plutonic rock, Volume 4: Biosphere model. Atomic Energy of Canada Limited Report AECL-11494-4. Pinawa, Canada.

APPENDIX A: USED FUEL INVENTORY UNCERTAINTY

A.1 INTRODUCTION

The radionuclide and chemical inventories in CANDU used fuel, as calculated by ORIGEN-S (Tait et al. 2000), are presented in Table 4.5, Table 4.6, Table 4.7 and Table 4.8 in Section 4.3. The uncertainties in these inventories are discussed below.

As noted in Section 4.3, the safety assessment calculations require the total radionuclide and chemical element inventories in a loaded container. The inventories in the container are uncertain due to:

- Uncertainties in the ORIGEN-S inventory calculations due to uncertainties in the data used by ORIGEN-S (e.g., nuclear cross-sections, fission product yields, decay constants, impurity levels, etc.) and perhaps model approximations.
- Variation in the average age of the fuel in each container.
- Variation in the average burnup and power rating of the fuel in each container.

In the sections below, the uncertainties in the nuclide inventories arising from these three sources are discussed.

A.2 VALIDATION OF ORIGEN-S FOR CANDU REACTORS AND ORIGEN-S UNCERTAINTIES

The used fuel radionuclide and chemical element inventories for CANDU fuel of various burnups were calculated by Tait et al. (2000, 2001) using the ORIGEN-S code. The ORIGEN series of codes are internationally recognized point depletion codes that have been widely used for predicting the characteristics of used reactor fuel, including radionuclide inventories, based on the irradiation history of the fuel. Following discharge of the fuel from the reactor, the code calculates radionuclide inventories as a function of decay time, accounting only for changes in nuclide inventory as a result of radionuclide decay and ingrowth.

Tait et al. (2000) used the ORIGEN-S (version SCALE 4.2) code together with a burnup dependent library developed for the CANDU 37-element natural UO₂ fuel bundle by Gauld et al. (1995) and Gauld and Litwin (1995). Burnup dependent CANDU cross-sections were compiled from two sources of multigroup data: (1) the AMPX-formatted ENDF/B-IV 27 group neutron library used in SCALE 4.2 and (2) the WIMS-AECL 89 group library (Griffiths 1994). Cross-sections for nuclides and reaction types not available from WIMS-AECL were obtained from the AMPX library.

Validation of the CANDU reactor 37-element and 28-element fuel cross-section libraries used with ORIGEN-S code are described in detail in Gauld et al. (1995) and Gauld and Litwin (1995). The CANDU reactor libraries were validated through a series of benchmark problems that included comparisons of code and library predictions against measured isotopes in depleted CANDU fuel, measured isotopes in depleted pressurized water reactor fuel in the Nuclear Energy Agency (NEA) ATM-104 benchmark test, measured decay heat from CANDU fuel bundles and comparison against the ANSI/ANS-5.1 decay heat standard. The validation studies demonstrated that the CANDU cross-section libraries could be used by ORIGEN-S code to accurately predict the properties and behaviour of irradiated CANDU fuel.

Here, only the validation tests in which the ORIGEN-S code and associated nuclear data libraries were benchmarked against experimental measurements of used fuel isotopic inventories are described. The ORIGEN-S code results were compared to experimental measurements of used fuel isotopic inventories for three CANDU reactor designs, including the Nuclear Power Demonstration (NPD), Bruce and Pickering reactors; and, the NEA ATM-104 benchmark on pressurized water reactor isotopic prediction. All of the ORIGEN-S inventory calculations were performed with cross-section libraries created specifically for the benchmark problems, using a power history that reflected the actual history of the assemblies used in the studies as closely as possible. Details of the computational methods and nuclear databases used in these benchmark tests are provided in Gauld and Litwin (1995) and Tait et al. (1995).

A.2.1 NPD Reactor Fuel

NPD fuel consists of a 19-element fuel bundle with natural uranium. Measurements were made on a fuel bundle with a burnup of about 6200 MWD/MgU (= 149 MWh/kgU). Measurements consisted of total plutonium and uranium mass and isotopic ratios. Samples were taken from each fuel element in the fuel bundle and the samples were combined in such a way to give representative sample of the outer ring, the middle ring and the central ring. From these measured values, bundle average inventories were calculated.

The ORIGEN-S depletion calculation, which directly provides the bundle averaged fuel composition, was ended when the U-235/U-238 ratio, an indicator of the burnup, equalled the experimentally measured U-235/U-238 ratio for the fuel bundle. The calculated and measured (bundle averaged) atom ratios for the NPD fuel study are compared in Table A.1.

Table A.1: Measured and Calculated Atom Ratios for NDP Fuel Study

Atom Ratio	Measured	ORIGEN-S	C/E*
U-235/U-238	2.849E-3 ± 0.3%	2.849E-3 [#]	1.00
Pu/U	3.13E-3 ± 0.7%	3.17E-3	1.01
Pu-239/Pu	7.334E-1 ± 0.1%	7.364E-1	1.00
Pu-240/Pu	2.204E-1 ± 0.3%	2.165E-1	0.98
Pu-241/Pu	3.815E-2 ± 0.2%	3.872E-2	1.01
Pu-242/Pu	8.12E-3 ± 0.3%	7.587E-3	0.93

*Ratio of calculated to experimental measured values.

[#]U-235/U-238 ratio used as an indicator of burnup (see text).

The ORIGEN-S results show good agreement with the measured ratios. The total plutonium production is within 1% of the measurement, while individual plutonium atom ratios are generally within about 2% with the exception of Pu-242 which was under predicted by about 7%.

A.2.2 Bruce Reactor Fuel

Bruce CANDU fuel consists of a 37-element fuel bundle with natural uranium. Measurements (isotopic analyses) were made on fuel bundle F21037C from the Bruce-A Nuclear Generating Station with an approximate burnup of 7800 MWd/MgU (= 187 MWh/kgU). Fuel assays were taken from several fuel pins at different radial positions within the bundle. These measurements were combined to generate averaged bundle inventories for use in the benchmark. Measurements consisted of plutonium and uranium atom ratios, measured primarily using mass spectroscopy. Pu-242 data were based on alpha-spectrometric counting.

The ORIGEN-S depletion calculation, which directly provides the bundle averaged fuel composition, was ended when the U-235/U atom ratio, an indicator of the burnup, equalled the experimentally measured U-235/U ratio for the fuel bundle. The calculated and measured results for the average bundle values of the atom ratios for the Bruce fuel study are compared in Table A.2.

Table A.2: Measured and Calculated Atom Ratios for Bruce Fuel Study

Atom Ratio	Measured	ORIGEN-S	C/E*
U-235/U	0.213 ± 2%	0.2121 [#]	1.00
U-236/U	0.080 ± 6%	0.0784	0.98
U-238/U	99.707 ± 0.05%	99.705	1.00
Pu-239/Pu	65.82 ± 1%	65.218	0.99
Pu-240/Pu	27.46 ± 1%	27.798	1.01
Pu-241/Pu	4.96 ± 3%	5.109	1.03
Pu-242/Pu	1.76 ± 5%	1.757	1.00

*Ratio of calculated to experimentally measured values.

[#]U-235/U ratio used as indicator for burnup (see text).

The ORIGEN-S results show good agreement with the measured values. The ORIGEN-S results lie within the experimental uncertainty for all quantities measured.

A.2.3 Pickering Reactor Fuel

ORIGEN-S was also verified using measured radionuclide inventories for a single outer element of a Pickering A non-CANLUB fuel bundle (Tait et al. 1995). These measurements are the most comprehensive published data for irradiated CANDU fuel. The bundle received uniform axial neutron flux as verified by high resolution gamma scans. The outer elements were irradiated at a linear power of about 40 kW/m and reached a burnup of 9208 MWd/MgU (= 221 MWh/kgU) based on the U-235/U-238 ratio.

Chemical analyses for actinides and fission products were performed on three samples from the middle of a single outer fuel element. Each sample consisted of an entire fuel pellet, with its Zircaloy cladding intact. Details of the analytical methods are provided in Tait et al. (1995).

ORIGEN-S was used to calculate the final discharge composition of the fuel using a series of burnup steps derived from the detailed power history of the fuel. Some special ORIGEN-S modelling was required to accurately represent just the outer element environment, rather than the bundle average environment simulated for the NPD and Bruce reactor fuels described

above. The details of the calculation method used to predict the inventories of the outer fuel element are described in Tait et al. (1995) and Gauld and Litwin (1995).

The ORIGEN-S calculated inventories are compared to the measured radionuclide concentrations in Table A.3. The ORIGEN-S predictions agree reasonably well with measured actinide and fission product inventories; the residual uncertainty is in many cases related more to the accuracy of the measured nuclide concentrations as shown in Table A.3.

Table A.3: Measured and Calculated Inventories for Pickering-A Fuel Study

Isotope	Measured ^{1,2} (Bq/kgU)	ORIGEN-S (Bq/kg U)	C/E ³
Cm-244	7.12E+08 ± 15%	7.44E+08	1.05
Am-241	1.86E+10 ± 20%	1.92E+10	1.03
Np-237	1.00E+06 ± 20%	8.51E+05	0.85
H-3	2.07E+09 ± 7%	2.23E+09	1.08
Sr-90	4.86E+11 ± 4%	5.03E+11	1.03
Tc-99	1.08E+08 ± 10%	1.50E+08	1.39
Ru-106	8.72E+07 ± 5%	2.52E+08	2.89
Sb-125	2.20E+09 ± 18%	2.56E+09	1.16
I-129	2.44E+05	3.62E+05	1.48
Cs-134	4.16E+09 ± 7%	4.03E+09	0.97
Cs-137	8.05E+11 ± 5%	7.88E+11	0.98
Eu-154	8.14E+09 ± 5%	9.07E+09	1.11
Eu-155	3.35E+09 ± 8%	3.13E+09	0.93
Isotope	Measured ^{1,2} (g/kg U)	ORIGEN-S (g/ kg U)	C/E
U-233	< 0.01	2.22E-07	--
U-234	0.0339 ± 55%	0.0423	1.25
U-235	1.64 ± 2.4%	1.64	1.00
U-236	0.802 ± 3.7%	0.813	1.01
U-238	983.5 ± 0.01%	983.5	1.00
Pu-238	0.0058 ± 5.6%	0.0053	0.91
Pu-239	2.69 ± 2.5%	2.72	1.01
Pu-240	1.22 ± 37%	1.25	1.03
Pu-241	0.134 ± 9%	0.142	1.06
Pu-242	0.094 ± 6.8%	0.0972	1.03

¹Data from Tait et al. (1995)

²Analytical or measurement uncertainty, σ_{meas} , expressed as a percentage.

³Ratio of calculated to experimentally measured value.

Large deviations are observed between the calculated and measured concentrations for I-129, Tc-99 and Ru-106 (see Table A.3). In each case, the calculated concentrations are significantly larger than the measured concentrations. The discrepancies for these isotopes, which are outside the analytical uncertainty, are attributed to: I-129, losses due to incomplete capture in the off-gas stream; Tc-99, incomplete recovery due to its association with the undissolved

metallic residue; and, Ru-106, poor counting (gamma) geometry for the solid metallic residue, as essentially all the Ru-106 is associated with this undissolved residue.

A.2.4 NEA Benchmark on Pressurized Water Reactor Isotopic Prediction

The NEA adopted one of a series of experiments designed to characterize irradiated fuel from light water reactors as a benchmark for validating isotopic predictions by depletion codes. The fuel used in these experiments was designated as an Approved Testing Material (ATM) and designated ATM-104 (Guenther et al. 1991). The fuel assembly was a standard 14 x 14 assembly with 176 uranium oxide fuel rods. The fuel achieved a moderately high burnup of about 42 MWd/kgU (= 1008 MWh/kgU).

The benchmark specified history parameters for three fuel samples, corresponding to exit burnup values of 27.35, 37.12 and 44.34 MWd/kgU. Only the 27.35 MWd/kgU (= 656 MWh/kgU) burnup sample was used in the validation test for the ORIGEN-S code and nuclear data libraries used for CANDU reactors (Gauld and Litwin 1995).

Chemical and radiochemical assays are available for the ATM-104 fuel pins for a number of actinide and fission product isotopes (Guenther et al. 1991). Burnup was determined by measured Nd-148 content, with a quoted uncertainty of about $\pm 2.5\%$.

The ORIGEN-S calculated results are compared in Table A.4 with experimentally measured values from the NEA ATM-104 benchmark.

The uranium and plutonium inventories are in good agreement, i.e., within the standard deviation of the measurements, except for U-234 and Pu-238. For U-234, one possible explanation is uncertainty in the initial concentration of U-234 in fresh fuel which is very low (typically < 0.05 wt%). Gauld and Litwin (1995) indicate that the underprediction for Pu-238 is likely due to missing alpha decay chain information for Cm-244 in WIMS-AECL.

Neptunium, americium and fission product inventories are generally within 10% of the measurements. However, large deviations are observed for Se-79 and Sn-126 which are overpredicted by about a factor of 10 and 3, respectively. These discrepancies were also observed in the calculations cited in the ATM-104 study (Guenther et al. 1991) and their cause was unresolved at that time, but is presumably due to uncertainties in the nuclear data for these isotopes. For example, since the time of this work, the half-lives of Se-79 and Sn-126 have been revised significantly to 2.95×10^5 years and 2.30×10^5 years, respectively, from the values of 3.3×10^4 years (Se-79) and 1.0×10^5 (Sn-126) used in ORIGEN-S (SCALE 4.2) (Tait et al. 2000, Appendix C).

Table A.4: Measured and Calculated Inventories for NEA ATM-104 Study

Isotope	Measured ^{1,2} (Ci/kgUO ₂)	ORIGEN-S (Ci/kg UO ₂)	C/E ³
Am-241	0.856 ± 4.9%	0.8279	0.97
Np-237	1.89E-04 ± 1.9%	1.696E-04	0.90
Se-79	4.55E-5 ± 4.9%	4.950E-4	10.8
Sr-90	45.9 ± 5.7%	49.84	1.09
Tc-99	9.59E-3 ± 3.9%	1.011E-02	1.05
Sn-126	1.25E-4 ± 10.2%	3.773E-4	3.02
Cs-135	4.16E-04 ± 14%	4.308E-04	1.04
Cs-137	67.1 ± 3.5%	68.11	1.02
Isotope	Measured ^{1,2} (g/kg U)	ORIGEN-S (g/ kg U)	Ratio (C/E)
U-234	0.16 ± 1.6%	0.1758	1.09
U-235	8.47 ± 1.6%	8.114	0.96
U-236	3.14 ± 1.6%	3.282	1.05
U-238	842.5 ± 1.6%	837.2	0.99
Pu-238	0.1012 ± 1.6%	0.08165	0.81
Pu-239	4.264 ± 1.6%	4.271	1.00
Pu-240	1.719 ± 1.6%	1.700	0.99
Pu-241	0.6812 ± 1.6%	0.6777	0.99
Pu-242	0.2886 ± 1.6%	0.2948	1.02

¹Data from Gauld and Litwin (1995)

²Analytical or measurement uncertainty, σ_{meas} , expressed as a percentage.

³Ratio of calculated to experimentally measured value.

A.2.5 More Recent Comparisons of ORIGEN with Measurements for Pressurized Water Reactor Fuel

More recent comparisons by SKB (2010) for pressurized water reactor fuel indicate that the ratio of measured to ORIGEN-S calculated inventories is 1.01 for U and Pu isotopes; 1.01 for fission products and 1.11 for actinides other than U and Pu. The agreement is good and within the uncertainty of the measured data. However, the details of these comparisons are unpublished (SKB 2010).

Recently, new isotopic capabilities have been implemented in release 6.1 of SCALE, which is the latest release of the modelling suite for nuclear safety analysis and design that includes ORIGEN, and is maintained by Oak Ridge National Laboratories (ORNL) (Bowman 2011, ORNL 2011). The SCALE 6.1 release includes updates to the data for ORIGEN, including improved ENDF/B-VII cross-section data, ENDF/B-VII nuclear decay data, and energy dependent fission product yields (Gauld et al. 2011).

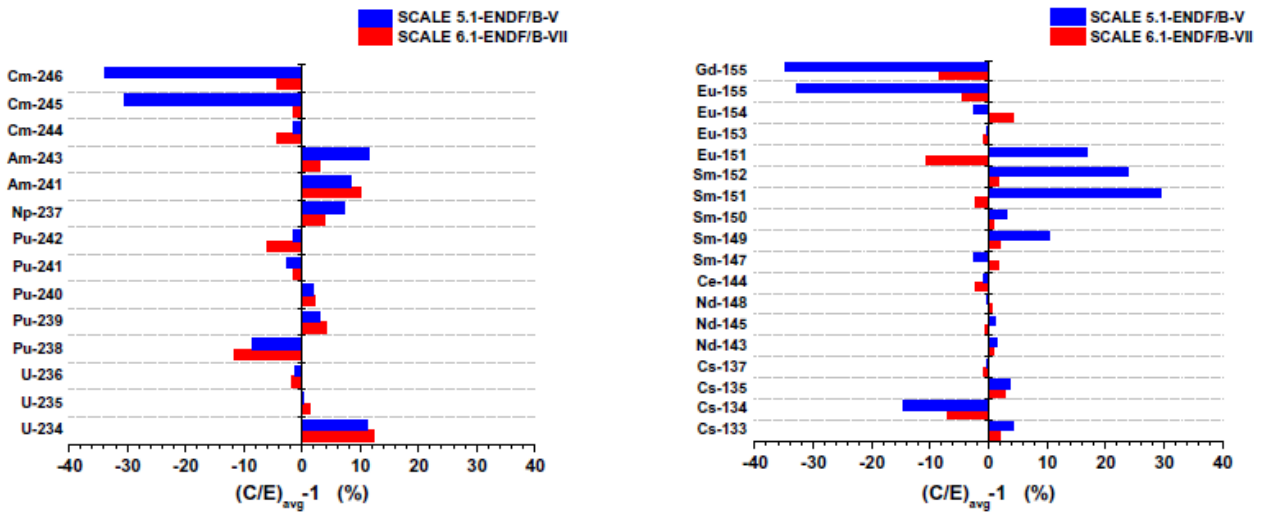
An assessment of the effect of these developments on the performance of ORIGEN was carried out by Ilas et al. (2012, and references therein). The analyses were focussed on evaluating the predictions for isotopic compositions using an extensive database of measured radionuclide

concentrations in pressurized water reactor spent nuclear fuel compiled by ORNL (Ilas et al. 2012).

Overall, the radionuclide inventories predicted by SCALE 6.1 showed good agreement with measured data, as shown in Figure A.1 which shows the average values of the calculated to experimental ratios for all spent fuels in the ORNL database for both the SCALE 5.1-ENDF/B-V and SCALE 6.1-ENDF/B-VII calculations (Ilas et al. 2012). Moreover, the comparison shows that the use of SCALE 6.1 and the new nuclear data from ENDF/B-VII leads to significant improvements in the estimation of the inventories of some fission product (particularly Cs-134, Sm-151, Sm-152, Eu-155 and Gd-155) and some minor actinides (Cm-245 and Cm-246).

Note that the calculated average C/E values were not weighted by the measurement uncertainties because of the observed large variation in data reported by different laboratories. In some cases, reported uncertainties refer only to instrument precision whereas the total uncertainty, which includes all sources of uncertainty along the analytical process (i.e., dissolution and separation yields, etc.), is required. Evaluation of the measurement data is an ongoing task being performed by members of the OECD/NEA Expert Group on Assay Data of Spent Nuclear Fuel (Ilas et al. 2012).

The results presented above indicate that SCALE 6.1 (and the new nuclear data libraries) provides an improved prediction of the used fuel concentrations of the isotopes of interest to criticality safety, reactor physics and radiation source terms. Additional studies are needed to determine if this is also the case for the isotopes of interest to nuclear waste management (e.g., C-14, Cl-36, I-129, Cs-135 and Se-79).



Note: $(C/E)_{avg}$ is the average of the calculated to experimental values for all fuels in the ORNL database

Figure A.1: Comparison of Calculated and Experimental Inventories for Actinide (left) and Fission Product (right) Using ENDF/B-V and ENDF/B-VII Libraries

A.2.6 ORIGEN-S Uncertainties for CANDU Fuel

As discussed above, the ORIGEN-S calculated inventories for CANDU fuel agree reasonably well with measured values. In most cases, the residual uncertainty is related more to the accuracy of the measured nuclide concentrations as shown in Tables A.1 to A.4.

Consequently, the uncertainty in the ORIGEN calculated inventories, σ_{OR} , for most radionuclides and chemical elements, was estimated as a normal probability density function with the predicted inventory as the mean value and the largest measurement (or analytical) uncertainty (σ_{meas} , see Table A.3 and Table A.4) as the standard deviation. If measurement uncertainties were not available then: (1) for progeny of well characterized parents, the standard deviation of the parent was used; or (2) a standard deviation of 7% was used, which is a typical uncertainty for fission products (Tait et al. 1995). Upper and lower bounds were chosen to be 5 standard deviations higher and lower than the mean. If the lower bound was not meaningful, i.e., less than zero, then the lower bound was set to 10 times smaller than the mean.

For short lived radionuclides, i.e., half-life < 2 years, the initial inventory is assigned a constant value because, soon after repository closure, the inventory of such short-lived nuclides would be determined by ingrowth from a long-lived parent nuclide.

A.3 INVENTORY UNCERTAINTY DUE TO AVERAGE AGE OF FUEL IN CONTAINERS

The design basis for the used fuel specifies a minimum fuel age of 30 years at time of placement. However, the Sixth Case Study assumes that fuel placed in the repository has cooled for exactly 30 years. This assumption is conservative for short-lived radionuclides such as Sr-90, and does not affect the inventory of the potentially most important dose contributors such as I-129 and Cl-36 because of their long half-lives. Therefore, uncertainty in the nuclide inventories arising from the uncertainty in the average fuel age is small and is neglected.

A.4 INVENTORY UNCERTAINTY DUE TO VARIATION IN AVERAGE BURNUP AND POWER RATING OF FUEL IN EACH CONTAINER

Uncertainty in average contaminant inventories in a container also arise due to the uncertainty in the average burnup and average power rating of the fuel bundles in the container. As discussed in the main text, the burnup uncertainty is conservatively treated in most safety assessment calculations by using calculated inventories for a reference burnup of 280 MWh/kgU, which represents, approximately, the 99th percentile of the fuel burnups for all CANDU fuel (Wilk 2013).

The reference burnup is also much larger than the median burnup on a station-specific basis, which is relevant as fuel bundles would likely be received and processed in the container encapsulation plant in groups from a particular station. The largest median burnup on a station-specific basis is 218 MWh/kgU for Bruce A for the years 2010 to 2012 (Wilk 2013). However, perhaps of more relevance to this discussion, is the fact that the distribution of bundle burnups for the Bruce A station is bimodal with peaks at approximately 130 and 246 MWh/kgU (Wilk 2013). The reference burnup of 280 MWh/kgU is also larger than 246 MWh/kgU.

The use of the reference burnup of 280 MWh/kgU is conservative because radionuclide inventories generally increase with burnup. Furthermore, given that the standard deviation in the distribution of bundle burnups (see Figure 4-1) is approximately 38 MWh/kgU, the standard deviation in the average container burnup is about $38/(48)^{1/2}$ MWh/kgU = 5.5 MWh/kgU for a container with 48 fuel bundles. This standard deviation is much less than 34 MWh/kgU (= 280 – 246 MWh/kgU); thus, the likelihood of having a container with an average container burnup greater than 280 MWh/kgU is less than 0.01%.

For the All Containers Fail scenario, all fuel bundles are eventually exposed to water and radionuclides are released from all fuel bundles in the repository. For this case, the inventories are calculated for a fuel burnup of 220 MWh/kgU, which represents the 80th percentile of the fuel burnups for all CANDU fuel bundles and is about 15% larger than the median burnup value of 192 MWh/kgU for all fuel bundles (Wilk 2013). This is considered to be sufficiently conservative for this scenario whereas use of the 280 MWh/kgU inventories would be overly conservative.

Nuclide inventories in used fuel bundles could also depend on the power rating of the fuel bundle (Tait et al. 2000). The inventories in Tait et al. (2000) were calculated for a reference bundle power rating of 455 kW/bundle and a screening analysis was done to determine the effect on the calculated inventories of lower and higher power ratings. These results were used to estimate inventory uncertainties arising from uncertainties in the average power rating of the bundles in a container as described below.

The distribution of Bruce fuel bundle power ratings has a standard deviation of approximately 140 kW/bundle (see Figure 4-3). However, if bundles are selected randomly, the standard deviation in the average power rating for the 48 bundles in a container would be about $140/48^{1/2}$ or 20.2 kW/bundle. The uncertainty in the nuclide inventory in a container, σ_{PR} , arising from the uncertainty in the average power rating of the bundles in the container was estimated as the maximum of the values calculated using Equations A.1a and A.1b

$$\sigma_{PR}(\%) = \frac{20.2 \text{ kW / bundle}}{(455 - 200) \text{ kW / bundle}} \left[100 \frac{I_{PR455} - I_{PR200}}{I_{PR455}} \right] \quad (\text{A.1a})$$

$$\sigma_{PR}(\%) = \frac{20.2 \text{ kW / bundle}}{(900 - 455) \text{ kW / bundle}} \left[100 \frac{I_{PR900} - I_{PR455}}{I_{PR455}} \right] \quad (\text{A.1b})$$

where in Equation A.1a, for example, the term in square brackets is the percentage difference in the nuclide inventories for bundle power ratings of 455 and 200 kW/bundle.

This analysis of inventory uncertainty due to bundle power rating found that the values of σ_{PR} are generally small (i.e., < 0.5%) for the radionuclides of interest, except for Cs-135 (7.4%).

A.5 SUMMARY OF INVENTORY UNCERTAINTIES

The uncertainty in the total contaminant inventories in a used fuel container is the sum of the following: (1) the uncertainties in the ORIGEN-S calculations, (2) the variation in the average age of the fuel in the container and (3) the variation in the average burnup and power rating of

the fuel in the container. These uncertainties have been estimated in Sections A.2, A.3 and A.4 above.

For all radionuclides and chemical elements except Cs-135, it is found that the total uncertainty in the container inventory is dominated by the estimated uncertainty in the calculated ORIGEN inventory of the radionuclide (or chemical element), σ_{OR} , as shown in Table 4-5, Table 4-6, Table 4-7, and Table 4-8. For Cs-135, the uncertainty due to variation in the fuel power rating is also important.

The inventory uncertainties of the different radionuclides (or chemical elements) are assumed to be uncorrelated given that the uncertainties arising from the variation in the average properties of the fuel in a container (i.e., age, burnup, and power rating) do not contribute significantly to the total uncertainty except for Cs-135.

REFERENCES

- Bowman, S.M. 2011. SCALE 6: Comprehensive nuclear safety analysis code system. Nucl. Tech. 174, 126-148.
- Gauld, I.C. and K.A. Litwin. 1995. Verification and validation of the ORIGEN-S code and nuclear data libraries. Atomic Energy of Canada Limited Report RC-1429, COG-I-95-150. Pinawa, Canada.
- Gauld, I.C., P.A. Carlson and K.A. Litwin. 1995. Production and validation of ORIGEN-S cross-section libraries for CANDU reactor fuel studies. Atomic Energy of Canada Limited Report RC-1442, COG-I-95-200. Pinawa, Canada.
- Gauld, I.C., G. Radulescu, G. Ilas, B.D. Murphy, M.L. Williams and D. Wiarda. 2011. Isotopic depletion and decay methods and analysis capabilities in SCALE. Nucl. Tech. 174, 169-195.
- Griffiths, J. 1994. WIMS-AECL users manual. Atomic Energy of Canada Limited Report RC-1176, COG-94-52. Chalk River, Canada.
- Guenther, R.J., D.E. Blahnik, U.P. Jenquin, J.E. Mendel, L.E. Thomas and C.K. Thornhill. 1991. Characterization of spent fuel approved testing material -- ATM-104. Pacific Northwest Laboratory Report PNL-5109-104/UC-802. Richland, Washington, USA.
- Ilas, G., I.C. Gauld and G. Radulescu. 2012. Validation of new depletion capabilities and ENDF/B-VII data libraries in SCALE. Ann. Nucl. Energy 46, 43-55.
- ORNL (Oak Ridge National Laboratory). 2011. SCALE: A comprehensive modeling and simulation suite for nuclear safety analysis and design. ORNL/TM-2005/39, Version 6.1. Available from Radiation Safety Information Computational Center at Oak Ridge National Laboratory as CCC-785. Oak Ridge, USA.
- SKB (Svensk Kärnbränslehantering AB). 2010. Spent nuclear fuel for disposal in the KBS-3 repository. SKB Technical Report SKB TR-10-13. Stockholm, Sweden.
- Tait, J.C., I.C. Gauld and A.H. Kerr. 1995. Validation of the ORIGEN-S code for predicting radionuclide inventories in used CANDU fuel. J. Nucl. Mat. 223, 109-121 (Also AECL-10891, COG-93-346, 1994).
- Tait, J.C., H. Roman and C.A. Morrison. 2000. Characteristics and radionuclide inventories of used fuel from OPG Nuclear Generating Stations. Volume 1 – Main report. Volume 2 – Radionuclide inventory data. Ontario Power Generation Report 06819-REP-01200-10029-R00. Toronto, Canada.
- Wilk, L. 2013. CANDU fuel burnup and power rating 2012 update. Nuclear Waste Management Organization Technical Report NWMO TR-2013-02. Toronto, Canada.

APPENDIX B: USED FUEL DISSOLUTION MODEL

B.1 UO₂ DISSOLUTION MODEL

The UO₂ ceramic fuel matrix is durable, and dissolves slowly in water. However, due to the radionuclides trapped within it, the rate of fuel dissolution is important.

The most important factor in the rate of dissolution of UO₂ in water is the redox conditions in the surrounding groundwater. Reducing conditions are expected to prevail in and around the container under the influence of the reducing groundwater, and consumption of any residual oxygen by reaction with the copper and steel container materials or with ferrous and organic material in the sealing materials. Under these reducing conditions, the UO₂ would dissolve very slowly.

However, the conditions at the used fuel surface are likely to be oxidizing for long time due to the production of oxidants in the water from radiolysis (Poinssot et al. 2005). (This water would have reached the fuel only after failure of the container and fuel cladding.) Radiolysis of the groundwater would be caused by the α -, β -, and γ -radiations emitted by the used fuel, at rates that depend on the radiation type and that decrease with time as the radiation fields decrease.

Shoesmith and Sunder (1991) used an electrochemical approach to predict the effect of α -, β - and γ -radiolysis on fuel dissolution. In this model, corrosion potential (E_{CORR}) measurements as a function of radiation source strength were combined with independent measurements of the fuel dissolution rate as a function of corrosion potential. This model formed the basis of the dissolution model for the Second Case Study (Johnson et al. 1996). However, this approach requires long extrapolations of the measurements at high doses to the low dose conditions expected at the fuel surface.

For this Case Study, an empirical model for radiolysis-driven dissolution is used. In this approach, the rates of dissolution of the used fuel matrix due to α -, β - and γ -radiolysis are assumed linear to the corresponding dose rates, i.e.,

$$R_{\alpha} = A_{cont} G_{\alpha} F_{\alpha} [D_{\alpha}(t+t_c)]^{a\alpha} \quad (B.1)$$

$$R_{\beta} = A_{cont} G_{\beta} F_{\beta} [D_{\beta}(t+t_c)]^{a\beta} \quad (B.2)$$

$$R_{\gamma} = A_{cont} G_{\gamma} F_{\gamma} [D_{\gamma}(t+t_c)]^{a\gamma} \quad (B.3)$$

with $a\alpha = a\beta = a\gamma = 1$; and the total matrix dissolution rate is given by

$$R_{TOT} = R_{\alpha} + R_{\beta} + R_{\gamma} + R_{ch} * A_{cont} \quad (B.4)$$

where

- R_{α} , R_{β} , and R_{γ} are the dissolution rates ($\text{mol}_U \cdot \text{a}^{-1}$) due to α -, β - and γ -radiation, respectively;
- R_{ch} is the chemical fuel dissolution rate, i.e., the dissolution rate of the fuel in the absence of radiolysis ($\text{mol}_U \cdot \text{m}^{-2} \cdot \text{a}^{-1}$);
- $D_{\alpha}(t+t_c)$, $D_{\beta}(t+t_c)$ and $D_{\gamma}(t+t_c)$ are the time-dependent dose rates ($\text{Gy} \cdot \text{a}^{-1}$);

- t is the time after placement of the fuel in the repository; t_c is the age of the fuel at the time of placement in the repository (i.e., the time between fuel removal from reactor and its placement in the repository) (years);
- G_α , G_β , and G_γ are empirical rate constants for fuel dissolution in the presence of alpha, beta and gamma radiation fields, respectively ($\text{mol}_U \cdot \text{m}^{-2} \cdot \text{Gy}^{-1}$);
- f_α , f_β , and f_γ are the alpha, beta and gamma dose variability factors; and
- A_{cont} is the effective surface area of the dissolving fuel, per container (m^2).

The remainder of this Appendix provides the basis for the values recommended for these parameters in this Case Study

B.2 FUEL SURFACE AREA IN A CONTAINER

The surface area of the fuel depends on the fragment size. The minimum possible surface area is that of the intact fuel pellets (about 12 mm diameter), or $0.043 \text{ m}^2/\text{kg}$. After irradiation, the fuel pellets are fragmented. Thus, the surface area of irradiated fuel would be greater than $0.043 \text{ m}^2/\text{kg}$. For example, the surface area would increase to about $0.062 \text{ m}^2/\text{kg}$ if each fuel pellet had two radial cracks. This is selected to be the minimum fuel surface area.

The geometric surface area of used fuel has been estimated to be about $0.2 \text{ m}^2/\text{kg}$, based on the size of fuel fragments from a Bruce bundle (Johnson 1982). In comparison, if the fuel were to be completely broken into small particles of about 0.6 mm, the surface area would be $1 \text{ m}^2/\text{kg}$.

The fuel surface area can also be estimated from the observation that the number of radial cracks in CANDU fuel is approximately equal to one-half of the linear heat rating expressed in kW/m (Lewis et al. 2009). The fuel pellets may also have circumferential and/or transversal cracks but these are rarer (Bain 1963, Hastings 1983).

The surface area of a cracked Bruce fuel pellet, which has a nominal diameter of 12.2 mm and length of 16 mm (Tait et al. 2000), was estimated assuming the following:

1. The fuel experienced a power rating of $38 \text{ kW}/\text{m}$ (see Section 4), suggesting that the pellet has 19 radial cracks. The radial cracks are assumed to extend from the outer surface of the pellet to the fuel centreline, even though cracks at the fuel centre could heal if the centreline temperature was sufficiently high for the UO_2 to become plastic (Bain 1963).
2. The fuel pellet has one circumferential crack that is located at $R/2$ where R is the radius of the fuel pellet.
3. The fuel pellet has one transversal crack.

Based on these assumptions, the surface area of Bruce fuel is about $0.27 \text{ m}^2/\text{kg}$. This is in fair agreement with the measured and selected value of $0.20 \text{ m}^2/\text{kg}$. Note that Bruce fuel would have a larger surface area per unit mass than Pickering fuel because the Bruce fuel pellets are smaller, i.e., the S/V ratio is larger.

The mass of UO_2 fuel in a container is 1048 kg, based on the 21.84 kg UO_2 per bundle and 48 bundles. Therefore, based on the range of geometric surface areas given above, A_{cont} is described using a lognormal distribution with a geometric mean of 209.3 m^2 , a geometric standard deviation of 1.8, and lower and upper bounds of 65 and 1048 m^2 , respectively.

Note that the effective surface area undergoing dissolution could be somewhat higher than the geometric surface area if the surface is rough. A typical value of the surface roughness factor is 3 (Grambow et al. 2000, p.27; Forsyth 1997 p.77). However, geometric surface areas are used here because the G_m ($m = \alpha, \beta$ or γ) values in Equation (B.1) to (B.3) are derived based on experimental dissolution rates calculated using the geometric surface area of the fuel.

B.3 FUEL RADIATION FIELDS

The alpha, beta and gamma radiation fields near the surface of a used fuel bundle within a water filled used fuel container have been calculated by Garisto et al. (2009) for the reference fuel burnup of 220 MWh/kg U and 280 MWh/kg U. These radiation field strengths are presented in Table B.1.

Based on the variability in alpha stopping power and nuclide inventories, the alpha dose rate variability factor f_α is described using a triangular probability density function with a most probable value of 1 and bounds of 0.8 to 1.2 (Garisto et al. 2009).

Based on the variability in beta stopping power and nuclide inventories, the beta dose rate variability factor f_β is described using a triangular probability density function with a most probable value of 1 and bounds of 0.8 to 1.2 (Garisto et al. 2009).

Based on the variability in nuclide inventories, the gamma dose rate variability factor f_γ is described using a triangular probability density function with a most probable value of 1 and bounds of 0.8 to 1.2 (Garisto et al. 2009).

Table B.1: Alpha, Beta and Gamma Dose Rates (Gy/a) for 220 MWh/kgU and 280 MWh/kgU Burnups

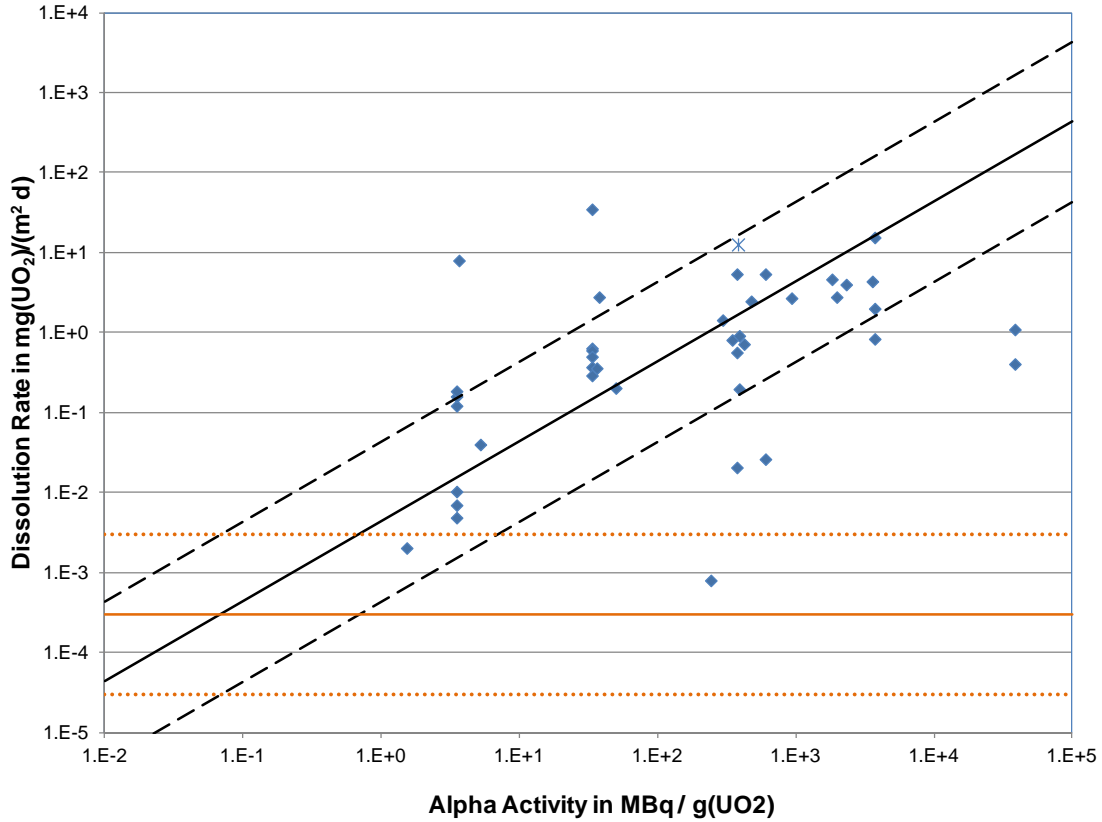
Time [a]	Alpha Dose Rate (Gy/a)		Beta Dose Rate (Gy/a)		Gamma Dose Rate (Gy/a)	
	220 MWh/kgU	280 MWh/kgU	220 MWh/kgU	280 MWh/kgU	220 MWh/kgU	280 MWh/kgU
10	1.42x10 ⁶	1.94x10 ⁶	4.56x10 ⁶	4.56x10 ⁶	7.11x10 ⁵	9.15x10 ⁵
20	1.72x10 ⁶	2.31x10 ⁶	3.41x10 ⁶	3.41x10 ⁶	5.30x10 ⁵	6.82x10 ⁵
30	1.89x10 ⁶	2.52x10 ⁶	2.66x10 ⁶	2.66x10 ⁶	3.95x10 ⁵	5.08x10 ⁵
40	1.99x10 ⁶	2.63x10 ⁶	2.08x10 ⁶	2.08x10 ⁶	2.95x10 ⁵	3.80x10 ⁵
50	2.03x10 ⁶	2.68x10 ⁶	1.63x10 ⁶	1.63x10 ⁶	2.20x10 ⁵	2.79x10 ⁵
60	2.05x10 ⁶	2.69x10 ⁶	1.28x10 ⁶	1.28x10 ⁶	1.74x10 ⁵	2.20x10 ⁵
75	2.04x10 ⁶	2.67x10 ⁶	8.92x10 ⁵	8.92x10 ⁵	1.23x10 ⁵	1.56x10 ⁵
100	2.00x10 ⁶	2.60x10 ⁶	4.90x10 ⁵	4.90x10 ⁵	6.87x10 ⁴	8.68x10 ⁴
150	1.88x10 ⁶	2.43x10 ⁶	1.50x10 ⁵	1.50x10 ⁵	2.16x10 ⁴	2.73x10 ⁴
200	1.77x10 ⁶	2.28x10 ⁶	4.85x10 ⁴	4.85x10 ⁴	6.80x10 ³	8.60x10 ³
300	1.58x10 ⁶	2.02x10 ⁶	8.48x10 ³	8.48x10 ³	1.02x10 ³	1.29x10 ³
500	1.30x10 ⁶	1.65x10 ⁶	3.56x10 ³	3.56x10 ³	2.28x10 ¹	3.08x10 ¹
1,000	9.03x10 ⁵	1.11x10 ⁶	2.01x10 ³	2.01x10 ³	1.55x10 ¹	2.15x10 ¹
10,000	3.21x10 ⁵	3.67x10 ⁵	4.66x10 ²	4.66x10 ²	1.65x10 ¹	2.18x10 ¹
100,000	1.80x10 ⁴	1.93x10 ⁴	1.91x10 ²	1.91x10 ²	2.84x10 ¹	3.20x10 ¹
1,000,000	6.24x10 ³	6.97x10 ³	1.59x10 ²	1.59x10 ²	3.84x10 ¹	3.90x10 ¹
10,000,000	4.19x10 ³	4.22x10 ³	1.15x10 ²	1.15x10 ²	3.58x10 ¹	3.57x10 ¹

B.4 G_α, G_β, and G_γ VALUES

The value of G_α is based on the experimental corrosion rate data compiled by Poinssot et al. (2005) (see also Shoesmith 2007) and plotted in Figure B.1. These corrosion rates are for α-doped UO₂, non-doped UO₂ (0.01 MBq/g) and used fuel. Search of the literature indicates that only a few additional experiments have been done since the compilation of Poinssot et al. (2005). The additional data from Muzeau et al. (2009) are also plotted in Figure B.1.

The results in Figure B.1 show a clear trend of increasing corrosion rates with increasing alpha activity. It also seems to show that there is a threshold activity below which no effect of alpha activity is observed (at approximately 1 MBq/g(UO₂)). Below the threshold activity, the corrosion rate of used UO₂ fuel is determined by the chemical dissolution rate R_{ch} (see Equation B.4).

A line with a slope of one (i.e., the corrosion rate is assumed to vary linearly with the alpha activity) was fitted through the experimental points, as shown in Figure B.1. This line describes the fuel dissolution rate as a function of alpha activity in fuel. The dashed lines show rates that are one order of magnitude lower and higher than the best estimate value. About 80% of the points fall within the two dashed lines.



Notes: The red lines show the selected chemical fuel dissolution rate and its bounds
 New data are identified using the * symbol

Figure B.1: Corrosion Rates Measured as a Function of Specific Alpha Activity

Based on the fit of the data in Figure B.1, it is found that

$$\text{Corrosion Rate (mgUO}_2\text{/m}^2\text{/d)} = 4.35 \times 10^{-3} * \text{Activity (MBq/g(UO}_2\text{))} \quad (\text{B.5})$$

The activity in used fuel (which can be calculated from the radionuclide inventory in Tait et al. (2000)) can be approximately expressed in terms of the alpha dose rate at the fuel surface, i.e.,

$$\text{Alpha Dose Rate (Gy/a)} = 4.2 \times 10^4 \text{ Activity (MBq/g(UO}_2\text{))} \quad (\text{B.6})$$

This relationship can be used to express the corrosion in Equation B.5 in terms of the alpha dose rate at the fuel surface.

$$\begin{aligned} \text{Corrosion Rate (molUO}_2\text{/m}^2\text{/a)} &= (4.35 \times 10^{-3} / 4.2 \times 10^4) \times 365(\text{d/a}) \times 3.7 \times 10^{-6}(\text{mol/mg}) \times D_\alpha \text{ (Gy/a)} \\ &= 1.4 \times 10^{-10} \times D_\alpha \text{ (Gy/a)} \end{aligned} \quad (\text{B.7})$$

Comparing Equations B.7 and B.1 it can be determined that $G_\alpha = 1.4 \times 10^{-10} \text{ mol/m}^2\text{/Gy}$.

Based on the variation of the experimental data in Figure B.1, G_α is described by a lognormal probability density function with geometric mean equal to 1.4×10^{-10} mol/m²/Gy, a geometric standard deviation of 6.0 and bounds of 3.5×10^{-12} to 2.1×10^{-9} mol/m²/Gy.

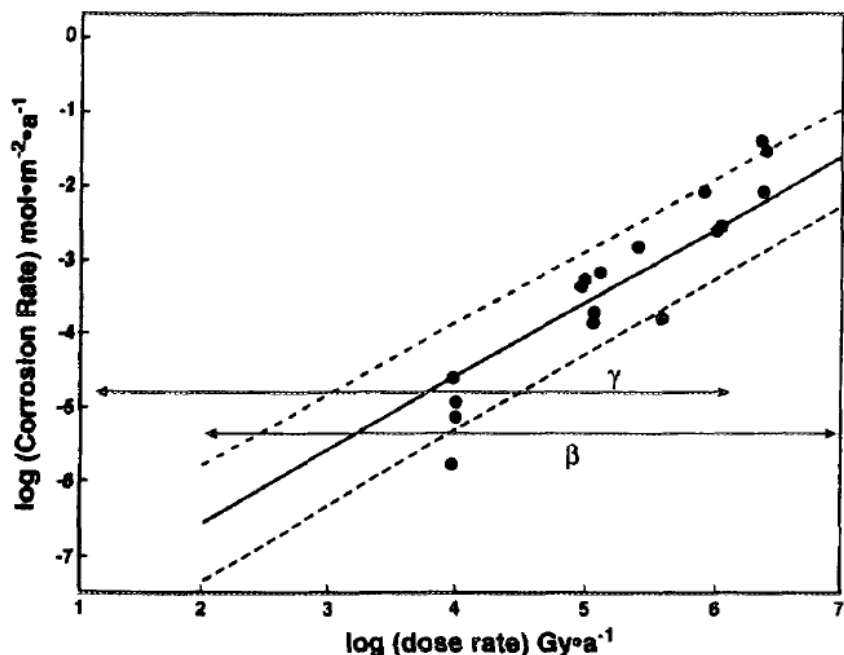
This selected value of G_α agrees well with the value 8.3×10^{-11} mol/m²/a for $G_{\text{eff}}(\alpha)$ used in the Third Case Study even though these two values were obtained using very different sets of experimental data.

As in previous assessments, it is assumed that $G_\beta = G_\gamma$ because beta and gamma radiation are both low linear energy (LET) radiation. Low LET radiation produces more radicals (e.g., H, O₂⁻) than high LET radiation, such as α -radiation, which results predominantly in the formation of molecular radiolysis products (e.g., H₂O₂).

The values of G_β and G_γ are obtained using the data in the Second Case Study (SCS) (Johnson et al. 1996). For convenience, Figure 5.6 of Johnson et al. (1996) is shown in Figure B.2 below. Based on the data in Table 5.2 of Johnson et al. (1996), for 100°C, $G_\beta = G_\gamma = 10^{-8.543}$ (mol/m²/Gy) or 2.86×10^{-9} mol/m²/Gy. The uncertainty in this value is about ± 0.74 log units (GSD = 5.5).

For the Sixth Case Study, the temperature in the vault is assumed to be 85°C throughout the simulation time. Using the activation energy of 33.5 kJ/mole (Johnson et al. 1996), $G_\beta = G_\gamma = 1.82 \times 10^{-9}$ mol/m²/Gy at 85°C. However, the temperature will only remain at 85°C briefly and rapidly cool as short lived radionuclides decay. Given the large range of temperature fluctuations over the time frames of interest, the Sixth Case Study assumes G_β and G_γ are described by loguniform probability density functions with bounds of 3.7×10^{-11} to 3.3×10^{-8} mol/m²/Gy. A value of 1.1×10^{-9} mol/m²/Gy is conservatively used for the Base Case and corresponds with a temperature of 70°C.

The selected value of G_β can be compared to the value 4.6×10^{-10} mol/m²/a for $G_{\text{eff}}(\beta)$ used in the Third Case Study. Again, the two values are similar.



Notes: The solid line is a fitted line and the dashed lines the $\pm 1\sigma$ values of this fit. The horizontal lines show the range of dose rates between the fuel ages of 10a and 1000a for beta and gamma radiation. Figure 5.6 from Johnson et al. 1996

Figure B.2: UO₂ (fuel) Corrosion Rates (calculated at 100°C) Plotted Logarithmically as a Function of the Gamma or Beta Radiation Dose Rate

B.5 CHEMICAL FUEL DISSOLUTION RATE

When the alpha-radiation field from used fuel becomes sufficiently low, chemical processes will drive fuel dissolution rather than the oxidative dissolution processes resulting from alpha-radiolysis of water. Under the reducing conditions expected in the repository, the chemical dissolution rate is low.

As defined, the chemical dissolution rate, R_{ch} , represents the intrinsic rate of UO₂ dissolution, i.e., the dissolution rate in the absence of solubility constraints and radiolysis. However, as the uranium concentration in solution approaches the solubility of UO₂, it is expected that the net fuel dissolution rate would decrease. In this case, the dissolution of the fuel can be described using a solubility limited dissolution model (Lemire and Garisto 1989, Grambow et al. 2010). Since the solubility of UO₂ is low under reducing conditions, the solubility limited dissolution rate can be substantially lower than the intrinsic chemical dissolution rate, if the rate of transport of uranium away from the container is constrained (e.g., small defect in the container). Thus, use of the intrinsic fuel dissolution rate is conservative.

Data on the chemical dissolution rate have been compiled from the literature. In many cases, these data actually represent the minimum observed fuel corrosion rate, which is taken here to be representative of the chemical dissolution rate. (The data may include radiolysis effects or be at measurement accuracy limits, and thus overestimate the true chemical dissolution rate.) The compiled chemical dissolution data are shown in Figure B.3. The data are from the following sources:

1. One of the first studies under reducing conditions was performed by Bruno et al. (1991). Using a continuous flow-through reactor, they found dissolution rates of $(6 \pm 2.5) \times 10^{-5}$ mol/(m² a), for neutral to alkaline conditions.
2. Grambow and Giffaut (2006) state that the dissolution rate of spent fuel under reducing conditions is less than 0.01 mg(UO₂)/(m² d), equivalent to 1.4×10^{-5} mol/(m² a).
3. The static dissolution tests of Ollila et al. (2003) using U-233 doped UO₂.
4. The data of Ollila (2007) from the NF-PRO project.
5. The dynamic tests under reducing conditions performed by SCK•CEN for the SFS project with alpha-doped UO₂ in Boom Clay water (Poinssot et al. 2005). Dissolution rates were independent of alpha activity. This is thought to be due to the reducing conditions imposed by the organic reductants in Boom Clay. If this is the case, then chemical dissolution would be expected to prevail.
6. The static dissolution tests of Saleh et al. (2006) using alpha-doped UO₂ in Boom clay suspensions suggest a dissolution rate of 9.7×10^{-6} mol/(m² a), independent of alpha activity. In these tests, the chemical dissolution rate may have been increased by sorption onto the suspended clay particles.

As noted above, the data in Figure B.3 are expected to overestimate the chemical dissolution rate. This is taken into account in selecting the value of the chemical dissolution rate to be used in the Sixth Case Study. The UO₂ chemical dissolution rate under reducing conditions (i.e., with no radiolysis effects) is selected to be loguniformly distributed with bounds of 4.0×10^{-8} to 4.0×10^{-6} mol/(m² a) and a median value of 4.0×10^{-7} mol/(m² a), which is about an order of magnitude higher than the median value used in the Third Case Study. The fuel dissolution rate at long times is expected to be much lower than this median value if the fuel is in equilibrium with the water in the defective container and the chemical dissolution rate is controlled by the diffusion of uranium out of the container.

Given the selected values of R_{ch} and G_{α} , and the alpha dose rate at the fuel surface, the dissolution rate due to alpha radiolysis will exceed the chemical dissolution rate for more than 10 million years.

With the selected median value of the chemical dissolution rate and the selected surface area of the fuel (0.2 m²/kg), all the fuel in a defective container would dissolve in about 13 million years. In comparison, SKB (2010) selects a (best-estimate) fractional fuel dissolution rate of 1.0×10^{-7} /year, based on the work of Werme et al. (2004); in which case all the fuel dissolves in 10 million years.

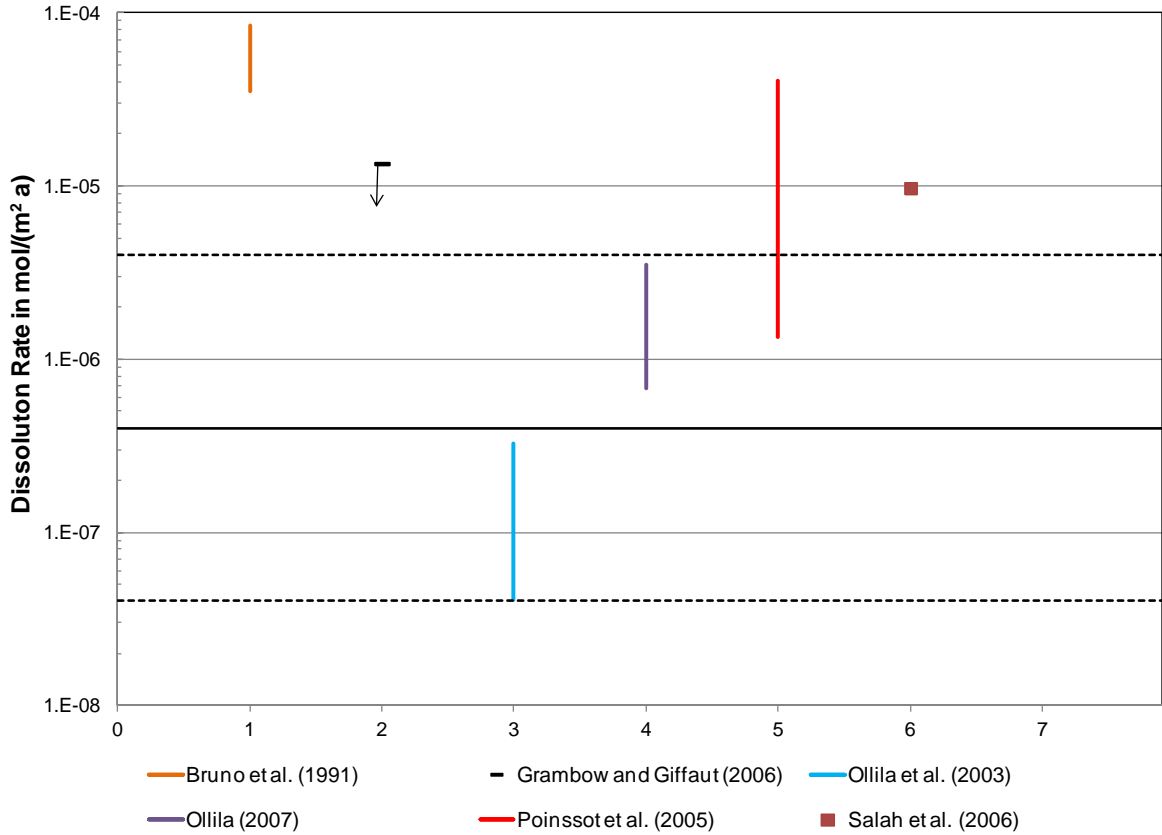


Figure B.3: UO₂ Corrosion Rates from Various Literature Sources

B.6 TOTAL FUEL DISSOLUTION RATE

Table B.1 summarizes the radiation dose rates at the used fuel surface as a function of time after discharge for 220 MWh/kgU and 280 MWh/kgU fuel. Figure B.4 shows the same data in a graphical form. After a few hundred years, the alpha contribution dominates. Figure B.5 shows the total used fuel dissolution rate calculated using Equation B.4 and the data given above.

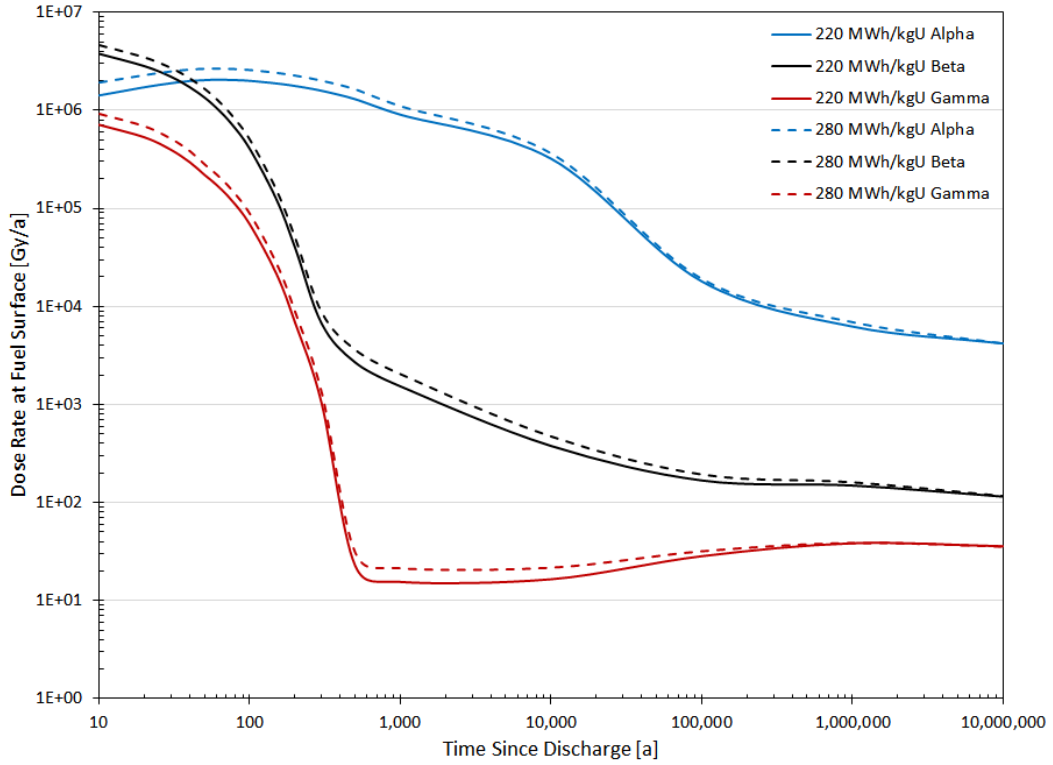


Figure B.4: Radiation Dose Rate in Water at the Fuel Surface (220 MWh/kgU burnup)

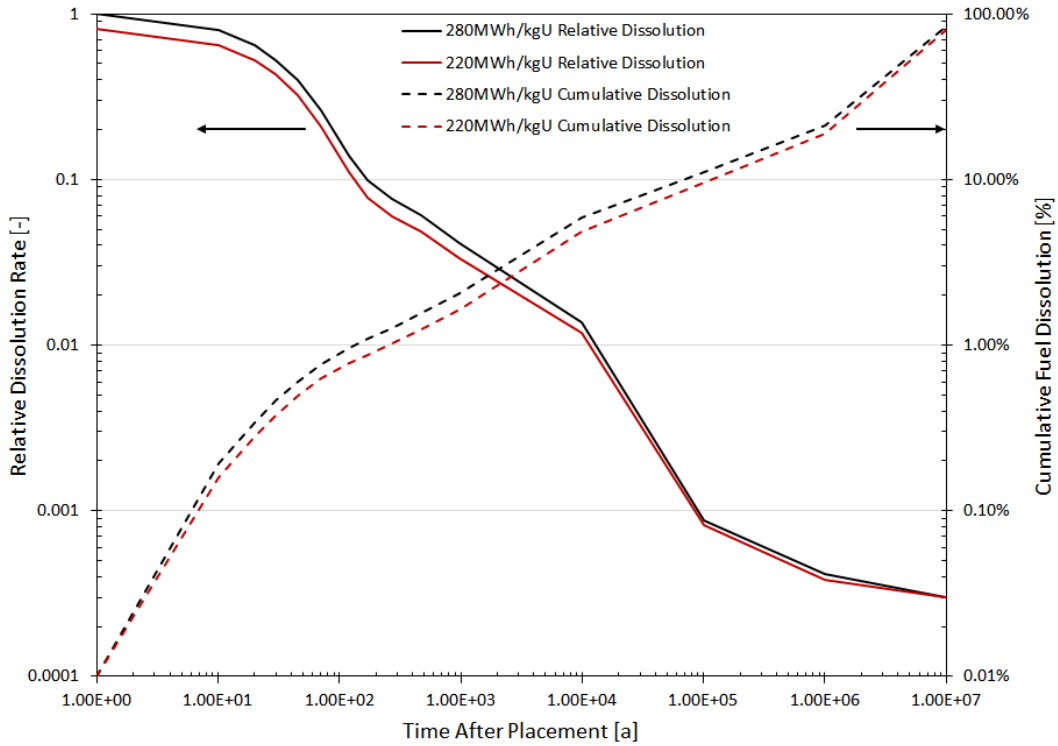


Figure B.5: Calculated Total Fuel Dissolution Rate

B.7 REFERENCES

- Bain, A.S. 1963. Cracking and bulk movement in irradiated uranium oxide fuel elements. Atomic Energy of Canada Limited Report AECL-1827. Chalk River, Canada.
- Bruno J., I. Casas and I. Puigdomènech. 1991. The kinetics of dissolution of UO_2 under reducing conditions and the influence of an oxidized surface layer (UO_{2+x}): Application of a continuous flow-through reactor. *Geochimica et Cosmochimica Acta*, 55, 647-658.
- Forsyth, R. 1997. The SKB spent fuel corrosion programmed. An evaluation of results from the experimental programme performed in the Studsvik Hot Cell Laboratory. SKB Technical Report TR 97-25. Stockholm, Sweden.
- Garisto, F., D.H. Barber, E. Chen, A. Inglot and C.A. Morrison. 2009. Alpha, beta and gamma dose rates in water in contact with used CANDU fuel. Nuclear Waste Management Organization Technical Report NWMO TR-2009-27. Toronto, Canada.
- Grambow, B.G. and E. Giffaut. 2006. Coupling of chemical processes in the near field. *Mat. Res. Soc. Symp. Proc.* Vol. 932, 55-66.
- Grambow, B., A. Loida, A. Martinez-Esparza, P. Diaz-Arocas, J. de Pablo, J.-L. Paul, G. Marx, J.-P. Glatz, K. Lemmens, K. Ollila and H. Christensen. 2000. Source term for performance assessment of spent fuel as a waste form. European Commission Report EUR 19140. Brussels, Belgium.
- Grambow, B., J. Bruno, L. Duro, J. Merino, A. Tamayo, C. Martin, G. Pepin, S. Schumacher, O. Smidt, C. Ferry, C. Jegou, J. Quiñones, E. Iglesias, N. Rodriguez Villagra, J. M. Nieto, A. Martínez-Esparza, A. Loida, V. Metz, B. Kienzler, G. Bracke (GRS), D. Pellegrini, G. Mathieu, V. Wasselin-Trupin, C. Serres, D. Wegen, M. Jonsson, L. Johnson, K. Lemmens, J. Liu, K. Spahiu, E. Ekeröth, I. Casas, J. de Pablo, C. Watson, P. Robinson, and D. Hodgkinson. 2010. MICADO model uncertainty for the mechanism of dissolution of spent fuel in nuclear waste repository. European Commission Report EUR 24597 EN. Brussels, Belgium.
- Hastings, I.J. 1983. Structure in irradiated UO_2 fuel from Canadian reactors. Atomic Energy of Canada Limited Report AECL-MISC-249. Chalk River, Canada.
- Johnson, L.H. 1982. The dissolution of irradiated UO_2 fuel in groundwater. Atomic Energy of Canada Limited Report AECL-6837. Pinawa, Canada.
- Johnson, L.H., D.M. LeNeveu, F. King, D.W. Shoesmith, M. Kolar, D.W. Oscarson, S. Sunder, C. Onofrei, and J.L. Crosthwaite. 1996. The disposal of Canada's nuclear fuel waste: A study of postclosure safety of in-room placement of used CANDU fuel in copper containers in permeable plutonic rock, Volume 2: Vault model. Atomic Energy of Canada Limited Report AECL-11494-2. Pinawa, Canada.
- Lemire, R.J. and F. Garisto. 1989. The solubility of U, Np, Pu, Th and Tc in a geological disposal vault for used nuclear fuel. Atomic Energy of Canada Limited Report AECL-10009. Pinawa, Canada.

- Lewis, B.J., F.C. Iglesias, R.S. Dickson and A. Williams. 2009. Overview of high-temperature fuel behaviour with relevance to CANDU fuel. *J. Nucl. Mater.* **394**, 67-86.
- Muzeau, B., C. Jegou, F. Delaunay, V. Brodic, A. Brevet, H. Catalette, E. Simoni and C. Corbel. 2009. Radiolytic oxidation of UO_2 pellets doped with alpha-emitters ($^{238/239}\text{Pu}$). *J. Alloys and Comps.* **467**, 578-589.
- Ollila, K. 2007. Dissolution of unirradiated UO_2 and UO_2 doped with ^{233}U in low and high ionic strength NaCl under anoxic and reducing conditions. European Commission NF-PRO Report D.1.5.11. Brussels, Belgium.
- Ollila, K. Y. Albinsson, V. Oversby and M. Cowper. 2003. Dissolution rates of unirradiated UO_2 , UO_2 doped with ^{233}U , and spent fuel under normal atmospheric conditions and under reducing conditions using an isotope dilution method. SKB Technical Report TR 03-13. Stockholm, Sweden.
- Poinssot, C., C. Ferry, M. Kelm, B.Grambow, A. Martinez-Esparza, L. Johnson, Z.Andriambololona, J. Bruno, C. Cacho, J-M. Cavendon, H. Christensen, C.Corbel, C. Jegou, K.Lemmens, A. Loida, P. Lovera, F. Miserque, J. de Pablo, A. Poulesquen, J. Quinones, V. Rondinella, K. Spahiu and D.Wegen. 2005. Final report of the European project spent fuel stability under repository conditions. European Commission Report CEA-R-6093. Brussels, Belgium.
- Saleh, S., C. Cacho, K. Lemmens and N. Maes. Static dissolution tests of alpha-doped UO_2 under repository relevant conditions: Influence of Boom Clay and alpha activity on fuel dissolution rates. *Mat. Res. Soc. Symp. Proc.* Vol. 932, 481-488.
- Shoesmith, D.W. 2007. Used fuel and uranium dioxide dissolution studies – A review. Nuclear Waste Management Organization Technical Report NWMO TR-2007-03. Toronto, Canada.
- Shoesmith, D.W. and S. Sunder. 1991. An electrochemistry-based model for the dissolution of UO_2 . Atomic Energy of Canada Limited Report AECL-10488. Pinawa, Canada.
- SKB (Svensk Kärnbränslehantering AB). 2010. Fuel and canister process report for the safety assessment SR-Site. SKB Technical Report SKB TR-10-46. Stockholm, Sweden.
- Tait, J.C., H. Roman and C.A. Morrison. 2000. Characteristics and Radionuclide Inventories of Used Fuel from OPG Nuclear Generating Stations, Volume 2 – Radionuclide Inventory Data. Ontario Power Generation Report 06819-REP-01200-10029-R00. Toronto, Canada.
- Werme, L., L.H. Johnson, V.M. Oversby, F. King, K. Spahiu, B.Grambow and D.W. Shoesmith. 2004. Spent fuel performance under repository conditions: a model for use in SR-Can. SKB Technical Report TR-04-19. Stockholm, Sweden.

APPENDIX C: SYVAC3-CC4 GEOSPHERE MODEL DATA

The SYVAC3-CC4 geosphere transport model (also called GEONET) uses a simplified representation of the groundwater flow results from FRAC3DVS-OPG. It uses a network of interconnected 1-D transport path segments to represent the transport of nuclides through the geosphere, from the repository to surface discharge points (see NWMO 2012b and Davison et al. 1994 for a description of the features of this model).

The input data for the network model used to represent the Sixth Case Study is listed in this appendix. The geosphere network model is derived from detailed groundwater flow modelling carried out using the FRAC3DVS-OPG code, and described in NWMO (2017). In particular, a detailed FRAC3DVS-OPG groundwater flow model was developed in which the fracture and permeability variation over the entire subregional area was represented. Particles were numerically released across the repository area and tracked to where they intercepted the surface. The particle tracks were then approximated by a network of 1-D segments to form the geosphere transport network described below, taking into account of direct paths for diffusion transport. These pathways are then used to create two similar, but different, SYVAC3-CC4 geosphere models:

- Simple Model: each of the 10 defective containers is modelled as a separate sector to allow for input of specific container failure times (i.e., the first container fails at 1000 years with the remaining containers failing every 100,000 years thereafter). The containers are clustered in the location that maximizes transport to the well, and their contaminants either discharge to the Well or to the Central Wetland area, depending on the well demand. No other containers are represented in this model. This model is used for the Normal Evolution Scenario and associated sensitivity studies, and for one of the two probabilistic assessment cases.
- Full Model: the entire repository is divided into sectors, where each sector contains multiple containers and where sectorization depends on commonality of transport times and transport endpoints. All containers in the repository are represented in this model. This is used for the All Containers Fail Disruptive Event Scenario and for one of the two probabilistic assessment cases.

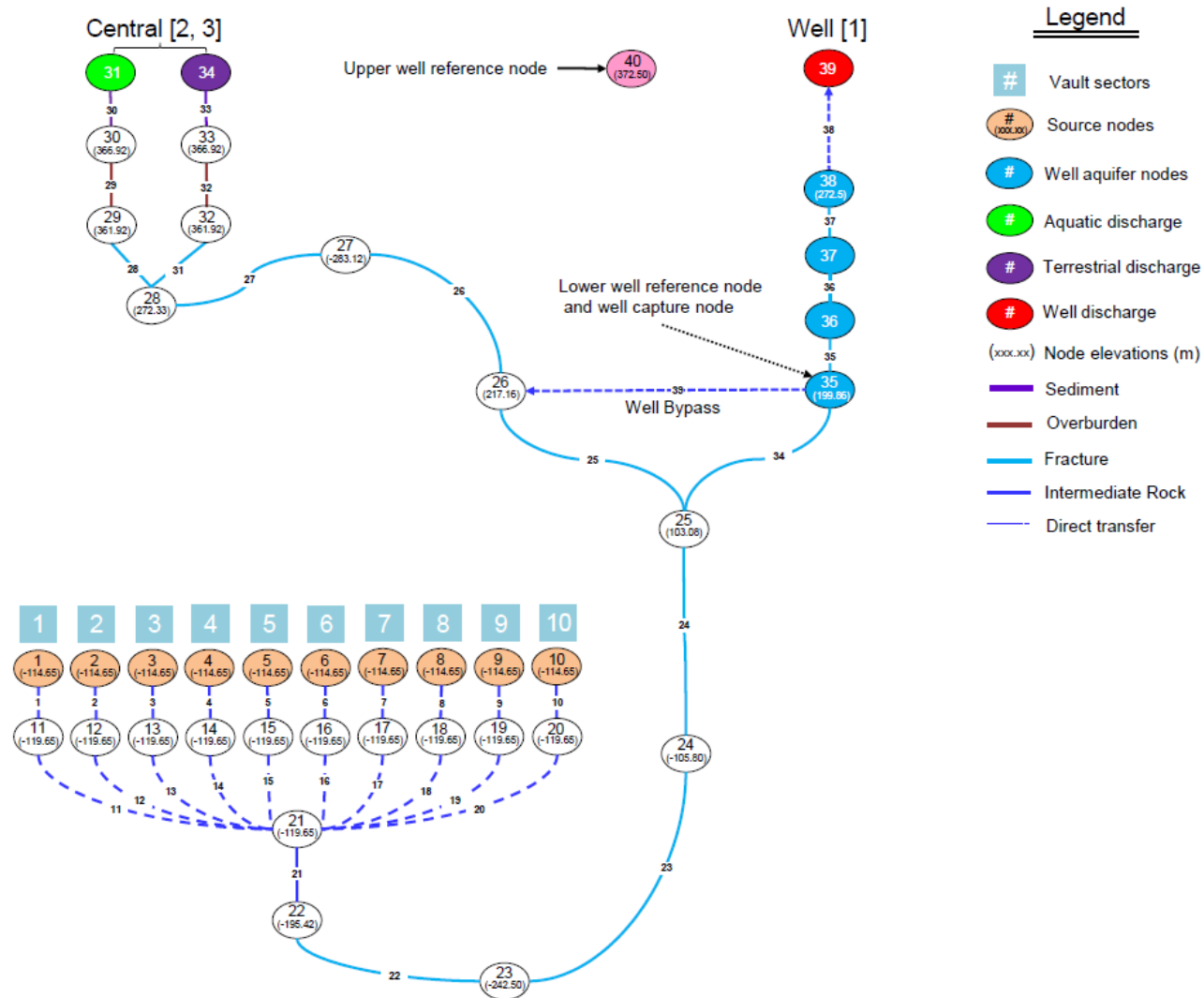
Figure C.1, Figure C.2, and Figure C.3 illustrates the transport network interconnections for the two models. Segments in the GEONET models have constant properties, characterized by a permeability, temperature (constant 20°C), groundwater flow rate, diffusivity and dispersivity. All transport paths end at the surface, either in the well or at a surface water discharge point. There are four surface discharge points at the Sixth Case Study site – the Well, the Central Discharge, the West River, and the East River. At the West and East river discharge locations the transport is further divided into a component that enters beneath the water body through sediments (aquatic discharge), and a portion that enters along the edge of the water body (terrestrial discharge). The Central discharge is a terrestrial discharge and the well is a unique discharge.

Depending on the well pumping rate, contaminants that would otherwise go to the river discharges may be captured by the well. This pumping-rate dependent branching occurs at several nodes across the larger GEONET model.

The Simple Model Data are listed the following tables. Table C.1 lists the nodes and the nodal input data. Table C.2 lists the segments and the segment input data. Table C.3 lists slope

values only for segments with variable source fractions indicated in Table C2. Table C.4 lists the data in the SYVAC3-CC4 Geosphere Network Input Files for the simple model.

The Full Model Data are listed the following tables. Table C.5 lists the nodes and the nodal input data. Table C.6 lists the segments and the segment input data. Table C.6 lists slope values only for segments with variable source fractions indicated in Table C7. Table C.8 lists the data in the SYVAC3-CC4 Geosphere Network Input Files for the simple model.



Notes: Only nodes (ellipses) with a particular function are colour coded. The line segments, representing the 1D transport pathways, are colour coded (see legend) to indicate the geosphere zone through which they pass.

Figure C.1: SYVAC3-CC4 Simple Model: Transport Network Connectivity

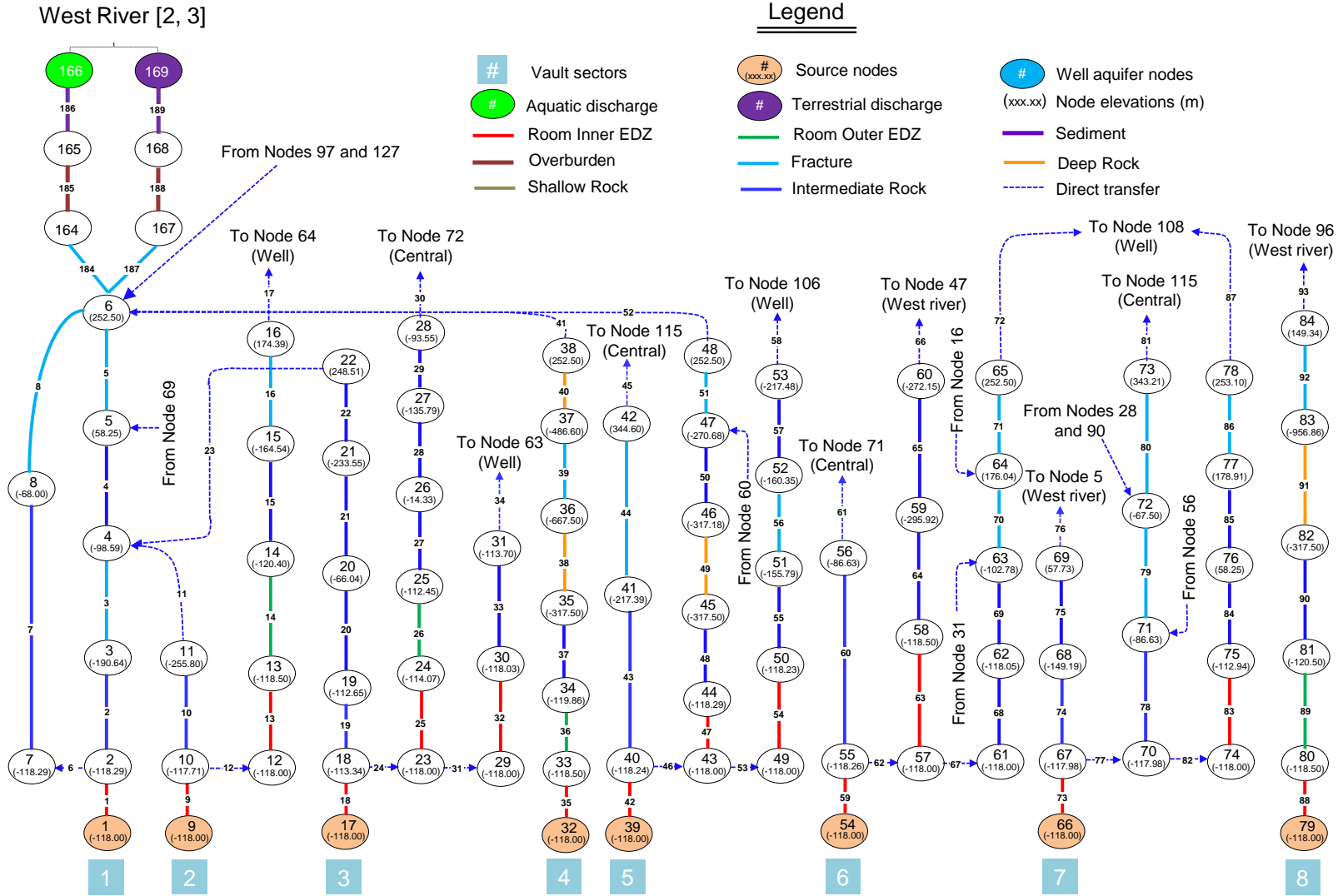


Figure C.2: SYVAC3-CC4 Full Model: Transport Network Connectivity – Part I

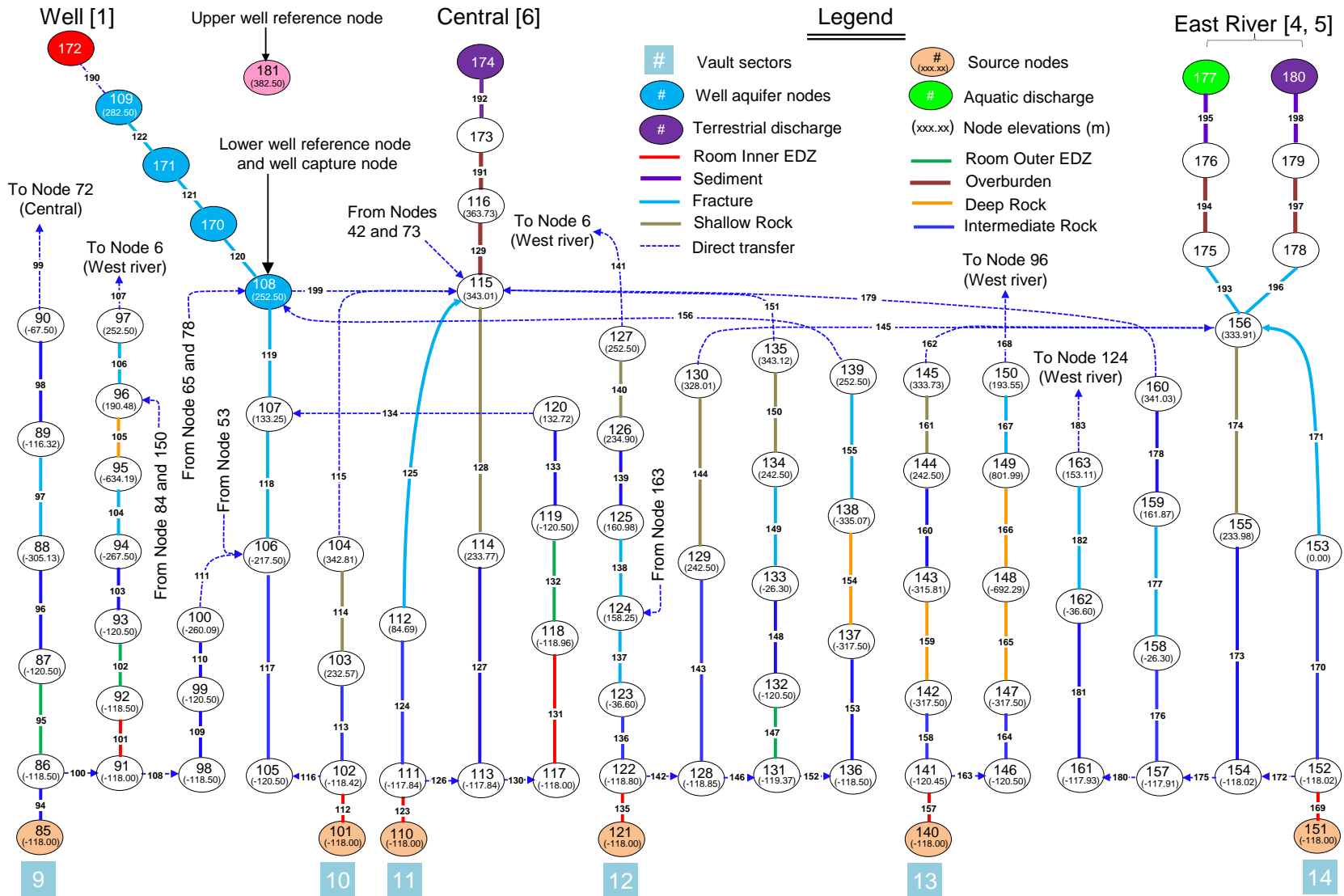


Figure C.3: SYVAC3-CC4 Full Model: Transport Network Connectivity – Part II

Table C.1: SYVAC3-CC4 Simple Geosphere Network - Node Data

Node #	X Position	Y Position	Z Position	NAQDA1
1	9.45E+02	3.82E+02	-1.15E+02	1.69E-04
2	9.47E+02	3.82E+02	-1.15E+02	1.69E-04
3	9.49E+02	3.82E+02	-1.15E+02	1.69E-04
4	9.51E+02	3.82E+02	-1.15E+02	1.69E-04
5	9.53E+02	3.82E+02	-1.15E+02	1.69E-04
6	9.55E+02	3.82E+02	-1.15E+02	1.69E-04
7	9.57E+02	3.82E+02	-1.15E+02	1.69E-04
8	9.59E+02	3.82E+02	-1.15E+02	1.69E-04
9	9.61E+02	3.82E+02	-1.15E+02	1.69E-04
10	9.63E+02	3.82E+02	-1.15E+02	1.69E-04
11	9.45E+02	3.82E+02	-1.20E+02	3.12E-05
12	9.47E+02	3.82E+02	-1.20E+02	3.12E-05
13	9.49E+02	3.82E+02	-1.20E+02	3.12E-05
14	9.51E+02	3.82E+02	-1.20E+02	3.12E-05
15	9.53E+02	3.82E+02	-1.20E+02	3.12E-05
16	9.55E+02	3.82E+02	-1.20E+02	3.12E-05
17	9.57E+02	3.82E+02	-1.20E+02	3.12E-05
18	9.59E+02	3.82E+02	-1.20E+02	3.12E-05
19	9.61E+02	3.82E+02	-1.20E+02	3.12E-05
20	9.63E+02	3.82E+02	-1.20E+02	3.12E-05
21	9.54E+02	3.82E+02	-1.20E+02	3.12E-05
22	8.28E+02	3.12E+02	-1.95E+02	2.99E-04
23	8.67E+02	-3.63E+02	-2.43E+02	8.26E-04
24	8.02E+02	-8.77E+02	-1.06E+02	1.51E-03
25	7.13E+02	-1.02E+03	1.03E+02	1.91E-03
26	6.69E+02	-1.05E+03	2.17E+02	1.44E-03
27	6.24E+02	-1.14E+03	2.83E+02	3.87E-04
28	6.14E+02	-1.28E+03	2.72E+02	8.31E-05
29	5.91E+02	-1.32E+03	3.72E+02	1.09E-06
30	5.91E+02	-1.32E+03	3.72E+02	1.09E-06
31	5.91E+02	-1.32E+03	3.72E+02	1.09E-06
32	5.91E+02	-1.32E+03	3.72E+02	1.09E-06
33	5.91E+02	-1.32E+03	3.72E+02	1.09E-06
34	5.90E+02	-1.32E+03	3.72E+02	1.09E-06
35	6.81E+02	-9.75E+02	2.00E+02	2.09E-03
36	6.70E+02	-8.79E+02	2.62E+02	5.83E-03
37	6.69E+02	-8.66E+02	2.70E+02	9.09E-03
38	6.69E+02	-8.62E+02	2.73E+02	1.23E-02

Node #	X Position	Y Position	Z Position	NAQDA1
39	6.69E+02	-8.62E+02	3.73E+02	6.87E-05
40	6.52E+02	-7.06E+02	3.73E+02	1.02E-04
41	0.00E+00	0.00E+00	0.00E+00	1.00E+00
...
200	0.00E+00	0.00E+00	0.00E+00	1.00E+00

Table C.2: SYVAC3-CC4 Simple Geosphere Network - Segment Properties

Segment #	Segment Hydraulic Conductivity [SGHYCO]	Segment Axial Dispersion Length [SGDSPF]	Source Fraction [SGSFRI]
1	1.26E-03	4.00E+00	1.00E+00
2	1.26E-03	4.00E+00	1.00E+00
3	1.26E-03	4.00E+00	1.00E+00
4	1.26E-03	4.00E+00	1.00E+00
5	1.26E-03	4.00E+00	1.00E+00
6	1.26E-03	4.00E+00	1.00E+00
7	1.26E-03	4.00E+00	1.00E+00
8	1.26E-03	4.00E+00	1.00E+00
9	1.26E-03	4.00E+00	1.00E+00
10	1.26E-03	4.00E+00	1.00E+00
11	0.00E+00	2.22E+00	1.00E+00
12	0.00E+00	2.86E+00	1.00E+00
13	0.00E+00	4.00E+00	1.00E+00
14	0.00E+00	6.67E+00	1.00E+00
15	0.00E+00	2.00E+01	1.00E+00
16	0.00E+00	2.00E+01	1.00E+00
17	0.00E+00	6.67E+00	1.00E+00
18	0.00E+00	4.00E+00	1.00E+00
19	0.00E+00	2.86E+00	1.00E+00
20	0.00E+00	2.22E+00	1.00E+00
21	1.26E-03	1.22E-01	1.00E+00
22	3.15E+01	2.95E-02	1.00E+00
23	3.15E+01	3.73E-02	1.00E+00
24	3.15E+01	7.49E-02	1.00E+00
25	3.15E+01	1.58E-01	1.00E+00
26	3.15E+01	1.68E-01	1.00E+00
27	3.15E+01	1.45E-01	1.00E+00
28	3.15E+01	1.90E-01	1.00E+00
29	3.15E+02	4.00E+00	1.00E+00

Segment #	Segment Hydraulic Conductivity [SGHYCO]	Segment Axial Dispersion Length [SGDSPF]	Source Fraction [SGSFRI]
30	3.15E+02	4.00E+00	1.00E+00
31	3.15E+01	1.90E-01	1.00E+00
32	3.15E+02	4.00E+00	1.00E+00
33	3.15E+02	4.00E+00	1.00E+00
34	3.15E+01	1.80E-01	0.00E+00
35	3.15E+01	2.04E-01	1.00E+00
36	3.15E+01	7.17E-01	1.00E+00
37	3.15E+01	2.15E+00	1.00E+00
38	0.00E+00	2.00E-01	1.00E+00
39	0.00E+00	1.00E+00	0.00E+00
40	0.00E+00	0.00E+00	0.00E+00
...
200	0.00E+00	0.00E+00	0.00E+00

Table C.3: SYVAC3-CC4 Simple Geosphere Network - Slope Values

Segment #	Slope Values [a/m3]		
	Well Demand Lower than BPA	Well Demand Higher than BPA but Lower than BPB	Well Demand Higher than BPB but Lower than BPC
1	0.00E+00	0.00E+00	0.00E+00
2	0.00E+00	0.00E+00	0.00E+00
3	0.00E+00	0.00E+00	0.00E+00
4	0.00E+00	0.00E+00	0.00E+00
5	0.00E+00	0.00E+00	0.00E+00
6	0.00E+00	0.00E+00	0.00E+00
7	0.00E+00	0.00E+00	0.00E+00
8	0.00E+00	0.00E+00	0.00E+00
9	0.00E+00	0.00E+00	0.00E+00
10	0.00E+00	0.00E+00	0.00E+00
11	0.00E+00	0.00E+00	0.00E+00
12	0.00E+00	0.00E+00	0.00E+00
13	0.00E+00	0.00E+00	0.00E+00
14	0.00E+00	0.00E+00	0.00E+00
15	0.00E+00	0.00E+00	0.00E+00
16	0.00E+00	0.00E+00	0.00E+00
17	0.00E+00	0.00E+00	0.00E+00
18	0.00E+00	0.00E+00	0.00E+00
19	0.00E+00	0.00E+00	0.00E+00
20	0.00E+00	0.00E+00	0.00E+00

21	0.00E+00	0.00E+00	0.00E+00
22	0.00E+00	0.00E+00	0.00E+00
23	0.00E+00	0.00E+00	0.00E+00
24	0.00E+00	0.00E+00	0.00E+00
25	1.00E+38	1.00E+38	1.00E+38
26	0.00E+00	0.00E+00	0.00E+00
27	0.00E+00	0.00E+00	0.00E+00
28	0.00E+00	0.00E+00	0.00E+00
29	0.00E+00	0.00E+00	0.00E+00
30	0.00E+00	0.00E+00	0.00E+00
31	0.00E+00	0.00E+00	0.00E+00
32	0.00E+00	0.00E+00	0.00E+00
33	0.00E+00	0.00E+00	0.00E+00
34	1.10E-03	0.00E+00	0.00E+00
35	0.00E+00	0.00E+00	0.00E+00
36	0.00E+00	0.00E+00	0.00E+00
37	0.00E+00	0.00E+00	0.00E+00
38	0.00E+00	0.00E+00	0.00E+00
39	0.00E+00	0.00E+00	0.00E+00
40	0.00E+00	0.00E+00	0.00E+00
...
200	0.00E+00	0.00E+00	0.00E+00

Table C.4: SYVAC3-CC4 Simple Geosphere Network - Input Data File

! 015-AUG-28 VERSION 01 M. GOBIEN
! external name of file 6CSBNetFileConnetivity.fxd
! Finalized nodes for determination of geosphere consequences for reference case

! List includes:
! - Well node 176,
! - River discharge nodes (Aquatic 170, 181, and 187) (Terrestrial 173, 184 and 190),
! - Central Wetland Terrestrial discharge node 178
! - Vault source node (Sector 8) 67

! Generated in 6CSBNetFileConnetivity01a.xlsx in

!
W:\Eba_shr\Projects\SA05_2012\Tasks\02D_4CS_GeosphereNetwork\07_NetworkDev\01_Net
work_FXD
! GEONET - NETWORK FIXED PARAMETER DATA FILE 'NETnn.FXD'

! INPUT FILE FOR SYVAC3-CC409

! Dimensions of 25 sectors (50 source nodes)

! 200 nodes

! 200 segments

! 10 discharges

! 10 unique glaciation states

! groundwater velocity function indicator []

! 1 = velocity input

! 2 = darcy velocity input

! 3 = hydraulic conductivity and head input and

! velocity calculated

! 4 = permeability and head input

! both hydraulic conductivity and

! velocity calculated from reference water properties

! 5 = permeability and temperature and head input

! both hydraulic conductivity and

! velocity calculated from variable water properties

! 6 = permeability and temperature and head input

! both hydraulic conductivity and

! velocity calculated from variable water properties

! with gravitational buoyancy term

3

&! geosphere fixed parameters for segments

&!response function flags []

&!1 =RSMINF, semi-infinite b.c. response function

&!2 =RMSTFR, mass transfer b.c. response function

&!3 =RZROCO, zero concentration b.c. response function

&	0	0	0	0	0	0	0	0	0	0	!90
&	0	0	0	0	0	0	0	0	0	0	!100
&	0	0	0	0	0	0	0	0	0	0	!110
&	0	0	0	0	0	0	0	0	0	0	!120
&	0	0	0	0	0	0	0	0	0	0	!130
&	0	0	0	0	0	0	0	0	0	0	!140
&	0	0	0	0	0	0	0	0	0	0	!150
&	0	0	0	0	0	0	0	0	0	0	!160
&	0	0	0	0	0	0	0	0	0	0	!170
&	0	0	0	0	0	0	0	0	0	0	!180
&	0	0	0	0	0	0	0	0	0	0	!190
&	0	0	0	0	0	0	0	0	0	0	!200

&!list of nonaquifer nodes for drawdown calculation

&	1	2	3	4	5	6	7	8	9	10	!10
&	11	12	13	14	15	16	17	18	19	20	!20
&	21	22	23	24	25	26	27	28	35	0	!30
&	0	0	0	0	0	0	0	0	0	0	!40
&	0	0	0	0	0	0	0	0	0	0	!50
&	0	0	0	0	0	0	0	0	0	0	!60
&	0	0	0	0	0	0	0	0	0	0	!70
&	0	0	0	0	0	0	0	0	0	0	!80
&	0	0	0	0	0	0	0	0	0	0	!90
&	0	0	0	0	0	0	0	0	0	0	!100
&	0	0	0	0	0	0	0	0	0	0	!110
&	0	0	0	0	0	0	0	0	0	0	!120
&	0	0	0	0	0	0	0	0	0	0	!130
&	0	0	0	0	0	0	0	0	0	0	!140
&	0	0	0	0	0	0	0	0	0	0	!150
&	0	0	0	0	0	0	0	0	0	0	!160
&	0	0	0	0	0	0	0	0	0	0	!170
&	0	0	0	0	0	0	0	0	0	0	!180
&	0	0	0	0	0	0	0	0	0	0	!190
&	0	0	0	0	0	0	0	0	0	0	!200

&!nodes in well aquifer bounding well position, upper then lower

& 40 35

&!list of biosphere discharge nodes

&	31	34	39	0	0	0	0	0	0	0	!10
---	----	----	----	---	---	---	---	---	---	---	-----

&!code number for biosphere discharge

&!1 = AQUA (aquatic discharge)

&!2 = WELL (well discharge)

&!3 = TERR (terrestrial discharge)

&!4 = BOG (swamp or bog discharge)

Table C.5: SYVAC3-CC4 Full Geosphere Network – Node Data

Node #	X Position	Y Position	Z Position	NAQDA1
1	1.79E+02	-7.65E+02	-1.18E+02	1.88E-04
2	1.85E+02	-7.67E+02	-1.18E+02	1.94E-04
3	8.22E+01	-1.23E+03	-1.91E+02	4.78E-06
4	4.90E+02	-1.75E+03	-9.86E+01	2.85E-06
5	3.88E+02	-1.80E+03	-4.83E+01	1.81E-06
6	3.45E+02	-1.93E+03	2.53E+02	3.60E-07
7	2.85E+02	-7.67E+02	-1.18E+02	1.94E-04
8	2.85E+02	-7.67E+02	-6.80E+01	4.78E-06
9	5.99E+01	-2.45E+02	-1.18E+02	8.95E-05
10	5.44E+01	-2.67E+02	-1.18E+02	8.96E-05
11	8.22E+01	-1.15E+03	-2.56E+02	5.11E-06
12	2.91E+02	5.42E+02	-1.18E+02	5.45E-05
13	3.45E+02	5.23E+02	-1.19E+02	6.54E-05
14	4.90E+02	4.60E+02	-1.20E+02	1.03E-04
15	8.18E+02	-3.46E+02	-1.65E+02	8.08E-04
16	7.08E+02	-8.71E+02	1.74E+02	3.39E-03
17	5.99E+01	6.82E+02	-1.18E+02	2.12E-05
18	9.71E+01	6.62E+02	-1.13E+02	2.37E-05
19	1.12E+02	6.60E+02	-1.13E+02	2.46E-05
20	2.21E+02	5.85E+01	-6.60E+01	8.78E-05
21	-2.13E+02	-9.75E+02	-2.34E+02	5.85E-06
22	8.22E+01	-1.25E+03	-2.49E+02	5.11E-06
23	2.09E+02	7.02E+02	-1.18E+02	3.04E-05
24	3.78E+02	6.64E+02	-1.14E+02	5.25E-05
25	4.69E+02	6.40E+02	-1.12E+02	6.77E-05
26	6.02E+02	-6.68E+01	-1.43E+01	1.65E-04
27	5.24E+02	-3.35E+02	-1.36E+02	2.91E-04
28	4.15E+02	-1.18E+03	-9.35E+01	6.50E-05
29	2.53E+02	5.02E+02	-1.18E+02	5.40E-05
30	6.73E+02	3.81E+02	-1.18E+02	1.67E-04
31	7.73E+02	-9.51E+01	-1.14E+02	4.88E-04
32	5.12E+02	7.22E+02	-1.18E+02	6.26E-05
33	6.07E+02	7.03E+02	-1.19E+02	7.77E-05
34	6.30E+02	7.00E+02	-1.20E+02	8.06E-05
35	8.63E+02	4.63E+01	-3.18E+02	5.16E-04
36	9.73E+02	-2.27E+02	-6.67E+02	7.63E-04
37	9.06E+02	-1.20E+03	-4.87E+02	1.00E-03
38	3.62E+02	-1.94E+03	2.53E+02	3.73E-07
39	6.61E+02	6.02E+02	-1.18E+02	1.05E-04

Node #	X Position	Y Position	Z Position	NAQDA1
40	6.73E+02	6.01E+02	-1.18E+02	1.09E-04
41	8.18E+02	5.85E+01	-2.17E+02	4.56E-04
42	6.04E+02	-1.32E+03	3.45E+02	8.78E-06
43	6.58E+02	5.82E+02	-1.18E+02	1.09E-04
44	6.63E+02	5.80E+02	-1.18E+02	1.10E-04
45	8.63E+02	-5.51E+01	-3.18E+02	5.82E-04
46	7.58E+02	-6.61E+02	-3.17E+02	9.80E-04
47	2.90E+02	-1.43E+03	-2.71E+02	4.91E-06
48	3.49E+02	-1.93E+03	2.53E+02	3.67E-07
49	6.61E+02	5.42E+02	-1.18E+02	1.19E-04
50	6.73E+02	5.41E+02	-1.18E+02	1.24E-04
51	7.88E+02	2.24E+02	-1.56E+02	3.22E-04
52	7.88E+02	1.72E+02	-1.60E+02	3.50E-04
53	8.23E+02	-2.79E+01	-2.17E+02	5.18E-04
54	5.72E+02	-1.85E+02	-1.18E+02	2.39E-04
55	5.69E+02	-1.87E+02	-1.18E+02	2.37E-04
56	4.25E+02	-1.18E+03	-8.66E+01	6.51E-05
57	3.90E+02	-1.65E+02	-1.18E+02	1.63E-04
58	9.26E+01	-3.26E+02	-1.19E+02	9.64E-05
59	-1.54E+02	-1.00E+03	-2.96E+02	5.18E-06
60	2.90E+02	-1.43E+03	-2.72E+02	4.90E-06
61	6.64E+02	3.22E+02	-1.18E+02	1.78E-04
62	6.73E+02	3.20E+02	-1.18E+02	1.84E-04
63	7.68E+02	-1.30E+02	-1.03E+02	5.02E-04
64	7.08E+02	-8.56E+02	1.76E+02	3.49E-03
65	6.77E+02	-8.63E+02	2.53E+02	7.71E-03
66	3.93E+02	-7.65E+02	-1.18E+02	6.75E-04
67	3.90E+02	-7.67E+02	-1.18E+02	4.85E-04
68	2.32E+02	-1.45E+03	-1.49E+02	4.06E-06
69	3.86E+02	-1.79E+03	5.77E+01	1.86E-06
70	4.73E+02	-7.67E+02	-1.18E+02	6.53E-04
71	4.09E+02	-1.09E+03	-8.66E+01	6.49E-05
72	6.21E+02	-1.38E+03	-6.75E+01	5.38E-05
73	7.23E+02	-1.45E+03	3.43E+02	3.82E-06
74	6.48E+02	-5.92E+02	-1.18E+02	7.95E-04
75	6.48E+02	-6.07E+02	-1.13E+02	8.16E-04
76	6.07E+02	-8.95E+02	5.83E+01	1.49E-03
77	6.54E+02	-9.53E+02	1.79E+02	2.60E-03
78	6.55E+02	-9.25E+02	2.53E+02	3.72E-03
79	1.50E+03	6.22E+02	-1.18E+02	4.44E-05

Node #	X Position	Y Position	Z Position	NAQDA1
80	1.49E+03	6.22E+02	-1.19E+02	4.50E-05
81	1.48E+03	6.21E+02	-1.21E+02	4.55E-05
82	1.39E+03	3.31E+02	-3.18E+02	1.12E-04
83	1.01E+03	-1.98E+03	-9.57E+02	3.13E-06
84	5.20E+02	-1.98E+03	1.49E+02	9.73E-07
85	1.21E+03	5.82E+02	-1.18E+02	8.35E-05
86	1.17E+03	5.82E+02	-1.19E+02	8.90E-05
87	1.15E+03	5.81E+02	-1.21E+02	9.25E-05
88	8.82E+02	4.32E+02	-3.05E+02	2.99E-04
89	7.58E+02	-1.17E+03	-1.16E+02	1.58E-03
90	6.09E+02	-1.36E+03	-6.75E+01	5.56E-05
91	1.08E+03	6.02E+02	-1.18E+02	1.00E-04
92	1.08E+03	6.02E+02	-1.19E+02	1.01E-04
93	1.05E+03	6.01E+02	-1.21E+02	1.05E-04
94	8.79E+02	5.13E+02	-2.68E+02	2.49E-04
95	1.38E+03	-1.38E+03	-6.34E+02	2.10E-04
96	5.20E+02	-2.00E+03	1.90E+02	7.20E-07
97	4.38E+02	-2.00E+03	2.53E+02	3.93E-07
98	1.06E+03	2.62E+02	-1.19E+02	1.81E-04
99	1.04E+03	2.61E+02	-1.21E+02	1.87E-04
100	8.62E+02	1.31E+02	-2.66E+02	4.46E-04
101	1.12E+03	-3.25E+02	-1.18E+02	3.60E-04
102	1.08E+03	-3.27E+02	-1.18E+02	3.94E-04
103	7.73E+02	-1.13E+03	2.33E+02	2.28E-04
104	9.42E+02	-1.38E+03	3.43E+02	1.99E-06
105	9.53E+02	1.81E+02	-1.21E+02	2.40E-04
106	8.37E+02	9.78E+01	-2.18E+02	4.39E-04
107	7.13E+02	-9.65E+02	1.33E+02	2.26E-03
108	6.74E+02	-8.73E+02	2.53E+02	7.23E-03
109	6.69E+02	-8.46E+02	2.83E+02	1.69E-02
110	9.54E+02	-7.65E+02	-1.18E+02	7.77E-04
111	9.52E+02	-7.67E+02	-1.18E+02	7.81E-04
112	9.52E+02	-7.67E+02	-6.88E-01	1.98E-04
113	9.52E+02	-7.67E+02	-1.18E+02	7.81E-04
114	9.00E+02	-1.25E+03	2.34E+02	3.49E-05
115	1.01E+03	-1.40E+03	3.43E+02	6.93E-07
116	1.04E+03	-1.40E+03	3.60E+02	2.00E-08
117	9.80E+02	-6.05E+02	-1.18E+02	6.09E-04
118	9.62E+02	-6.23E+02	-1.19E+02	6.44E-04
119	9.58E+02	-6.24E+02	-1.21E+02	6.49E-04

Node #	X Position	Y Position	Z Position	NAQDA1
120	7.23E+02	-9.66E+02	1.33E+02	2.25E-03
121	1.29E+03	-1.85E+02	-1.18E+02	2.09E-04
122	1.26E+03	-1.87E+02	-1.19E+02	2.23E-04
123	1.20E+03	-1.34E+03	-3.66E+01	1.14E-04
124	6.50E+02	-1.34E+03	1.58E+02	4.00E-05
125	6.49E+02	-1.45E+03	1.61E+02	3.48E-05
126	5.79E+02	-1.55E+03	2.35E+02	5.19E-06
127	3.64E+02	-1.86E+03	2.53E+02	3.40E-07
128	1.36E+03	-1.67E+02	-1.19E+02	1.74E-04
129	1.67E+03	-1.61E+03	2.43E+02	2.20E-07
130	1.69E+03	-1.61E+03	3.28E+02	2.00E-08
131	1.27E+03	-4.23E+02	-1.19E+02	2.64E-04
132	1.27E+03	-4.25E+02	-1.21E+02	2.66E-04
133	1.28E+03	-1.25E+03	-2.63E+01	1.00E-04
134	6.64E+02	-1.46E+03	2.43E+02	2.20E-05
135	6.03E+02	-1.56E+03	3.43E+02	9.73E-07
136	1.29E+03	1.21E+02	-1.19E+02	1.44E-04
137	9.74E+02	-3.99E+02	-3.18E+02	7.42E-04
138	9.27E+02	-4.75E+02	-3.35E+02	9.47E-04
139	6.71E+02	-8.97E+02	2.53E+02	5.58E-03
140	1.50E+03	1.22E+02	-1.18E+02	9.28E-05
141	1.49E+03	1.20E+02	-1.20E+02	9.41E-05
142	1.47E+03	-5.47E+02	-3.18E+02	2.00E-04
143	1.76E+03	-1.28E+03	-3.16E+02	5.54E-05
144	1.74E+03	-1.59E+03	2.43E+02	1.80E-07
145	1.73E+03	-1.59E+03	3.34E+02	6.67E-09
146	1.52E+03	4.61E+02	-1.21E+02	5.67E-05
147	1.48E+03	1.31E+02	-3.18E+02	1.18E-04
148	1.91E+03	-1.25E+03	-6.92E+02	6.26E-05
149	1.28E+03	-2.25E+03	-8.02E+02	1.82E-06
150	5.20E+02	-2.01E+03	1.94E+02	6.87E-07
151	1.56E+03	-7.65E+02	-1.18E+02	1.11E-04
152	1.57E+03	-7.67E+02	-1.18E+02	1.02E-04
153	1.57E+03	-7.67E+02	0.00E+00	2.76E-05
154	1.57E+03	-7.67E+02	-1.18E+02	1.02E-04
155	1.78E+03	-2.08E+03	2.34E+02	2.40E-07
156	1.77E+03	-1.57E+03	3.34E+02	1.33E-08
157	1.44E+03	-7.67E+02	-1.18E+02	1.50E-04
158	1.46E+03	-9.52E+02	-2.63E+01	4.40E-05
159	1.53E+03	-1.03E+03	1.62E+02	2.12E-05

Node #	X Position	Y Position	Z Position	NAQDA1
160	1.48E+03	-1.42E+03	3.41E+02	1.13E-07
161	1.30E+03	-7.67E+02	-1.18E+02	2.25E-04
162	1.26E+03	-1.30E+03	-3.66E+01	1.05E-04
163	6.51E+02	-1.45E+03	1.53E+02	3.60E-05
164	3.09E+02	-2.00E+03	3.57E+02	0.00E+00
165	3.09E+02	-2.00E+03	3.57E+02	0.00E+00
166	3.09E+02	-2.00E+03	3.57E+02	0.00E+00
167	3.09E+02	-2.00E+03	3.53E+02	0.00E+00
168	3.09E+02	-2.00E+03	3.57E+02	0.00E+00
169	3.09E+02	-2.00E+03	3.57E+02	0.00E+00
170	6.71E+02	-8.60E+02	2.68E+02	1.69E-02
171	6.69E+02	-8.50E+02	2.79E+02	1.69E-02
172	6.69E+02	-8.46E+02	3.83E+02	-2.05E-04
173	1.04E+03	-1.40E+03	3.64E+02	2.00E-08
174	1.04E+03	-1.40E+03	3.64E+02	2.00E-08
175	1.77E+03	-1.58E+03	3.55E+02	0.00E+00
176	1.77E+03	-1.58E+03	3.59E+02	0.00E+00
177	1.77E+03	-1.58E+03	3.60E+02	0.00E+00
178	1.77E+03	-1.58E+03	3.56E+02	0.00E+00
179	1.77E+03	-1.58E+03	3.60E+02	0.00E+00
180	1.77E+03	-1.58E+03	3.60E+02	0.00E+00
181	6.49E+02	-7.56E+02	3.83E+02	-3.42E-04
182	0.00E+00	0.00E+00	0.00E+00	0.00E+00
...
200	0.00E+00	0.00E+00	0.00E+00	0.00E+00

Table C.6: SYVAC3-CC4 Full Geosphere Network – Segment Properties

Segment #	Segment Hydraulic Conductivity [SGHYCO]	Segment Axial Dispersion Length [SGDSPF]	Source Fraction [SGSFRI]
1	2.80E-01	3.36E+00	1.00E+00
2	1.21E-03	3.82E-02	9.90E-01
3	3.16E+01	3.16E-02	1.00E+00
4	1.21E-03	1.03E-01	1.00E+00
5	3.16E+01	8.46E-02	1.00E+00
6	0.00E+00	0.00E+00	1.00E-02
7	1.21E-03	6.28E-02	1.00E+00
8	3.16E+01	1.70E-02	1.00E+00
9	2.80E-01	8.94E-01	1.00E+00
10	1.21E-03	2.01E-02	1.00E+00
11	0.00E+00	0.00E+00	1.00E+00
12	0.00E+00	0.00E+00	0.00E+00
13	2.80E-01	3.51E-01	1.00E+00
14	3.88E-02	1.27E-01	1.00E+00
15	1.21E-03	2.29E-02	1.00E+00
16	3.16E+01	3.15E-02	1.00E+00
17	0.00E+00	0.00E+00	1.00E+00
18	2.80E-01	4.72E-01	1.00E+00
19	3.88E-02	1.30E+00	1.00E+00
20	1.21E-03	3.26E-02	1.00E+00
21	1.21E-03	1.76E-02	1.00E+00
22	1.21E-03	4.95E-02	1.00E+00
23	0.00E+00	0.00E+00	1.00E+00
24	0.00E+00	0.00E+00	0.00E+00
25	2.80E-01	1.15E-01	1.00E+00
26	3.88E-02	2.13E-01	1.00E+00
27	1.21E-03	2.75E-02	1.00E+00
28	1.21E-03	6.57E-02	1.00E+00
29	1.21E-03	2.36E-02	1.00E+00
30	0.00E+00	0.00E+00	1.00E+00
31	0.00E+00	0.00E+00	0.00E+00
32	2.80E-01	4.57E-02	1.00E+00
33	1.21E-03	4.11E-02	1.00E+00
34	0.00E+00	0.00E+00	1.00E+00
35	2.80E-01	2.08E-01	1.00E+00
36	3.88E-02	8.38E-01	1.00E+00
37	1.21E-03	2.77E-02	1.00E+00

Segment #	Segment Hydraulic Conductivity [SGHYCO]	Segment Axial Dispersion Length [SGDSPF]	Source Fraction [SGSFRI]
38	3.15E-04	4.37E-02	1.00E+00
39	3.16E+01	2.02E-02	1.00E+00
40	3.15E-04	1.70E-02	1.00E+00
41	0.00E+00	0.00E+00	1.00E+00
42	2.80E-01	1.60E+00	1.00E+00
43	1.21E-03	3.51E-02	1.00E+00
44	3.16E+01	1.33E-02	1.00E+00
45	0.00E+00	0.00E+00	1.00E+00
46	0.00E+00	0.00E+00	0.00E+00
47	2.80E-01	4.12E+00	1.00E+00
48	1.21E-03	2.88E-02	1.00E+00
49	3.15E-04	3.25E-02	1.00E+00
50	1.21E-03	2.23E-02	1.00E+00
51	3.16E+01	2.75E-02	1.00E+00
52	0.00E+00	0.00E+00	1.00E+00
53	0.00E+00	0.00E+00	0.00E+00
54	2.80E-01	1.60E+00	1.00E+00
55	1.21E-03	5.90E-02	1.00E+00
56	3.16E+01	3.86E-01	1.00E+00
57	1.21E-03	9.48E-02	1.00E+00
58	0.00E+00	0.00E+00	1.00E+00
59	2.80E-01	6.13E+00	1.00E+00
60	1.21E-03	2.00E-02	1.00E+00
61	0.00E+00	0.00E+00	1.00E+00
62	0.00E+00	0.00E+00	0.00E+00
63	2.80E-01	5.90E-02	1.00E+00
64	1.21E-03	2.71E-02	1.00E+00
65	1.21E-03	3.25E-02	1.00E+00
66	0.00E+00	0.00E+00	1.00E+00
67	0.00E+00	0.00E+00	0.00E+00
68	1.21E-03	2.11E+00	1.00E+00
69	1.21E-03	4.34E-02	1.00E+00
70	3.16E+01	2.57E-02	1.00E+00
71	3.16E+01	2.41E-01	1.00E+00
72	0.00E+00	0.00E+00	1.00E+00
73	2.80E-01	5.00E+00	1.00E+00
74	1.21E-03	2.85E-02	1.00E+00
75	1.21E-03	4.71E-02	1.00E+00

Segment #	Segment Hydraulic Conductivity [SGHYCO]	Segment Axial Dispersion Length [SGDSPF]	Source Fraction [SGSFRI]
76	0.00E+00	0.00E+00	1.00E+00
77	0.00E+00	0.00E+00	0.00E+00
78	1.21E-03	4.80E-02	1.00E+00
79	3.16E+01	6.86E-02	1.00E+00
80	3.16E+01	4.65E-02	1.00E+00
81	0.00E+00	0.00E+00	1.00E+00
82	0.00E+00	0.00E+00	0.00E+00
83	1.21E-03	1.29E+00	1.00E+00
84	1.21E-03	5.93E-02	1.00E+00
85	1.21E-03	1.41E-01	1.00E+00
86	3.16E+01	2.52E-01	1.00E+00
87	0.00E+00	0.00E+00	1.00E+00
88	2.80E-01	2.48E+00	1.00E+00
89	3.88E-02	3.75E+00	1.00E+00
90	1.21E-03	5.52E-02	1.00E+00
91	3.15E-04	8.25E-03	1.00E+00
92	3.16E+01	1.65E-02	1.00E+00
93	0.00E+00	0.00E+00	1.00E+00
94	2.80E-01	5.65E-01	1.00E+00
95	3.88E-02	9.45E-01	1.00E+00
96	1.21E-03	5.58E-02	1.00E+00
97	3.16E+01	1.23E-02	1.00E+00
98	1.21E-03	8.29E-02	1.00E+00
99	0.00E+00	0.00E+00	1.00E+00
100	0.00E+00	0.00E+00	0.00E+00
101	2.80E-01	4.02E+00	1.00E+00
102	3.88E-02	9.04E-01	1.00E+00
103	1.21E-03	8.15E-02	1.00E+00
104	3.16E+01	1.01E-02	1.00E+00
105	3.15E-04	1.49E-02	1.00E+00
106	3.16E+01	1.95E-01	1.00E+00
107	0.00E+00	0.00E+00	1.00E+00
108	0.00E+00	0.00E+00	0.00E+00
109	3.88E-02	9.53E-01	1.00E+00
110	1.21E-03	7.52E-02	1.00E+00
111	0.00E+00	0.00E+00	1.00E+00
112	2.80E-01	5.27E-01	1.00E+00
113	1.21E-03	2.16E-02	1.00E+00

Segment #	Segment Hydraulic Conductivity [SGHYCO]	Segment Axial Dispersion Length [SGDSPF]	Source Fraction [SGSFRI]
114	6.31E-02	6.27E-02	1.00E+00
115	0.00E+00	0.00E+00	1.00E+00
116	0.00E+00	0.00E+00	0.00E+00
117	1.21E-03	7.39E-02	1.00E+00
118	3.16E+01	1.78E-02	1.00E+00
119	3.16E+01	1.29E-01	1.00E+00
120	3.16E+01	9.58E-01	1.00E+00
121	3.16E+01	1.33E+00	1.00E+00
122	3.16E+01	4.00E+00	1.00E+00
123	2.80E-01	4.51E+00	1.00E+00
124	1.21E-03	4.75E-02	1.50E-01
125	3.16E+01	5.29E-02	1.00E+00
126	0.00E+00	0.00E+00	8.50E-01
127	1.21E-03	3.33E-02	1.00E+00
128	6.31E-02	9.41E-02	1.00E+00
129	3.15E-01	6.55E-01	1.00E+00
130	0.00E+00	0.00E+00	1.00E+00
131	2.80E-01	7.79E-01	1.00E+00
132	3.88E-02	4.58E+00	1.00E+00
133	1.21E-03	4.12E-02	1.00E+00
134	0.00E+00	0.00E+00	1.00E+00
135	2.80E-01	7.55E-01	1.00E+00
136	1.21E-03	1.73E-02	0.00E+00
137	3.16E+01	3.39E-02	1.00E+00
138	3.16E+01	7.72E-01	1.00E+00
139	1.21E-03	1.42E-01	1.00E+00
140	6.31E-02	5.29E-02	1.00E+00
141	0.00E+00	0.00E+00	1.00E+00
142	0.00E+00	0.00E+00	0.00E+00
143	1.21E-03	1.32E-02	1.00E+00
144	6.31E-02	2.26E-01	1.00E+00
145	0.00E+00	0.00E+00	1.00E+00
146	0.00E+00	0.00E+00	0.00E+00
147	3.88E-02	5.68E+00	1.00E+00
148	1.21E-03	2.41E-02	1.00E+00
149	3.16E+01	2.83E-02	1.00E+00
150	6.31E-02	1.30E-01	1.00E+00
151	0.00E+00	0.00E+00	1.00E+00

Segment #	Segment Hydraulic Conductivity [SGHYCO]	Segment Axial Dispersion Length [SGDSPF]	Source Fraction [SGSFRI]
152	0.00E+00	0.00E+00	0.00E+00
153	1.21E-03	3.13E-02	1.00E+00
154	3.15E-04	2.19E-01	1.00E+00
155	3.16E+01	2.61E-02	1.00E+00
156	0.00E+00	0.00E+00	1.00E+00
157	2.80E-01	2.71E+00	1.00E+00
158	1.21E-03	2.87E-02	1.00E+00
159	3.15E-04	2.55E-02	1.00E+00
160	1.21E-03	3.13E-02	1.00E+00
161	6.31E-02	2.18E-01	1.00E+00
162	0.00E+00	0.00E+00	1.00E+00
163	0.00E+00	0.00E+00	0.00E+00
164	1.21E-03	5.18E-02	1.00E+00
165	3.15E-04	1.34E-02	1.00E+00
166	3.15E-04	1.69E-02	1.00E+00
167	3.16E+01	1.57E-02	1.00E+00
168	0.00E+00	0.00E+00	1.00E+00
169	2.80E-01	1.03E+00	1.00E+00
170	1.21E-03	9.17E-02	1.50E-01
171	3.16E+01	2.33E-02	1.00E+00
172	0.00E+00	0.00E+00	8.50E-01
173	1.21E-03	2.45E-02	1.00E+00
174	6.31E-02	1.44E-01	1.00E+00
175	0.00E+00	0.00E+00	0.00E+00
176	1.21E-03	9.61E-02	1.00E+00
177	3.16E+01	9.38E-02	1.00E+00
178	1.21E-03	4.62E-02	1.00E+00
179	0.00E+00	0.00E+00	1.00E+00
180	0.00E+00	0.00E+00	0.00E+00
181	1.21E-03	3.71E-02	1.00E+00
182	3.16E+01	3.06E-02	1.00E+00
183	0.00E+00	0.00E+00	1.00E+00
184	3.16E+01	1.59E-01	1.00E+00
185	3.15E-01	4.00E+00	1.00E+00
186	3.15E+02	2.00E+01	1.00E+00
187	3.16E+01	1.58E-01	1.00E+00
188	3.15E-01	4.00E+00	1.00E+00
189	3.15E+02	0.00E+00	1.00E+00

Segment #	Segment Hydraulic Conductivity [SGHYCO]	Segment Axial Dispersion Length [SGDSPF]	Source Fraction [SGSFRI]
190	0.00E+00	2.00E-01	1.00E+00
191	3.15E-01	4.00E+00	1.00E+00
192	3.15E+02	0.00E+00	1.00E+00
193	3.16E+01	9.32E-01	1.00E+00
194	3.15E-01	4.00E+00	1.00E+00
195	3.15E+02	2.00E+01	1.00E+00
196	3.16E+01	8.91E-01	1.00E+00
197	3.15E-01	4.00E+00	1.00E+00
198	3.15E+02	2.00E+01	1.00E+00
199	0.00E+00	0.00E+00	0.00E+00
200	0.00E+00	0.00E+00	0.00E+00

Table C.7: SYVAC3-CC4 Full Geosphere Network – Slope Values

Segment #	Slope Values [a/m3]		
	Well Demand Lower than BPA	Well Demand Higher than BPA but Lower than BPB	Well Demand Higher than BPB but Lower than BPC
1	0.00E+00	0.00E+00	0.00E+00
2	0.00E+00	0.00E+00	0.00E+00
3	0.00E+00	0.00E+00	0.00E+00
4	0.00E+00	0.00E+00	0.00E+00
5	0.00E+00	0.00E+00	0.00E+00
6	0.00E+00	0.00E+00	0.00E+00
7	0.00E+00	0.00E+00	0.00E+00
8	0.00E+00	0.00E+00	0.00E+00
9	0.00E+00	0.00E+00	0.00E+00
10	1.00E+38	1.00E+38	1.00E+38
11	0.00E+00	0.00E+00	0.00E+00
12	0.00E+00	7.86E-05	1.72E-04
13	0.00E+00	0.00E+00	0.00E+00
14	0.00E+00	0.00E+00	0.00E+00
15	0.00E+00	0.00E+00	0.00E+00
16	0.00E+00	0.00E+00	0.00E+00
17	0.00E+00	0.00E+00	0.00E+00
18	0.00E+00	0.00E+00	0.00E+00
19	1.00E+38	1.00E+38	1.00E+38
20	0.00E+00	0.00E+00	0.00E+00
21	0.00E+00	0.00E+00	0.00E+00
22	0.00E+00	0.00E+00	0.00E+00
23	0.00E+00	0.00E+00	0.00E+00
24	6.73E-04	1.52E-04	2.24E-05
25	1.00E+38	1.00E+38	1.00E+38
26	0.00E+00	0.00E+00	0.00E+00
27	0.00E+00	0.00E+00	0.00E+00
28	0.00E+00	0.00E+00	0.00E+00
29	0.00E+00	0.00E+00	0.00E+00
30	0.00E+00	0.00E+00	0.00E+00
31	9.61E-04	1.22E-04	2.45E-05
32	0.00E+00	0.00E+00	0.00E+00
33	0.00E+00	0.00E+00	0.00E+00
34	0.00E+00	0.00E+00	0.00E+00
35	0.00E+00	0.00E+00	0.00E+00
36	0.00E+00	0.00E+00	0.00E+00
37	0.00E+00	0.00E+00	0.00E+00

Segment #	Slope Values [a/m3]		
	Well Demand Lower than BPA	Well Demand Higher than BPA but Lower than BPB	Well Demand Higher than BPB but Lower than BPC
38	0.00E+00	0.00E+00	0.00E+00
39	0.00E+00	0.00E+00	0.00E+00
40	0.00E+00	0.00E+00	0.00E+00
41	0.00E+00	0.00E+00	0.00E+00
42	0.00E+00	0.00E+00	0.00E+00
43	1.00E+38	1.00E+38	1.00E+38
44	0.00E+00	0.00E+00	0.00E+00
45	0.00E+00	0.00E+00	0.00E+00
46	1.10E-03	0.00E+00	0.00E+00
47	1.00E+38	1.00E+38	1.00E+38
48	0.00E+00	0.00E+00	0.00E+00
49	0.00E+00	0.00E+00	0.00E+00
50	0.00E+00	0.00E+00	0.00E+00
51	0.00E+00	0.00E+00	0.00E+00
52	0.00E+00	0.00E+00	0.00E+00
53	8.78E-04	-8.04E-05	-1.68E-04
54	0.00E+00	0.00E+00	0.00E+00
55	0.00E+00	0.00E+00	0.00E+00
56	0.00E+00	0.00E+00	0.00E+00
57	0.00E+00	0.00E+00	0.00E+00
58	0.00E+00	0.00E+00	0.00E+00
59	0.00E+00	0.00E+00	0.00E+00
60	1.00E+38	1.00E+38	1.00E+38
61	0.00E+00	0.00E+00	0.00E+00
62	8.84E-04	1.03E-04	6.73E-05
63	1.00E+38	1.00E+38	1.00E+38
64	0.00E+00	0.00E+00	0.00E+00
65	0.00E+00	0.00E+00	0.00E+00
66	0.00E+00	0.00E+00	0.00E+00
67	6.91E-04	3.58E-04	5.27E-05
68	0.00E+00	0.00E+00	0.00E+00
69	0.00E+00	0.00E+00	0.00E+00
70	0.00E+00	0.00E+00	0.00E+00
71	0.00E+00	0.00E+00	0.00E+00
72	0.00E+00	0.00E+00	0.00E+00
73	0.00E+00	0.00E+00	0.00E+00
74	1.00E+38	1.00E+38	1.00E+38
75	0.00E+00	0.00E+00	0.00E+00

Segment #	Slope Values [a/m3]		
	Well Demand Lower than BPA	Well Demand Higher than BPA but Lower than BPB	Well Demand Higher than BPB but Lower than BPC
76	0.00E+00	0.00E+00	0.00E+00
77	7.31E-04	3.27E-04	7.08E-05
78	1.00E+38	1.00E+38	1.00E+38
79	0.00E+00	0.00E+00	0.00E+00
80	0.00E+00	0.00E+00	0.00E+00
81	0.00E+00	0.00E+00	0.00E+00
82	4.19E-04	5.37E-04	1.51E-04
83	0.00E+00	0.00E+00	0.00E+00
84	0.00E+00	0.00E+00	0.00E+00
85	0.00E+00	0.00E+00	0.00E+00
86	0.00E+00	0.00E+00	0.00E+00
87	0.00E+00	0.00E+00	0.00E+00
88	0.00E+00	0.00E+00	0.00E+00
89	0.00E+00	0.00E+00	0.00E+00
90	0.00E+00	0.00E+00	0.00E+00
91	0.00E+00	0.00E+00	0.00E+00
92	0.00E+00	0.00E+00	0.00E+00
93	0.00E+00	0.00E+00	0.00E+00
94	0.00E+00	0.00E+00	0.00E+00
95	1.00E+38	1.00E+38	1.00E+38
96	0.00E+00	0.00E+00	0.00E+00
97	0.00E+00	0.00E+00	0.00E+00
98	0.00E+00	0.00E+00	0.00E+00
99	0.00E+00	0.00E+00	0.00E+00
100	9.15E-04	-1.70E-04	1.33E-04
101	1.00E+38	1.00E+38	1.00E+38
102	0.00E+00	0.00E+00	0.00E+00
103	0.00E+00	0.00E+00	0.00E+00
104	0.00E+00	0.00E+00	0.00E+00
105	0.00E+00	0.00E+00	0.00E+00
106	0.00E+00	0.00E+00	0.00E+00
107	0.00E+00	0.00E+00	0.00E+00
108	8.38E-04	3.18E-04	-1.28E-04
109	0.00E+00	0.00E+00	0.00E+00
110	0.00E+00	0.00E+00	0.00E+00
111	0.00E+00	0.00E+00	0.00E+00
112	0.00E+00	0.00E+00	0.00E+00
113	1.00E+38	1.00E+38	1.00E+38

Segment #	Slope Values [a/m3]		
	Well Demand Lower than BPA	Well Demand Higher than BPA but Lower than BPB	Well Demand Higher than BPB but Lower than BPC
114	0.00E+00	0.00E+00	0.00E+00
115	0.00E+00	0.00E+00	0.00E+00
116	1.09E-03	1.57E-05	0.00E+00
117	0.00E+00	0.00E+00	0.00E+00
118	0.00E+00	0.00E+00	0.00E+00
119	0.00E+00	0.00E+00	0.00E+00
120	0.00E+00	0.00E+00	0.00E+00
121	0.00E+00	0.00E+00	0.00E+00
122	0.00E+00	0.00E+00	0.00E+00
123	0.00E+00	0.00E+00	0.00E+00
124	0.00E+00	0.00E+00	0.00E+00
125	0.00E+00	0.00E+00	0.00E+00
126	0.00E+00	0.00E+00	0.00E+00
127	1.00E+38	1.00E+38	1.00E+38
128	0.00E+00	0.00E+00	0.00E+00
129	0.00E+00	0.00E+00	0.00E+00
130	3.00E-05	5.89E-04	3.13E-04
131	0.00E+00	0.00E+00	0.00E+00
132	0.00E+00	0.00E+00	0.00E+00
133	0.00E+00	0.00E+00	0.00E+00
134	0.00E+00	0.00E+00	0.00E+00
135	0.00E+00	0.00E+00	0.00E+00
136	1.00E+38	1.00E+38	1.00E+38
137	0.00E+00	0.00E+00	0.00E+00
138	0.00E+00	0.00E+00	0.00E+00
139	0.00E+00	0.00E+00	0.00E+00
140	0.00E+00	0.00E+00	0.00E+00
141	0.00E+00	0.00E+00	0.00E+00
142	6.12E-04	3.53E-06	6.97E-05
143	1.00E+38	1.00E+38	1.00E+38
144	0.00E+00	0.00E+00	0.00E+00
145	0.00E+00	0.00E+00	0.00E+00
146	7.33E-04	2.74E-04	8.55E-05
147	1.00E+38	1.00E+38	1.00E+38
148	0.00E+00	0.00E+00	0.00E+00
149	0.00E+00	0.00E+00	0.00E+00
150	0.00E+00	0.00E+00	0.00E+00
151	0.00E+00	0.00E+00	0.00E+00

Segment #	Slope Values [a/m3]		
	Well Demand Lower than BPA	Well Demand Higher than BPA but Lower than BPB	Well Demand Higher than BPB but Lower than BPC
152	6.93E-04	2.83E-04	9.79E-05
153	0.00E+00	0.00E+00	0.00E+00
154	0.00E+00	0.00E+00	0.00E+00
155	0.00E+00	0.00E+00	0.00E+00
156	0.00E+00	0.00E+00	0.00E+00
157	0.00E+00	0.00E+00	0.00E+00
158	1.00E+38	1.00E+38	1.00E+38
159	0.00E+00	0.00E+00	0.00E+00
160	0.00E+00	0.00E+00	0.00E+00
161	0.00E+00	0.00E+00	0.00E+00
162	0.00E+00	0.00E+00	0.00E+00
163	1.02E-05	3.30E-04	3.75E-04
164	0.00E+00	0.00E+00	0.00E+00
165	0.00E+00	0.00E+00	0.00E+00
166	0.00E+00	0.00E+00	0.00E+00
167	0.00E+00	0.00E+00	0.00E+00
168	0.00E+00	0.00E+00	0.00E+00
169	0.00E+00	0.00E+00	0.00E+00
170	0.00E+00	0.00E+00	0.00E+00
171	0.00E+00	0.00E+00	0.00E+00
172	0.00E+00	0.00E+00	0.00E+00
173	1.00E+38	1.00E+38	1.00E+38
174	0.00E+00	0.00E+00	0.00E+00
175	5.97E-05	3.87E-05	1.42E-04
176	1.00E+38	1.00E+38	1.00E+38
177	0.00E+00	0.00E+00	0.00E+00
178	0.00E+00	0.00E+00	0.00E+00
179	0.00E+00	0.00E+00	0.00E+00
180	0.00E+00	1.04E-03	1.76E-04
181	0.00E+00	0.00E+00	0.00E+00
182	0.00E+00	0.00E+00	0.00E+00
183	0.00E+00	0.00E+00	0.00E+00
184	0.00E+00	0.00E+00	0.00E+00
185	0.00E+00	0.00E+00	0.00E+00
186	0.00E+00	0.00E+00	0.00E+00
187	0.00E+00	0.00E+00	0.00E+00
188	0.00E+00	0.00E+00	0.00E+00
189	0.00E+00	0.00E+00	0.00E+00

Segment #	Slope Values [a/m3]		
	Well Demand Lower than BPA	Well Demand Higher than BPA but Lower than BPB	Well Demand Higher than BPB but Lower than BPC
190	0.00E+00	0.00E+00	0.00E+00
191	0.00E+00	0.00E+00	0.00E+00
192	0.00E+00	0.00E+00	0.00E+00
193	0.00E+00	0.00E+00	0.00E+00
194	0.00E+00	0.00E+00	0.00E+00
195	0.00E+00	0.00E+00	0.00E+00
196	0.00E+00	0.00E+00	0.00E+00
197	0.00E+00	0.00E+00	0.00E+00
198	0.00E+00	0.00E+00	0.00E+00
199	0.00E+00	0.00E+00	0.00E+00
200	0.00E+00	0.00E+00	0.00E+00

Table C.8: SYVAC3-CC4 Full Geosphere Network – Input Data File

```

! 016-Sept-28 VERSION 01 R. Guo
!     external name of file 6CSBNetFileConnetivity.fxd
!     Finalized nodes for determination of geosphere consequences for reference case

!     List includes:
!     - Well node 172,
!     - River discharge nodes (Aquatic 166 and 177) (Terrestrial 169 and 180),
!     - Central Wetland Terrestrial discharge node 174
!     - Vault source node (Sector 14) 14
! Generated in 6CSBNetFileConnetivity01a.xlsx in

!
! GEONET - NETWORK FIXED PARAMETER DATA FILE 'NETnn.FXD'

! INPUT FILE FOR SYVAC3-CC409

!     Dimensions of 25 sectors (50 source nodes)

!         200 nodes

!         200 segments

!         10 discharges

!         10 unique glaciation states

! groundwater velocity function indicator []

```

- ! 1 = velocity input
- ! 2 = darcy velocity input
- ! 3 = hydraulic conductivity and head input and
! velocity calculated
- ! 4 = permeability and head input
! both hydraulic conductivity and
! velocity calculated from reference water properties
- ! 5 = permeability and temperature and head input
! both hydraulic conductivity and
! velocity calculated from variable water properties
- ! 6 = permeability and temperature and head input
! both hydraulic conductivity and
! velocity calculated from variable water properties
! with gravitational buoyancy term

3

&! geosphere fixed parameters for segments

&!response function flags []

&!1 =RSMINF, semi-infinite b.c. response function

&!2 =RMSTFR, mass transfer b.c. response function

&!3 =RZROCO, zero concentration b.c. response function

&!4 =pass without change, no response function

&!5 =MULTIC, compartment model mimic a semi-infinite b.c.

&!6 =MULTIC, compartment model mimic a zero concentration b.c.

&	1	1	1	1	1	4	1	1	1	1	!10
&	4	4	1	1	1	1	4	1	1	1	!20
&	1	1	4	4	1	1	1	1	1	4	!30
&	4	1	1	4	1	1	1	1	1	1	!40
&	4	1	1	1	4	4	1	1	1	1	!50
&	1	4	4	1	1	1	1	4	1	1	!60

&	4	4	1	1	1	4	4	1	1	1	!70
&	1	4	1	1	1	4	4	1	1	1	!80
&	4	4	1	1	1	1	4	1	1	1	!90
&	1	1	4	1	1	1	1	1	4	4	!100
&	1	1	1	1	1	1	4	4	1	1	!110
&	4	1	1	1	4	4	1	1	1	1	!120
&	1	1	1	1	1	4	1	1	1	4	!130
&	1	1	1	4	1	1	1	1	1	1	!140
&	4	4	1	1	4	4	1	1	1	1	!150
&	4	4	1	1	1	4	1	1	1	1	!160
&	1	4	4	1	1	1	1	4	1	1	!170
&	1	4	1	1	4	1	1	1	4	4	!180
&	1	1	4	1	1	1	1	1	1	4	!190
&	1	1	1	1	1	1	1	1	4	0	!200

&! chemical property class

&	10	2	4	2	4	20	2	4	10	2	!10
&	20	20	10	11	2	4	20	10	11	2	!20
&	2	2	20	20	10	11	2	2	2	20	!30
&	20	10	2	20	10	11	2	1	4	1	!40
&	20	10	2	4	20	20	10	2	1	2	!50
&	4	20	20	10	2	4	2	20	10	2	!60
&	20	20	10	2	2	20	20	2	2	4	!70
&	4	20	10	2	2	20	20	2	4	4	!80
&	20	20	10	2	2	4	20	10	11	2	!90
&	1	4	20	10	11	2	4	2	20	20	!100
&	10	11	2	4	1	4	20	20	11	2	!110
&	20	10	2	3	20	20	2	4	4	4	!120
&	4	4	10	2	4	20	2	3	7	20	!130
&	10	11	2	20	10	2	4	4	2	3	!140
&	20	20	2	3	20	20	11	2	4	3	!150
&	20	20	2	1	4	20	10	2	1	2	!160
&	3	20	20	2	1	1	4	20	10	2	!170
&	4	20	2	3	20	2	4	2	20	20	!180
&	2	4	20	4	7	8	4	7	8	20	!190
&	7	8	4	7	8	4	7	8	20	0	!200

&! physical property class

&	10	2	4	2	4	20	2	4	10	2	!10
&	20	20	10	11	2	4	20	10	11	2	!20
&	2	2	20	20	10	11	2	2	2	20	!30
&	20	10	2	20	10	11	2	1	4	1	!40
&	20	10	2	4	20	20	10	2	1	2	!50
&	4	20	20	10	2	4	2	20	10	2	!60
&	20	20	10	2	2	20	20	2	2	4	!70
&	4	20	10	2	2	20	20	2	4	4	!80
&	20	20	10	2	2	4	20	10	11	2	!90
&	1	4	20	10	11	2	4	2	20	20	!100
&	10	11	2	4	1	4	20	20	11	2	!110
&	20	10	2	3	20	20	2	4	4	4	!120
&	4	4	10	2	4	20	2	3	7	20	!130

&	10	11	2	20	10	2	4	4	2	3	!140
&	20	20	2	3	20	20	11	2	4	3	!150
&	20	20	2	1	4	20	10	2	1	2	!160
&	3	20	20	2	1	1	4	20	10	2	!170
&	4	20	2	3	20	2	4	2	20	20	!180
&	2	4	20	4	7	8	4	7	8	20	!190
&	7	8	4	7	8	4	7	8	20	0	!200

&!node index number for node at inlet of segment

&	1	2	3	4	5	2	7	8	9	10	!10
&	11	10	12	13	14	15	16	17	18	19	!20
&	20	21	22	18	23	24	25	26	27	28	!30
&	23	29	30	31	32	33	34	35	36	37	!40
&	38	39	40	41	42	40	43	44	45	46	!50
&	47	48	43	49	50	51	52	53	54	55	!60
&	56	55	57	58	59	60	57	61	62	63	!70
&	64	65	66	67	68	69	67	70	71	72	!80
&	73	70	74	75	76	77	78	79	80	81	!90
&	82	83	84	85	86	87	88	89	90	86	!100
&	91	92	93	94	95	96	97	91	98	99	!110
&	100	101	102	103	104	102	105	106	107	108	!120
&	170	171	110	111	112	111	113	114	115	113	!130
&	117	118	119	120	121	122	123	124	125	126	!140
&	127	122	128	129	130	128	131	132	133	134	!150
&	135	131	136	137	138	139	140	141	142	143	!160
&	144	145	141	146	147	148	149	150	151	152	!170
&	153	152	154	155	154	157	158	159	160	157	!180
&	161	162	163	6	164	165	6	167	168	109	!190
&	116	173	156	175	176	156	178	179	108	0	!200

&!node index number for node at outlet of segment

&	2	3	4	5	6	7	8	6	10	11	!10
&	4	12	13	14	15	16	64	18	19	20	!20
&	21	22	4	23	24	25	26	27	28	72	!30
&	29	30	31	63	33	34	35	36	37	38	!40
&	6	40	41	42	115	43	44	45	46	47	!50
&	48	6	49	50	51	52	53	106	55	56	!60
&	71	57	58	59	60	47	61	62	63	64	!70
&	65	108	67	68	69	5	70	71	72	73	!80
&	115	74	75	76	77	78	108	80	81	82	!90
&	83	84	96	86	87	88	89	90	72	91	!100
&	92	93	94	95	96	97	6	98	99	100	!110
&	106	102	103	104	115	105	106	107	108	170	!120
&	171	109	111	112	115	113	114	115	116	117	!130
&	118	119	120	107	122	123	124	125	126	127	!140
&	6	128	129	130	156	131	132	133	134	135	!150
&	115	136	137	138	139	108	141	142	143	144	!160
&	145	156	146	147	148	149	150	96	152	153	!170
&	156	154	155	156	157	158	159	160	115	161	!180
&	162	163	124	164	165	166	167	168	169	172	!190
&	173	174	175	176	177	178	179	180	115	0	!200

&!unique glaciation states

&! 1 Bora1 !Normal Boreal

&! 2 PrmT1 !Permafrost Talik

&! 3 IceC1 !Icesheet Coldbase

&! 4 PrmT0 !Permafrost No Talik

&! 5 IceW1 !Icesheet Warmbase

&! 6 ProL1 !Proglacial Lake

&! 7 Bora2 !Normal Boreal 2

&! 8 sta08 !state 8

&! 9 sta09 !state 9

&! 10 sta10 !state 10

&!identification of states with impermeable zone and pathway through

&! 0 = no impermeable zone

&! 1 = impermeable zone but no open pathway

&! 2 = impermeable zone with open pathway

& 0 0 0 0 0 0 0 0 0 0 0 !10

&!list of segments in open pathway passing through impermeable zone

& 0 0 0 0 0 0 0 0 0 0 0 !10

& 0 0 0 0 0 0 0 0 0 0 0 !20

& 0 0 0 0 0 0 0 0 0 0 0 !30

& 0 0 0 0 0 0 0 0 0 0 0 !40

& 0 0 0 0 0 0 0 0 0 0 0 !50

& 0 0 0 0 0 0 0 0 0 0 0 !60

& 0 0 0 0 0 0 0 0 0 0 0 !70

& 0 0 0 0 0 0 0 0 0 0 0 !80

& 0 0 0 0 0 0 0 0 0 0 0 !90

& 0 0 0 0 0 0 0 0 0 0 0 !100

& 0 0 0 0 0 0 0 0 0 0 0 !110

& 0 0 0 0 0 0 0 0 0 0 0 !120

& 0 0 0 0 0 0 0 0 0 0 0 !130

& 0 0 0 0 0 0 0 0 0 0 0 !140

& 0 0 0 0 0 0 0 0 0 0 0 !150

& 0 0 0 0 0 0 0 0 0 0 0 !160

& 0 0 0 0 0 0 0 0 0 0 0 !170

& 0 0 0 0 0 0 0 0 0 0 0 !180

REFERENCES

- Davison, C.C., T. Chan, A. Brown, M. Gascoyne, D. Kamineni, G. Lodha, T. Melnyk, B.W. Nakka, P. O'Connor, D. Ophori, N. Scheier, N. Soonawala, F. Stanchell, D. Stevenson, G. Thorne, T. Vandergraaf, P. Vilks and S. Whitaker. 1994. The disposal of Canada's nuclear fuel waste: The geosphere model for postclosure assessment. Atomic Energy of Canada Limited Report AECL-10719, COG-93-9. Pinawa, Canada.
- Kitson, C., T. Melnyk, L. Wojciechowski, and T. Chshyolkova. 2012. SYVAC3-CC4 User Manual. Nuclear Waste Management Organization Technical Report NWMO TR-2012-21. Toronto, Canada.
- NWMO (Nuclear Waste Management Organization). 2017. Postclosure Safety Assessment of a Used Fuel Repository in Crystalline Rock. Nuclear Waste Management Organization Technical Report NWMO-TR-2017-02. Toronto, Canada.
- NWMO (Nuclear Waste Management Organization). 2012. SYVAC3-CC4 Theory Manual. Nuclear Waste Management Organization Technical Report NWMO TR-2012-22. Toronto, Canada.